

The University of Sheffield

Development of a Gut-on-a-Chip models in a 3D microfluidic platform (OrganoPlate®)



Elena Naumovska

Supervisor: Dr. Kai Erdmann

A thesis submitted in partial fulfilment of the requirements for the degree of
Doctor of Philosophy

in the
Faculty of Science
Department of Biomedical sciences

April 20

“The world hates change, yet it is the only thing that has brought progress.”- Charles F. Kettering

Acknowledgments

This work would not be possible with constant support from so many people, especially my supervisors Dr. Dorota Kurek and Dr. Henriette Lanz for the continuous support during my PhD journey. I had a very enjoyable time and the whole process was even easier with the help of my colleagues from MIMETAS. Furthermore, I would like to thank my academic supervisor Dr. Kai Erdman for his support throughout the PhD journey and my advisors Dr. Elizabeth Seward and Prof. Elizabeth Smythe for their hard questions and insightful comments which helped a lot during the writing of this thesis.

But most important, I would like to thank my family, my father Gligor, my mother Trajanka and my brother Tome which supported and encouraged me over the years to pursue a scientific career, even though that meant that I will be far away from them. Moreover, I would like to extend my deepest thanks to my husband Jane for being the best husband, a friend and a father to our little baby girl as well as for his love and for his support during my studies. And finally, I would like to thank my beautiful baby girl Emily for being the best thesis buddy and for also teaching me to be a better organized person for the final days of writing. Mommy loves you so much.

Contents

Acknowledgments-----	iii
Declaration -----	vi
Funding -----	vii
Abstract -----	viii
List of Figures -----	ix
List of Tables -----	xi
Chapter 1 Introduction-----	1
Gastrointestinal (GI) tract-----	1
Inflammatory bowel disease-----	1
In-vitro and ex-vivo experimental models of the intestine-----	26
The OrganoPlate® -----	32
Chapter 2 Aims, outline and approach -----	34
Project aims and summary -----	34
Approach -----	36
Chapter 3 Material and Methods -----	37
Materials -----	37
Cell culture -----	39
Cell seeding in the OrganoPlate® -----	42

Directed differentiation of induced pluripotent stem cells -----	45
Assays-----	47
Statistical analysis-----	55
Graphics -----	55
Chapter 4 Membrane-free culture and real-time barrier integrity assessment of perfused intestinal epithelium tubes -----	58
Chapter 5 Development of a Gut-on-a-Chip Model for High Throughput Disease Modelling and Drug Discovery-----	74
Chapter 6 Developing a complex tetra co-culture model suitable for modelling the inflamed intestinal mucosa in a 3D microfluidic platform - a plug and play approach-----	98
Chapter 7 Directed differentiation of induced pluripotent stem cells towards gut-on-a-chip in a 3D microfluidic platform-----	123
Chapter 8 Discussion -----	140
Benefit of Organs on a chip (OOC)-----	140
No single model can rule them all -----	140
Modelling IBD with organs-on-a-chip -----	142
Outlook -----	149
References-----	150

Declaration

All sentences or passages quoted in this document from other people's work have been specifically acknowledged by clear cross-referencing to author, work and page(s). Any illustrations that are not the work of the author of this report have been used with the explicit permission of the originator and are specifically acknowledged. I understand that failure to do this, amount to plagiarism and will be considered grounds for failure.

Name: **Elena Naumovska**

Date: April 6, 2020

Signature:

A handwritten signature in black ink, appearing to read 'Elena Naumovska', written in a cursive style.

Funding

The work in this thesis is funded from the initial training network MIMIC (ITN-MIMIC). ITN-MIMIC has received funding from the European Union's Horizon 2020 research and innovation program under grant agreement No 674983



Abstract

A common bottleneck in any drug development processes is finding an accurate model that will closely mimic disease development and progression. Conventional *in-vitro* drug screen experiments often rely on two-dimensional (2D) culture systems. These models often provide useful information and insights especially about drug metabolism and penetration. However, at the same time these models have more regularly failed to predict drug targets. Therefore, there is an unmet need for models that will bridge the gap between preclinical models and their predictive value throughout the stages of drug development. I described in this thesis the development and characterization of 3D gut-on-chip models developed on high throughput microfluidics platform – OrganoPlate. The *in-vitro* models were directed towards a disease state by applying downstream signalling molecule of activated immune cells. With this approach I was able to mimic several main characteristics of inflammatory bowel disease (IBD), like loss of barrier integrity and cell activation. After which these diseased gut-on-chip models were used for small scale phenotypic studies. Moreover, the work in this thesis describes four different high throughput models with increasing level of complexity, from simple Caco-2 based *in-vitro* models to more complex iPSC based ones, to complex tetra-co-culture model where several parts of human physiology are combined to achieve more predictable *in vitro* models.

..

List of Figures

FIGURE 1.1 DIFFERENCES BETWEEN CROHN’S DISEASE (CD) AND ULCERATIVE COLITIS (UC).....	3
FIGURE 1.2 AETIOLOGY OF IBD.	5
FIGURE 1.3 LOCI ASSOCIATED WITH THE DIFFERENT FORMS OF IBD ,	7
FIGURE 1.4 <i>NOD2</i> ACTIVATION	9
FIGURE 1.5 SCHEMATIC REPRESENTATION OF THE INTESTINAL EPITHELIUM WITH UNDERLYING LAMINA PROPRIA CONTAINING IMMUNE CELLS.	15
FIGURE 1.6 TIGHT JUNCTIONS AND THEIR ROLE IN DISEASE.....	16
FIGURE 1.7 ACTIVATION OF TNF- α , INF- γ AND IL-1 β SIGNALLING PATHWAYS.	19
FIGURE 1.8 CONCEPTUAL FRAMEWORK FOR THE PATHOGENESIS OF IBD.	22
FIGURE 1.9 <i>IN-VITRO</i> AND <i>EX-VIVO</i> INTESTINAL MODELS.....	29
FIGURE 1.10 THE ORGANOPLATE 3-LANE AND SCHEMATIC REPRESENTATION OF TUBULE SEEDING.	32
FIGURE 3.1 SCHEMATIC REPRESENTATION OF SIMPLIFIED ORGANOPLATE AGAINST GEL CELL SEEDING (TUBULE SEEDING).....	43
FIGURE 3.2 SCHEMATIC REPRESENTATION OF DIRECTED DIFFERENTIATION PROTOCOL OF INDUCED PLURIPOTENT STEM CELLS INTO GUT-ON-A-CHIP IN A MICROFLUIDIC DEVICE THE ORGANOPLATE®	46
FIGURE 3.3 SCHEMATIC OVERVIEW OF THE BARRIER INTEGRITY ASSAY IN A 3-LANE ORGANOPLATE®.....	48
FIGURE 3.4 ORGANOTEER	49
FIGURE 6.1 DEVELOPMENT OF A COMPLEX TETRA CO-CULTURE INTESTINAL MODEL	109
FIGURE 6.2 OPTIMIZATION OF MUCUS PRODUCING TUBULES	111
FIGURE 6.3 CHARACTERIZATION OF MUCUS PRODUCING 2CC.....	113
FIGURE 6.4 OPTIMIZATION OF THE TETRA CO-CULTURE MODEL	115
FIGURE 6.5 CHARACTERIZATION OF THE TETRA CO-CULTURE (4CC)	116
FIGURE 6.6 TRIGGER DYNAMICS AND INDUCING INFLAMMATION IN THE 4CC.....	117
FIGURE 6.7 PREVENTION OF THE INTESTINAL INFLAMMATORY-LIKE PHENOTYPE INDUCED BY CYTOKINES IN THE INTESTINE ON-A-CHIP MODEL BY ADDITION OF THE ANTI-INFLAMMATORY COMPOUND TPCA-1	119

FIGURE 8.1 APPLICABILITY OF ORGANS-ON-A-CHIP IN THE DRUG DEVELOPMENT PIPELINE	141
---	-----

List of Tables

TABLE 1-1 SUMMARY OF THERAPIES AVAILABLE FOR THE TREATMENT OF IBD.	24
TABLE 1-2 A SUMMARY OF ADVANTAGES AND DISADVANTAGES IN MODELLING DISEASES WITH <i>IN-VITRO</i> CELLULAR MODELS.....	26
TABLE 1-3 CHARACTERISTICS AND DESIGN OF INTESTINAL OOC	31
TABLE 2-1 REQUIREMENTS FOR HIGH-THROUGHPUT <i>IN-VITRO</i> MODELS.....	34
TABLE 2-2 IBD CHARACTERISTICS THAT CAN BE MODELLED WITH DIFFERENT CELL TYPES AND CONFIGURATION	35
TABLE 3-1 LIST OF EQUIPMENT USED	37
TABLE 3-2 LIST OF COMMERCIALY AVAILABLE KITS	38
TABLE 3-3 COMPONENTS OF DIRECTED DIFFERENTIATION MEDIA	47
TABLE 3-4 COMMONLY USED FLUORESCENTLY LABELLED DEXTRAN'S FOR PERFORMING THE BARRIER INTEGRITY ASSAY	48
TABLE 3-5 LIST OF PRIMARY AND SECONDARY ANTIBODIES AND CELL STAINS USED IN IMMUNOHISTOCHEMISTRY	52
TABLE 3-6 COMPONENTS MASTER MIX FOR CDNA SYNTHESIS	54
TABLE 3-7 SYBR GREEN PROBES	56
TABLE 3-8 LIST OF TAQMAN PROBES USED IN EXPERIMENTS.....	57

Chapter 1 Introduction

Gastrointestinal (GI) tract

In vitro modelling of the gastrointestinal track has many applications, mainly in the areas of toxicology, tissue engineering, nutraceuticals and drug testing (Costa and Ahluwalia 2019). In the drug development, the oral drug delivery has long been considered an attractive manner of administration of medicine. Although there are challenges associated with this method, what makes this delivery so interesting for pharmaceutical companies is the ease of administration, the long shelf life of solid formulation and the intensified immune response (Viswanathan, Muralidaran, and Ragavan 2017; Hamman, Demana, and Olivier 2007). The importance of the GI tract comes from its role in development of food antigens tolerance, self-antigens, non-pathogenic commensal bacteria and thereby maintaining immune homeostasis. Additionally, the GI tract protects the host organism from pathogenic organisms by mounting inflammatory responses towards them (Ahluwalia, Magnusson, and Öhman 2017). Therefore, it is not a surprise that when disrupted, this fine line between tolerance and inflammation of the GI track, may result in disease (Ahluwalia et al. 2018a)

Inflammatory bowel disease

Observed since ancient times, inflammatory bowel disease (IBD) is a complex idiopathic disease that becomes a big problem in westernized nations (Kaplan 2015). One major characteristic of IBD is a severe inflammation of the small bowel and/or colon, which in turn leads to recurrent diarrhoea, fever and abdominal pain. Severity of the disease is highly heterogenous and currently is clinically classified in two major pathological subtypes: Crohn's disease and ulcerative colitis (Tontini et al. 2015). Despite both being chronic and relapsing, they can be distinguished by the

inflammation location and by the histological changes on the intestinal wall as shown in Figure 1.1 (Matricon, Barnich, and Ardid 2010). Crohn's disease (CD) is characterized by a transmural inflammation with skip lesions that may involve any part of the GI tract from mouth to anus, but mostly affecting the terminal ileum. On the other hand, Ulcerative colitis (UC) is characterized by continuous colonic mucosal inflammation starting from the rectum moving upwards. Major symptoms for both diseases include bloody diarrhoea, tenesmus and abdominal pain (Mulder et al. 2014).

Epidemiology

Inflammatory bowel disease (IBD) is a disabling disease affecting the quality of life, with varying symptoms resulting in chronic pain and fatigue (Cohen et al. 2014). Compared to the general population, the longevity or mortality of IBD patients is not changed and no significant differences in the prevalence between man and female is observed (Kaplan 2015b; Ananthakrishnan 2015). However, most IBD cases are found in young adults and thus affecting individuals in their most formidable and productive years of their life (Ananthakrishnan 2015).

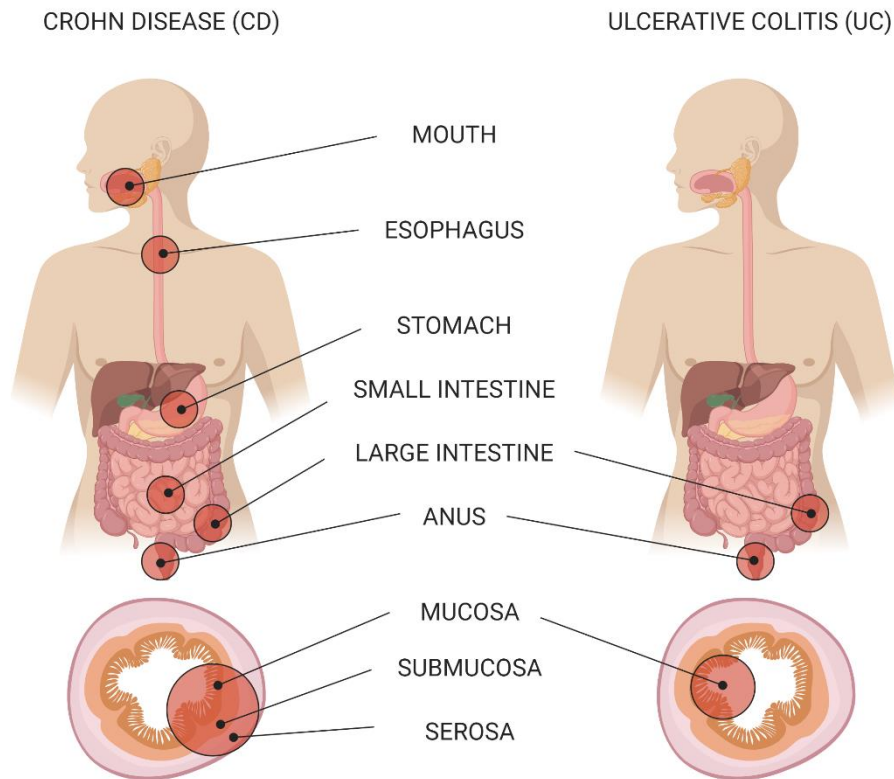


Figure 1.1 Differences between Crohn's disease (CD) and Ulcerative colitis (UC).

Both subtypes of IBD have different disease localization with striking difference is their effect on the intestinal wall. CD is characterized by transmural inflammation (all the layers of the gut) with skip lesions, whereas, UC is superficial (only the mucosa) continuous inflammation starting from the rectum and moving upwards. According Nasser-Moghaddam 2012

Looking at ethnicity and race, the prevalence of IBD seems to affect mostly African American and Caucasian population, whereas Hispanics and Asians seems to be less affected (Arebi et al. 2018). The highest risk population for developing IBD are Ashkenazi Jews with approximate prevalence of 2–4 times higher than Caucasian non-Jewish population (Henry, Randall, and Gershon 2004; Kenny et al. 2012)

Geographically speaking, IBD incidences seem to stretch from less incidents in the southern to more in the northern hemisphere. Furthermore, modernized countries have a higher number of IBD incidents, where North America ranges from 5 to 29/100,000/year giving approximately 1.4 million Americans that are affected (Matricon, Barnich, and Ardid 2010). In Europe IBD is a vastly prevalent disease that affects 2.5-3 million people. This is associated to a higher socioeconomical burden costing roughly about 4.6–5.6 bn Euros a year as direct healthcare cost (Burisch et al. 2013).

Aetiology

From an aetiological point of view, IBD is considered a non-Mendelian polygenic disorder, where several factors lead into the development of the disease (Figure 1.2). These include environmental, genetic, microbiological and immunological factors. There are extensive data collections available for each of the single components involved in IBD, however their interactions and the percentage of each single component in the development of the disease is still elusive (Noble et al. 2006, Hu et al. 2011).

Environmental factors

Multiple theories have been proposed to explain the influence of environmental factors in developing abnormal inflammatory responses to intestinal microorganisms (Molodecky and Kaplan 2010a). For both IBD and majority of autoimmune diseases, a theory is postulated to explain the development of a dysregulated immune system. The so-called hygiene hypothesis suggests that the rise of immunologic disorders can be attributed to the lack of childhood exposure to enteric pathogens, mainly due to increased sanitary practice (Gent et al. 1994).

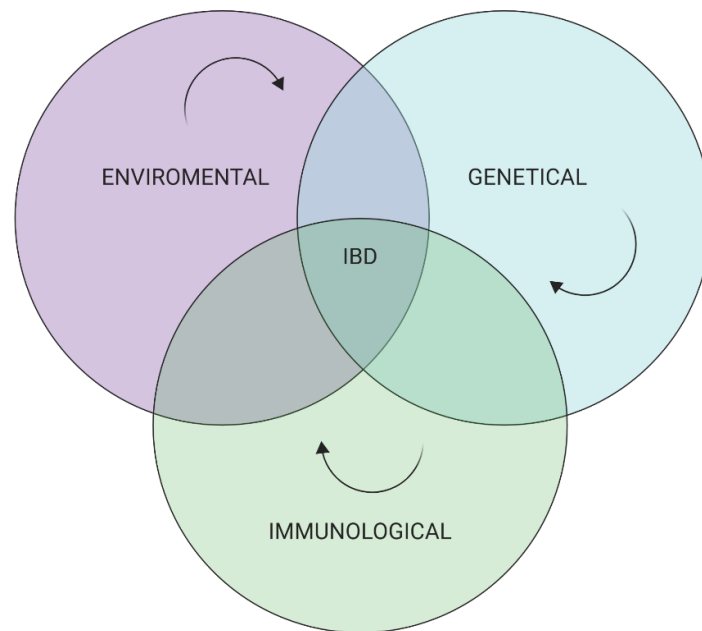


Figure 1.2 Aetiology of IBD.

Interaction of various factors that contribute to the chronic intestinal inflammation: an uncontrolled immune response to luminal microbiota in a genetically susceptible host, where environmental triggers are also necessary for the onset of the disease. Modified from (Hu et al. 2011)

The improved sanitation and hygiene together with the decreased exposure to enteric organisms during childhood, results in increased susceptibility to development of improper immunologic responses towards common microorganisms and antigens (Molodecky and Kaplan 2010b). Multiple studies have been done to pinpoint the environmental risk factors associated to IBD including appendectomy, oral contraceptives (OC), diet, breastfeeding, infections/vaccinations, antibiotics and childhood hygiene (Molodecky and Kaplan 2010b). However, there are inconsistent and sometimes opposite findings, therefore more studies are needed to further clarify the risks of certain environmental factor towards the development of IBD. Smoking is a consensual environmental factor associated with IBD (Ng et al. 2013; Kikut et al. 2018) where striking

difference in impact to both forms of IBD. In UC, smoking was found to have protective effect and improved outcome in the course of the disease and thereby decreasing the need for surgical removal of the colon (Kikut et al. 2018). Contrary to UC, smoking has close to two-fold increased risk for development of CD (Russel et al. 1996). Smoking also increases the severity of the CD with increased flare-up. Furthermore, heavy smokers suffering from CD are more likely to need surgery which in turn affects dramatically their quality of life (Russel et al. 1996).

Genomic factors

With the help of technological advances in the past two decades, genome-wide associated studies identified more than 200 loci that confer risk of IBD (see Figure 1.3; de Souza and Fiocchi 2016, Ek, D'Amato, and Halfvarson 2014). The function of the majority of these genes is associated with immune regulation, cytokine production, T-cell function and defective bacterial processing (de Souza and Fiocchi 2016).

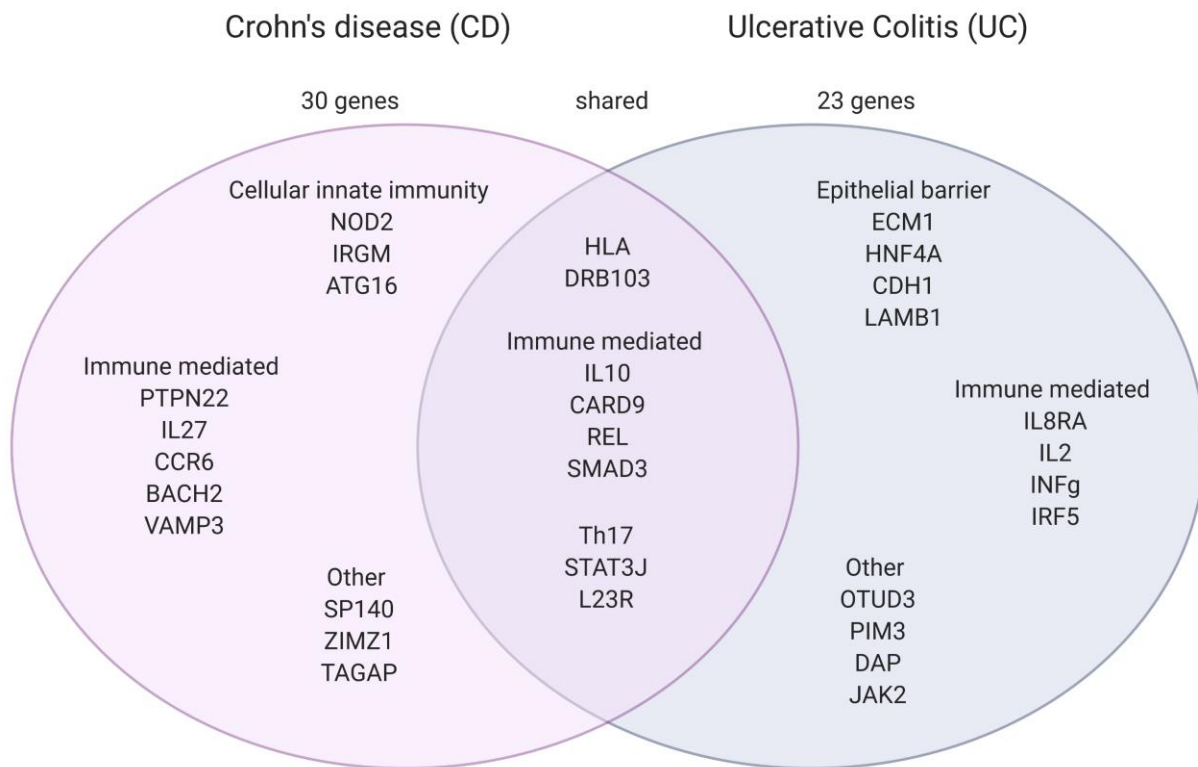


Figure 1.3 Loci associated with the different forms of IBD ,

There are more than 200 loci involved in the development of IBD, where 30 are associated to CD (in pink), 23 are associated to UC (in purple) and the rest are associated with both forms of IBD. Modified from Ek, D'Amato, and Halfvarson 2014

One of the first genes discovered to be a major genetic risk factor for CD development is Nucleotide-binding and oligomerization domain 2 (NOD2) (Ek, D'Amato, and Halfvarson 2014). *NOD2* is a 110 kDa cytosolic protein (1040 amino acids) containing 2 Caspase activation and recruitment domains (CARDs) that is a primary receptor to muramyl dipeptide (MDP) (Eckmann and Karin 2005). MDP is part of the bacterial wall of both Gram-positive and Gram-negative bacteria. *NOD2* gene is located on human chromosome 16p21 and is highly expressed in myeloid cells (macrophages and dendritic cells), Paneth cells and in lesser extent in T cells (Sidiq et al.

2016). Notably, *NOD2* expression is induced by several components including vitamin D, lipopolysaccharide (LPS), short-chain fatty acids (e.g., butyrate), and pro-inflammatory cytokines (Clark and Mach 2016, Hamman, Demana, and Olivier 2007). *NOD2* loss, leads to increased inflammation due to improper bacterial clearance this can be seen as one of the key pathogenic events in the development of CD (Noguchi et al. 2009; Shaw et al. 2011; Yamamoto and Ma 2009). This role of *NOD2* in the development of CD may also be supported by its role in other chronic inflammatory diseases of the barrier organs like skin, liver, spleen, and eyes (Negroni et al. 2018a). *NOD2* is involved in regulating NF kappaB activation as part of the innate immune system of intestinal epithelial cells and therefore when disrupted, can lead to the development of CD (Schreiber et al. 2005). A peptidoglycan derived from Gram-positive bacteria and Gram-negative bacteria, N-acetylmuramyl-l-alanyl-d-isoglutamine (MDP) is recognized by the C-terminus of the receptor which leads to *NOD2* activation and oligomerization See Figure 1.4. This leads to the recruitment of kinase receptor interacting protein 2 (RIP2), which is facilitated by CARD-CARD homophilic interactions. Other molecules then are recruited to this *NOD2*-RIP2 platform including two E3 ligases: TNF receptor associated factor 6 (TRAF6) and TRAF2. These interactions lead to the ubiquitination of NF- κ B essential modulator (NEMO). Ubiquitinated NEMO together with TGF β -activated kinase 1 (TAK1) forms a complex that leads to the activation of I κ B kinase (IKK) and thereby initiation of the NF- κ B signalling pathway by phosphorylation and subsequent degradation of I κ B- α . The free NF- κ B translocate into the nucleus and activates transcription of pro-inflammatory molecules (Negroni et al. 2018b)

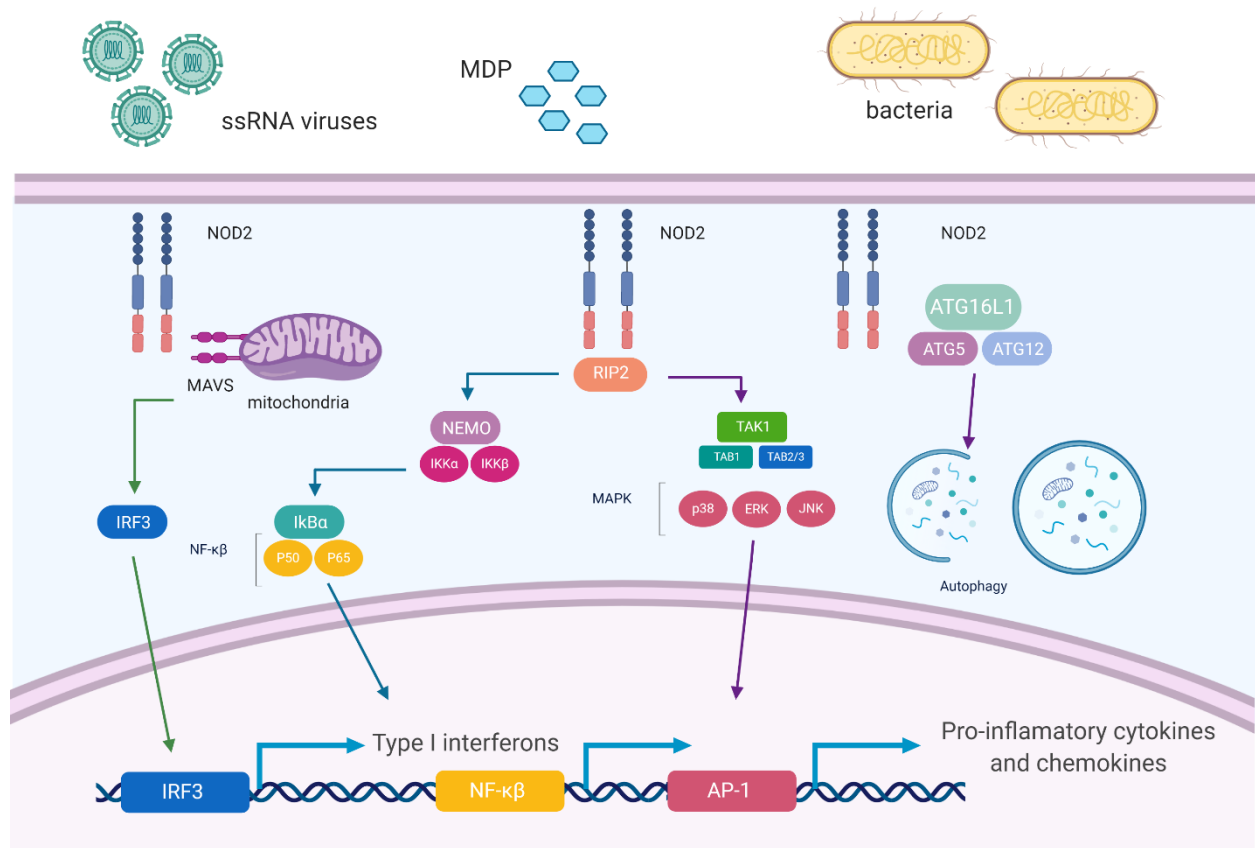


Figure 1.4 *NOD2* activation .

Abbreviations: AP-1, activator protein-1; ATF6, activating transcription factor 6; ATG, autophagy-related genes; ATG16L1, autophagy related 16 like 1; ER, endoplasmic reticulum; ERK, extracellular signal-regulated kinase; IFNs, interferons; IKB, NF- κ B inhibitor; IKK, I κ B kinase; IRF3, interferon response factor 3; JNK, c-Jun N-terminal kinase; MAVS, mitochondrial antiviral signalling; MDP, muramyl dipeptide; NEMO, NF- κ B essential modulator; NOD, nucleotide-binding oligomerization domain; PERK, protein kinase RNA-like endoplasmic reticulum kinase; RIP2, receptor-interacting protein kinase 2; TAB, TGF- β activated kinase; TAK1, targets transforming growth factor- β activated kinase 1. Modified from Negroni et al., 2018.

NOD2 activation also leads to the activation of the mitogen-activated protein kinases (MAPK), through TRAF6-dependent manner that leads to downstream activation of JNK, p38 and ERK. Depending on the cell, the activation of these two pathways leads to the production of myriad of cytokines and chemokines and in Paneth cells defensins like IL-6, TNF- α , IL-8/CXCL8, IFN- γ , IL-1 β and α -defensin (Parlato et al. 2014).

In RIP2 and NF- κ B independent mechanism, *NOD2* can recruit autophagy proteins to the plasma membrane at the bacterial entry site. This is important because *ATG16L1* is involved in the wrapping of invading bacteria by autophagosomes. *ATG16L1* is also one of the most commonly mutated genes found in CD (Hoefkens et al. 2013). Moreover, single nucleotide polymorphisms in both *ATG16L1* and *NOD2* are implicated in increased susceptibility to CD (Cadwell 2010; Homer et al. 2010). These studies suggest that *NOD2-ATG16L1* axis is probably a critical pathway and its dysregulation is closely connected to the onset of CD. However, single genetic variants are not connected and therefore cannot explain the development of CD or UC. In addition to this, these associated to IBD variants can also be found in healthy individuals (Cho and Brant 2011). Therefore, to understand the contribution of the different genetic components in IBD development, we need to focus on more integrative approaches where other factors are included which will shed more light on the disease pathogenesis (Travassos et al. 2010; Negroni et al. 2018b).

Microbiological factors

The GI tract is the residing place to large microbial community (Hillman et al. 2017). Early gut colonization with these microorganisms is important for proper development of the immune system (Schokker et al. 2015). This is mainly due to the establishment of symbiotic relationship and homeostasis with our microbiota and also to the development of tolerance against these commensal microorganisms (de Souza and Fiocchi 2016). Many studies have focused on characterizing the IBD gut microbiota, however the most important unanswered question is whether the gut dysbiosis in IBD is the cause or the consequence of the disease (Ananthakrishnan 2015). Additionally, it remains elusive whether the host genotype directly influences the bacterial microbiota or whether external factors, like diet and antibiotics, directly influence in the bacterial dysbiosis (Ananthakrishnan 2015). No single microorganism can be associated to the gut

dysbiosis, but several trends are constantly reported which are mainly connected with reduced bacterial diversity. Most studies show decrease in several genera including *Bacteroidetes* and *Firmicutes* as well as decrease in specific anti-inflammatory microorganisms like *Bifidobacterium adolescentis* and *Faecalibacterium prausnitzii* (Joossens et al. 2011). These decrease results in an increase in *Enterobacteriaceae* and *Fusobacterium* genera, from which the most common is *Escherichia coli*. Moreover, with the increase of opportunistic pathogenic bacteria there is also increase of virulence markers like enterotoxin, haemoglobin protease, haemolysin A, haemolysin B, cytotoxic necrotizing factor 1, and secreted autotransporter toxin, suggesting a possible critical role of these virulence factors in IBD pathology (Zuo and Ng 2018).

One of the hallmarks for IBD is an enhanced immune reactivity against microbial agents. CD patients, commonly have increased serum antibodies to commensal microorganisms like *Saccharomyces cerevisiae* and *Escherichia coli* that can be used as a prognostic factor of the disease severity (Mow et al. 2004). Although a bacterial dysbiosis may influence the risk of development of IBD, it is not sufficient to cause IBD by itself (Hold et al. 2014).

Immunity

The development of intestinal inflammation is a normal physiological process that occurs constantly in the organism. A defence response reaction can be caused by internal factors (associated with the body cells) and by external factors, which include infections and exposures to inflammatory agents like food and smoking (Kikut et al. 2018). The main purpose of the defence response is to protect tissues against their further destructive event and to eliminate the internal and external agents that caused the inflammation (Kikut et al. 2018).

Since the 70's, immunity dominated the investigation of the pathogenesis of IBD. This research interest is justified considering that one of the earliest signs of inflammation in IBD is the infiltration of classical innate immune cells like neutrophils, dendritic cells and macrophages. Both adaptive and innate immune systems are involved in the pathogenesis of IBD and though several mechanisms of action including the impairment of the epithelial barrier function, release of multiple inflammatory mediators and tissue destruction (Ahluwalia et al. 2018b; Marks and Segal 2008; Elia et al. 2015; Siegmund and Zeitz 2011)

Specialized cells of the adaptive immune system, such as dendritic cells (DCs), macrophages, intestinal myofibroblast and intestinal epithelial cells (IEC) express receptors for sensing structural motifs of the intestinal microbiota known as pathogen associated molecular patterns (PAMPs) (Mogensen 2009). This allows the rapid initiation of immune responses towards invading pathogenic microorganisms and the development of immune tolerance towards the resident microbiota (Pott and Hornef 2012). Moreover, the function of the dendritic cells as professional antigen presenting cells, allows the crosstalk between the innate and adaptive immunity, as they are responsible of activating and polarizing T-cells (Gaudino and Kumar 2019).

Based on studies done on animal models and IBD patients, CD and UC show particular type of immune response and the secreted cytokine profiles (Nemeth et al. 2017). The directed immune responses rely on the polarization of lymphocytes such as type 1 T helper (Th1), type 2 T helper (Th2) and type 17 T helper (Th17) responses (Geremia et al. 2014a). Th1 cells are known to produce several cytokines, with the most important being IFN- γ (Berger 2000). Combined with innate-related cytokines like IL-1 β , tumour necrosis factor (TNF)- α , and IL-6, IFN- γ is pivotal for the development of CD (Strober and Fuss 2011). During intestinal inflammation, IFN- γ , together with TNF- α released by activated mucosal macrophages, are responsible for intestinal epithelial

cell beta catenin signalling (D. H. Kim and Cheon 2017). Effects of these two effector molecules lead to limited differentiation and proliferation of the intestinal epithelial cells (Zuo and Ng 2018). TNF- α is also produced by Th1 cells and is considered one of the central cytokines in IBD, thus it affects several other intestinal cells. For example, in stromal cells TNF- α induces the differentiation into myofibroblasts. This increases the production of matrix metalloproteinases (MMPs) which are tissue-degrading enzymes (Bonnans, Chou, and Werb 2014). MMPs are a group of zinc-dependent proteolytic enzymes that work on the digestion of the basement membrane (mainly collagen), resulting in cells losing an important contact dependent stimulus from the environment which leads to further IEC apoptosis (Valatas et al. 2017). Th2 cells are important in UC and are responsible for the production of IL-4 and IL-13. IL-4 and IL-13 exert potent effects on intestinal epithelial cells by increasing the permeability. Moreover, they are also associated with the beginning of epithelial apoptosis by inducing enterocyte differentiation and expression of the pore-forming tight junction protein Claudin-2 (Zuo and Ng 2018).

In addition to the traditional Th1/Th2 subtypes, other polarized cells are found in IBD. Th17 cells are a unique subset of IL-17-producing T-cells. They play an important role in maintaining commensal population, but in the settings of autoimmune diseases, Th17 can often aggravate the disease (Abusleme and Moutsopoulos 2017). Th17 differentiation is driven by both IL-6 and TGF- β and stabilized by IL-23 and IL-1 β . The main cytokine produced by Th17 is IL-17A which induces further neutrophil recruitment and up-regulation of a number of pro-inflammatory triggers, such as inducible nitric oxide synthase (iNOS) and IL-1 β (Geremia et al. 2014b).

The simplistic assumption that only one type of polarized cell is responsible for the development of the different forms of IBD is often contradicted by studies that show fluctuation of Th1 and Th2 responses especially during the course of the disease (de Souza, Fiocchi, and

Iliopoulos 2017). Isolate immune parameters cannot by itself mediate IBD and several different immune cell subpopulation exist at the same time carrying complex gene signatures and performing multiple functions (Wang, Han, and Ma 2016). Consequently, interfering with the interpretation of immune responses, the immune system involvement in gut inflammation can be fully understood only in the context of specific signals received by the other factors involved in the pathogenesis of IBD (Wang, Han, and Ma 2016).

Intestinal epithelial cells, Mucosal Inflammation and intestinal permeability

The largest of the body mucosal surface is the intestine, and the epithelial monolayer is the main component of this surface and make the epithelial barrier (Vancamelbeke and Vermeire 2017). It is covered by simple columnar epithelial cells organized in two distinct structures, protrusions into the lumen called villi and invagination called crypts (Peterson and Artis 2014b).

These cells are the first line of defence from the outside environment, however, this is also the site where most nutrients are absorbed. Therefore the function of the intestinal epithelial cells (IEC's) comprises of providing a physical barrier, absorption, mucus production and to act as non-professional antigen presenting cells (Peterson and Artis 2014a).

There are several types of differentiated intestinal epithelial cells including absorptive cells (enterocytes), mucus producing cells (goblet cells), hormone producing cells (enteroendocrine cells), defensins and stem cell niche cell (Paneth cells), antigen presenting cells (M cells), chemosensory cells (Tuft cells); all of which differentiate from epithelial stem cells or Lgr5+ cells located in the base of the crypts (von Martels et al. 2017; Sato, Vries, Snippert, Van De Wetering, et al. 2009). See Figure 1.5. There is a constant renewal of new cells in which precursor cells are

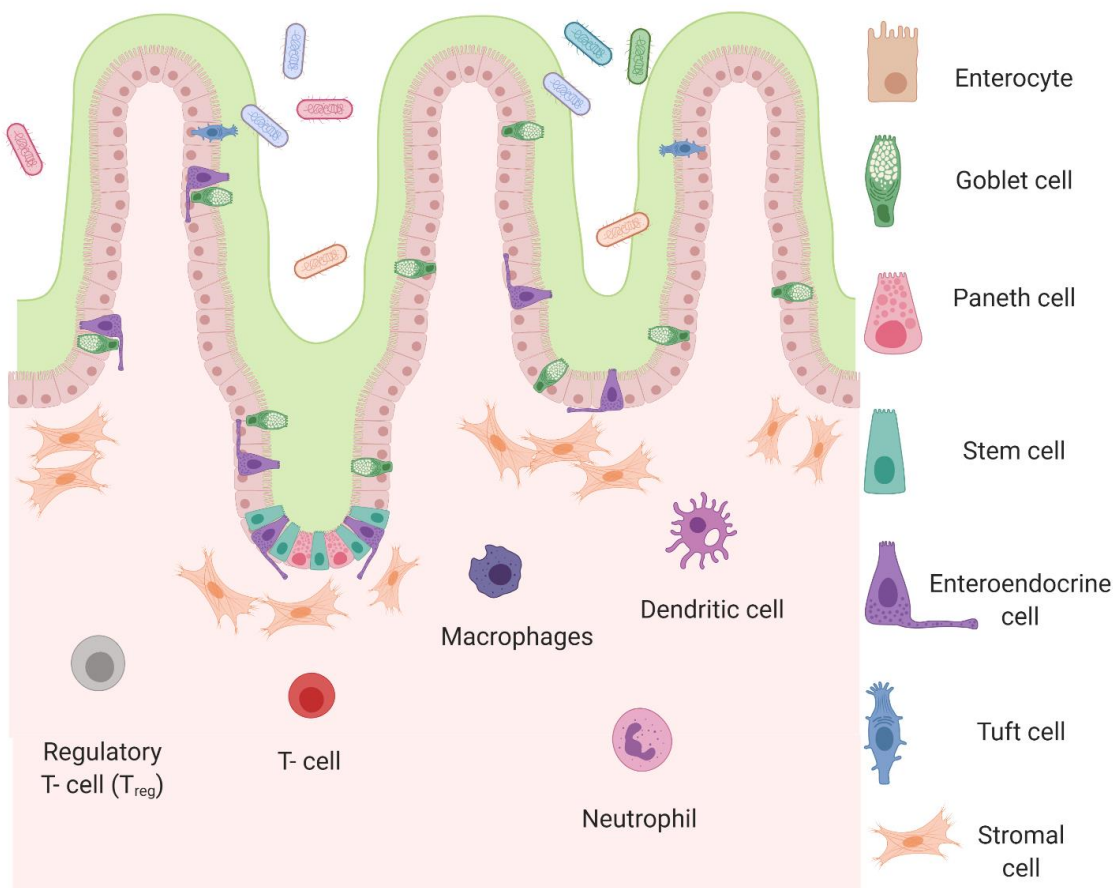


Figure 1.5 Schematic representation of the intestinal epithelium with underlying lamina propria containing immune cells.

Enterocytes comprise the majority of IEC (brown), the second biggest population of cells are goblet cells (green) with few enteroendocrine cells (purple). In the base of the crypts Paneth (pink) and LGR5+ stem cell (mint) reside. Beneath them in the lamina propria are the stromal cell and depending on the inflammation status different types of immune cells both from the innate and the adaptive branches. Modified from Abreu, 2010.

constantly made by the Lgr5⁺ stem cells located in the base of the crypts. As they travel, they differentiate to the top of the villi and they are shed into the lumen of the gut; a process that takes between 5-6 days. (Peterson and Artis 2014a; Gassler 2017; Abreu 2010).

The epithelial monolayer acts as a protective physical barrier which is mediated by three types of specialized junctional complexes: desmosomes, adherent junctions, and tight junctions (TJs) (Alberts et al. 2002). The first two complexes, desmosomes and adherent junctions, are involved in the attachment of cells, while the TJs are apically located and responsible in the regulation of the barrier integrity and paracellular permeability. In the formation of TJs four different types of

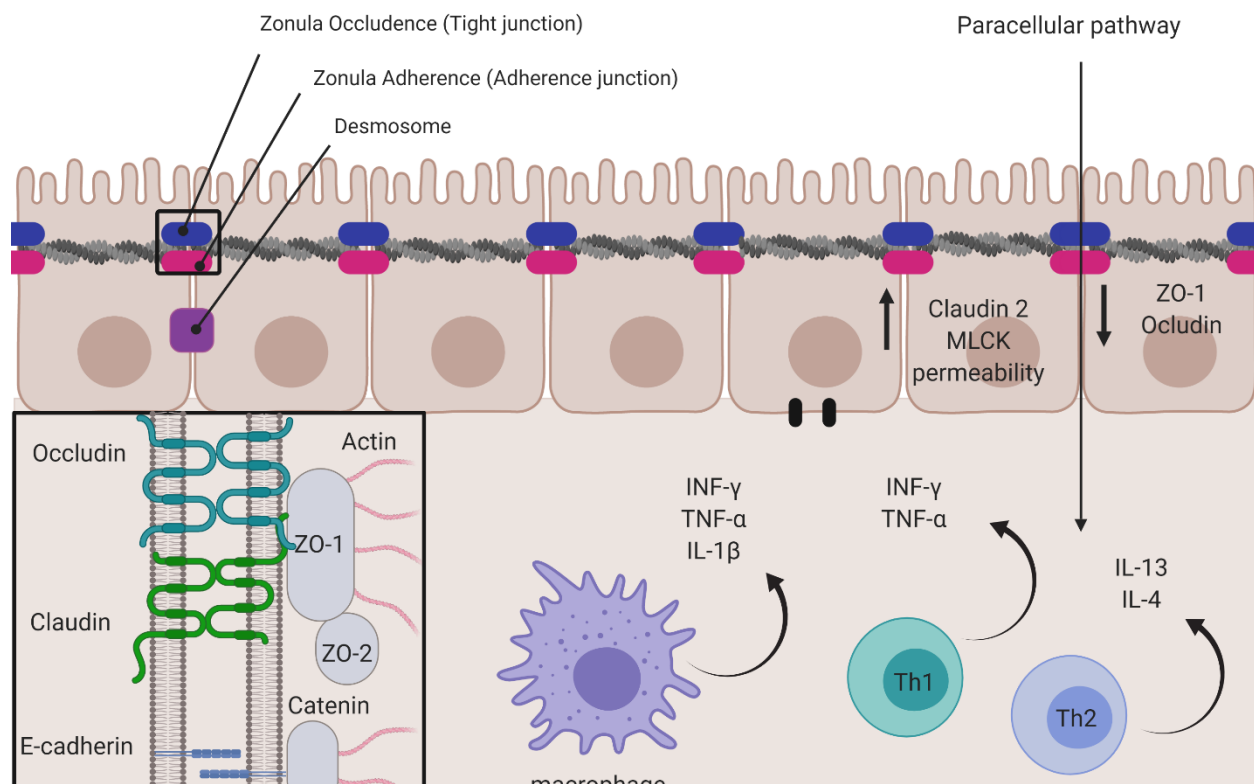


Figure 1.6 Tight junctions and their role in disease.

TJ (blue) are situated apically and are responsible maintain tissue homeostasis. Several molecules affect this barrier mainly affecting the TJ as a result of this the barrier becomes leaky resulting in IBD and systemic inflammation.

Modified from **Laukoetter et al. 2008**

proteins are included such as junctional adhesion molecules, occluding, claudins and tricellulin (Groschwitz and Hogan 2009; Laukoetter, Nava, and Nusrat 2008)

The main function of the TJs is to seal the paracellular space between epithelial cells, thus separating the cell membrane into apical and basolateral domains. This is forming a physical barrier where antigens are excluded. In fact, one of the hallmarks of IBD pathogenesis is an intrinsic defect of the intestinal barrier and the associated mucus layer. Structural changes of the intestinal TJ proteins are closely associated to this process (see Figure 1.6, Roda et al. 2010). This is widely reported in CD patients with active flare-ups (Bjarnason et al. 1983). It is known that a multitude of pathologic conditions, especially cytokine mediated, contribute to changes in paracellular permeability (Capaldo and Nusrat 2009). Moreover, several clinical studies show that in IBD patients levels of several cytokines like TNF- α , IFN- γ , IL-1 β , IL-6, and IL-17 are elevated and these cytokines are known to disturb intestinal barrier function (S. H. Lee 2015).

Interferon- γ (IFN- γ)

IFN- γ is the only interferon type II, that does not share homology sequence with the other interferons from group II. However, IFN- γ possesses immunomodulatory properties and is critical molecule for both innate and adaptive immune system (Tau and Rothman 1999). IFN- γ is a 16kDa non-glycosylated protein, which in his active form is a noncovalently linked homodimer. This dimer interacts with the IFN- γ receptor (IFNGR). IFNGR is a complex heterodimer complex comprised of two IFN- γ R1/CD119 subunits and IFN- γ R2 subunits which interact with Jak1 and Jak2, respectively. Both Jak1 and Jak2 activation results in recruitment and phosphorylation of STAT1. Phosphorylated STAT1 then forms homodimers and translocate to the nucleus where it binds to IFN- γ -activated sequence (GAS) elements regulating the production of transcription

factors mainly responsible for the activation of many secondary response genes (Schroder et al. 2004). Additionally, IFN- γ can activate MAPK, PI 3-K-Akt, and NF-kappa B signalling pathways. Even though IFN- γ is known to be cytotoxic and cytostatic molecule, multiple studies have also suggested that IFN- γ may also have proliferative and pro-tumorigenic effects (Zaidi and Merlino 2011).

IFN- γ is mainly involved in inflammatory immune responses, however it is also involved in the increase of paracellular permeability in IEC through the redistribution and expression of TJ proteins and the rearrangement of the actin cytoskeleton. In the case of actin-myosin contractility IFN- γ mechanism of action is through Rho-associated kinase-dependent manner. Exposure to IFN- γ activates RhoA, a small GTPase and powerful regulator of actin remodelling. RhoA activation increases the expression of Rho associated kinase (ROCK). ROCK then phosphorylates myosin light chain (MLC), leading to biochemical and morphological reorganization of perijunctional F-actin and TJ proteins like occludin, and ZO-1 (Bruewer et al. 2005; Utech et al. 2005; Shen et al. 2006).

Tumour necrosis factor- α (TNF- α) is one of the key cytokines involved in the pathogenesis of IBD. Clinical studies found to be elevated in the serum, intestinal mucosa and stools of patients (Muzes et al. 2012). There are two forms of TNF- α : membrane bound and soluble form. The membrane bound is 26 kD protein produced as a 233 amino acids long type II transmembrane protein, arranged as a stable homotrimer. It can be proteolytically cleaved from metalloprotease like TNF- α converting enzyme (TACE, ADAM17). Once released, quickly loses its bioactivity. The soluble form of TNF- α is a 17-kDa a homotrimer. Both the membrane bound and the soluble TNF- α have overlapping and distinct activities (Idriss and Naismith 2000).

Their biological activity comes after interacting with their receptor, tumour necrosis factor receptor (TNFR) which is type I membrane protein.

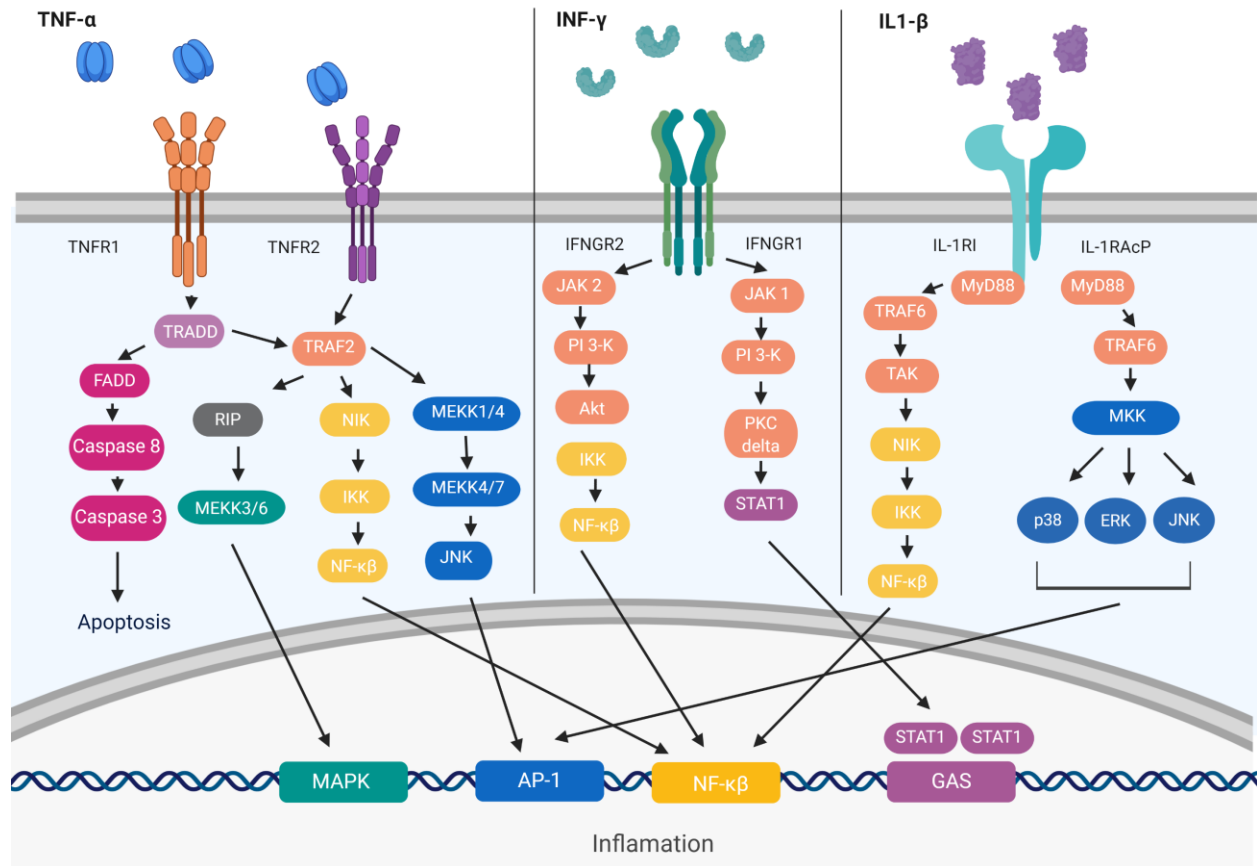


Figure 1.7 Activation of TNF- α , INF- γ and IL-1 β signalling pathways.

Signalling pathways of TNF- α , INF- γ and IL-1 β converge and are known to activate the NF- κ B pathway which is considered as master key regulator in the development of IBD. AP-1, activator protein-1; GAS, Gamma interferon activation site element; IFNs, interferons; IFN-, interferons IKB, NF- κ B inhibitor; IKK, I κ B kinase; IFNGR1, Interferon gamma receptor 1; IKK, I κ B kinase; IFNGR2, Interferon gamma receptor 2; JAK1 Janus kinase1; JAK2 Janus kinase2 JNK, c-Jun N-terminal kinase, nuclear factor (NF)- κ B; STAT1 signal transducer and activator of transcription 1; TRADD, TNF-R1-associated death domain protein; TRAF2, TNF receptor-associated factor; TNFR1, TNF- α receptor I; TNFR2, TNF- α receptor II;

There are two types of TNFR, TNFR1 and TNFR2 which form trimeric complexes upon binding of TNF- α . Both forms have four parts: signal peptide, extracellular domain, transmembrane domain and intracellular domain. The main difference between the two is the lack of death domain (DD) in the TNFR2, but is present in the TNFR1. TNF- α is to be known to mediate two signalling

pathways: one for apoptosis and the other for inflammation and survival (Idriss and Naismith 2000).

TNF- α influences the intestinal epithelium directly and is known to induce apoptosis and inflammatory response, as well as impair the TJ barrier by inducing ZO-1 redistribution. In epithelial cells TNF- α induces decrease transepithelial electrical resistance by myosin light chain phosphorylation, but also through increase of expression of claudin-2 which is a pore forming complex (Bruewer et al. 2005; Utech et al. 2005).

Interleukin-1 β (IL-1 β) plays a central role in the intestinal inflammatory process as is noticeably elevated in CD patients (Al-Sadi and Ma 2007). IL-1 β binds to a Type I IL-1 receptor (IL-1RI) which is a heterodimer with IL-1 receptor accessory protein (IL-1RAcP). This leads to activation of NF- κ B through different signalling mechanisms one of which is through the recruitment of two receptor associated kinases, IRAK-1 and IRAK-2. They recruit and activate TRAF6 which then leads to subsequent oligomerization of TRAF6. The oligomerization of TRAF6 leads to the formation of TAK1 and MEKK3 signalling complexes and activation of NF- κ B-inducing kinase (NIK) which further relays the signal to I-kappaB kinases (IKK-1 and -2) and subsequent activation and translocation to the nucleus of NF- κ B (Acuner Ozbabacan et al. 2014). However, IL-1 β also leads to the activation of other mitogen activated protein kinases like JNKs and p38 MAPK as well as subsequent AP-1 activation. The activation of these pathways plays an important role in mediating IL-1 associated responses mainly activation the transcription of IL-8, IL-6, iNOS, COX2, cyclinD1 and β -defensin2 all known to be IL-1 target genes (Acuner Ozbabacan et al. 2014).

One of the effects of the activation of IL-1 β in the intestinal epithelium is decreasing TEER by decreasing occludin expression and by activating the Nf- κ B pathway (Al-Sadi and Ma 2007).

Moreover, there is a synergistic effect on the intestinal epithelial barrier when these separate cytokines are combined which is the situation in-vivo. Additional to their effect on the barrier integrity several other important changes happen and have been identified in IBD when the IEC are exposed to immunomodulatory molecules for a prolonged time period. These include different mucus and its component production, apoptosis, differential production of Toll-like and NOD-like receptors (Coskun 2014).

Framework for the pathogenesis of IBD

The development of IBD is a slow process where an excessive reaction to commensal microorganisms in genetically susceptible individuals is found. It is suspected that in the first phase

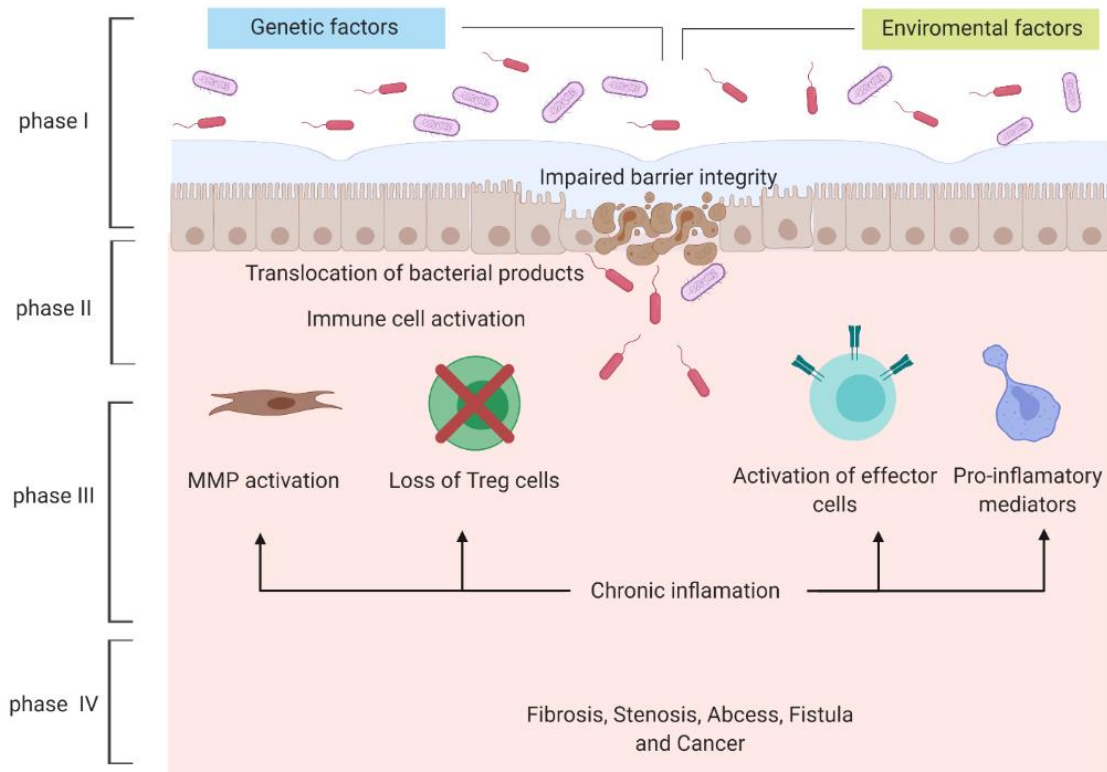


Figure 1.8 Conceptual framework for the pathogenesis of IBD.

Combination of factors induce a barrier dysfunction which allows the translocation of bacterial products. This leads to immune cell activation and immune response that can't be dampened. Leading to chronic inflammation and complications of the disease. Abbreviations MMP matrix metalloproteinases, Treg, regulatory T-cells. Modified from Neurath 2014.

of the disease, both the work of environmental and host factors induce impairment of the barrier function in the intestinal mucosa. In some patient the trigger of these events might be induced by bacterial or viral infections. In the second phase of the disease progression, the diminished function of the intestinal barrier in turn allows the translocation of commensal bacteria and their products from the lumen of the intestine to the lamina propria. This apical to basal side translocation leads to the activation of residing immune cells, mainly dendritic cells and macrophages, which causes

increased cytokine production and release. At this point this is a normal immunological reaction, which in time is dampened. However, in IBD, this leads to prolonged inflammation that further activates the resident intestinal cells. In the third phase a chronic intestinal inflammation develops and if the initial activation response can't be dampened, there is further tissue destruction and cytokine production. All of this leads to the last and final phase, where the un-dampened immune activation leads to several complications of the disease including abscess, fistula, fibrosis, stenosis and cancer Figure 1.8(Neurath 2014).

Therapies available for IBD treatment

Available treatments for IBD come in the form of medicines, diet and lifestyle changes. Their main goal is only to alleviate symptoms, decrease of underlying inflammation and prevent major complications of the disease. Current drugs therapies fail under several categories (summarized in Table 1-1): anti-inflammatory drugs, antibiotics and immune system suppressors (Al-Sadi and Ma 2007).

The mechanisms of action of the anti-inflammatory drugs is to reduce overall inflammation and to prevent/decrease flare-ups. Depending of the affected intestine area, several anti-inflammatory molecules such as corticosteroids and aminosalicylates (olsalazine (Dipentum), mesalamine (Asacol HD, Delzicol), and balsalazide (Colazal)) can be used.

Immunosuppressant drugs affect the activation of immune systems by suppression of T cell function and natural killer cell activity. This category include cyclosporine (Gengraf, Neoral, Sandimmune), mercaptopurine (Purinethol, Purixan), methotrexate (Trexall) and azathioprine (Azasan, Imuran). Part of this group, medications called biologics are widely used and highly effective for both forms of IBD. These drugs are anti-TNF- α monoclonal antibodies, that bind to

TNF-alpha and neutralize its action. Several drugs are on the market like Infliximab (Remicade), adalimumab (Humira) and certolizumab pegol (Cimzia, Atreya et al. 2011).

Table 1-1 Summary of therapies available for the treatment of IBD.

(Al-Sadi and Ma 2007; Lamb et al. 2019; Chudy-Onwugaje et al. 2019)

Class of therapy	Mechanism	CD or UC	Type used
Antibiotics	Reducing the number of intestinal bacteria	CD and UC	
Aminosalicytes (ASAs)	Topical anti-inflammatory drugs that interfere with the ability to control inflammation	Mild to moderate UC	Balsalazide, Mesalamine, Olsalazine, Sulfasalazine
Corticosteroids	Very fast acting anti-inflammatory drugs (effective in inducing remission)	CD and UC	Budesonide (mild to moderate CD), used in acute phase, Hydrocortisone
Immunomodulators	Helps regulate the immune system	CD and UC	Azathioprine, 6-mercaptopurine, metotraxate
Biologics	Specifically block inflammation by targeting specific pathways	CD and UC	Anti-TNFalpha –Adalimumab (Humira), Infliximab (Remicade) Integrin receptor antagonist- block leucocytes from infiltrating in the gut - Natalizumab IL-12/23 antagonist-Ustekinumab
Jak inhibitors	Small molecule based medicines that are and directly absorbed and influence specific pathway	CD and UC	Tofacitinib (Xeljans)

In order to reduce bacterial infection, antibiotics are prescribed. Ciprofloxacin (Cipro) and metronidazole (Flagyl) are the most widely used (Al-Sadi and Ma 2007; Lamb et al. 2019; Chudy-Onwugaje et al. 2019).

If all the above-mentioned treatments fail to relief the signs and symptoms of IBD, the last option is in the form of surgery. Proctocolectomy is a surgical procedure used for UC where complete removal of the colon and the rectum is performed and usually cures the disease. In the case of CD,

surgeons remove just the diseased portion of the digestive tract, however this doesn't cure the disease and sometimes the disease recurs in the reconnected tissue (Burisch et al. 2013).

In-vitro and ex-vivo experimental models of the intestine

Vast majority of information has been collected over the years regarding the number of cells and signalling molecules involved in the pathogenesis of IBD. Nevertheless, building of effective model for developing medicines, a reductionist approach has been advocated by many researches (McKay, Philpott, and Perdue 1997). This is mainly because several aspects of IBD remain obscure and *in-vivo* models are too complex to dissect and address each of the components. For this reason, there are advantage and disadvantages in the use of *in-vitro* models, summarized in Table 1-2.

Table 1-2 A summary of advantages and disadvantages in modelling diseases with *in-vitro* cellular models

Modified from McKay, Philpott, and Perdue 1997

Advantages	Disadvantages
<ul style="list-style-type: none"> • Characterized cell population • Culture conditions are controlled • Specific outcomes can be measured over time • Effects of specific mediators can be examined • Effects of specific type of cells can be examined • Order of reagent addition can be varied 	<ul style="list-style-type: none"> • Single cells do not exist in physiologically relevant context • Culture conditions might not mimic the local environment • Transformed cells may have unique properties • Unknown factors can be present in the culture media • Essential features of the model can be missing

Static models

The most widely used cell line, Caco-2, is considered as “golden standard” in pharmacological, nutritional, and microbiological fields. It was derived in the 1970's from human colorectal adenocarcinoma (Pearce, Coia, et al. 2018). Even though derived from human colon, this cell line has a unique feature where upon reaching confluency, can spontaneously differentiate into enterocyte-like cells with absorptive properties. It mimics small intestinal phenotype by expressing

several important differentiation markers including: brush border, TJs, enzymes and transporters characteristic of the intestinal epithelium (Hidalgo, Raub, and Borchardt 1989). This makes the cell line most desirable for studying bacterial adhesion/invasion, transport kinetics, intestinal barrier function and innate immune response (Shi et al. 2017). In standard settings, Caco-2 cells are usually grown on membrane inserts where they are left to differentiate in a 2D manner in the span of 21 days (see Figure 1.9). Drawback of this models is that there isn't a mucus layer present and there is a low paracellular permeability (Béduneau et al. 2014). To overcome some of these limitation, a co-culture of Caco-2 and HT-29 was made to make the model more physiologically and functionally relevant. HT-29-MTX cells are clones of the parental HT-29 cell treated with methotrexate to differentiate these cells into goblet mucus producing like cells (Béduneau et al. 2014). HT29-MTX cells produce both secretory and membrane bound MUC2, MUC5AC, MUC6 and MUC1, MUC3, MUC4 mucins (Huet et al. 1995).

Another model considers the specialized M-cells present in intestinal epithelium. There, a triple co-culture has been developed by co-culturing Caco-2 absorptive cells, HT29-MTX mucus-producing cells and Raji B lymphocytes. Under these conditions Caco-2 cells develop into M-like phenotype. This is useful model for predicting intestinal permeability (Araújo et al. 2016).

An *ex vivo* model of the porcine intestine was developed by TNO. InTESTine™ (see Figure 1.9), utilizes freshly isolated tissue from multiple segments of the GI tract (Pearce, Coia, et al. 2018). The model contains mucus layer that can be useful for culturing tissue microbiome. Other *ex vivo* models are based on the Ussing chamber, which was developed for studying transport across variety of epithelial tissues. Two halves of the chamber are isolated by the polarized epithelia and since the chamber has incorporated electrodes, can be used for permeability/transport studies by measuring voltage and short-circuit current (Al-Sadi and Ma 2007).

Most of the concerns regarding the previously described *in vitro* gut models is related to the physiological relevance, as they lack some important parts of the small intestine such as epithelial mucosa, variety of intestinal epithelial cells, 3 dimensionality, stromal layer and mechanical cues (Williams et al. 2015). Therefore recent scientific discoveries in cultivation of adult intestinal organoids as well as differentiation of embryonic and induced pluripotent stem cells (iPSC) towards gut lineages were aimed to overcome some of these issues (Sinagoga and Wells 2015; Barker et al. 2007). Organoids made from adult LGR5⁺ stem cells can now be continuously passaged and propagated *in vitro*. This opens an entire new world, because for decades the limiting factor in culturing intestinal cells was their life span (Sato, Vries, Snippert, van de Wetering, et al. 2009). These cells can now be differentiated in any of intestine cell types with directed differentiation methods (Pearce, Al-Jawadi, et al. 2018). Moreover, they also contain functional enteroendocrine cells, which is useful to model and study the gut-brain axis (Hampton 2017).

Another source of primary human intestinal epithelium can be obtained from iPSC, where in a multistep directed differentiation process guides the iPSC into distinct phenotype, forming structures known as human intestinal organoids (HIO). During the directed differentiation, the cells go through definitive endoderm stage, then hindgut stage and later develop into of epithelial structures (Workman et al. 2018). Additionally, they also contain a stromal layer with supporting cells and are useful for studies of epithelial and mesenchymal interactions in health and disease.

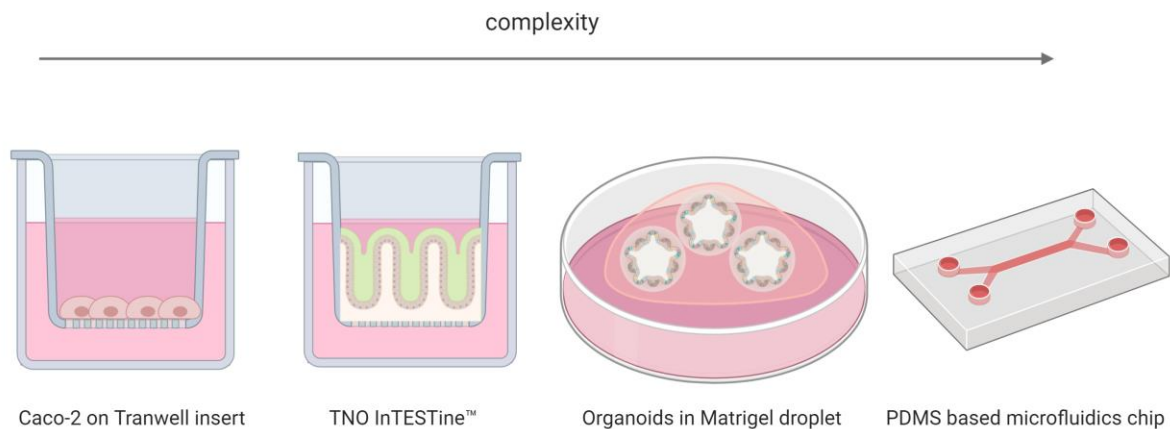


Figure 1.9 *In-vitro* and ex-vivo intestinal models.

Different *in-vitro* and ex-vivo models of the intestine that can be applied for disease modelling and drug discovery. Increasing complexity and physiological relevance from left to right.

Even though these 3D cultures are extremely useful for looking at barrier integrity and interaction of different cells in microbiological studies, they are very difficult to culture and the experimentally is a time consuming process since the organoids are embedded in extracellular matrix and their polarity is in an “inside-out” conformation Figure 1.9. This means that their apical side is in the inside and the basal side protruding outwards. That is why there are effort of further developing these models into more physiologically relevant models; for example, employing different mechanisms that reconstitute an *in vivo* situation like flow, cyclic stretching and gradients.

Dynamic models - Biomimetic microsystems (Organs on a chip)

In recent years, there are numerous biomedical advances in the *in vitro* modelling field, that come from the microfluidic Organ Chip models which are *in vitro* models built on a biomimetic microsystems or chips (Sosa-Hernández et al. 2018). These models have so far, the best potential

to mimic complex multi-organ or multi-layer systems where complex physiological environments can be reconstituted to reproduce fundamental biological processes. For example, the chemical and physical cues that cells receive in 3D conformation, or from concentration and gradients of molecular signals, ECM stiffness, can be easily applied in these systems, making the biomimetic microsystems useful for studying tissue development and cellular processes found *I -vivo*. This allows for better understanding of the disease processes, drug functions and toxicity.

Until now, several microfluidic organ-on-a-chip models of the human intestine have been developed with increasing levels of complexity, from simple Caco-2 based chips (Shah et al. 2016b; Shim et al. 2017a; H. J. Kim et al. 2012b), to more complex using LGR5⁺ (Kasendra et al. 2018c) and iPSC (Shah et al. 2016b) derived organoids. Their physiological relevance comes from having all the relevant cell types, as well as from being able to dissect several factors involved in health and disease, such as microbiome and environmental factors which is not possible in animal models.

The choice of material for these devices is usually polydimethylsiloxane (PDMS), a flexible, gas-permeable, polymer which has favourable manufacturing properties (see Figure 1.10 and Table 1-3). However, one of the drawbacks in PDMS chips is that they are difficult to image and are known to absorb drugs especially small and hydrophobic molecules (Halldorsson et al. 2015). Furthermore, the usability of these devices for drug discovery comes from the robustness, compatibility with existing equipment, automation, cost, and ease of use. In the literature, large majority of the publications on gut-on-a-chip, although complex, show low-throughput models (see Table 1-3) and therefore rendering their applicability in a high-throughput drug discovery studies (Junaid et al. 2017).

Table 1-3 Characteristics and design of Intestinal OOC

(Bein et al. 2018)

Type of microfluidics platform	Cell type used	Used for	Disease modelling	Assays used	Suitable for high throughput	Reff.
Silicon based	Caco-2/HT29-MTX	Evaluating nanoparticle interactions with human tissues	No	Permeability assay	No	(Sosa-Hernández et al. 2018)
Porous PC membrane sandwiched between two PDMS substrates	Caco-2	Drug permeability studies	No	Permeability assay and Mass spectrometry	No	(Gao et al. 2013)
Layers of polydimethylsiloxane (PDMS) with a slide glass and a polyester (PET) membrane	Caco-2	Drug permeability and metabolism studies	No	qPCR, Immunostaining, enzyme activity and TEM	No	(Shim et al. 2017b)
Polydimethylsiloxane (PDMS) with a slide glass	Ex-vivo tissue of the epithelium and serosa	Modelling disease	Yes	Viability Permeability studies	No	(Dawson et al. 2016)
Two polycarbonate (PC) enclosures, which sandwich silicone rubber gaskets, which are themselves attached to semi-permeable PC membranes	CCD-18Co or Caco-2 Primary immune cells	Research into gastrointestinal microbiome involvement in human health and disease	No	Oxygen sensing Cytokine profiling Barrier integrity Metabolomics	No	(Shah et al. 2016a)
Polydimethylsiloxane (PDMS) with a slide glass	Small intestinal organoids	Studies of metabolism, nutrition, infection, and drug pharmacokinetics, as well as personalized medicine	Yes	qPCR, morphological studies	No	(Kasandra et al. 2020, 2018a)

The OrganoPlate®

OrganoPlate® is a high-throughput microfluidic 3D culture plate which is developed to support between 40 (3-lane) (see Figure 1.10) and up to 96 tissue models (2-lane) on a single 384 well plate.

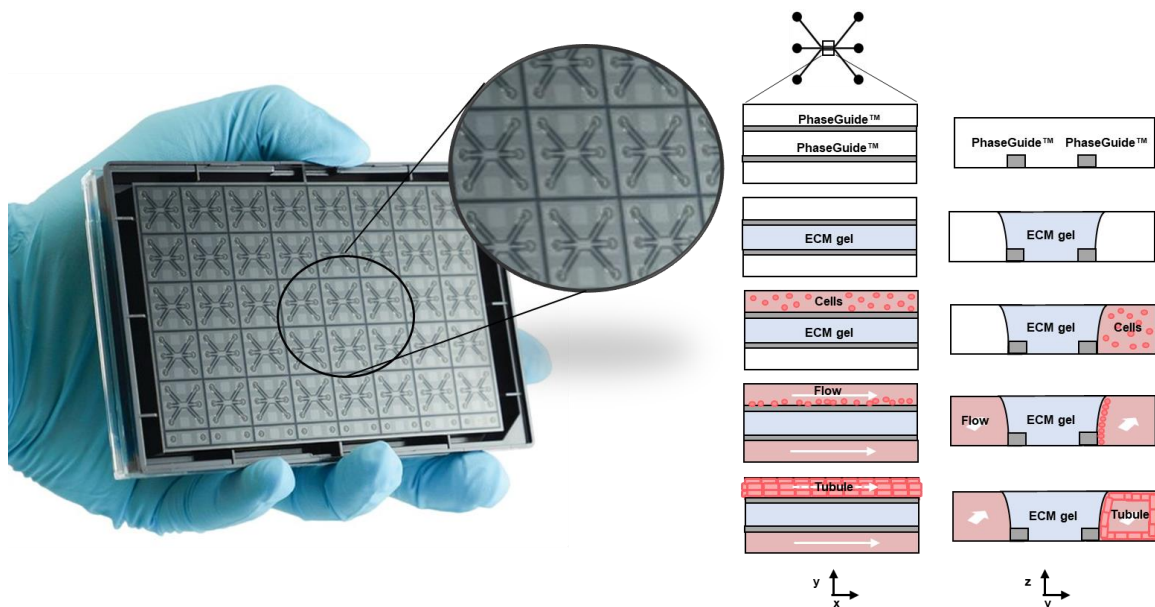


Figure 1.10 The OrganoPlate 3-lane and schematic representation of tubule seeding.

The OrganoPlate features 40 independent cell culture microfluidics chips each supporting adjacent in-gel culture and 2 perfusion channels, that can be used for seeding perfused tubular tissues or other in gel seeded cells.

The OrganoPlate® is based on a key-technology called PhaseGuides™ which is a small ridge in the OrganoPlate® that allows extracellular matrix loading without the overflowing between two adjacent channels using the meniscus pinning effect. Upon gelation, adjacent lanes are filled with either more ECM containing cells or cells in suspension for tubule formation. MIMETAS employs a unique microfabrication platform that allows for thin glass microfluidics on a microtiter plate making this technology compatible with standard laboratory equipment and with industrial high-

throughput robotics and screening equipment. Moreover, due to its transparent design cells are fully visual accessible for microscopic readout therefore several non-end point assays can be performed at the same time (Trietsch et al. 2013). The different OrganoPlate® designs allow to combine several cell types to achieve fully physiologically relevant tissue and disease models.

Chapter 2 Aims, outline and approach

Project aims and summary

The overall aim of this research project was to develop a 3D gut-on-a-chip model on a high-throughput microfluidics platform, the Organoplate, that will be compatible with high-scale preclinical drug studies. The different models developed in this thesis needed to qualify for the usage in drug development therefore it was imperative that they meet several criteria summarized in Table 2-1.

Table 2-1 Requirements for high-throughput *in-vitro* models

	Characteristics of the model	Techniques used to confirm
Model	Simple	
	Robust	
	Reproducible	
Monolayer integrity	Tightness of the cell layer	Transepithelial electrical resistance (TEER)
		Transepithelial flux (Barrier integrity assay)
Differentiation character	Expression of markers characteristic for the model	Immunocytochemistry (ICH)
		RT-qPCR
		Electron microscopy
Functionality	Expression and activity of different transporters	Immunocytochemistry (ICH)
		Efflux/ influx studies

Moreover, the model developed also needs to be fit for purpose due to their simplistic approach. That is why in this thesis I worked in developing several complementary models that will cover most of the characteristics of IBD see Table 2-3. but at the same time comply with the requirements mentioned above

Table 2-2 IBD characteristics that can be modelled with different cell types and configuration

IBD characteristics	Model	Cell types	Chapter
Loss of barrier integrity	Epithelial	Caco-2	IV and V
Loss of goblet cells/ decreased mucus production	Mucus producing	Caco-2/HT-29-MTX	VI
Myofibroblast induced tissue destruction	Epithelial-mesenchymal interaction model	Caco-2+/- HT-29-MTX and Intestinal myofibroblast	
Increase of cytokine production	Inflamed intestinal mucosal model	Caco-2/HT-29-MTX/THP-1/MUTZ-3	VI
Loss of Paneth cells	Personalized gut-on-a-chip model	Organoids or iPSC	VII

Approach

Recent studies have confirmed that a prolonged exposure of intestinal epithelial cells (IEC) to proinflammatory cytokines affects the intestinal epithelial homeostasis in a negative way, by downregulation of TJ proteins, differentiation and apoptosis. Thus, worsening the disease progression. Moreover, in the management of inflammatory bowel diseases (IBD) several studies identified mucosal healing (Assche, Vermeire, and Rutgeerts, n.d.; Cintolo 2016) as a key prognostic parameter, therefore making the mucosal healing a treatment goal for IBD. The structural basis of mucosal healing is an intact barrier function of the gut epithelium that prevents translocation of commensal bacteria into the mucosa and submucosa with subsequent immune cell activation. In this thesis, I focused in building 3D high-throughput gut-on-a-chip models both healthy and IBD-like that can be used in drug discovery pipeline. By mainly focusing on successful modelling of the intestinal epithelium and/or underlying tissues and cells with different levels of complexity. In addition, since these models can be directed towards an IBD-like state with the application of downstream molecules of activated immune system like IL-1b, TNF-a and INF-gamma known to recapitulate key aspects of IBD pathology. Making these models useful tools for investigation of disruption of epithelial barrier, IEC cell activation and as you can see in chapter VI activation of immune components. I was also able to show in a small-scale drug discovery studies that single molecules are able to revert the IBD-like phenotype.

Chapter 3 Material and Methods

Materials

Table 3-1 List of equipment used

Equipment	Product info/ supplier
Laminar flow hood	Teslar, Biovanguard green line
Centrifuge	VWR, macrostar 3.0R
Micro centrifuge	Eppendorf, Centrifuge 5424
Incubator	Binder, CB170
OrganoTEER	MIMETAS, OrganoTEER
PCR machine	Roche, LightCycler® 96 Instrument
Vortex orbital shaker	Sartorius ,Vortex 2 S000
Drop spectrophotometer	Thermo Fisher Scientific, NanoDrop™ One/OneC Microvolume UV-Vis Spectrophotometer with Wi-Fi
High content phase contrast and fluorescent microscope	Molecular Devices, ImageXpress Micro XL/XLS
High content Confocal microscope	Molecular Devices, ImageXpress Micro Confocal
Plate reader	Thermo Fisher Scientific, Fluorskan Ascent FL
Electronic repeating multichannel pipette	Sartorius , Picus 8-ch 50-1200 uL
Electronic repeating pipette	Sartorius Picus 0,2-10 uL

Aspiration system with multichannel insert	Integra Biosciences, VACUSAFE
3-lane 400µm-Organoplate®	MIMETAS, 4003-400-B
Rocker platform	MIMETAS, Perfusion Rocker™ Mini

Table 3-2 List of commercially available kits

Kit	Company	Cat.No
IL-8 DuoSet ELISA kit	R&D	DY208-05
IL-6 DuoSet ELISA kit	R&D	DY206-05
IL-1b DuoSet ELISA kit	R&D	DY205-10
TNF-alpha DuoSet ELISA kit	R&D	DY210-05
RNAasy micro kit	Quiagen	74004
Live/dead cytotoxicity kit	Thermo Fisher	L3224
Mounting Medium with DAPI	VectorLaboratories	H-1200

Cell culture

Caco-2

Human colon adenocarcinoma cell line Caco-2 (Sigma, 86010202) were cultured on T75 flasks in EMEM (ATCC,30-2003,) supplemented with 10% (v/v) FBS (Gibco, 16140-071), 1% (v/v) Non-essential amino acids (NEAA) (Gibco, 11140-050) and 1% (v/v) penicillin/streptomycin solution (Sigma, P4333). Cells were cultured in a humidified incubator at 37°C with 5% CO₂. Because Caco-2 cells start to differentiate once they reach confluency they were cultured up until 80% confluency and then either subculture or used for the experiments. For passaging cells were washed 1x with PBS (LifeTech, 20012019,) and then detached with 0.25% Trypsin (Gibco, 15290-046) and 0.53 mM EDTA (AM9260G, Ambion). The flask was placed in an incubator 37°C with 5% CO₂ for 3-5min. Neutralization was done by adding 2 volumes of complete media (Caco-2 media) and resuspending the cells several times to get rid of clumps. Then cells were counted and centrifuged at 200g for 5min. The supernatant was discarded, and cells were re-suspended in complete media. All experiments were performed on cells between passage 47 and 60. Cells were routinely tested for mycoplasma and were found negative.

HT-29-MTX-E12

HT29-MTX-E12 a human colorectal adenocarcinoma cell line (Sigma, 86010202) was cultured in T75 flasks with DMEM media (D6546, Sigma) supplemented with 10% (v/v) FBS (Gibco, 16140-071), 1% (v/v) NEAA (Life Tech, 11140-050), 1% (v/v) Glutamax (Gibco, 35050-061) and 1% (v/v) penicillin/streptomycin (Sigma, P4333). For sub-culturing the cells were washed once with PBS (LifeTech , 20012019) and detached with 0.25% Trypsin (Gibco, 15290-046) and 0.53 mM EDTA (AM9260G, Ambion). The flask was placed in an incubator at 37°C with 5% CO₂ for

3-5min. After this neutralization was done by adding 2 volumes of complete media (HT-29 media) and cells were resuspended several times to get rid of clumps. Then cells were counted and centrifuged at 200gx5min. The supernatant was discarded, and cells resuspended in complete media. Sub-confluent cultures (70-80%) were split in 1:3 to 1:10 or adding approximately 5x1E5 cells/T75 flask. All experiments were performed on cells between passage 50 and 70. Cells were routinely tested for mycoplasma and were found negative.

THP-1

The human acute monocytic leukemia cell line THP-1 (ATCC, Tib-202) was cultured in T25 flask placed upright and containing RPMI 1640 (R0883, Sigma) supplemented with 10% FBS (v/v) (Gibco, 16140-071), 1% (v/v) Glutamax (Gibco, 35050-061) and 1% (v/v) penicillin/streptomycin (Sigma, P4333). Because THP-1 is a suspension culture therefore there was no need for detachment step. For sub-culturing the cells were counted and then centrifuged at 300g for 5min. The supernatant was discarded, and cell concentration was adjusted to 0.2x10E6 cells/mL in a complete (THP-1) media. Cell concentration was maintained below 1.0x10E6 cells/mL. All experiments were performed on cells between passage 5 and 15. Cells were routinely tested for mycoplasma and were found negative.

MUTZ-3

MUTZ-3 human acute myelomonocytic leukemia cell line (DSMZ, ACC 295,) was cultured in T25 flask placed upright and containing Alpha-MEM (Sigma, M4526) supplemented with 20% (v/v) FBS (16140-071, Gibco), 1% (v/v) Glutamax (Gibco, 35050-061), 1% (v/v) penicillin/streptomycin (P4333, Sigma) and 10% (v/v) conditioned medium of 5637 cells (ATCC, HTB-9). Cells were cultured in a humidified incubator (37°C, 5% CO₂) and maintained below cell

concentration of 1.0×10^6 cells/mL. For sub-culturing the cells were counted and then centrifuged at 300g for 5min. The supernatant was discarded, and cell concentration was adjusted to 0.2×10^6 cells/mL in a complete (MUTZ-3) media. All experiments were performed on cells between passage 5 and 15. Cells were routinely tested for mycoplasma and were found negative.

5637 cell line and preparation of conditioned media

The human bladder carcinoma cells (ATCC, HTB-9) were cultured with RPMI 1640 (R0883, Sigma) supplemented with 10% FBS (v/v) (Gibco, 16140-071), 1% (v/v) Glutamax (Gibco, 35050-061) and 1% (v/v) penicillin/streptomycin (Sigma, P4333). Confluent cultures were split in 1:5 ratio using 0.25% Trypsin (Gibco, 15290-046) and 0.53 mM EDTA (AM9260G, Ambion) for 5 to 10 min. For conditioned media preparation the supernatant medium, containing some free-floating cells, was collected after 2 days post splitting, centrifuged, and filtered through a 0.2-µm Millipore filter. This conditioned medium was labeled “low” and stored at -20°C. Fresh media was added to the cultures and the same procedure was repeated after 2 more days of culturing. This media was labeled “high” and stored at -20°C. For preparing conditioned medium of 5637 cells, 50% from the “low” and 50% from the “high” media was added.

Induced pluripotent stem cells (iPSC)

Human induced pluripotent stem cells (hiPSC; UOSi001-A) University of Sheffield (Sheffield, United Kingdom) were routinely cultured on 6-well cell culture plates pre-coated with 0.5 mg/mL Vitronectin Recombinant Human Protein (VTN) (Thermo Fisher.14700) diluted in Phosphate Buffered Saline (PBS) (ATCC, 30-2200). Plates were coated prior use for 60 min at room temperature (RT) and either used immediately or stored at 4°C up to a week. Cells were passaged before reaching a 60-70% confluency and discarded if any sign of differentiation in the

cultures was present. This was done by removing the old media and rinsing the cells once with PBS. After that a 0.5 mM EDTA (15-575-020, UltraPure 0.5M EDTA, pH 8.0, Invitrogen) was added and cultures were incubated at 37°C for app.1-2 min. EDTA was removed by pipette and cells were flushed once with fresh E8 media (Thermo Fisher, A1517001). For sub culturing small clumps of cells were added in 1/4 or 1/6 ratio in media supplemented with 10 μ M Y-27623 ROCK inhibitor (Merck , 688000) for the initial 24h. Media change was done every day and cells were cultured at 5% CO₂ at 37°C

Cell seeding in the OrganoPlate®

Monoculture cell seeding against gel (Tubule seeding)

Before ECM loading, 50ul of HBSS (Sigma, 55037C) was added in all observation windows of the OrganoPlate (4003-400-B, Mimetas). The ECM collagen-I (Cultrex, 3447-020-01) was diluted to 4 mg/ml, on ice using 100 mM HEPES (Thermo Fisher, 15630-122) and 3.7 mg/ml NaHCO₃ (Sigma, S5761) in a 8:1:1 ratio. Then 2ul of the ECM was dispensed in the gel inlet (MI) of the OrganoPlate®. Then the plate was placed in humidified incubator (37°C 5% CO₂) for approximately 15 min to allow the ECM polymerization. In the meantime, cells are trypsinized with 0.25% Trypsin (Gibco, 15290-046) and 0.53 mM EDTA (AM9260G, Ambion), and cell concentration is adjusted after centrifugation to 10E6 cells /mL. Then we added 2ul of the adjusted cell suspension (20.000 cells) in the top channel of a 3-lane 400 μ m OrganoPlate®, followed by 50ul of media added to the top inlet only. The plate was put on a 75-degree angle for 2-4h in the incubator, followed by media addition in the remaining channels. Perfusion was started by placing the OrganoPlate® (on a rocker (7° angle per 8 minutes) thus allowing bi-directional flow.

Simplified schematics of the procedure can be seen in Figure 3.1.

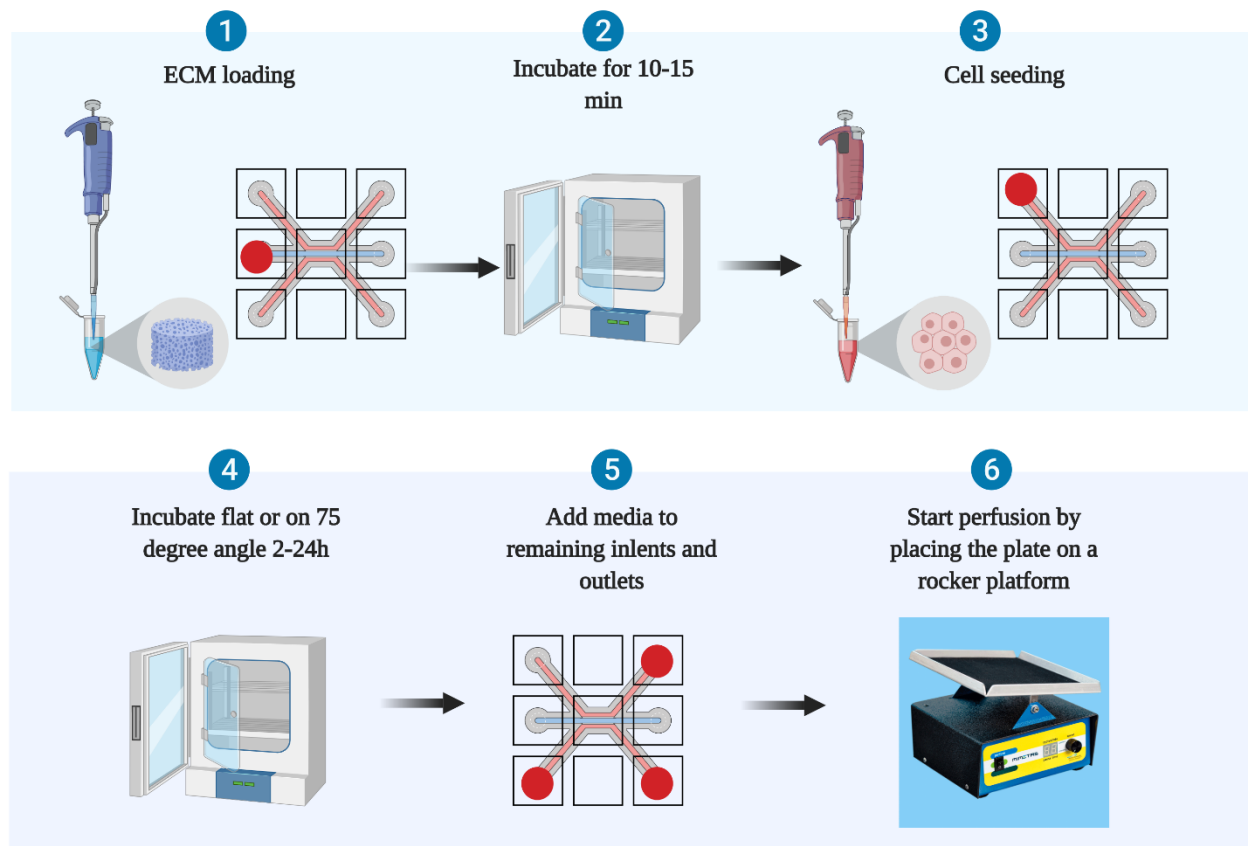


Figure 3.1 Schematic representation of simplified Organoplate against gel cell seeding (tubule seeding)

Tetra co-culture seeding in the OrganoPlate

2 μl of cell suspension made by mixing Caco-2 at 10×10^6 cells/mL and HT29 cells at 10×10^6 cells/mL in a ratio of 6:1 in Caco-2 complete medium was injected in the inlet of the top medium channel, followed by an addition of 50 μl medium to the same well. The OrganoPlate was placed on the side for 3.5 hours at 37°C to allow the cells to sediment and attach to the ECM. Afterwards, an additional 50 μl of culture medium was added to each of the remaining in- and outlets of the top and bottom medium channels. Subsequently, the OrganoPlate was placed horizontally in a humidified incubator (37°C , 5% CO_2) on an interval rocker switching between a $+7^\circ$ and -7° inclination every 8 min (Mimetas Rocker Mini, Mimetas BV), allowing bi-directional flow. At

day 4 of culture, the immune cells were added. Differentiated THP-1 and MUTZ-3 were collected, aliquoted and pelleted (300 x g, 5 min) in separate Eppendorf tubes. 2x concentration of each of the cell lines at 6×10^6 cells/ml was prepared. THP-1 and MUTZ-3 were premixed at a ratio of 1:1 in EMEM supplemented Caco-2 medium at a final concentration for each of the cell lines at 3×10^6 cells/ml. Medium was aspirated from the bottom perfusion channel and 2 μ l of cell suspension (6000 cells each, 12 000 immune cells total) was injected in the inlet of the bottom medium channel. Cells were forced into the channel by pipetting 0.5-1 μ l of the cell suspension from the outlet into the inlet. This was repeated 3 times followed by placing the OrganoPlate on the side for 30 min at 37°C to allow the immune cells to attach to the ECM. Finally, 50 μ l of medium was added all inlets and outlets and the OrganoPlate was placed horizontally on the interval rocker with the same settings as mentioned above.

Induced pluripotent stem cell seeding

IPS cell seeding follows the same procedures for ECM seeding as mono/co-culture cell seeding against gel described previously (Trietsch et al. 2017b). After solidification of the gel, the Organoplates were coated with 0.5 mg/L Vitronectin for 60 min at room temperature (RT). Cells were dissociated to single cells following procedure see Figure 3.2 and resuspended in mTeSR medium supplemented with 10 μ M Y-27623 ROCK inhibitor. Cell concentration was adjusted to 1×10^7 cells/mL from which 2 μ L was added in the top medium outlet. Followed by removal of 1 μ L from the top medium inlet. Then 50 μ L of mTeSR with Y-27623 ROCK inhibitor (Rocki) was added to the top medium inlet. The plates Organoplates were placed flat in a humidified incubator to allow cell attachment for 24h. After that mTeSR medium without Rocki was added to the remaining inlets and outlets and perfusion was started by placing the plate in humidified incubator (37°C, 5% CO₂) on an interval rocker switching between a +7° and -7° inclination every 8 min overnight. Differentiation procedure was started after 24h.

Directed differentiation of induced pluripotent stem cells

Directed differentiation of iPSC cells was started after 48 hours post seeding. Definitive endoderm differentiation was started by adding 50ul of DE1 media followed by 24h of DE2 media. Hindgut was added after 2 days of DE differentiation and cells were treated for 72h in Hindgut (HG) media. Once Hindgut was established cells were treated with mature intestine (MI) media up to three

weeks. Media was changed every 3 to 4 days. Detailed media composition for the media used can be seen in Table 3-3 Overview of the differentiation process can be seen in Figure 3.2.

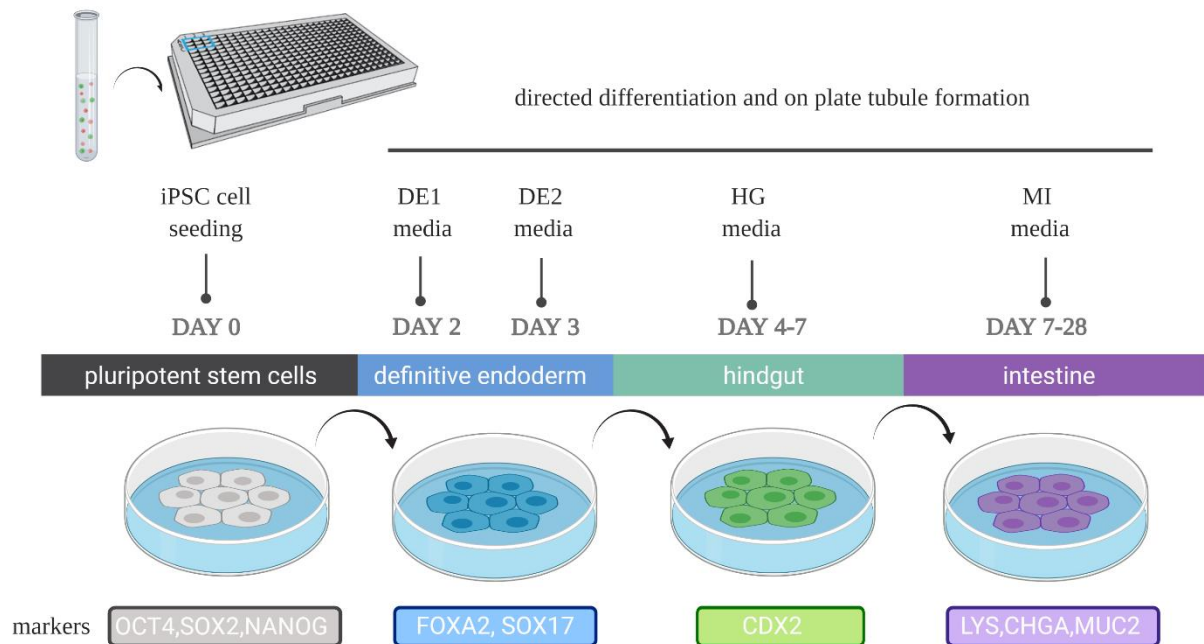


Figure 3.2 Schematic representation of directed differentiation protocol of induced pluripotent stem cells into gut-on-a-chip in a microfluidic device the OrganoPlate®.

Table 3-3 Components of directed differentiation media

Stage of differentiation	Abbreviation	Component	Final concentration
Definitive endoderm	DE1	RPMI-1640 Medium	/
		Penicillin-Streptomycin	1x
		Non-essential amino acids	1x
		B27 with insulin	1x
		CHIR99021	3 uM
	DE2	RPMI-1640 Medium	/
		Penicillin-Streptomycin	1x
		Non-essential amino acids	1x
		B27 with insulin	1x
Hindgut	HG	RPMI-1640 Medium	/
		Penicillin-Streptomycin	1x
		Non-essential amino acids	1x
		FBS	1x
		CHIR99021	2 uM
		FGF 4	500ng/mL
		Noggin	100ng/mL
Mature intestine	MI	DMEM/F12 Medium	/
		HEPES	/
		Penicillin-Streptomycin	15mM
		Non-essential amino acids	1x
		B27 with insulin	1x
		Noggin	1x
		R-spondin	100 ng/mL
		EGF	500 ng/mL
		MMP-8	100 ng/mL
	10 uM		

Assays

Barrier integrity assay (BI assay)

This assay is performed to assess the barrier tightness of a boundary tissue and can be used as one of the criteria for optimizing a tissue model, to select for leak-tight tissues for a transport or toxicant exposure study and to detect compound-induced disruption of the barrier (end point or in real-time) Figure 3.3 In short the apical medium inlet is perfused with 40ul and the outlet with 30ul of the commonly used fluorescent dextrans Table 3-4 dissolved in basal media. In the middle and bottom inlets and outlets only 20ul of basal media is added. Measuring the leakage of the

fluorescent dye from the lumen of the tubules into the ECM compartment is performed by real-time imaging with the ImageXpress Micro (37°C, 5% CO₂) set to take images on interval every 3-5min for the duration of 15 or 30min. For a long time, cytotoxic exposures, experiments were done by taking point measurements every 12-24h. The leak tightness of the tubules was determined by analyzing the ration between the fluorescent signal in the basal and apical region in Fiji

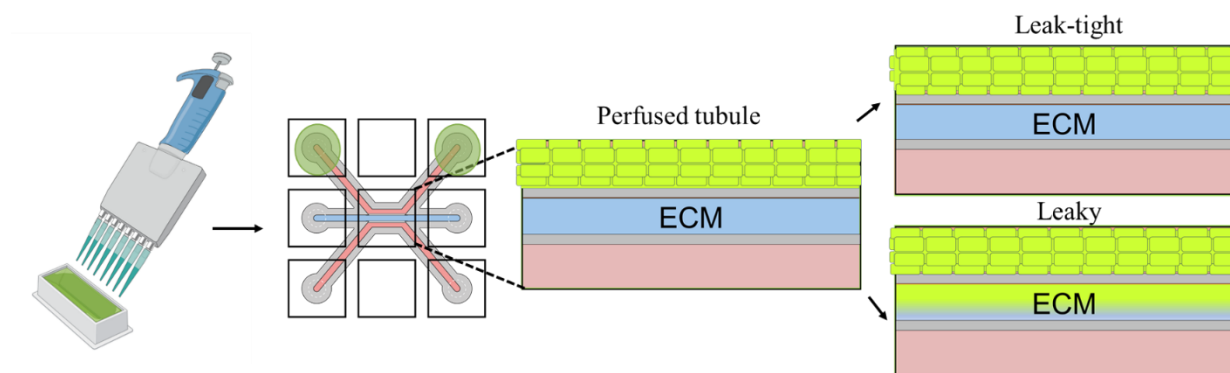


Figure 3.3 Schematic overview of the barrier integrity assay in a 3-lane OrganoPlate®

Table 3-4 Commonly used fluorescently labelled dextran's for performing the Barrier integrity assay

	Company	Cat.No	Size (kDa)	Stock concentration (mg/mL)	Working concentration (mg/mL)
Tetramethylrhodamine isothiocyanate dextran (TRITC-Dextran)	Sigma	T1287	155	25	0.5
Fluorescein isothiocyanate dextran (FITC-Dextran)	Sigma	46946	150	25	0.5
Fluorescein isothiocyanate dextran (FITC-Dextran)	Sigma	FD10s	10	25	0.5
Tetramethylrhodamine isothiocyanate dextran (TRITC-Dextran)	Sigma	T1037	4.4	25	0.5

The following approach was used for quantifying the barrier integrity in the OrganoPlate®. The fluorescent signal ratio was determined by measuring the intensity of the fluorescent signal in the medium channel (the lumen of the tubule-apical region) and the fluorescent signal from the adjacent gel channel (the basal region) of a chip over time. The fluorescence from the basal side was divided by the fluorescence of the apical side which in turn gives us a number from 0 till 1. In the case of a leak-tight barrier tissue this ratio remains constant and relatively low however when we have a leaky barrier tissue this ratio increases over time, eventually approaching 1. This is because the fluorescent signal leaks in the basal region from the apical region over time.

Transepithelial electrical resistance (TEER)

Transepithelial electrical resistance (TEER) was used as a measurement that can help us assess the barrier function of epithelial cells. The electrical impedance was assessed by applying a continuous current to the cells on both apical and basal side (Chen, Einspanier, and Schoen 2015).



Figure 3.4 OrganoTEER

Transepithelial electrical resistance measurement (TEER) was performed using an automated

multichannel impedance spectrometer specifically designed for use with the OrganoPlate® (OrganoTEER, Mimetas) see Figure 3.4. Before the start of every experiments the OrganoTEER electrode board was sterilized by spraying them with 70% Ethanol and leaving them for an hour under the hood to dry out. Plates were taken out of the incubator and medium was added in the middle inlets and outlets the OrganoPlate® were left to equilibrate for 30 min at room temperature before the measurement. Since the OrganoTEER is matched to the OrganoPlate® each of the electrode pairs from the electrode board are dipped in the inlet and outlet wells of all the microfluidics chips thus connecting to the basal and apical side of all tubes. Point impedance measurements were performed by frequency sweep from 5Hz to 1MHz (75 points at precision 0) with TEER values going up to $1000 \Omega \cdot \text{cm}^2$.

Data was analysed using the OrganoTEER software, which automatically extracts the TEER contribution (in Ohm) from the measured spectra and normalizes it to $\text{Ohm} \cdot \text{cm}^2$ by multiplying by the tubule-ECM interface (estimated at 0.0056 cm^2). The TEER values of our models would be compared to values of the small intestinal epithelium.

Immunohistochemistry (IHC)

Immunohistochemistry was used to detect target specific cellular biomolecules expressed by our cultures. The detection of the bound antibodies was performed by high content fluorescence microscopy using either the Micro XLS-C High Content Imaging Systems or (Molecular Devices) and analyzed in Fiji.

Fixation was preform by adding freshly prepared fixative 3.7% formaldehyde diluted in PBS with Ca^{2+} and Mg^{2+} (14040117, Thermo Fisher) from 37% formaldehyde stock (252549, Sigma) in a 1/10 ratio. Media was aspirated from all of the chips and $50 \mu\text{L}$ was added to all inlets and outlets. Plates were incubated for 10-15min at RT placed on an angle or on a rocker followed by removal

of the fixative and 3x5 minutes of wash steps with 50 μ L D-PBS (20012068, Life Tech) (in all inlets and outlets) All subsequent steps were performed on room temperature. Cells were permeabilized with 50 μ L of freshly prepared permeabilization buffer 0.3% Triton X-100 (T8787, Sigma) in PBS added in all inlets and outlets for 10 minutes. After this the chips were washed once with washing solution 4% FBS (16140-071, Gibco) in PBS and blocked with blocking solution 2% FBS 2% bovine serum albumin (BSA) (A2153, Sigma), 0.1% Tween20 (P9416, Sigma) in PBS) for 30-45 min with blocking solution (50 μ L in all inlets and outlets). After this the primary antibody was added in a blocking solution at correct dilution. The cells were incubated for 1-2 hours at RT. Then plates were washed 3x 5 min with washing solution (50 μ L in all inlets and outlets) and incubated with the secondary antibody at RT for 30 min in the dark. Cells were again washed with washing solution 3x 5 min and constrained if needed with stain cells with direct stains (e.g. DAPI, Hoechst or ActinRed) for up to 30min. Lastly the cells were washed 1x5min with D-PBS and 50 μ L D-PBS was added in all of the inlets and outlets.

All the incubation and washing steps are performed by creating perfusion by placing the OrganoPlate on a regular rocker platform on low switching interval and small angle (i.e. 5° angle, 2-5 min interval).

Enzyme-linked immunosorbent assay (ELISA)

Media was collected from the different compartments and inlets and outlets were pooled together. All samples were stored at -80°C until further analysis and were thawed only once. The concentration different chemokines and cytokines was determined using the commercially available kits see Table 3-2 according to the manufacturer's protocols. The absorbance of the samples was measured using the Multiskan™ FC Microplate Photometer (Thermo Fisher) at 450 nm.

Table 3-5 List of primary and secondary antibodies and cell stains used in immunohistochemistry

Primary						
Antibody	Species Reactivity	Host / Isotype	Class	Company	Cat	Dilution
ZO-1	Dog, Human, Rat	Rabbit / IgG	Polyclonal	Thermo Fisher	61-7300	1:125
Occludin	Dog, Human, Rat	Rabbit / IgG	Polyclonal	Thermo Fisher	71-1500	1:125
E-cadherin	Human, Mouse	Rabbit / IgG	Monoclonal	Cell Sig.Tech	3195S	1:100
Ezrin (Villin II)	Dog, Human	Mouse/ IgG1	Monoclonal	BD	610602	1:50
Ac.tubulin	Human, Monkey	Mouse/ IgG2b	Monoclonal	Sigma	T6793	1:2000
MUC2	Human, Mouse	Mouse/ IgG1	Monoclonal	Sigma	MA512345	1:100
MUC5AC	Human, Mouse	Mouse/ IgG1	Monoclonal	Sigma	MA512178	1:100
SOX17	Human	Mouse/ IgG1	Monoclonal	R&D	MAB19241	1:100
FOXA2	Human	Goat / IgG	Polyclonal	R&D	AF2400	1:100
CDX2	Human	Goat / IgG	Polyclonal	R&D	AF2400	1:100
LGR5	Human, Mouse	Mouse/ IgG1	Monoclonal	SanBio	TA503316	1:200
SI	Human	Goat / IgG	Polyclonal	Santa Cruz	Sc-27603	1:100
Villin	Human	Mouse/ IgG1	Monoclonal	Santa Cruz	58897	1:200
Lysozyme	Human	Mouse/ IgG1	Monoclonal	Thermo Fisher	MA182873	1:200
Isotype		Rabbit / Ig	Control	Thermo Fisher	31235	1:250
Isotype		Goat / IgG	Control	Thermo Fisher	026202	1:250

isotype		Mouse / Ig	Control	Thermo Fisher	08-6599	1:250
Secondary antibodies						
anti-Goat Alexa Fluor 488		Donkey		Invitrogen	A11055	1:250
anti-Mouse Alexa Fluor 555		Donkey		Thermo Fisher	1736967	1:250
anti-Rabbit Alexa Fluor 647		Donkey		Sigma	SAB46001 77	1:250
Cell stains						
Actin Green 488				Life Tech	R37110	2 drops/mL
Actin Red 555				Life Tech	R37112	2 drops/mL
Hoechst 33342				Thermo Fisher	H3570	1/1000

Gene expression analysis (qRT-PCR)

Gene expression analysis of key differentiation and polarization markers was used to assess and compare gut tubules over the course of several days. RNA isolation was performed using the RNeasy Micro kit according to manufacturer instructions see Table 3-2. Lysates from several chips were pooled together and stored at -80 until further use. For cDNA synthesis we first determined the RNA concentration with NanoDrop OneC Microvolume UV-Vis Spectrophotometer (Thermo Fischer) Which was adjusted to a min concentration of 30 ng/ μ L in DEPC-treated milliQ water. Then we proceeded with adding the isolated RNA and a MasterMix Table 3-6 to Applied Biosystems™ MicroAmp™ Optical 8-Tube Strip with Attached Optical Caps, 0.2 mL (Thermo Fisher, 15527575)

Table 3-6 Components Master Mix for cDNA synthesis

Component	Stock concentration	Working concentration	Supplier	Cat.No
UltraPure™ DNase/RNase-Free Distilled Water	/	/	Thermo	10977035
First strand buffer	5x	1x	Invitrogen	28025013
dNTP's	12.5 mM	3.7nM	Invitrogen	10297018
Random primers	3 µg/µl	0.34 µg/µl	Invitrogen	48190011
DTT	0.1 M	13.3 mM	Invitrogen	28025013
RNAsin	40 U/µl	1.33 U/µl	Promega	N2511
M-MLV Reverse Transcriptase	200U/µl	13.3 U/µl	Invitrogen	28025013

Reverse transcription was carried out in a Light Cycler 96 instrument (Roche). Finally, qPCR was performed by using FastStart Essential DNA Green Master (Roche, 06402712001) for SYBR Green I-based real-time PCR and FastStart Essential DNA Probe Master (Roche, 06402682001) for TaqMan based real-time PCR. For primers used either SYBR Green or Taqman see Table 3-7 and Table 3-8 .

Mucus staining with Alcian blue

Alcian blue was used to detect mucopolysaccharides. Cultures were fixed for 20 min with 0.1% glutaraldehyde (G5882, Sigma) diluted in HBSS (Hank's Balanced Salt solution, H6648, Sigma) at RT followed by three washing steps. Then a 1% Alcian blue (B8438, Sigma) in 3% acetic acid (A6238, Sigma, pH 2.5) solution was added and incubated for 2 hours by starting a perfusion. Either by placing the OrganoPlate on the rocker platform or tilting the plate on an angle. After this

the chips were washed once with 3% acetic acid, two times with HBSS and stored in HBSS. Image acquisition was performed using the EVOST[™] FL Auto 2 Imaging System (Thermo Fisher, US).

Statistical analysis

Data was analysed using software described in the assay methods and GraphPad Prism software version 6, 7 and 8 (GraphPad Software, La Jolla, CA, USA) was used to graph and determine statistical significance. Unless stated otherwise, values are expressed as mean \pm Standard deviation (SD). All experiments are represented with minimum of three technical replicates or $n \geq 3$. For two groups a two-tailed, unpaired Student's t-test was used as for three or more groups ANOVA was applied. Differences with $p < 0.05$ were considered significant (ns $p > 0.05$, * $p < 0.05$, ** $p < 0.01$, *** $p < 0.001$, **** $p < 0.0001$). Number of chips and independent experiments in each experiment are mentioned in the figure legends.

Graphics

Majority of figures were created with BioRender.com under a paid academic subscription.

Table 3-7 SYBR Green probes

Gene ID		Primer sequence 5' - 3'
ACTIN	Forward:	CTCTTCCAGCCTTCCTTCCT
	Reverse:	AGCACTGTGTTGGCGTACAG
GAPDH	Forward:	CAATGACCCCTTCATTGACC
	Reverse:	GACAAGCTTCCC GTTCTCAG
MUC5AC	Forward:	CAGGGGTAGACCCTCCTCTC
	Reverse:	AGGCCTGTGTCTGCACCTAC
MUC13	Forward:	TCCTCCTCAGATTACCAAGCA
	Reverse:	GTTTAGGGTGCTGGTCTCCA
MUC12	Forward:	CCTGGAAACCTTAGCACCAG
	Reverse:	GACAGACGCATTGTTTTCCAT
MUC16	Forward:	AGTGGACCTTGGGACCTCA
	Reverse:	CACAGGGCCAGCAGATGTAG
SI	Forward:	GTAAGGAGAAACCGGGAAGC
	Reverse:	TGTCCATGGTCATGCAAATC
CCL20	Forward:	GCAAGCAACTTTGACTGCTG
	Reverse:	GATGTCACAGCCTTCATTGG
IL-8	Forward:	AGACAGCAGAGCACACAAGC
	Reverse:	ATGGTTCCTTCCGGTGGT

Table 3-8 List of TaqMan probes used in experiments

Gene ID	Gene	Accession number	Type
OCT4	Octamer-binding transcription factor 4	Hs04260367_gH	FAM
NANOG	Homeobox protein Nanog	Hs04260366_g1	FAM
SOX17	Sex Determining Region Y Box 17	Hs00751752_s1	FAM
FOXA2	Forkhead Box A2	Hs05036278_s1	FAM
CDX2	Homeobox protein CDX-2	Hs01078080_m1	FAM
ALB	Albumin	Hs00609411_m1	FAM
PDX1	Insulin promoter factor 1	Hs00236830_m1	FAM
MUC2	Mucin 2	Hs03005103_g1	FAM
VIL	Villin	Hs01031722_g1	FAM
LYS	Lysozyme	Hs00426232_m1	FAM
CHRA	ChromograninA	Hs00900375_m1	FAM
LGR5	Leucine-rich repeat-containing G-protein coupled receptor 5	Hs00969422_m1	FAM
ACTB	Actin Beta	Hs01060665_g1	VIC

Chapter 4

Membrane-free culture and real-time barrier integrity assessment of perfused intestinal epithelium tubes

The main goal of the study was to build a simple gut-on-a-chip model based on Caco-2 cells that exhibits the proper cell polarity and transporter expression in a high throughput microfluidic platform the OrganoPlate® and it is compatible for toxicological study.

The main results of this research have been published in the Nature Communication on 15th of August 2017 and went through a peer review process.

Author contributions

I optimized the cell culturing and performed the experiments (involved in the generation of data for figures 2 d and e; figure 3 d-i; figure 4; figure 5; Supplementary figure 3 and Supplementary figure 4) optimized the exposure setup under flow and the assay method. Was involved in the basic data analysis and in the reviewing of the manuscript.

ARTICLE

DOI: 10.1038/s41467-017-00259-3

OPEN

Membrane-free culture and real-time barrier integrity assessment of perfused intestinal epithelium tubes

Sebastiaan J. Trietsch¹, Elena Naumovska¹, Dorota Kurek¹, Meily C. Setyawati¹, Marianne K. Vormann¹, Karlijn J. Wilschut¹, Henriëtte L. Lanz¹, Arnaud Nicolas ¹, Chee Ping Ng¹, Jos Joore¹, Stefan Kustermann², Adrian Roth², Thomas Hankemeier³, Annie Moisan² & Paul Vulto¹

In vitro models that better reflect in vivo epithelial barrier (patho-)physiology are urgently required to predict adverse drug effects. Here we introduce extracellular matrix-supported intestinal tubules in perfused microfluidic devices, exhibiting tissue polarization and transporter expression. Forty leak-tight tubules are cultured in parallel on a single plate and their response to pharmacological stimuli is recorded over 125 h using automated imaging techniques. A study comprising 357 gut tubes is performed, of which 93% are leak tight before exposure. EC₅₀-time curves could be extracted that provide insight into both concentration and exposure time response. Full compatibility with standard equipment and user-friendly operation make this Organ-on-a-Chip platform readily applicable in routine laboratories.

¹Mimetas BV, JH Oortweg 19, 2333CH Leiden, The Netherlands. ²Roche Innovation Center Basel, F. Hoffmann-La Roche Ltd, Grenzacherstrasse 124, 4070 Basel, Switzerland. ³Leiden Academic Centre for Drug Research, Leiden University, Einsteinweg 55, Leiden 2333CC, The Netherlands. Annie Moisan and Paul Vulto contributed equally to this work. Correspondence and requests for materials should be addressed to P.V. (email: p.vulto@mimetas.com)

Dysfunction of epithelial barriers as a result of pathological states or drug-induced toxicity can lead to life-threatening conditions and halt drug development at all clinical stages. Epithelial barrier disruption is mainly manifested by an increased para-cellular permeability of the epithelium. In vitro testing of para-cellular permeability of epithelial barriers is most commonly achieved by cultivating cells on a rigid membrane that separates two medium-containing chambers under static conditions. Such conventional Transwell systems are poorly

suited for high-resolution kinetic measurements and image-based readouts, and therefore provide only limited information on the underlying mechanisms, leading to barrier disruption. More importantly, it does not comply with the current paradigm in cell culture that is steadily shifting towards three-dimensional cultures, extracellular matrix (ECM) embedment and addition of perfusion flow^{1–5}.

The field of microfluidics has rapidly gained momentum in the realm of in vitro modeling³. Inherent to its dimensions,

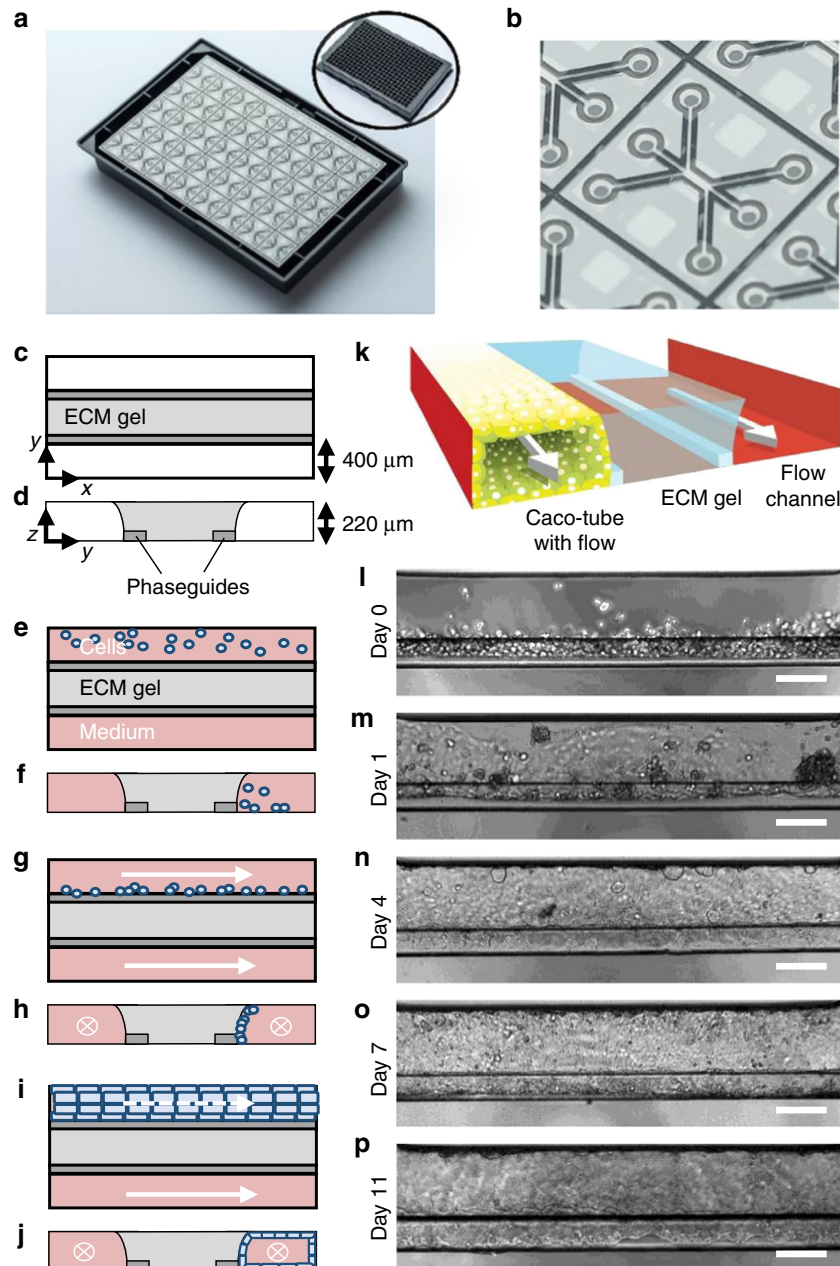


Fig. 1 Overview of the method for modeling intestinal tubules in the OrganoPlate platform. **a** Photograph of the bottom of an OrganoPlate showing 40 microfluidic channel networks with inlay showing the top view of the 384-well plate format device; **b** Zoom-in on a single microfluidic channel network comprising three channels that join in the center. **c, e, g, i** Horizontal projection and **d, f, h, j** vertical cross section of center region for subsequent steps in establishing the gut model. **c, d** An extracellular matrix gel (light gray) is patterned by two phaseguides (dark gray), **e, f** culture medium is introduced in the two lanes adjacent to the ECM gel, one of which comprises cells. **g, h** Cells are allowed to settle against the ECM gel surface by placing the plate on its side. **i, j** Upon application of flow, cells form a confluent layer lining the channel and gel surfaces, resulting in a tubular shape. **k** 3D artist impression of the center of a chip comprising a tubule, an extra cellular matrix gel and a perfusion lane; two phaseguides (white bars) are present that define the three distinct lanes in the central channel. The tubule has a lumen at its apical side that is perfused. **l–p** Phase-contrast images of the formation of the tubular structure at day 0, 1, 4, 7, and 11, respectively. Scale bars are 100 μm

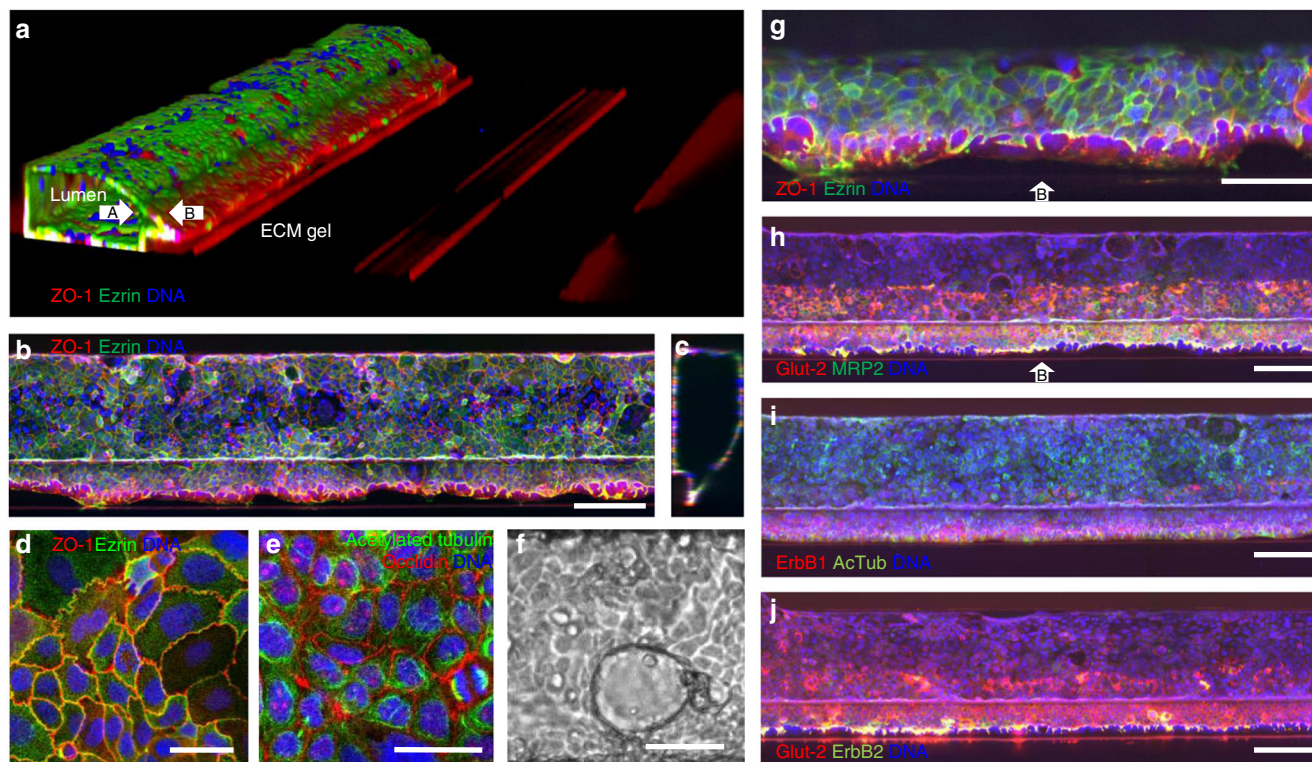


Fig. 2 Tubule characterization by immunofluorescent staining. **a** 3D reconstruction of a confocal z-stack showing tubular morphology with a lumen. White arrows indicate the apical (A) and basal (B) sides. The tube is stained for tight junctions (ZO-1 in red) and brush borders (ezrin in green). **b** Max projection and **c** vertical cross-section of the tubular structure in **a**; **d**, **e** zoom of the epithelial layer at the bottom of the tube exhibiting **d** tight junctions (ZO-1 in red) and brush borders (ezrin in green), and **e** acetylated tubulin (green) and occluding (red). **f** Phase-contrast image showing dome formation. **g** Zoom of a z-slice of the tube in **a** of the cell layer on top of the phaseguide showing apical positioning of ezrin, indicating polarization of the tube (white arrow indicates basal side B). **h** Expression of glucose and MRP2 transporters, respectively stained with Glut-2 in red and MRP2 stain in green. Both Glut-2 and MRP2 show significantly higher signal against the collagen gel compared to the regions that are not exposed to the collagen, indicating increased expression levels. Both stains clearly stain the apical side of the tube. For z-slices above the phaseguide at a higher magnification see Supplementary Fig. 2b. **i** ErbB1 (red) and acetylated tubulin (green) expression. ErbB1 expression levels appear higher against the collagen. **j** Co-staining of Glut-2 transporter and ErbB2 receptor; both stains show higher signal levels against the collagen gel. ErbB2 is primarily expressed pericellularly (see also Supplementary Fig. 2d for a zoom). All tubes are fixed after 4 days in culture. Nuclei are stained blue with DraG5 (**a-c**, **g-j**) and DAPI (**d**, **e**). Scale bars in white are 100 μm with the exception of **d**, **e**, **f**, and **g**, where they are 50 μm . Z-slices just above the phaseguide at higher magnification of the images **g-j** are available in Supplementary Fig. 2. All images are representative of at least three biological and at least three technical replicates

microfluidic techniques are uniquely suitable to connect with epithelia of tubular shapes in order to provide shear stress and continuous medium refreshment through perfusion. Typical microfluidic solutions make use of artificial membranes to enable apical-basal access to the epithelia⁶, thus not accommodating an ECM that is a crucial parameter in cell signaling involved in differentiation and epithelial-to-mesenchymal transition. Also, microfluidic techniques, which are typically presented as single chips⁷, need to be parallelized in order to deliver readouts for multiple compounds, dilutions, replicates and controls. User-friendly operation and compatibility with state-of-the-art readouts, such as high content imaging (HCI)-based multiplexed cellular and molecular analyses, are crucial prerequisites for perfused, ECM-embedded cell culture techniques to become a new standard.⁸

We developed a methodology to culture perfused, ECM-supported epithelia and interrogate their barrier function in a membrane-free manner. As an example, we developed a model of intestinal tract epithelium that exhibits cellular polarization, tight junction formation, and expression of key receptors. Forty gut models were grown in a tubular shape in the OrganoPlate platform that was accessible from both the apical and basal sides. The tubes were assessed for barrier integrity and exposed to staurosporine and acetylsalicylic acid (aspirin) for 125 h. From

330 tubes used in these experiments, 93% were leak tight before exposure. The experiment was repeated using real-time parallel time-lapse imaging, in which tubes were stable up till 6 to 8 h. EC₅₀-time curves provide insight in concentration response at increasing exposure time in one single experimental run.

Results

Intestinal tube culture in OrganoPlate. Figure 1 shows the OrganoPlate platform, which encompasses 40 microfluidic cell culture structures embedded in a standard 384-well microtiter plate format (Fig. 1a, b)^{9, 10}. Each microfluidic channel structure is comprised of three lanes that are connected to corresponding wells of a microtiter plate that function as inlets and outlets to access the microfluidic culture. The lanes join in the centre of the structure where two capillary pressure barriers are present called phaseguides¹¹. Figure 1c–j shows a schematic representation of vertical and horizontal cross-sections of the centre of a microfluidic structure and the method of growing a tubular structure. First, an ECM gel is introduced in the central lane (Fig. 1c, d). The phaseguides are used to selectively pattern the ECM gel in the central lane by meniscus pinning. The meniscus stretches beyond the phaseguide, leading to a curved shape. After ECM gelation, epithelial cells are seeded in one

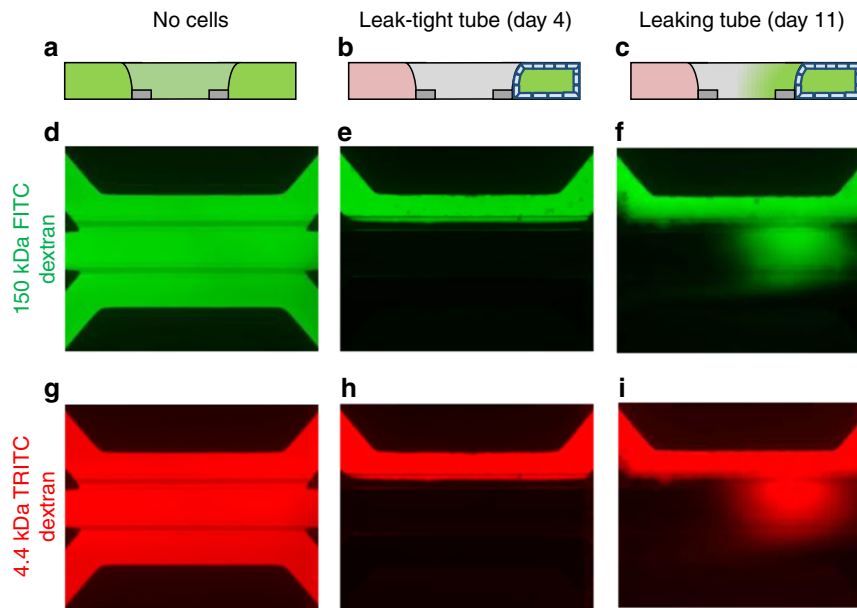


Fig. 3 Barrier integrity assay in OrganoPlate. A fluorescent dye is inserted in the channel comprising the tube. Integrity of the tube barrier is quantified by measuring the amount of dye that is leaking out of the tube into the adjacent gel channel. **a–c** Sketch in vertical cross section showing fluorescence distribution: **a** in absence of a tube, **b** for the case of a leak-tight tube and **c** for a leaky tube. **d–i** Fluorescent images of microfluidic chips perfused with fluorescent molecules show experimental results for: gel only (**d, g**), leak-tight tube (**e, h**), and leaky tube (**f–i**) using both 150 kDa FITC-dextran and 4.4 kDa TRITC-Dextran during the same experiment

lateral lane, allowing them to sediment directly against the ECM gel by placing the titre plate in a vertical position, i.e., standing on one side (Fig. 1e–h). Upon attachment of the cells, the plate is horizontally placed on an interval rocker that induces flow by reciprocal leveling between reservoirs (Supplementary Fig. 1). Upon application of flow, cells proliferate and start lining all surfaces of the perfusion channel, forming a confluent tubular structure (Fig. 1i, j). The tubules have a lumen that is connected to the in- and outlet of the respective lanes, making then accessible for perfusion with medium and for apical compound exposure. The basal side of the epithelium is facing the ECM gel and can be accessed by the second perfusion lane on the opposite side of the ECM gel lane. Figure 1k depicts an artist impression of the 3D configuration of the tube, showing that the tube is grown directly against the ECM, without the presence of artificial membranes (Fig. 1k).

For modeling of the intestinal barrier, the human intestinal colorectal adenocarcinoma cell line (Caco-2) was used. Figure 1l–p shows phase-contrast pictures of tube formation at day 0, 1, 4, 7, and 11, respectively. On day 0, cells are seeded against the ECM and start colonizing the glass walls to form a confluent tube (Fig. 1n–p). Perfusion was crucial for tube formation. Tubes were formed in 3 days and optimal barrier function was found at day 4 (Supplementary Fig. 1).

Differentiation and polarization marker expression. Figure 2a shows a 3D reconstruction of confocal fluorescence micrographs of the gut tube. The tube has a clear lumen and lines the perimeter of the gel and perfusion lane. Caco-2 cells in the confluent tubule display tight junctions and brush border formation as shown by immunofluorescence staining of ZO-1 and ezrin, respectively¹² (Fig. 2a–d, g). Figure 2e shows localization of acetylated tubulin (microtubules) and occludin (tight junctions)¹³. Dome-formation is observed, indicative of active fluid transport and intact epithelial barrier function^{14, 15} (Fig. 2f). Figure 2h–j shows maximum intensity projection images of tubes stained for Glut-2, MRP2, ErbB1, and ErbB2. Cells in

contact with the ECM showed a strongly increased expression of the transporters Glut-2, MRP2 and to a lesser extend ErbB1 and ErbB2 receptors.¹⁶ These staining results illustrate the crucially instructive role that the ECM plays in cellular differentiation and protein expression. Furthermore, characteristics of the ECM gel surface, such as its (bio-)chemical composition and mechanical characteristics, allow the formation of tissue structures observed in vivo.¹⁷ Polarization of the cell layer against the gel is best visualized at the contact line between the gel meniscus and the phaseguide, at the bending point of the cell layer where apical-basal polarization is in the horizontal plane. This is the most right-hand part of the tube in Fig. 2a or the bottom side of the tube in Fig. 2b. Figure 2g and Supplementary Fig. 2 show single z-slices at this bending point, just above the phaseguide. Tubes are the same as the images of Fig. 2b, h–j, but depicted as single z-slices and at higher magnification. Polarization is confirmed by localization of brush borders (ezrin) and the MRP2 transporter on the apical side as shown in Fig. 2g, and Supplementary Fig. 2a, b, while ErbB2 is positioned pericellularly (see Supplementary Fig. 2d). At least 10 Caco tubes were stained with each marker that were grown on at least four different days for at least four different passage numbers of cells prior to seeding. Figures show a representative selection of results.

Barrier integrity. Barrier function of the Caco-2 tubes was assessed by perfusion with a fluorescent probe in culture medium through the tube lumen, followed by the determination of fluorescence levels in the basal gel region, normalized to the fluorescence in the lumen. This is illustrated in Fig. 3a–i. Both a high molecular weight fluorescent probe (150 kDa FITC-dextran) and a lower molecular weight probe (4.4 kDa TRITC-dextran) were added to the medium that is perfused through the lumen of the tube. In absence of an intact tubular structure, the fluorescent probes leak into the gel and the basal side perfusion channel (Fig. 3a, d, g), while for a fully intact barrier, the fluorescent probes are retained in the lumen of the tube (Fig. 3b, e, h). Upon (partial) loss of barrier function, e.g., through drug-induced

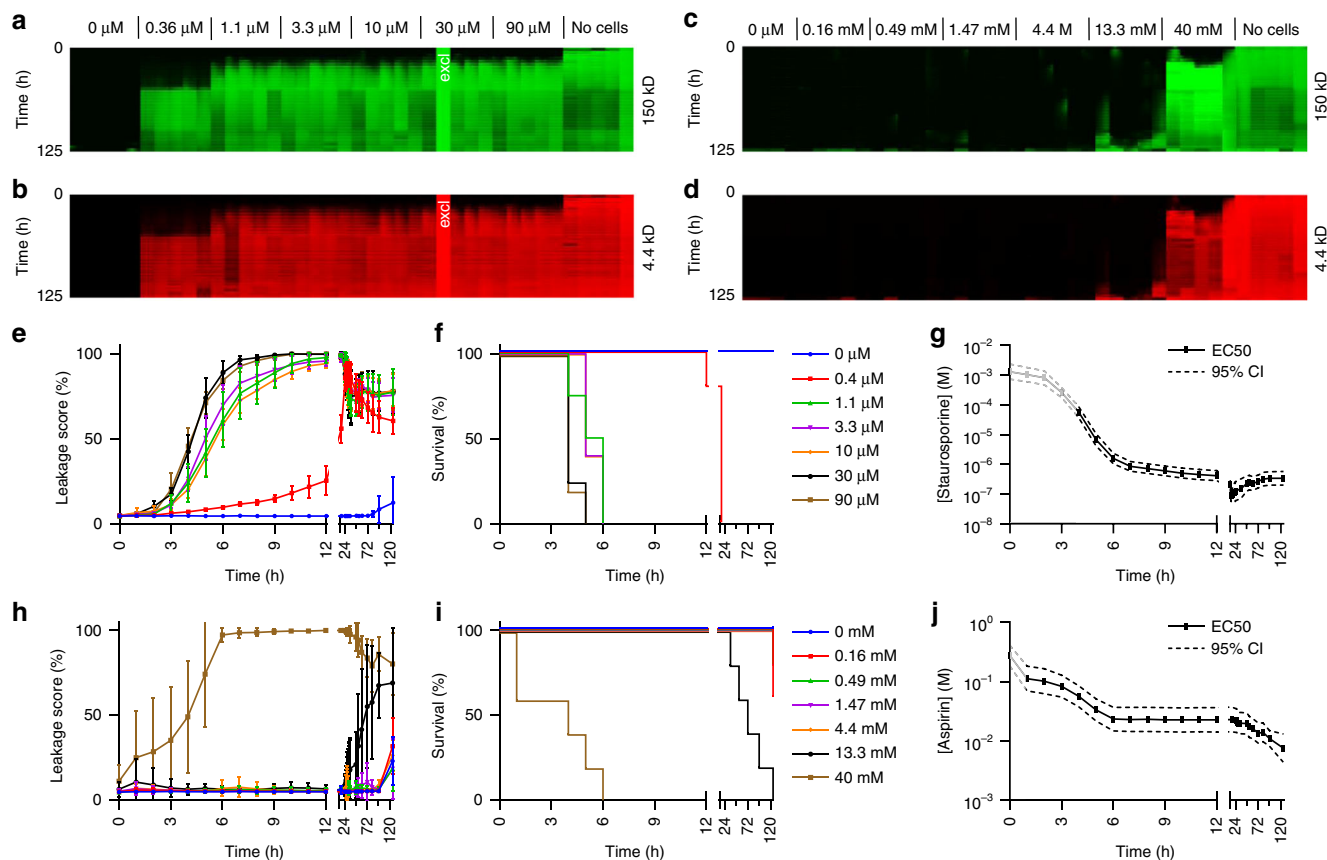


Fig. 4 Drug-induced loss of barrier integrity is observed over time in a concentration-dependent manner. Results shown for staurosporine (**a, b, e–g**) and aspirin (**c, d, h–j**). **a–d** Array of fluorescence micrographs of the gel region showing distribution of the 150 kDa FITC-Dextran (**a, c**), and 4.4 kDa TRITC-Dextran (**b, d**) over time and for various compound concentrations; the loss of barrier integrity results in an increased fluorescent signal. Measurements are taken at 1-h intervals up to 12 h, at 16 h, from 24 to 36 h at 1 h interval, and at 48, 53, 60, 72, 82, 96, and 125 h. In between each interval, the OrganoPlate was placed back into the incubator on the interval rocker platform to maintain the perfusion flow. Five technical replicates of each concentration of a compound were measured on a single plate. One well was excluded from further data analysis, because of a pipetting error (marked with “excl” in white). **e, h** The progression of the loss of barrier function over time is plotted as the ratio between fluorescent signal in apical and basal regions for the various concentrations of staurosporine (**e**) and aspirin (**h**), where the plotted *line* is the mean of five replicate exposures and *error bars* depict the standard deviation. **f, i** Kaplan–Meier curves were generated where survival was defined as showing a leakage score below 40%. Overlapping curves were shifted by 1% for clarity purposes. **g, j** EC₅₀ values are plotted as a function of exposure time. EC₅₀ values were obtained by fitting a concentration–response curve at each time point based on non-linear regression of leakage scores using normalized response and standard slope and were plotted including 95% confidence interval (CI). EC₅₀ values obtained from time points before the first event in the Kaplan–Meier plot, as indicated by a grayed out line, should be interpreted with caution as the curve fit could be dominated by noise rather than biological effect. All shown graphs were derived from data acquired using 150 kDa FITC dextran. Technical replicates are defined as tubes seeded on the same plate and exposed in the same experimental session. Independent full replicate series were run for both staurosporine and aspirin that are displayed in Supplementary Figs. 3 and 4

toxicity, the fluorescent probe leaks out of the lumen towards the basal side, yielding a higher signal in the ECM (Fig. 3c, f, i). Barrier integrity was measured using a HCI system, allowing monitoring of 40 tubes in parallel. To quantify the integrity of the barrier, the fluorescence level was measured in the gel region and normalized to the fluorescence level in the luminal side to compensate for bleaching effects. Upon reaching a fluorescence value of 0.4, barrier integrity of a tube was considered lost. The barrier integrity of 24 tubes was tracked on day 4, 7 and 11 of culture. As depicted in Supplementary Fig. 1c, it was found that, at day 4, all tubes were leak tight, while at day 7 and 11, three and seven tubes were leaky, respectively. Therefore, barrier integrity measurements are performed at 4 days of culture.

Drug-induced barrier disruption. Barrier integrity of 4-day-old Caco-2 tubes was assessed during a 125-h apical exposure to various concentrations of staurosporine (0.4–90 μ M), an inducer of apoptosis,¹⁸ and aspirin which affects tight junctions¹⁹

(0.16–40 mM). Fluorescence levels were measured at 1-h intervals from 1 to 12 h, and 24 to 36 h, as well as at 16, 48, 53, 60, 72, 82, 96, and 125 h. Between measurements, the OrganoPlate was placed back on the rocker platform to maintain flow. Figure 4a–d depicts arrays of images showing the fluorescence in the gel at each time-point for both FITC- and TRITC-dextran. Measurements for each compound were taken on a single OrganoPlate with five replicates per concentration. The staurosporine and aspirin studies were executed five and three times, respectively in separate experimental sessions (see Supplementary Fig. 4).

Fluorescence images of one single OrganoPlate depicted in the arrays of Fig. 4a–d and their quantification as depicted in Fig. 4e, h show that barrier integrity gradually diminished over time for all concentrations of staurosporine and for the two highest concentrations of aspirin. Results can also be visualised by generating Kaplan–Meier plots for loss of barrier integrity, in which events are defined as the fluorescence ratio reaching 40%

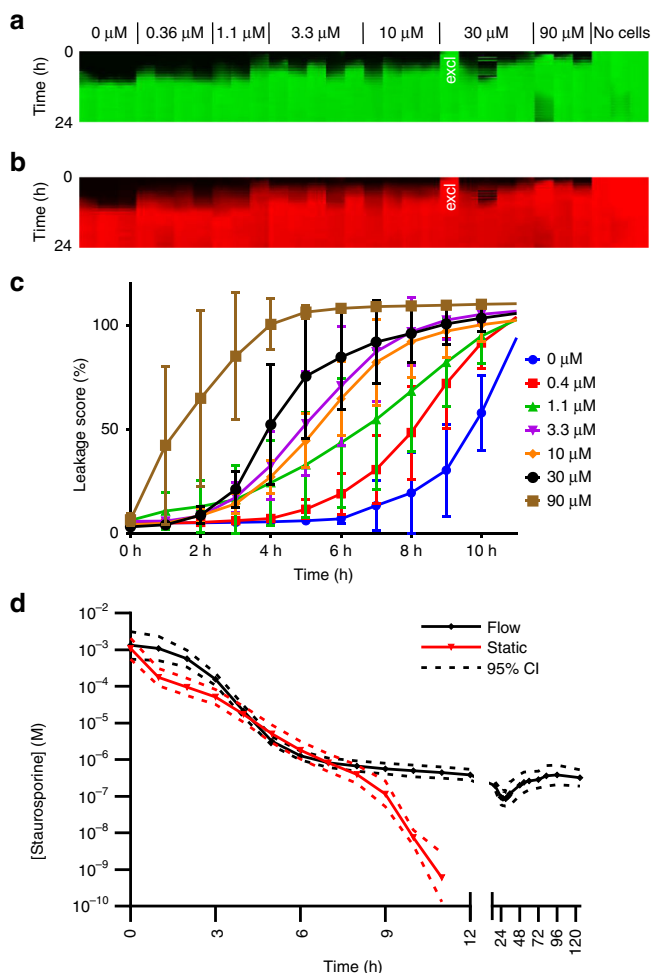


Fig. 5 Drug-induced loss of barrier integrity as a function of staurosporine concentration measured in real-time. **a, b** Array of fluorescence micrographs of the gel region showing distribution of the 150 kDa FITC-Dextran (**a**) and 4.4 kDa TRITC-Dextran (**b**) over time and as a function of compound concentration; the OrganoPlate was continuously kept in an incubated automated microscope. Pictures were taken at 1 h intervals. One data point was excluded for the fact that the tube appeared leaky at the first time point (marked with “excl” in white). **c** The progression of the loss of barrier function over time shows that untreated controls lose barrier integrity at 6–8 h due to lack of flow. The plotted line is the mean of 3–5 technical replicate exposures and error bars depict the standard deviation. **d** EC_{50} values over time for real-time measurement without flow and for measurement in intervals with flow induced between measurement (overlay with the graph of Fig. 4g). EC_{50} values with and without flow are similar for the initial 8 h of measurement

(Fig. 4f, i). This approach is particularly useful for less potent toxicants, where EC_{50} determination suffers from a lack of data of high effect. Aspirin, which has a different mode of action, involving tight junction disruption and proliferation inhibition, instead of apoptosis induction^{20, 21}, causes much less barrier disruption at relevant concentration. The Kaplan–Meier curve, however, does show a highly significant trend of loss-of-barrier function at higher concentration ($P < 0.0001$ for both curve difference and trend significance, derived from log-rank tests) (Fig. 4i). An EC_{50} value was estimated for each time point by fitting the concentration-response curve based on non-linear regression of the logarithm of the compound concentration vs. the normalized fluorescence, assuming a top and bottom plateau at 0 and 100% fluorescence. With increasing exposure times, a

shift of EC_{50} toward lower compound concentrations was observed (Fig. 4g, j). The 95% confidence interval of the extracted EC_{50} values indicates the robust data over the entire exposure time. EC_{50} values extracted at time points before the first event in the Kaplan–Meier plots should be interpreted with caution, as baseline fluorescence is likely to dominate the curve fitting rather than a biologically relevant signal.

Supplementary Fig. 3 shows an independent repeat of the study in Fig. 4 using cells seeded at different passage numbers in separate experimental sessions. Supplementary Fig. 3h–j, n–p also shows the data analysis for 4.4 kDa TRITC-dextran.

Supplementary Fig. 4 shows an overlay of the EC_{50} curves for 5 independent experimental series of staurosporine (Supplementary Fig. 4a, b) and aspirin (Supplementary Fig. 4c, d), based on both 150 kDa FITC-dextran (Supplementary Fig. 4a, c) and 4.4 kDa TRITC-dextran (Supplementary Fig. 4b, d) analysis. Independent experimental series were performed using cells at different passage numbers, separate plates, and separate experimental sessions. The high degree of similarity between the EC_{50} time curves for the full replicate series are a powerful illustration of the robustness of the method.

In parallel to fluorescence images, phase-contrast pictures were taken at selected time points. An example of tube morphology as a response to 96 h of staurosporine exposure is included in the Supplementary Information (Supplementary Fig. 5). Tubes are fully deteriorated for the highest concentration staurosporine and damages can be observed for exposure to 30 μ M staurosporine. For lower concentrations, tubes appear intact, while fluorescence images show that barrier integrity is lost. This indicates that loss of barrier function at higher concentrations of staurosporine is primarily due to cell death. Dead cells are flushed away by the perfusion flow.

For comparison, a similar experiment in a conventional Transwell was performed, which revealed a lower sensitivity for barrier disruption compared to the OrganoPlate, showing no significant difference between controls and staurosporine exposed wells after 4 h (Supplementary Fig. 6), while a clear effect is already apparent in the OrganoPlate results. In addition to improved morphological maturity of the 3D-perfused culture, the increased sensitivity of the model can be attributed to a decreased dead volume and higher surface-to-volume ratio of the microfluidic system as compared to Transwell systems. In a Transwell, the FITC-dextran was strongly diluted in the large target volume when crossing the barrier. By contrast, in OrganoPlates, the fluorescence is measured directly in the ECM after crossing the epithelial membrane. Since no dilution step is involved here, a much higher signal-to-noise ratio is obtained. Sensitivity of the microfluidic assay is such that it can be used as a binary assay, in which the exposure time at which leakage is observed is indicative of the toxicity of the compound.

Real-time measurement. Figure 5 shows another concentration response experiment with staurosporine, but this time the OrganoPlate was continuously kept inside the microscope throughout the experiment. A conditioned high content imager was used to maintain appropriate CO_2 , temperature and humidity. Flow was absent in this experiment, as the high content imager did not provide rocking. As can be observed in fluorescent images and quantification thereof, vehicle control tubes started leaking after 6 to 8 h of imaging. This can most likely be attributed to suboptimal conditions, including a lack of perfusion flow. Nevertheless, a clear concentration-response effect could be observed. An EC_{50} -time curve was extracted and overlaid in red with the curve from the experiments with rocking in black (as shown previously in Fig. 4g), showing similar curves for up to 8 h

(Fig. 5c). The advantage of incubation in the microscope is that a higher time resolution can be obtained.

In the experimental series of Figs. 4, 5, Supplementary Fig. 3 and Supplementary Fig. 4 10 OrganoPlates were used, comprising a total of 357 gut tubes and 33 ECM-only negative controls in total. Two tubes were excluded because of pipetting errors and 26 because of insufficient barrier function after 1 h, yielding 93% of leak-tight tubes at the onset of drug exposure.

Discussion

In summary, we present a unique methodology for assessing the barrier integrity of 40 leak-tight, polarized epithelial gut tubes in parallel using HCI. It is for the first time that a comprehensive method is presented to interrogate perfused epithelia tubules that are exposed to an ECM. The system allows sensitive, real-time interrogation of compound effects on barrier integrity, yielding insight in both exposure concentration and exposure time effects. The method has been robustly demonstrated for over 350 gut tubes and over 20,000 datapoints, making this to our knowledge the largest published Organ-on-a-Chip data set so far. The method can be applied to other epithelia as well as translated to disease models. The co-culture capabilities of the platform⁹ can be explored to create complex tissue configurations, for example, by incorporating mesenchymal and immune cells in the ECM adjacent to the epithelial tubes. The system outperforms classical techniques such as Transwell systems in terms of sensitivity, ease of use and (multiplexed) readout flexibility, as well as reagent, cell and time consumption. More importantly, it allows for the first time non-expert end-users to adopt Organ-on-a-Chip technology in their laboratories, without need for specific microfluidic skills or dedicated equipment.

Methods

Cell culture. The human colon adenocarcinoma cell line Caco-2 (86010202, Sigma-Aldrich) was cultured on T75 flasks in EMEM (No. 30-2003, ATCC), 10% FBS (No. F4135, Sigma), 1% NEAA (No. 11140-050, Life Technologies) and 1% penicillin/streptomycin (Sigma #P4333). Caco-2 cells between passage 45 and 60 were used for all experiments. Cells were routinely tested for mycoplasma contamination and found negative.

OrganoPlate culture. OrganoPlate culture was performed using three-lane OrganoPlates with 400 $\mu\text{m} \times 220 \mu\text{m}$ ($w \times h$) channels (Mimetas BV, the Netherlands). Phaseguides had dimensions of 100 $\mu\text{m} \times 55 \mu\text{m}$ ($w \times h$). Gel and perfusion channels have a length of 9 mm and 13 mm, respectively. 2 μl of gel composed of 4 mg/ml Collagen I (AMSBio Cultrex 3D Collagen I Rat Tail, 5 mg/ml, Cat. 3447-020-01), 100 mM HEPES (Life Technologies, 15630-122) and 3.7 mg/ml NaHCO_3 (Sigma, Cat. S5761) was dispensed in the gel inlet and incubated 30–45 min at 37 °C. Caco-2 cells were trypsinized using 0.5% trypsin in PBS/EDTA (Sigma, T3924), aliquoted and pelleted (5 min, 100 $\times g$). The cells were applied to the system by seeding 2 μl of 1×10^7 of cells/ml in the outlet of the top medium channel. Subsequently, the OrganoPlate was put on the side for 20 min to allow the cells to sediment against the ECM. This was followed by addition of 50 μl medium to the outlet of the top medium channel and the OrganoPlate was again incubated on the side for 3–4 h at 37 °C to complete cell attachment. After incubation, medium was added up to a total of 50 μl on both inlets and both outlets. The OrganoPlate was placed horizontally in the incubator (37 °C 5% CO_2) on an interval rocker switching between a +7° and -7° inclination every 8 min (Mimetas Rocker Mini), allowing bi-directional flow. Medium (50 μl each on inlet and outlet) was refreshed every 2–3 days.

Transwell culture. Caco-2 cells (60×10^3 cells per cm^2) were seeded on Transwell inserts (24-well, Transwell, Costar #3470-Clear, 0.4 μm pore size) and cultured for 21 days in EMEM supplemented with 10% fetal calf serum (FCS), and penicillin/streptomycin (Sigma #P4333). Medium was refreshed every 2–3 days, both 100 μl on apical (insert) and 500 μl on basal side of the Transwell.

Immunohistochemistry. Caco-2 tubules were fixed with 3.7% formaldehyde (Sigma No. 252549) in PBS (phosphate-buffered saline, Life Tech No. 20012068) for 15 min washed twice for 5 min with PBS and permeabilized with 0.3% Triton X-100 (Sigma # T8787) in PBS for 10 min. After washing with 4% FCS in PBS, cells were incubated with blocking solution (2% FCS, 2% bovine serum albumin (BSA) (Sigma # A2153), 0.1% Tween 20 (Sigma # P9416) in PBS) for 45 min.

Subsequently, cells were incubated with primary antibodies for 60 min or at 4 °C overnight, washed three times, incubated with secondary antibodies for 30 min and washed three times with 4% FCS in PBS. The following antibodies were used for immunohistochemistry: Rabbit a-ZO-1 (Invitrogen No. 617300, 1:125), Mouse a-acetylated tubulin (Sigma No. T6793, 1:2000), Rabbit a-ErbB1 (Novusbio No. NBP-1-51439, 1:200), Mouse a-MRP-2 (Santa Cruz No. SC-59608, 100 $\mu\text{g}/\text{ml}$, 1:10), Rabbit a-Glut-2 (Santa Cruz No. SC-9117, 200 $\mu\text{g}/\text{ml}$, 1:20), Mouse a-Ezrin (BD Transduction No. 610602, 1:50), Mouse a-ErbB2 (Thermo Scientific No. MS-229-P0, 200 $\mu\text{g}/\text{ml}$, 1:20), Rabbit a-Occludin (ThermoFisher No. 71-1500, 0.25 mg/ml, 1:100), Rabbit isotype (Life Tech No. 86199), Mouse isotype (Life Tech No. 86599), Goat isotype (Life Tech No. 02-6202), Goat a-Rabbit AlexaFluor 488 (Thermo Scientific, No. A11008, 1:250), Goat a-Rabbit AlexaFluor 555 (Life Tech, A21428, 1:250), Goat a-Mouse AlexaFluor 488 (Life Technologies, A11001, 1:250), Goat a-Mouse AlexaFluor 555 (Life Tech, A21422, 1:250), Goat a-Mouse AlexaFluor 647 (Life Tech, A-21236, 1:250), Donkey a-Rabbit AlexaFluor 647 (Life Tech, A-31573, 1:250). After nuclear stain (DraQ5, Abcam No. ab108410 or DAPI, H-1200, Vector Laboratories) cells were stored in PBS or Vectashield (H-1200, Vector Laboratories). All steps were performed at room temperature (RT). Cells were imaged with ImageXpress Micro XLS and Micro XLS-C HCI Systems (Molecular Devices, US) and SP5 laser point scanning confocal microscope (Leica).

Compound exposure. Caco-2 cells in OrganoPlates and Transwells were exposed to staurosporine or aspirin and barrier integrity was measured. Staurosporine was tested separately on five experiments of Caco-2 tubes cultured in OrganoPlate at passages: 48, 51, 53, 54, and 59. Aspirin was tested separately on three experiments of Caco-2 tubes cultured in OrganoPlate at passages: 48, 51, and 56. Cells were exposed for 125 h for interval measurements and for 24 h for real-time measurements. Concentrations of aspirin were 0, 0.1, 0.33, 1.11, 3.67, 12.12, 40 mM (Sigma No. A5376), and concentrations of staurosporine were 0, 0.4, 1.1, 3.3, 10, 30, 90 μM (Sigma No. S4400). Aspirin was dissolved in medium. Staurosporine was dissolved in medium with 0.9% DMSO (Sigma, No. D8418) for 90 μM and 0.3% for the other concentrations. Staurosporine preparations for the shorter-term exposure also contained 9% tox medium for 90 μM staurosporine and 3% tox medium for the other concentrations (500 ml of MEM α (Sigma No. M4526) with 6.25 ml of L-glutamine (Sigma No. G7513), 6 ml Tox Supplement (Sigma No. MTOXRTSUP).

Barrier integrity assay in OrganoPlate. Medium in the apical perfusion channel was replaced by medium containing 0.5 mg/ml FITC-dextran (150 kDa, Sigma No. 46946) and TRITC-dextran (4.4 kDa, Sigma No. T1037) and increasing concentrations of staurosporine or aspirin. Leakage of the fluorescent probe from the lumen of the tubular structure into the ECM compartment was automatically imaged using an ImageXpress XLS Micro HCI system at 37 °C and 5% CO_2 . For long-term exposure, imaging was performed at 1-h intervals up to 12 h, and from 24 to 36 h, and at 16, 35, 36, 48, 53, 60, 72, 82, 96, and 125 h. Between each interval, the OrganoPlate was placed back into the incubator on the interval rocker platform in order to maintain perfusion flow. For real-time measurement, automatic imaging was performed every hour for 24 h without removing the OrganoPlate from the HCI system. The ratio between the fluorescent signal in the basal and apical region of the tube was analyzed using Fiji²².

Barrier integrity assay in Transwell. 14–21 h prior to start of the experiment, media was changed to phenol-red free media (DMEM/F12 (Gibco, 11039-021), 10% FBS HI (Sigma, F4135), 1% NEAA (Life Tech, 11140050), 1% pen/strep (Sigma, P4333)). At the start of the compound exposure, medium was replaced. A total of 550 μl was added to the basolateral side, 250 μl of FITC-dextran solution (0.125 mg/ml medium) mixed with the compound of choice was added to the apical side. At each timepoint a 75 μl aliquot was collected from the basolateral side. 75 μl of fresh medium was added to the basolateral side after the 2 h aspirin timepoint. The fluorescence intensity was measured with a multi-well plate fluorimeter (Fluoroskan Ascent FL, Thermo Fisher) with excitation at 485 nm and emission at 535 nm.

Statistics and data analysis. Barrier integrity assay images were analyzed using Fiji²². Fluorescence intensities where measured in the apical and basal regions of the tubes and the ratio between these was reported. Tubes that reached a 40% fluorescent intensity ratio at first hour of measurement were considered non-leak tight and discarded. GraphPad Prism 6 (GraphPad Software Inc., La Jolla, CA) was used to generate Kaplan-Meier curves using the Survival Analysis – Survival Curve function defining an event as showing a basal to apical fluorescence intensity ratio over 40%. To prevent the overlapping data, curves were nudged by 1 data point each for clarity. Curve difference was estimated using log-rank (Mantel–Cox) test. Trend significance was evaluated using log-rank test.

Concentration-response curves were fitted using non-linear regression of the logarithm of the compound concentration vs. the normalized fluorescence assuming a top and bottom plateau at 0 and 100% and standard slope (hill slope = 1). The estimated EC_{50} values and 95% confidence interval were plotted vs. time.

Data availability. The data that support the findings of this study are available from the corresponding author upon reasonable request.

Received: 4 October 2016 Accepted: 14 June 2017

Published online: 15 August 2017

References

- Pampaloni, F., Reynaud, E. G. & Stelzer, E. H. K. The third dimension bridges the gap between cell culture and live tissue. *Nat. Rev. Mol. Cell Biol.* **8**, 839–845 (2007).
- Weaver, V. M. et al. Reversion of the malignant phenotype of human breast cells in three-dimensional culture and in vivo by integrin blocking antibodies. *J. Cell. Biol.* **137**, 231–245 (1997).
- van Duinen, V., Trietsch, S. J., Joore, J., Vulto, P. & Hankemeier, T. Microfluidic 3D cell culture: from tools to tissue models. *Curr. Opin. Biotechnol.* **35**, 118–126 (2015).
- Tibbitt, M. W. & Anseth, K. S. Hydrogels as extracellular matrix mimics for 3D cell culture. *Biotechnol. Bioeng.* **103**, 655–663 (2009).
- Huh, D., Hamilton, G. A. & Ingber, D. E. From 3D cell culture to organs-on-chips. *Trends. Cell. Biol.* **21**, 745–754 (2011).
- Kim, H. J., Li, H., Collins, J. J. & Ingber, D. E. Contributions of microbiome and mechanical deformation to intestinal bacterial overgrowth and inflammation in a human gut-on-a-chip. *Proc. Natl Acad. Sci.* **113**, E7–E15 (2015).
- Shah, P. et al. A microfluidics-based in vitro model of the gastrointestinal human–microbe interface. *Nat. Commun.* **7**, 11535 (2016).
- Junaid, A., Mashaghi, A., Hankemeier, T. & Vulto, P. An end-user perspective on organ-on-a-chip: assays and usability aspects. *Curr. Opin. Biomed. Eng.* **1**, 15–22 (2017).
- Trietsch, S. J., Israëls, G. D., Joore, J., Hankemeier, T. & Vulto, P. Microfluidic titer plate for stratified 3D cell culture. *Lab. Chip.* **13**, 3548–3554 (2013).
- Wevers, N. R. et al. High-throughput compound evaluation on 3D networks of neurons and glia in a microfluidic platform. *Sci. Rep.* **6**, 38856 (2016).
- Vulto, P. et al. Phaseguides: a paradigm shift in microfluidic priming and emptying. *Lab. Chip.* **11**, 1596–1602 (2011).
- Giepmans, B. N. G. & van Ijzendoorn, S. C. D. Epithelial cell–cell junctions and plasma membrane domains. *Biochim. Biophys. Acta. Biomembr.* **1788**, 820–831 (2009).
- Liang, T. W. et al. Characterization of huJAM: evidence for involvement in cell–cell contact and tight junction regulation. *Am. J. Physiol. Cell Physiol.* **279**, C1733–C1743 (2000).
- Lever, J. E. Inducers of mammalian cell differentiation stimulate dome formation in a differentiated kidney epithelial cell line (MDCK). *Proc. Natl. Acad. Sci. USA.* **76**, 1323–1327 (1979).
- Chantret, I., Barbat, A., Dussaux, E., Brattain, M. G. & Zweibaum, A. Epithelial polarity, villin expression, and enterocytic differentiation of cultured human colon carcinoma cells: a survey of twenty cell lines epithelial polarity, villin expression, and enterocytic differentiation of cultured human colon carcinoma. *Cancer Res.* **48**, 1936–1942 (1988).
- Pfister, A. B., Wood, R. C., Salas, P. J. I., Zea, D. L. & Ramsauer, V. P. Early response to ErbB2 over-expression in polarized Caco-2 cells involves partial segregation from ErbB3 by relocalization to the apical surface and initiation of survival signaling. *J. Cell. Biochem.* **111**, 643–652 (2010).
- Johnson, L. R. *Physiology of the Gastrointestinal Tract*. (Academic Press, 2012).
- Belmokhtar, C. A., Hillion, J. & Ségal-Bendirdjian, E. Staurosporine induces apoptosis through both caspase-dependent and caspase-independent mechanisms. *Oncogene.* **20**, 3354–3362 (2001).
- Oshima, T., Miwa, H. & Joh, T. Aspirin induces gastric epithelial barrier dysfunction by activating p38 MAPK via claudin-7. *Am. J. Physiol. Cell. Physiol.* **295**, C800–C806 (2008).
- Ricchi, P. et al. Effect of aspirin on cell proliferation and differentiation of colon adenocarcinoma Caco-2 cells. *Int. J. Cancer* **73**, 880–884 (1997).
- Matsui, H. et al. The pathophysiology of non-steroidal anti-inflammatory drug (NSAID)-induced mucosal injuries in stomach and small intestine. *J. Clin. Biochem. Nutr.* **48**, 107–111 (2011).
- Schindelin, J. et al. Fiji: an open-source platform for biological-image analysis. *Nat. Methods* **9**, 676–682 (2012).

Acknowledgements

We thank Professor Dr Hans Tanke for the use of the imaging facilities at the Department of Molecular Cell Biology, Leiden University Medical Center, and Joop Wiegant and Annelies van der Laan for their assistance. We thank Kitty Joore for generating artist impressions. E.N. and A.N. were supported by the EU Horizon 2020 program under project 674983 (Mimic) and 641639 (Biopol), respectively.

Author contributions

S.J.T. developed the concept of tube-formation in OrganoPlates and is responsible for the statistical data analysis and image processing. E.N. and M.C.S. performed all the experiments and produced the images. A.N., C.P.N., and M.K.V. developed the assay methods, K.J.W. and D.K. supervised the research, and H.L.L., D.K., and A.M. contributed to the experimental design and interpretation of the data. P.V. wrote the manuscript with comments from the authors. J.J., P.V., S.K., A.R., T.H., and A.M. oversaw the research.

Additional information

Supplementary Information accompanies this paper at doi:10.1038/s41467-017-00259-3.

Competing interests: S.J.T., E.N., M.C.S., M.K.V., K.J.W., H.L.L., A.N., C.P.N., D.K., J.J., and P.V. are employees of MIMETAS BV, the Netherlands, which is marketing the OrganoPlate. P.V., J.J., T.H. and S.J.T. are shareholders of that same company. OrganoPlate is a trademark of MIMETAS. A.R., S.K., and A.M. are employees of F. Hofmann-LaRoche Ltd and A.M. is a shareholder of F. Hofmann-LaRoche Ltd.

Reprints and permission information is available online at <http://npg.nature.com/reprintsandpermissions/>

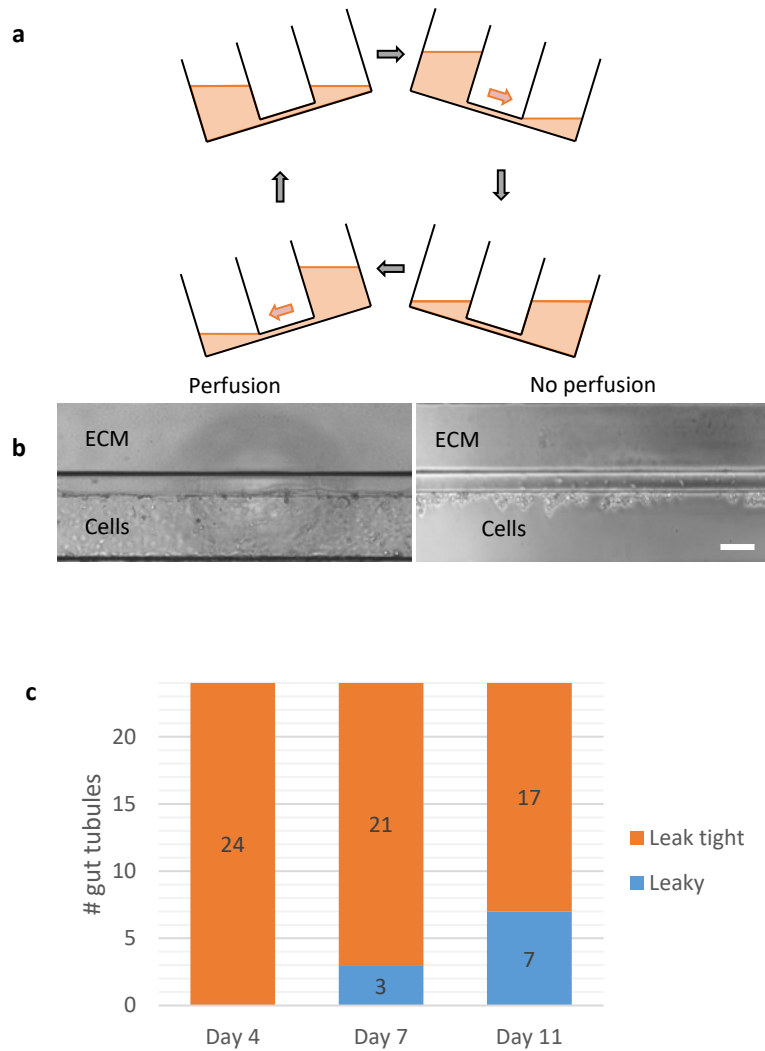
Publisher's note: Springer Nature remains neutral with regard to jurisdictional claims in published maps and institutional affiliations.



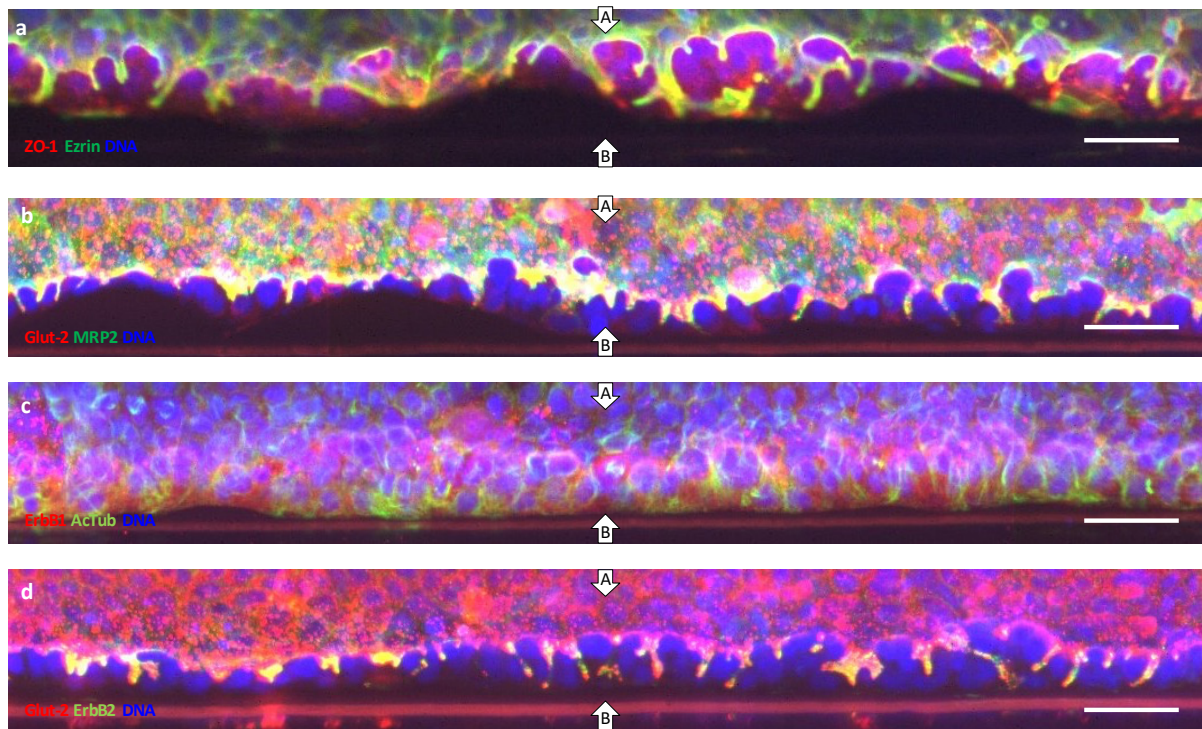
Open Access This article is licensed under a Creative Commons Attribution 4.0 International License, which permits use, sharing, adaptation, distribution and reproduction in any medium or format, as long as you give appropriate credit to the original author(s) and the source, provide a link to the Creative Commons license, and indicate if changes were made. The images or other third party material in this article are included in the article's Creative Commons license, unless indicated otherwise in a credit line to the material. If material is not included in the article's Creative Commons license and your intended use is not permitted by statutory regulation or exceeds the permitted use, you will need to obtain permission directly from the copyright holder. To view a copy of this license, visit <http://creativecommons.org/licenses/by/4.0/>.

© The Author(s) 2017

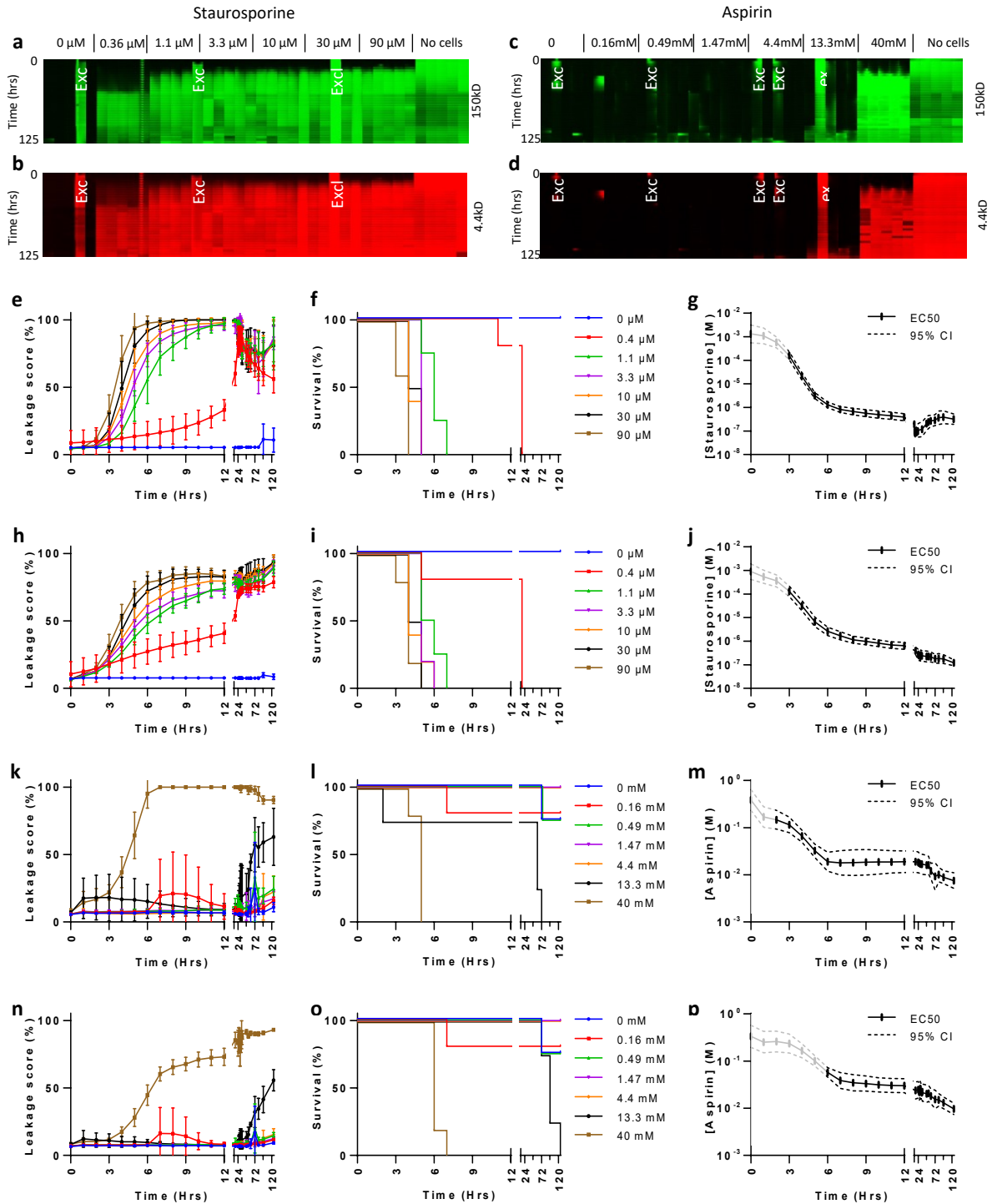
File name: Supplementary Information
Description: Supplementary Figures



Supplementary Fig. 1 | Flow induction in OrganoPlate. (a) Flow is induced by leveling between two reservoirs that are connected by the perfusion channel. By placing the plate under an angle on an interval rocker that inverts the angle at regular intervals, a continuous bi-directional flow through the perfusion channel is induced. **(b)** Influence of flow on tube formation: A confluent tube of Caco-2 cells is formed within three days when perfused (left), while few cells survive culture without perfusion (right). Scale bars are 100 μm. **(c)** Number of leak tight and leaky tubes in a single experimental run. Fluorescence intensity in the gel is measured and normalized to the fluorescence level in the tube channel. Upon crossing a threshold value of 0.4, a tube is considered leaky. At day 4 all tubes are leak tight, while at day 11 approximately 29% of tubes are leaking.

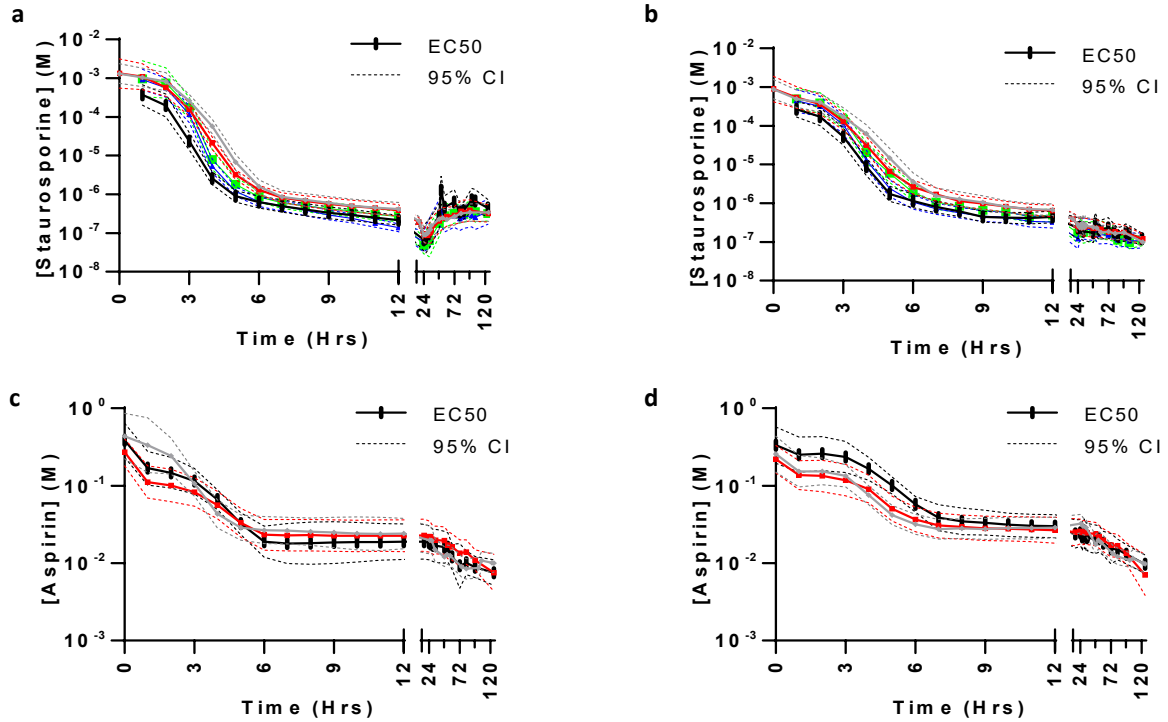


Supplementary Fig. 2 | Tubule characterization by immunofluorescent staining. Z-slices at higher magnification of confocal fluorescence micrographs of tubes from **fig. (2)** focusing on barrier morphology against ECM at approx. 50 μm above the bottom of the tube. An optical slice of the cells attached to the ECM is shown with white arrows indicating the apical (A) and basal (B) sides. The tube is stained for tight junctions (ZO-1 in red) and brush borders (Ezrin in green) showing apical positioning of Ezrin indicating polarization of the tube and invaginations expressing transport proteins. **(b)** expression of glucose and MRP2 transporters respectively stained with Glut-2 in red and MRP2 stain in green. Both stains clearly stain the apical side of the tube. **(c)** ErbB1 (red) and acetylated tubulin (green) expression. **(d)** Co-staining of Glut-2 transporter (red) and ErbB2 receptor (green); ErbB2 is primarily expressed pericellularly (here appearing as yellow). All tubes are fixated after four days in culture. Scale bars in white are 50 μm . Images are representative of at least three biological and at least three technical replicates.

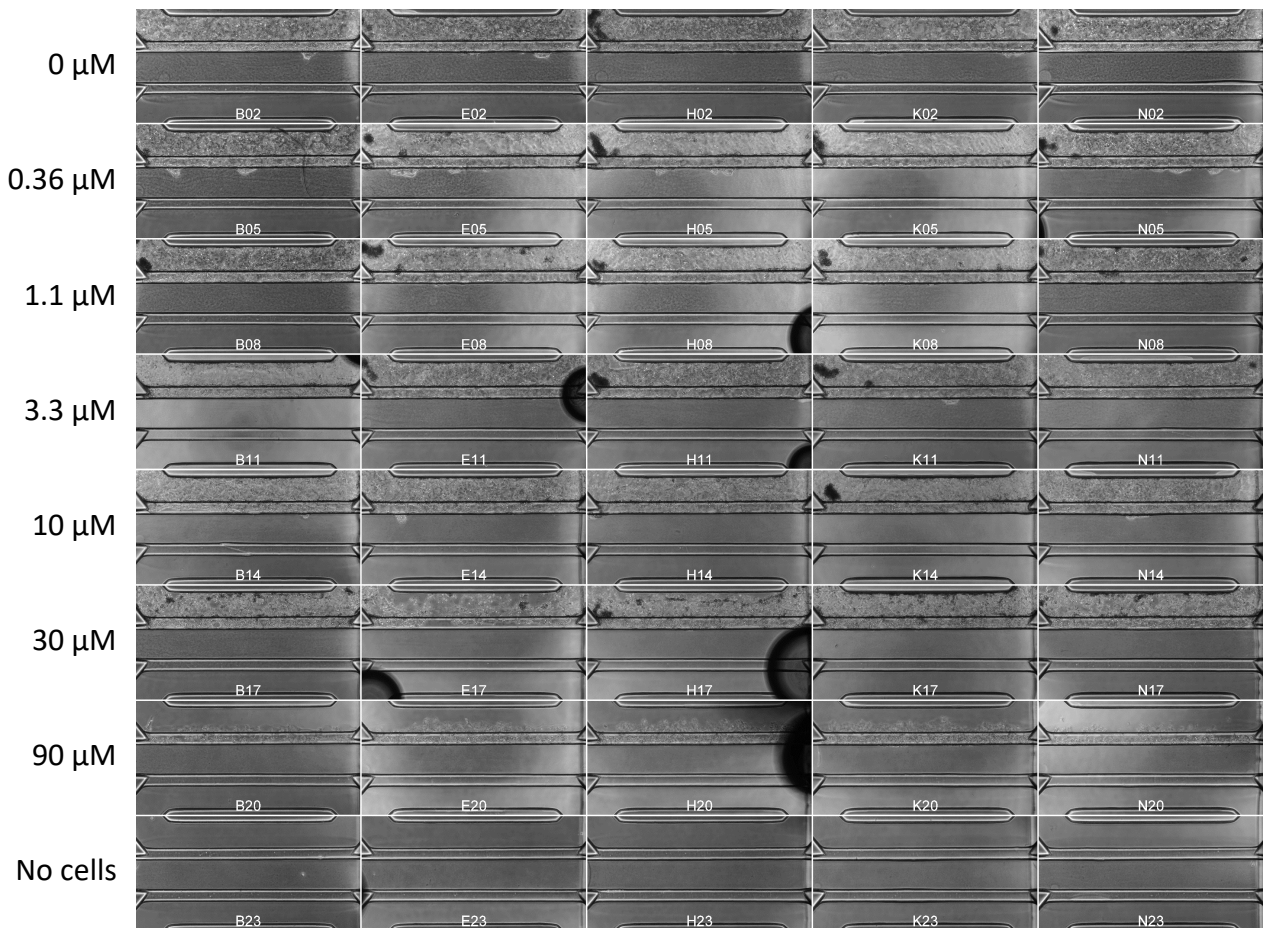


Supplementary Fig. 3 | Replicate of the experimental series in Figure 4 using cells at a different passage number, in which loss of barrier integrity is observed over time in a concentration-dependent manner for staurosporine (a, b, e-j) and aspirin (c, d, k-p). (a-d) Array of fluorescence micrographs of the gel region showing distribution of the 150kDa FITC-Dextran (a, c) and 4.4kDa TRITC-Dextran (b, d) over time and as a function of compound concentration; the loss of barrier integrity is shown by an increased fluorescent signal. Measurements are taken at 1-hour intervals up to 12 hours, at 16 hours, from 24 to 36 hours at 1-hour interval, and at 48, 53, 60, 72, 82, 96 and 125 hours. In between each interval, the OrganoPlate was placed back into the incubator on the interval rocker platform. Five technical

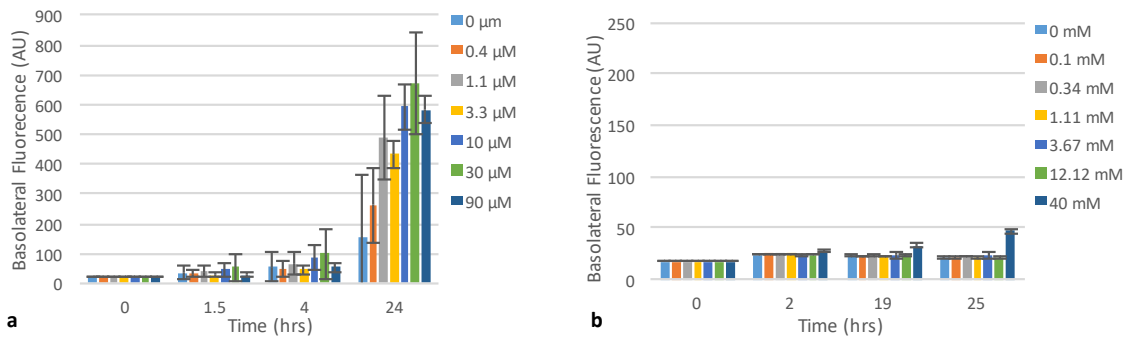
replicates of each concentration of a compound were measured on one single plate. Seven tubes were excluded from further data analysis, because the tubes appeared leaky at the first measurement (indicated with “Excl^{*}”) and one run was excluded because of a pipetting error (indicated with “Excl^{**}”). **(e, h, k, n)** The progression of the loss of barrier function over time is plotted as the ratio between fluorescent signal in apical and basal regions for the various concentrations of staurosporine **(e, h)** and aspirin **(h, n)**; **(e, k)** show barrier integrity measurement using 150 kDa FITC dextran as a leakage marker, while **(h, n)** show barrier integrity measurement using 4.4 kDa TRITC-dextran as a leakage marker. The plotted line is the mean of 5 technical replicate exposures minus excluded datapoints and error bars depict the standard deviation **(f, i, l, o)** Kaplan-Meier curves were generated where survival was defined as showing a leakage score below 40%. Overlapping curves were shifted by 1% for clarity purposes. **(g, j, m, p)** EC50 values as a function of exposure time. EC50 values were obtained by fitting a concentration response curve at each time point based on non-linear regression of normalized leakage scores using standard slope. EC50 values obtained from time points before the first event in the Kaplan-Meier plot, as indicated by grayed out line, should be interpreted with caution as the curve fit could be dominated by noise rather than biological effect. Technical replicates represent tubes seeded on the same plate and exposed in the same experimental session. Further independent replicate series for both staurosporine and aspirin are compared in **Supplementary Fig. 4**.



Supplementary Fig. 4 | Overlay of EC50 time curves of staurosporine and aspirin. The robustness of the assay was evaluated by comparing multiple replicate series of the experiments depicted in figure 4 and S13 executed in separate experimental sessions using cells at different passage numbers. The EC50 time curves were generated for 5 independent staurosporine studies (**a**, **b**) and 3 independent aspirin studies (**c**, **d**). Figures **a**, **c** show results for 150kDa FITC-Dextran and figures **b**, **d** show results for 4.4kDa TRITC-Dextran. Independent experimental series show comparable results, confirming the robustness of the assays. The EC50 curves represent a total of 330 Caco-2 tubes and over 18,000 datapoints.



Supplementary Fig. 5 | Phase contrast images of Caco-2 tubes after 96 hours of staurosporine exposure. Even though all concentration already show leakage at this time point, a confluent monolayer is still observed at all but the highest concentration. At 90 μM tubes have fully deteriorated. Dead cells detach and are flushed away by the perfusion flow. Images are representative of 5 experimental series in quintuplicate.



Supplementary Fig. 6 | Barrier integrity on Caco-layers in conventional Transwell systems exposed to (a) staurosporine and (b) aspirin. Caco-2 cells were seeded at a density of 60×10^3 cells/cm² on 6.5 mm polyester Transwell inserts with 0.4 μm pores. Media was replaced three times per week (DMEM, 10% FCS, 1% NEAA, glutamax, p/s) for three weeks. After three weeks, the apical medium was replaced with 250 μL of medium containing a fluorescent probe (150kD FITC dextran) and staurosporine (a) or aspirin (b) at varying concentrations. The basolateral media was replaced with 550 μL fresh medium. At various time points, 75 μL basolateral medium was sampled to perform fluorescence measurements using a Fluoroskan FL plate reader. 75 μL fresh medium was added after the aspirin 2hr timepoint to maintain sufficient sample for the remaining sampling time points. Fresh medium was used for 0 hour measurements. Four technical replicas were used for aspirin at 0 to 0.34 mM and three for the remaining concentrations. For staurosporine 4, 3, 3, 3, 4, 3, and 4 replicates were performed at 0, 0.4, 1.1, 3.3, 10, 30 and 90 μM respectively.

Chapter 5

Development of a Gut-on-a-Chip Model for High Throughput Disease Modelling and Drug Discovery

The main goal of the study was to further develop the simple gut-on-a-chip model based on Caco-2 to mimic IBD-like characteristics and to validate this model applicability for high throughput target screening and drug discovery.

The main results of this research have been published in the International Journal of Molecular Sciences on 12th of November 2019 and the manuscript went through a peer review process.

Authors contributions

I was responsible for designing and performing the experimental work (included in the manuscript : figure 1, together with CB figure 2 and figure 4, and part of figure 5). I performed the data analysis and co-wrote the manuscript with comments from authors.

.



Article

Development of a Gut-on-a-Chip Model for High Throughput Disease Modeling and Drug Discovery

Claudia Beurivage ^{1,2,†}, Elena Naumovska ^{2,3,†}, Yee Xiang Chang ¹, Edo D. Elstak ¹ , Arnaud Nicolas ³, Heidi Wouters ¹, Guido van Moolenbroek ³ , Henriëtte L. Lanz ³, Sebastiaan J. Trietsch ³, Jos Joore ³ , Paul Vulto ³, Richard A.J. Janssen ¹, Kai S. Erdmann ², Jan Stallen ^{1,*} and Dorota Kurek ^{3,*}

¹ Galapagos BV, Zernikedreef 16, 2333 CL Leiden, The Netherlands; claudia.beurivage@glpg.com (C.B.); y.x.chang@students.uu.nl (Y.X.C.); edo.elstak@glpg.com (E.D.E.); Heidi.Wouters-EXT@glpg.com (H.W.); richard.janssen@glpg.com (R.A.J.J.)

² Department of Biomedical Sciences, University of Sheffield, Western Bank, Sheffield S10 2TN, UK; e.naumovska@mimetas.com (E.N.); k.erdmann@sheffield.ac.uk (K.S.E.)

³ Mimetas BV, J.H. Oortweg 16, 2333 CH Leiden, The Netherlands; a.nicolas@mimetas.com (A.N.); g.t.van.moolenbroek@umail.leidenuniv.nl (G.v.M.); h.lanz@mimetas.com (H.L.L.); s.trietsch@mimetas.com (S.J.T.); j.joore@mimetas.com (J.J.); p.vulto@mimetas.com (P.V.)

* Correspondence: jan.stallen@crl.com (J.S.); d.kurek@mimetas.com (D.K.); Tel.: +31-7170-20012 (J.S.); +31-8588-83161 (D.K.)

† These authors contributed equally to this work.

Received: 3 October 2019; Accepted: 8 November 2019; Published: 12 November 2019



Abstract: A common bottleneck in any drug development process is finding sufficiently accurate models that capture key aspects of disease development and progression. Conventional drug screening models often rely on simple 2D culture systems that fail to recapitulate the complexity of the organ situation. In this study, we show the application of a robust high throughput 3D gut-on-a-chip model for investigating hallmarks of inflammatory bowel disease (IBD). Using the OrganoPlate platform, we subjected enterocyte-like cells to an immune-relevant inflammatory trigger in order to recapitulate key events of IBD and to further investigate the suitability of this model for compound discovery and target validation activities. The induction of inflammatory conditions caused a loss of barrier function of the intestinal epithelium and its activation by increased cytokine production, two events observed in IBD pathophysiology. More importantly, anti-inflammatory compound exposure prevented the loss of barrier function and the increased cytokine release. Furthermore, knockdown of key inflammatory regulators *RELA* and *MYD88* through on-chip adenoviral shRNA transduction alleviated IBD phenotype by decreasing cytokine production. In summary, we demonstrate the routine use of a gut-on-a-chip platform for disease-specific aspects modeling. The approach can be used for larger scale disease modeling, target validation and drug discovery purposes.

Keywords: inflammation; inflammatory bowel disease; gut-on-a-chip; Organ-on-a-Chip; microfluidic; drug discovery; disease modeling

1. Introduction

Inflammatory bowel disease (IBD), including ulcerative colitis (UC) and Crohn's disease (CD), is a complex chronic idiopathic disease severely incapacitating the life of more than 2.5 to 3 million Europeans, bringing a high socio-economic burden to society [1–3]. The aetiology of the disease remains elusive; however, it is known to involve the interaction of genetic, environmental, microbiological and immunological factors [3,4]. There is a general consensus in the scientific community that IBD arises from a dysregulated activation of immune effectors in response to commensal microbiota, which

is triggered by environmental factors in a genetically-susceptible host [5,6]. Important and frequent primary events in IBD include loss of function of the epithelial barrier and an impaired balance between pro- and anti-inflammatory mediators secreted by intestinal epithelial cells (IECs) or immune cells [6,7].

The multifactorial nature of IBD makes it extremely difficult to develop realistic disease models that will be able to grasp and recapitulate the complexity of the disease development and progression. This is particularly important knowing that 25% to 30% of patients fail to respond to standard IBD therapy and more than 20% have to discontinue ongoing treatments due to unforeseen side-effects [8]. The need for deeper understanding of the disease's mechanisms and for the development of new medicines is therefore urgent.

Different *in vivo*, *ex vivo* and *in vitro* models are currently used to study IBD aetiology [9–12]. Despite the interspecies difference, animal models have proven to be extremely useful to understand IBD mechanisms such as the essential role of microbiota and T cells [13,14]. However, manipulation of individual IBD parameters, such as barrier function of the epithelium and cell-type specific activation, are difficult to achieve in these complex models, which proves to complicate matters and in turn leads to poor prognosis of drug candidates [15]. Furthermore, from a drug discovery perspective, high throughput screening of compounds cannot be achieved in such models. On the other hand, *ex vivo* models such as intestinal explants come from a limited source with an extremely limited lifespan, making them unsuitable for drug discovery purposes [10,16,17]. Standard *in vitro* setups usually include the static culture of epithelial cells on rigid membranes separating two different chambers, sometimes comprising an immune component [18]. Such conventional membrane insert-based systems, often called 2.5D or Transwell systems, are a useful tool with medium throughput but do not recapitulate 3D cell organization, which has proven to be important for increased physiological relevance [19]. Given the limitations of existing models, there is a need for a tool that will mimic key aspects of IBD in a robust manner that is compatible with high throughput screening equipment.

The recently emerged field of Organ-on-a-Chip technology offers a potential alternative to traditional 2D cell cultures and animal models. Recent studies have shown enormous progress in both gut-on-a-chip and IBD research [20,21]. In most cases, chips made out of a silicon rubber material are seeded with either cell lines, induced pluripotent stem cells (iPSCs) or Lgr5⁺-derived organoids [22,23]. These studies are extremely valuable to assess the impact of micro engineering techniques on the physiological relevance of cell culture models. Nevertheless, there are some shortcomings associated with such silicon rubber chips including the lack of scalability and the reduction of bioavailability of some drugs and small molecules due to unspecific adsorption [24,25].

To overcome these limitations and to allow the integration of Organ-on-a-Chip in the drug development process, we further adapted a recently published gut-on-a-chip system [26] to mimic inflammatory conditions. This model, based on the use of Caco-2 cells, has already been proven to be easy-to-use, robust and reproducible as well as relatively fast; Caco-2 cells form 3D leak-tight polarized tubules with accessible apical and basal sides after only 4 days of culture. The platform we used in this study, the OrganoPlate, offers a high throughput alternative to silicon rubber chips and allows compound screening due to its glass composition.

To mimic inflammatory characteristics in this model, we applied an optimised immune-relevant cytokine trigger that mimics the effect of *E. coli*-activated dendritic cells (DCs) on the IECs [27–29]. We assessed the effect of this trigger on two main aspects of IBD—the integrity of the intestinal barrier as well as the cellular activation of IECs. To assess barrier integrity, we measured transepithelial electrical resistance (TEER) values of Caco-2 tubules in a high throughput manner and assessed the localisation of cell junction-associated protein E-CADHERIN. The production of epithelial-relevant inflammatory cytokines by Caco-2 cells was used as a readout for cellular activation following trigger.

To assess the applicability of the model for target and drug discovery processes, we performed direct on-chip adenoviral transduction of validated shRNAs against proinflammatory targets RELA and MYD88. We further addressed the ability of the model to respond to a well-known anti-inflammatory compound, TPCA-1 [30,31]. Overall, our results show that this 3D model can be used as an *in vitro* tool

for drug development in an accelerated manner and opens the way to more physiologically relevant models usable in high throughput experiments.

2. Results

2.1. Establishing Leak-Tight 3D Caco-2 Tubules Controlled by TEER Measurements

In this study, we employed the OrganoPlate platform in order to establish a 3D in vitro model recapitulating key IBD characteristics. We successfully established this IBD model by adapting our previously published gut-on-a-chip model where Caco-2 cells grow in 3D tubules following medium perfusion [26]. Figure 1 shows the 3-lane OrganoPlate where 40 microfluidic chips are organized at the bottom side of a standard 384-well plate format (Figure 1A). Each of these chips has three microfluidic channels with dedicated inlets and outlets as well as an observation window allowing real-time monitoring of the 3D culture (Figure 1B). An extracellular matrix (ECM) precursor is loaded into the middle channel and patterned with a surface tension technique called phase guiding [32]. After gelation, fluids can be inserted in adjacent channels, allowing membrane-free co-culture of several cell types. In our study, we seeded Caco-2 cells in the top channel against an ECM gel while the bottom channel was kept free of cells (Figure 1C). Data from our previous study showed that, upon medium perfusion, Caco-2 cells form a complete and polarized leak-tight tubule after 4 days of culture in OrganoPlate (Figure 1D). In those earlier studies, we determined the barrier integrity using a FITC-labeled dextran leakage assay [26]. In the current study, we assessed the barrier integrity by measuring the transepithelial electrical resistance (TEER) values of the Caco-2 tubules, leading to more sensitive and accurate data [33]. We show that the TEER values of Caco-2 tubules continuously increase and stabilise after 4 days of culture until the end of the experimentation (Figure 1E).

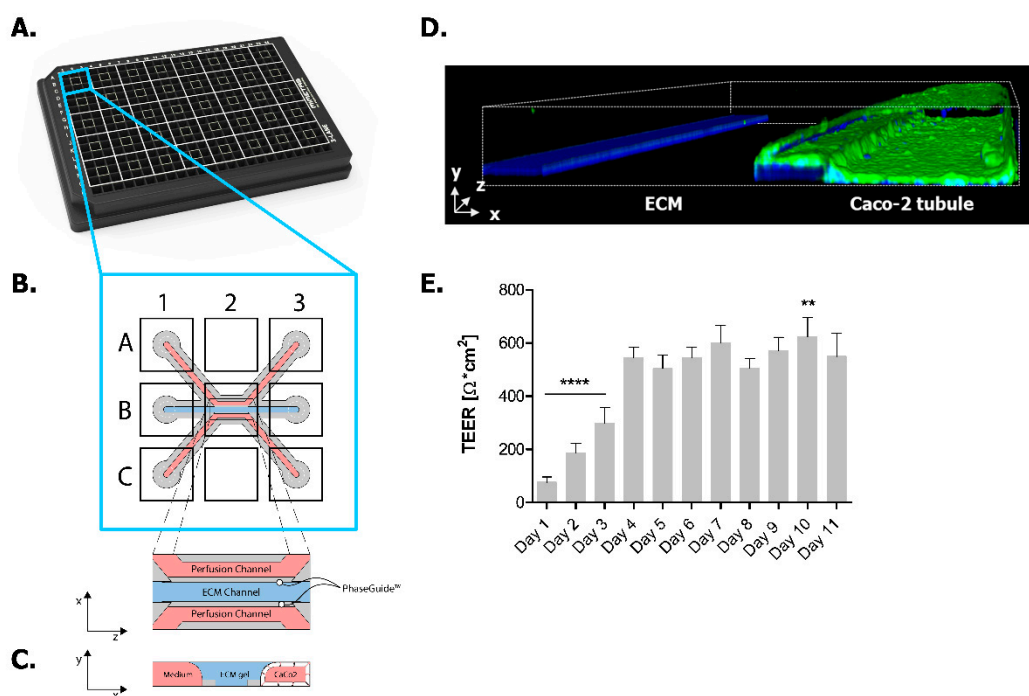


Figure 1. Caco-2 tubules in the 3-lane OrganoPlate. (A) Photograph of the 3-lane OrganoPlate. Each plate contains 40 individual microfluidic chips. (B) Schematic representation of a microfluidic chip; each chip has three microfluidic channels each containing two medium channels (pink) and a gel channel (blue). Each channel has an inlet (A1, B1 and C1) and an outlet (A3, B3 and C3). Real-time imaging is done through the observation window (B2). (C) Transversal view of a microfluidic view;

Caco-2 cells adhere to the ECM meniscus created by the PhaseGuide™ technology. Upon medium perfusion, Caco-2 cells form tubules covering the walls of the top channel. (D) 3D reconstruction image of a Caco-2 tubule at Day 4 stained for ACTIN (green) and DNA (blue), depicting the nuclei. (E) Transepithelial electrical resistance (TEER) values of Caco-2 tubules over time until Day 11. Data is represented as mean \pm SEM. ** $p < 0.01$; **** $p < 0.0001$ by one-way ANOVA with Dunnett's post-hoc test compared to Day 4 ($n = 13$).

2.2. Induction of Inflammatory State in Caco-2 Tubules

Based on previous literature [34], we optimised a cytokine cocktail that replicates the effect of *E. coli*-activated DCs on the cytokine secretion of Caco-2 cells in the Transwell system. We first optimised the composition of the trigger and found that a combination of IL-1 β , TNF- α and IFN- γ led to the highest cytokine production in Caco-2 cells (Figure A1). We then compared the trigger's effect to the effect of different concentrations of *E. coli*-activated DCs on the cytokine production of Caco-2 cells (Figure A2). The optimised trigger led to comparable cytokine production levels as the presence of *E. coli*-activated DCs by Caco-2 cells, supporting the immunological relevance of the cytokine cocktail as an inflammatory trigger.

We consequently adapted the concentration of the trigger to the OrganoPlate platform. Because of the difference between the Transwell and the OrganoPlate systems, which is mainly explained by the medium diffusion rate through the ECM gel in the OrganoPlate and in order to recapitulate the effects seen in the Transwell system, concentrations of 2, 100 and 100 ng/mL were set for IL-1 β , TNF- α and IFN- γ , respectively (results not-shown). Caco-2 cells were triggered basally at Day 4 or Day 7 leading to short or long trigger times. Overall, the morphology of Caco-2 cells did not change upon trigger. However, Caco-2 cells submitted to a prolonged inflammatory trigger frequently started to invade the ECM (Figure 2A). As a change in the epithelium permeability is often an important event in IBD etiology [35], we assessed whether the cytokine trigger affected the TEER values of the tubules. The TEER values increased over time in non-triggered Caco-2 tubules (Figure 2B). However, upon triggering, the TEER values of the Caco-2 tubules decreased significantly for all trigger times when compared to non-triggered conditions. The prolonged trigger resulted in the lowest TEER values (Figure 2B).

To assess the effect of the inflammatory trigger on the cellular activation of Caco-2 cells, the production of epithelial cytokines IP-10, IL-8 and CCL-20 were quantified. Caco-2 cells secreted low amounts of these epithelial cytokines in non-triggered conditions (Figure 2C–E). After trigger, both apical and basal secretion of all analyzed cytokines was increased significantly, with no major differences between short and long trigger times (Figure 2C–E). However, the effect of the long trigger on secretion of IL-8 was marginal (Figure 2D). In summary, both short and long inflammatory triggers induced a loss of barrier function of Caco-2 tubules as well as an increased cell activation, depicted with an elevated cytokine production in both apical and basal compartments.

In an attempt to further understand the impaired TEER values of the Caco-2 cells upon trigger, we investigated the expression levels and localisation pattern of the *zonula adherens* protein E-CADHERIN (ECAD). It has been reported that in vitro wounded HT-29 monolayer models as well as CD and UC tissue have reduced levels of ECAD membranous expression [36–38]. To determine if this also occurs in our model, we stained Caco-2 cells for ECAD and the cytoskeleton marker ACTIN (Figure 3A). The organisational pattern of the ECAD staining was segmented and quantified based on two characteristics: compactness and major axis length of signal. A disorganized epithelial cell layer will display a fragmented ECAD phenotype with short major axes and low compactness values. Short and prolonged triggers both induced a significant reduction of these two characteristics in Caco-2 cells (Figure 3B,C). The compactness of the ECAD signal also showed a reduction following the early short trigger (D4-D7), but for this condition there was no significant effect on the length of the major axis. The reduction in epithelial cell layer organization confirmed the reduced TEER values of the triggered

tubules. These results highlight that IBD-like conditions such as loss of barrier function and cytokine production can be induced in Caco-2 cells using a relevant cytokine trigger.

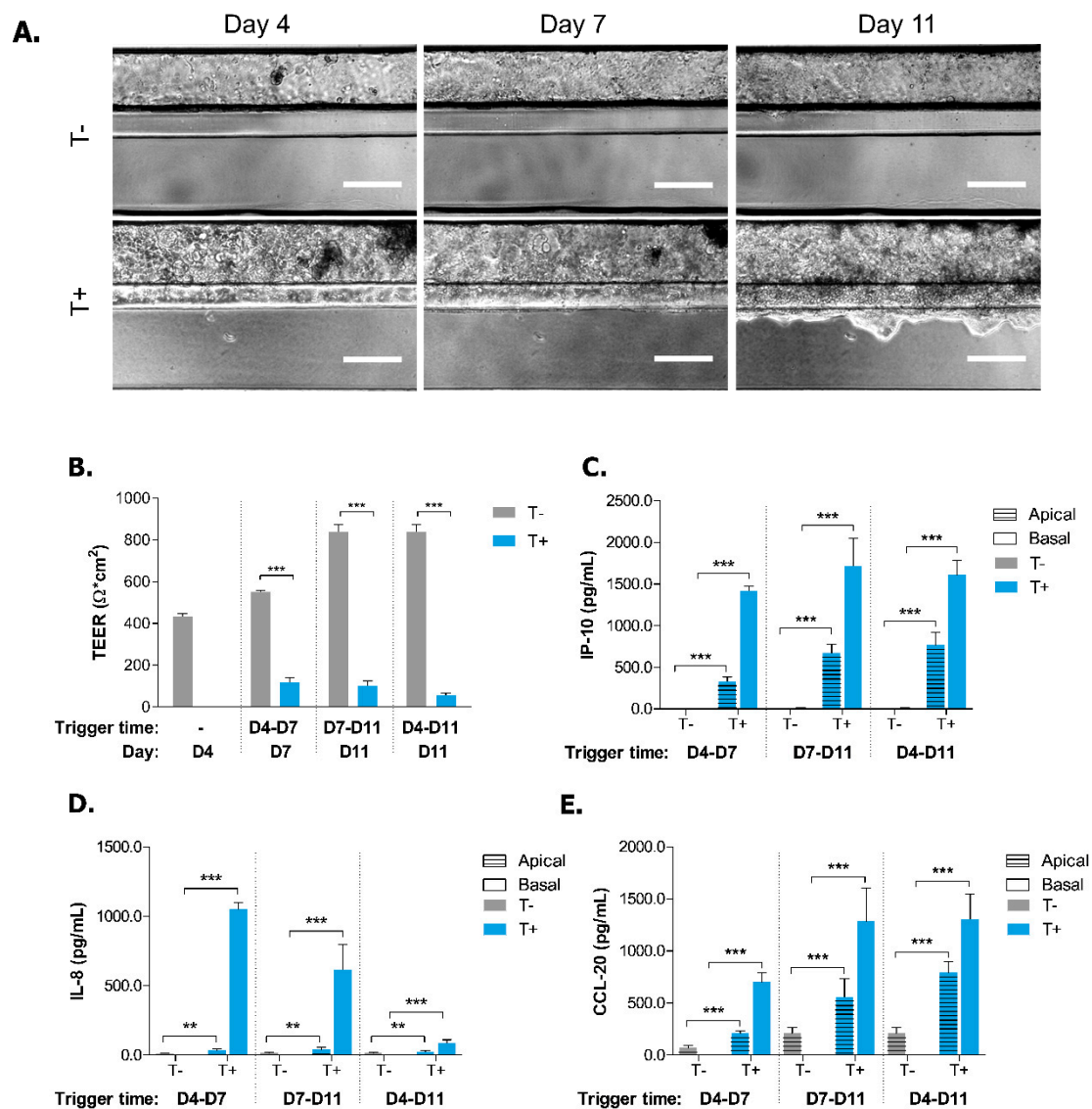


Figure 2. Effect of short and long cytokine trigger on morphology and integrity of Caco-2 tubules. (A) Representative 4X phase contrast images of triggered (T+) and non-triggered (T-) Caco-2 tubules at Days 4, 7 and 11. Scale bars = 100 μm . (B) TEER values of triggered (T+) and non-triggered (T-) Caco-2 tubules at Days 4, 7 and 11. Data is presented as mean \pm SEM. ** $p \leq 0.01$; *** $p \leq 0.001$ by two-way ANOVA with Bonferroni corrected post-hoc test compared to T- of each time point ($n = 3-10$). (C-E) Secretion of IP-10 (C), IL-8 (D) and CCL-20 (E) in apical and basal compartments of triggered (T+) and non-triggered (T-) Caco-2 tubules at Days 7 or 11. Data is represented as mean \pm SEM. * $p < 0.05$; ** $p < 0.01$; *** $p < 0.001$ by two-way ANOVA with ArcSinh transformation and Holm corrected post-hoc test and compared to apical and basal T- of each time point ($n = 3-5$).

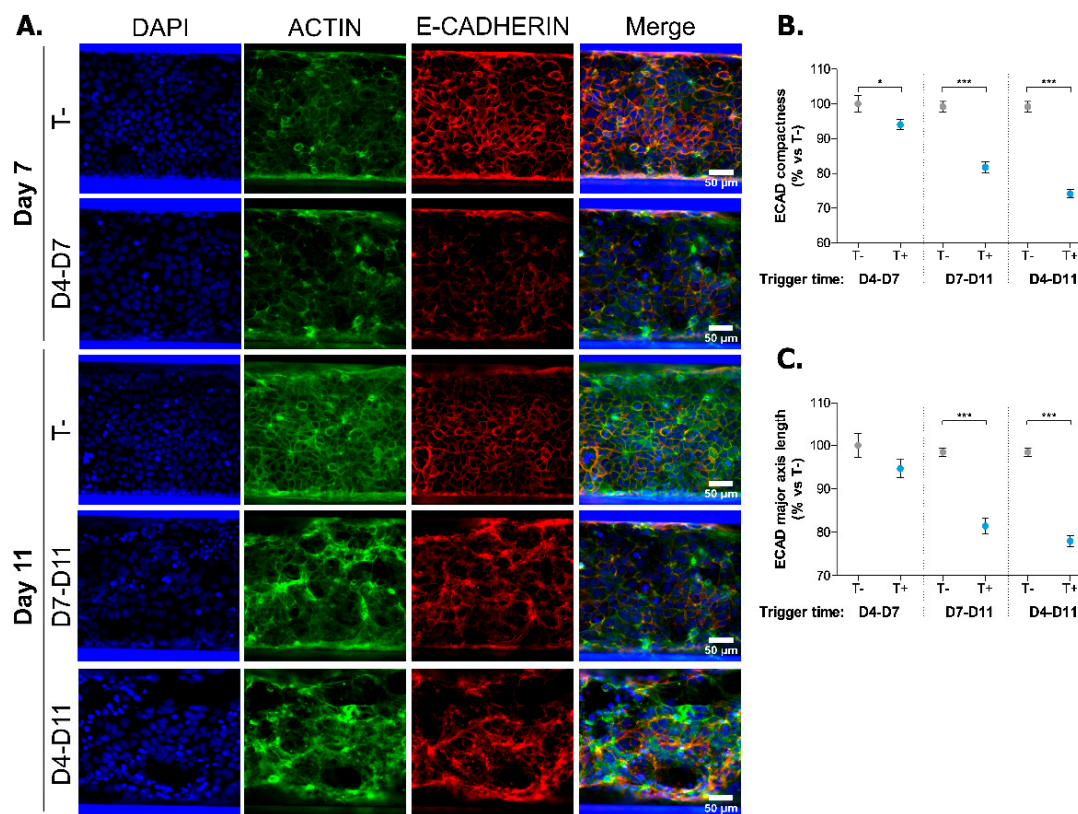


Figure 3. Short and long cytokine triggers induce morphological changes in Caco-2 tubules (A) Representative 20X images of Caco-2 tubules stained for cytoskeleton marker ACTIN, *zonula adherens* marker E-CADHERIN and nucleus marker DAPI at Day 7 and Day 11 in non-triggered (T-) or triggered (T+; D4–D7, D7–D11, D4–D11) conditions. Scale bars = 50 μm . (B,C) Compactness (B) and major axis length (C) of E-CADHERIN (ECAD) staining normalized to T- at Day 7. Data is represented as mean \pm SEM. * $p < 0.05$; *** $p < 0.001$ by two-tailed Student's *t*-test and compared to T- of each time point ($n = 8$ –14). Segmentation process of ECAD staining is showed in Figure A3.

2.3. Exposure to TPCA-1 Prevent the Inflammatory State of Caco-2 Tubules

In order to confirm the validity of our model for drug discovery purposes, we treated Caco-2 cells to a well-known anti-inflammatory compound, TPCA-1. TPCA-1 is a selective inhibitor of human I κ B kinase-2 (IKK-2) [30]. Under normal conditions, IKK-2 phosphorylates the inhibitor of NF- κ B (I κ B α). When phosphorylated, I κ B α releases NF- κ B allowing its nuclear translocation to activate transcription of numerous genes involved in inflammation. Therefore, by inhibiting IKK-2, TPCA-1 prevents the nuclear translocation of NF- κ B, leading to an anti-inflammatory effect.

Cells were exposed to TPCA-1 for two hours before a 72 h pro-inflammatory trigger was added in the continued presence of the compound. We determined the cytokine production levels in both the apical and basal supernatants. TPCA-1 induced a concentration-dependent inhibition of both apical and basal secretion of IP-10, IL-8 and CCL-20 by activated Caco-2 cells (Figure 4A–C). At concentrations of 5 and 20 μM , TPCA-1 could inhibit the secretion of all analytes to levels lower than non-triggered cells (results not shown). However, these higher TPCA-1 concentrations also suppressed the barrier integrity (Figure 4D) and the viability of the cells (Figure 4E). At a concentration of 1.25 μM , TPCA-1 led to a high percentage of inhibition (PIN) of cytokine production without significantly altering cell viability while restoring the barrier function of Caco-2 cells, when compared to triggered but TPCA-1 untreated tubules. These results clearly show that TPCA-1 exposure drastically decreases apical and basal cytokine secretion by Caco-2 cells and proves the suitability of the system to perform future compound exposure studies.

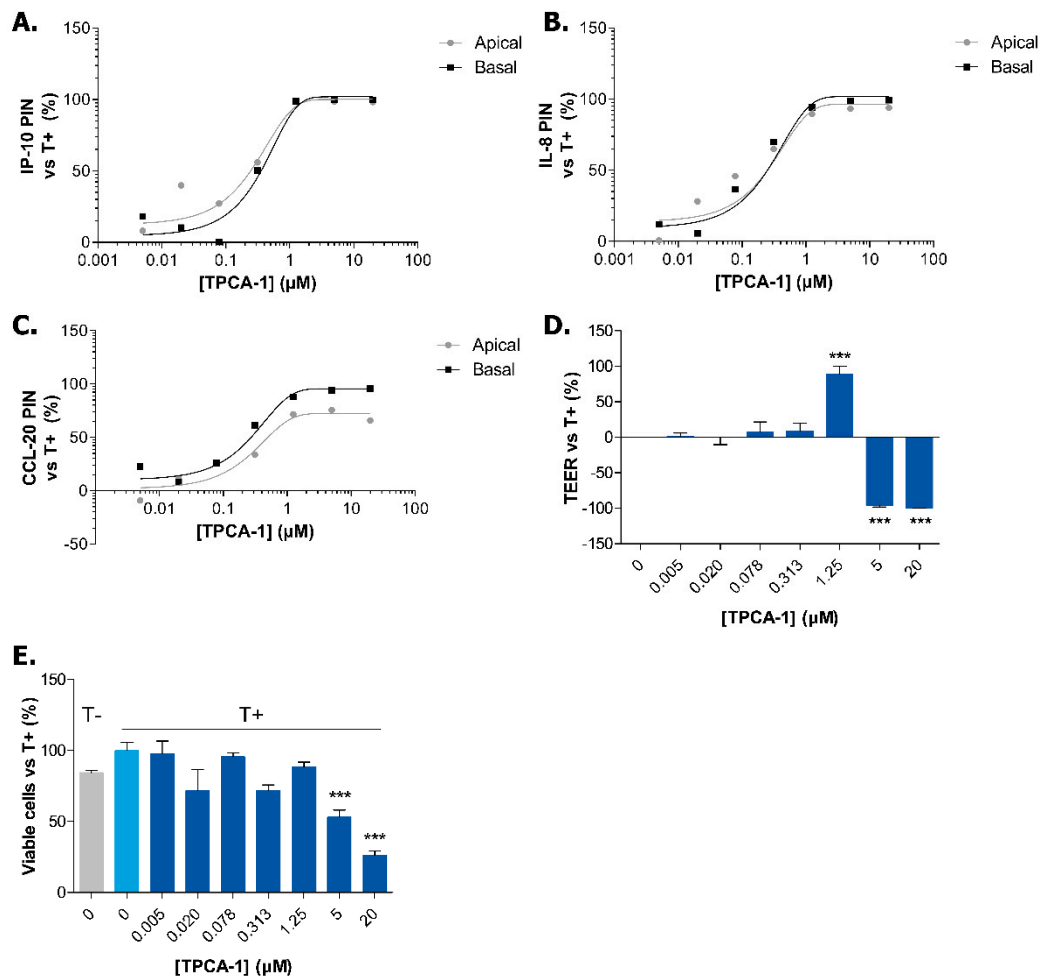


Figure 4. TPCA-1 exposure decreases cytokine secretion of Caco-2 tubules in a dose-dependent manner. (A–C) Percentage of inhibition (PIN) of IP-10 (A), IL-8 (B) and CCL-20 (C) secretion by Caco-2 cells at Day 7 following a 72 h TPCA-1 exposure in apical and basal compartments. Dots represent the PIN mean normalized to triggered (T+) but TPCA-1 untreated tubules. The line depicts a non-linear regression between [TPCA-1] and cytokine secretion ($n = 4-5$). (D) TEER values of TPCA-1 treated tubules at Day 7. Data is represented as percentage of triggered (T+) but TPCA-1 untreated tubules \pm SEM. *** $p < 0.001$ by one-way ANOVA with Dunnett's post-hoc test compared to triggered (T+) but TPCA-1 untreated tubules ($n = 3-5$). (E) Percentage of viable cells after TPCA-1 treatment at Day 7. Data is represented as percentage of triggered (T+) but TPCA-1 untreated tubules \pm SEM. *** $p < 0.001$ by one-way ANOVA with Dunnett's post-hoc test compared to triggered (T+) but TPCA-1 untreated tubules ($n = 3-4$).

2.4. Adenoviral Knockdown of Inflammatory Effectors Prevents IBD-like Phenotype in Caco-2 Tubules

To further evaluate whether the inflamed state of Caco-2 cells could be prevented, we designed and tested several putative negative- and positive-control recombinant shRNA-expressing adenoviruses (AdV; Tables A1 and A2) based on their ability to reduce CCL-20 production by Caco-2 cells (Figure A4). The results allowed us to select two non-targeting AdV (AdV-shmmNr1h3, AdV-shluc) and two AdV expressing validated shRNAs against MYD88 and RELA (AdV-shMYD88, AdV-shRELA) to be used in this study (Table 1). RELA is a subunit of NF- κ B, a main player in inflammatory pathways that controls the expression of various pro-inflammatory genes such as chemokines, cytokines and adhesion molecules [39]. MYD88 is an adaptor protein downstream in the Toll-like receptor (TLR) and IL-1 signaling pathway involved in innate immune responses [39].

We chose to transduce cells directly in the chip. Recently, microfluidic transduction has been shown to be faster and more efficient than static transduction using clinically processed GFP-carrying lentiviruses [40]. We demonstrate, for the first time, the use of direct on-chip adenoviral transduction to conduct knockdown studies. In order to evaluate the transduction efficiency of on-chip AdV-mediated delivery, Caco-2 cells were transduced with a recombinant AdV expressing a ZsGreen DNA (AdV-ZsGreen). Microscopic evaluation confirmed that the delivery of 5 infectious units (IU) of ZsGreen-carrying virus per cell resulted in almost 100% transduction of Caco-2 cells at Day 4 (Figure 5A,B). We thus concluded that transduction experiments could be efficiently performed directly in the OrganoPlate.

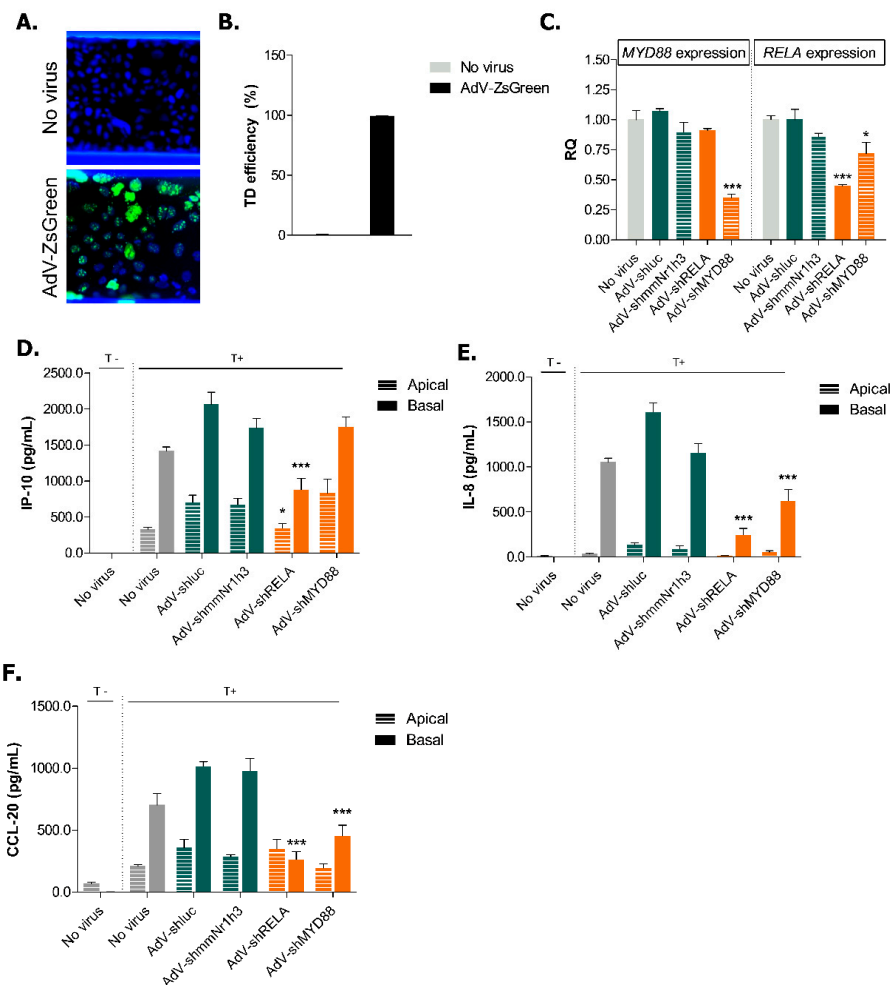


Figure 5. Efficient knockdown of inflammatory effectors decreases basal cytokine secretion in triggered Caco-2 tubules. (A) Representative 10× pictures of Caco-2 cells 72 h after on-chip transduction with a ZsGreen-carrying virus (AdV-ZsGreen). Green shows ZsGreen signal and blue shows DAPI signal. (B) On-chip transduction (TD) efficiency 72 h post-transduction. The number of ZsGreen-positive cells was quantified in 2 fields of 10X per chip and normalised to the number of total nuclei. Data is represented as mean ± SEM ($n \geq 4$). (C) Knockdown efficiency of *RELA* and *MYD88* at Day 11. Data is represented as mean ± SEM normalised to *GAPDH* expression. * $p < 0.05$; *** $p < 0.001$ by two-way ANOVA with Bonferroni post-test compared to no virus condition ($n = 2-3$). (D–F) Secretion of IP-10 (D), IL-8 (E) and CCL-20 (F) in apical and basal compartments of non-triggered and triggered Caco-2 tubules at Day 7. Data is represented as mean ± SEM. * $p < 0.05$; *** $p < 0.001$ by two-way ANOVA with ArcSinh transformation and Holm corrected post-hoc test compared to AdV-shluc ($n = 3-5$). The non-transduced condition is shown in grey, negative control viruses in green and viruses carrying shRNA for inflammatory effectors in orange.

Table 1. shRNA adenoviruses selected for the study.

Insert Name	Target Sequence
AdV-shluc	GGTACCTAAGGGTGTGGC
AdV_shmmNr1h3	CACACATATGTGGAGGCC
AdV_shMYD88	GGTCATCACTGTCTGCCA
AdV_shRELA	GATTGAGGAGAAACGTAAA

The knockdown efficiency was further assessed on Day 11 and confirmed a 65% reduction of *MYD88* mRNA expression by AdV-shMYD88 and a 55% reduction of *RELA* mRNA expression by AdV-shRELA (Figure 5C). Previous studies have shown that *Myd88*-knockout in murine bone marrow-derived macrophages show decreased levels of NF- κ B p65 subunit (RELA) activation following *Enterococcus faecalis* infection [41]. This suggests that MYD88 might be involved at some level in the regulation of RELA expression or activation, which could in turn explain the 28% reduction of *RELA* mRNA expression following MYD88 knockdown (Figure 5C).

After having confirmed that the adenoviral technology induces effective knockdown, we investigated how the knockdown of *RELA* and *MYD88* could alleviate the IBD phenotype in Caco-2 cells. We could not determine whether the knockdown could prevent the loss of barrier integrity as the adenoviral delivery of non-targeting constructs affected the TEER values of the Caco-2 tubules (Figure A5). We started by investigating if the cytokine production of Caco-2 cells in non-triggered conditions was affected. The adenoviral transduction itself induced the apical production of IP-10, CCL-20 and IL-8 by Caco-2 cells (Figures A6 and 5D–F). However, when compared to the negative control AdV-shluc, *MYD88* knockdown reduced both the apical and basal production of IL-8 as well as the basal production of CCL-20 in non-triggered conditions (Figure A6). The knockdown of *RELA* reduced the apical production of IP-10, both the apical and basal production of IL-8 but did not affect CCL-20 production. However, the production of these pro-inflammatory cytokines in Caco-2 cells is low in non-triggered conditions (note the difference in the range of the Y-axis in Figure A6 in comparison to the triggered samples in Figure 5D,F). However, we were particularly interested to know whether we could prevent the IBD phenotype establishment in our model and we therefore analyzed cytokine production in triggered Caco-2 cells. Compared to AdV-shluc, AdV-shRELA significantly inhibited the apical and basal secretion of IP-10 (Figure 5D) as well as the basal secretion of both IL-8 and CCL-20 (Figure 5E,F). The reduced expression of *MYD88* also caused a decrease in secretion of basal IL-8 and CCL-20 (Figure 5E,F). We did not observe a complete reduction of cytokine production after *RELA* and *MYD88* knockdown likely due to partial redundancy in underlying signaling pathways leading to cytokine production and due to incomplete knockdown. However, we show that our model could lead to potential target discovery, even by using a trigger composed of a mixture of different cytokines.

3. Discussion

When developing new disease models, users presently often have to choose between the level of throughput they want to achieve and the physiological relevance of their model. From a drug development perspective, achieving a high level of throughput is an important factor to consider as it significantly decreases the time and costs associated with screening activities. The Organ-on-a-Chip technology offers a valid alternative that promises increased throughput while achieving higher physiological relevance when compared to current traditional membrane inserts such as Transwells. When compared to membrane inserts, the OrganoPlate platform used in this study decreases media and reagent consumption by up to 10-fold depending on the assay, while offering an increased scalability. Furthermore, it also decreased the experimental time needed to obtain a differentiated epithelium from 21 days to only 4 to 5 days [26]. In comparison with silicon-based microfluidic chips, the OrganoPlate offers an easy-to-handle technology on a 384-well plate format that is tube- and pump-free and compatible with all lab instruments and high content imagers. Furthermore, Organ-on-a-Chip technology could be of great interest to pharmaceutical companies as one recent estimate anticipates

an overall reduction of 10% to 26% in total research and development costs if organs-on-a-chip are implemented in a standard drug development process [42–44].

In this study, we show a robust and reliable 3D gut-on-a-chip model that can be used in drug discovery. More importantly, by applying specific downstream cues of immune activation on Caco-2 cells, we were able to recapitulate key physiological aspects of IBD pathology; the loss of barrier integrity and an increased cytokine production.

For the first time, we could simultaneously monitor the barrier integrity of 40 membrane-free Caco-2 tubules in a real-time manner by measuring the TEER values of the tubules. In non-triggered conditions, Caco-2 tubules could reach up to 600–800 $\Omega\cdot\text{cm}^2$ in TEER values after 11 days of culture. Upon inflammatory trigger, we show a significant reduction in TEER values, highlighting the impaired barrier function of the tubules. In the Transwell system, the TEER values of Caco-2 monolayers generally vary between 250–400 $\Omega\cdot\text{cm}^2$, but TEER values as high as 1200 $\Omega\cdot\text{cm}^2$ have also been reported [33,45,46]. We have also observed slight variations in the TEER values of non-triggered Caco-2 tubules over different experiments. Variations in TEER values have been reported before due to factors such as temperature, medium formulation, cell culture period and passage number of cells [33]. This high variability in the range of TEER values of Caco-2 cells makes it difficult to fully integrate our results in the light of recent literature and to understand their physiological relevance. Recent studies have also started to further investigate the problematic in order to understand the variation in TEER values between the Transwell system and microfluidic platforms [47]. Nevertheless, this novel method allowed us to constantly monitor the barrier integrity of Caco-2 tubules in order to further validate the Caco-2 gut-on-a-chip model previously described [26], before establishing IBD-like conditions.

It was previously shown that protein expression of IL-1 β [48] and IFN- γ [49] as well as mRNA expression of IFN- γ [50,51] are upregulated in the mucosa of patients with active IBD. Our data clearly demonstrates that an inflammatory state, reflected by an increased cell activation and a decreased barrier function, can be induced in the Caco-2 gut-on-a-chip model following trigger with immune-relevant cytokines IL-1 β , IFN- γ and TNF- α . Since cell activation and loss of barrier function are key inevitable events of IBD pathogenesis [52], the increased cytokine release by IECS and the drop of TEER values upon the induction of IBD-like conditions support the relevance of our model to study disease-specific mechanisms of IBD. Interestingly, Caco-2 cells secreted low cytokine levels in basal conditions as expected [53]. Upon inflammatory trigger, both apical and basal production of epithelial inflammatory cytokines IL-8, IP-10 and CCL-20 were increased. However, the basal secretion of these cytokines was consistently higher when compared to their apical production. As both cytokine receptors and pro-inflammatory molecules are localised and secreted basally in polarized IECs in order to recruit immune cells to the site of inflammation [53,54], the increased basal cytokine production by Caco-2 cells upon trigger therefore reflects the in vivo physiology of the gastrointestinal tract in inflamed conditions.

Furthermore, we showed that the decreased barrier function of Caco-2 cells was associated with a fragmented localisation of *adherens junction* (AJ) protein ECAD upon inflammatory trigger. Mislocalisation of ECAD has been observed in CD patients and may be linked with the decreased intestinal barrier function of these patients [55]. Tight junctions (TJ) have also been shown to be affected in IBD patients, with notably elevated levels of CLAUDIN-2 protein in colonic biopsies of UC patients [56]. To this day, it is still unclear whether the loss of barrier function is a cause or a consequence of the establishment of inflammation in IBD patients. It would therefore be interesting to use this model to investigate how and when AJ and TJ are affected in IBD pathology.

Throughout our research, we used different inflammatory trigger timelines to induce IBD characteristics. The initial rationale behind the idea was that using a short or a long trigger time would induce different degrees of phenotype severity; the shorter trigger leading to a milder phenotype and the longer trigger leading to a more severe one. However, we did not observe any differences in cytokine production by Caco-2 cells between the short and the long triggers nor did we observe any striking differences in TEER values or ECAD localization. These results suggest that the increased

cytokine production and the loss of barrier function in Caco-2 happen shortly after trigger and that the time of exposure does not further modulate these characteristics. In the future, the concentration of the cytokines used in the trigger could potentially be optimized in order to illustrate different levels of severity of the IBD phenotype in this gut-on-a-chip model. Nevertheless, we did observe that Caco-2 cells started to invade the ECM after a prolonged exposure to cytokines. It is known that many cytokines are able to regulate proliferation and invasion of Caco-2 cells and a prolonged exposure to IFN- γ , TNF- α and IL-1 β might affect those processes [57].

Interestingly, when assessing the effect of the trigger on cell activation, we observed that a prolonged cytokine trigger did not increase IL-8 production by Caco-2 cells compared to non-triggered conditions. This could be explained by the fact that the triggering medium was refreshed at Day 7, before cytokine production levels were assessed at Day 11. Indeed, it is known that IL-8 is rapidly produced after TNF- α triggering of Caco-2 cells and that the secretion is stopped approximately 12 h after trigger [58]. It is plausible that, by refreshing the medium at Day 7, levels of IL-8 were back to normal and the exhausted Caco-2 cells could not produce any additional IL-8.

Finally, we showed the functionality of this simple gut-on-a-chip model in IBD target and drug discovery by preventing the effect of the IBD-like trigger through compound and gene knockdown intervention. We used direct on-chip transduction to knockdown the expression of *MYD88* and *RELA*. We showed that the increased cytokine production induced in triggered Caco-2 cells could be partially suppressed by *MYD88* and *RELA* knockdowns, making the system applicable for large-scale knockdown screens. Once again, it was noticed that the basal production of the analytes was more affected by the knockdown than the apical production. As IECs generally recruit immune cells to the damaged epithelium by secreting pro-inflammatory cytokines in the subjacent intestinal mucosa [53,54], these results support the physiological relevance of our model to study IBD mechanisms. Nevertheless, we observed residual effect of the trigger cocktail on cytokine production after *RELA* and *MYD88* knockdowns. This can first be explained by the partial knockdown induced by the shRNA-carrying viruses. Furthermore, the cytokines we quantified as readouts of the inflammation are involved in several of the pathways activated by the trigger cocktail and the knockdown of a single effector of these pathways is not sufficient to completely prevent cytokine release. Nevertheless, we showed that this gut-on-a-chip is suitable for target discovery, even in a set-up using a mixture of different cytokines, reflecting the actual pathological situation in IBD.

The effect of the knockdown of inflammatory genes on barrier integrity could not be assessed as AdV transduction affected the TEER values of the Caco-2 tubules. The interaction between AdV and its receptors might have, amongst others, affected TJ or cell–cell interaction which may have impaired attachment of the cells and therefore, decreased TEER values. As *MYD88* and *RELA* are immune regulators and are not expected to play a significant role in the maintenance of barrier integrity, it would be interesting to determine whether the knockdown of genes involved in barrier function such as *HNF4A* or *ECM1* could rescue the effect of AdV transduction on TEER values of Caco-2 tubules. Furthermore, we could potentially overcome this limitation of our model by establishing stable knockdown Caco-2 cell lines before seeding them in the OrganoPlate.

Finally, by using a compound treatment we could not only prevent the increased release of inflammatory cytokines but also the loss of barrier function in triggered Caco-2 tubules. Namely, Caco-2 tubules treated with 1.25 μ M of TPCA-1 retained their barrier integrity without affecting cell viability. The lower TPCA-1 concentrations did not significantly decrease cytokine release and the higher concentration caused cell death, which affected the barrier function of the epithelium. These results suggest that this model could be used to assess the effect of compounds on both cell activation and barrier integrity.

Our system shows the potential for further improvements by replacing Caco-2 cells with intestinal organoids or gut epithelium derived from iPSCs, thus making it more physiologically relevant. By including patient-derived material, we would be able to test and predict individual responsiveness to medication and find the optimal treatment for a given IBD patient. Research groups have started to use

such primary cells in order to develop gut-on-a-chip models [22,59], but they are of limited throughput and their application to disease modeling and drug screening has yet to be performed. Overall, these types of models could be of tremendous help in the rise of the personalized medicine field. In addition to the culture of human primary material, the membrane-free OrganoPlate platform is also ideally suited for co-cultures with immune cells, adding further complexity and relevance. This would allow the elicitation of epithelial-immune crosstalk mechanisms and could be of particular interest if microbial products are added to the model. There is consensus that gut microbiota is directly engaging with immune cells in the intestinal tissue and that this interaction is an important factor contributing to IBD pathogenesis, however the nature of this causal relationship has yet to be confirmed [60–62]. By using a high-throughput platform that allows different microbial taxa to interact directly with the intestinal epithelium, together with unprecedented imaging capabilities and the possibility to model low oxygen levels, we could gain a deeper understanding of the relation between microbiota and IBD.

In summary, this study establishes for the first time a robust and reliable gut-on-a-chip model allowing the recapitulation of key aspects of IBD pathogenesis in a high throughput manner. This work provides a foundation for upcoming large-scale 3D microfluidic modeling of IBD and screening of relevant therapeutic targets, allowing us to further study and understand gut inflammation.

4. Materials and Methods

4.1. Ethics Statement

The research described here has been performed according to applicable Dutch national ethics regulations and was conducted within Galapagos BV (Leiden, The Netherlands). Scientists from Galapagos BV are qualified to perform research using human material and have appropriate facilities and equipment available to comply with applicable laws, regulations and internal rules related to handling and storage of the material. The human material was obtained from Sanquin (Amsterdam, The Netherlands). The supplier has confirmed to Galapagos BV that informed consent from the donors to use the material for research purposes was received. The cells were solely used for target and drug discovery and were not used for human experimentation or therapy. All material is and will remain anonymized.

4.2. Cells

Human colon adenocarcinoma cell line Caco-2 (ECACC 86010202) was cultured in Caco-2 medium composed of EMEM (ATCC, Manassas, VA, USA) supplemented with 10% FBS (Gibco, Waltham, MA, USA), 1% NEAA (Gibco, Waltham, MA, USA) and 1% penicillin/streptomycin (Gibco, Waltham, MA, USA). Cells were cultured at 37 °C in a humidified atmosphere with 5% CO₂ up to 80% confluency and then either sub-cultured or used for the experiments. All experiments were performed on cells between passages 47 and 60.

4.3. OrganoPlate Seeding and Tubule Formation

Detailed extracellular matrix (ECM) loading and seeding procedures of Caco-2 cells in three-lane OrganoPlate were performed as previously reported [26]. In summary, 20,000 Caco-2 cells were seeded against a pH-buffered 4 mg/mL Collagen I gel (Cultrex, Gaithersburg, MD, USA) in a 3-lane 400 µm OrganoPlate (Mimetas, Leiden, The Netherlands) and allowed to attach against the gel for 4 h (37 °C, 5% CO₂). After attachment, Caco-2 medium was added to medium inlets and outlets and perfusion was started by putting the plate on an interval rocker (Perfusion Rocker Mini, Mimetas, Leiden, The Netherlands) switching between a +7° and –7° inclination every 8 min (37 °C, 5% CO₂) thus allowing bi-directional flow. Medium was refreshed every 3 days post-seeding.

4.4. Triggering of IBD-like Conditions

Caco-2 cells were triggered basally with an adapted cocktail of human recombinant cytokines (ImmunoTools, Friesoythe, Germany) composed of IL-1 β , IFN- γ and TNF- α at respectively 2, 100 and 100 ng/mL dissolved in Caco-2 media. Three trigger times were used throughout experiments (Day 4 to 7, Day 7 to 11 or Day 4 to 11); the Day 4 to 7 trigger is shown unless stated otherwise.

4.5. Cytokine Secretion of Caco-2 Cells

Media was harvested separately from the top and bottom inlets and outlets, reflecting the apical and basal secretion of analytes by Caco-2 cells, and stored at -20°C until further assessment. The concentrations of macrophage inflammatory protein-3 (CCL-20/MIP3A), IFN-Gamma-Inducible Protein 10 (IP-10/CXCL10), Interleukin-8 (IL-8/CXCL8), Interleukin-6 (IL-6), Interleukin-1-Beta (IL-1 β) and Tumor Necrosis Factor-Alpha (TNF- α) were quantified using a human multiplex assay (Thermo Fischer, Waltham, MA, USA) on a Luminex FlexMap 3D (Merck Millipore, Burlington, MA, USA) according to manufacturer protocol.

4.6. TEER Measurements

Transepithelial electrical resistance (TEER) was measured at different time points using an automated multichannel impedance spectrometer designed for use with the OrganoPlate (OrganoTEER, Mimetas, Leiden, The Netherlands). Before measurement, medium was added in the gel inlets and outlets and the OrganoPlate was returned to the incubator (37°C , 5% CO_2) to equilibrate for an hour. The electrode board of the OrganoTEER is matched to the OrganoPlate such that when an OrganoPlate is placed in the OrganoTEER, electrode pairs are dipped in the medium in all inlet and outlet wells connecting to the basal and apical side of all tubes. Point impedance measurements were performed by frequency sweep from 5 Hz to 1 MHz (75 points at precision 0) with TEER values going up to $1000\ \Omega\cdot\text{cm}^2$. Data was analyzed using OrganoTEER software, which automatically extracts the TEER contribution (in Ohm) from the measured spectra and normalises it to $\text{Ohm}\cdot\text{cm}^2$ by multiplying by the tubule-ECM interface (estimated at $0.0056\ \text{cm}^2$).

4.7. Immunohistochemistry

Caco-2 tubules were fixed with 3.7% formaldehyde (Sigma-Aldrich, St. Louis, MI, USA) in PBS for 10 min and prepared for immunohistochemistry as previously described [26]. The primary antibody mouse α -E-CADHERIN (Abcam AB1416, 1:100, Cambridge, UK) and the secondary antibody donkey α -mouse AlexaFluor647 (Molecular Probes A31571, 1:250; Eugene, OR, USA) were used. Actin was stained using ActinGreenTM 488 ReadyProbesTM Reagent (Thermo Fisher, R37110, Waltham, MA, USA) and nuclei was stained using NucBlueTM Fixed Cell ReadyProbesTM Reagent (Thermo Fisher, Waltham, MA, USA). Both reagents were added in the secondary antibody solution according to the manufacturer's instructions. All steps were performed at room temperature on an interval rocker (Perfusion Rocker Mini, Mimetas) switching between a $+7^{\circ}$ and -7° inclination every 1 min. Cells were imaged on the InCell 6000 (GE Healthcare Life Sciences, Marlborough, MA, USA) and the Micro XLS-C HCI System (Molecular Devices, San Jose, CA, USA).

The organization of the epithelial cell layer forming the Caco-2 tubule was quantified by segmentation of the E-CADHERIN (ECAD) positive cell junctions with Cell Profiler 3.0 [63]. ECAD signals were enhanced using a neurite tubeness method to amplify the junction patterns. Subsequently the junctions were identified with a three classes adaptive Otsu threshold. To reduce fragmentation, the objects were merged and filtered with area of >600 pixels. The MeasureObjectSizeShape module was used to extract non-intensity related features of the ECAD objects and the MeasureImageIntensity module for extraction of intensity-related measurements from the ECAD objects. Input images and final output segmentation overlays are printed in Figure A3. Based on this segmentation process, two characteristics of the organizational pattern of the ECAD staining were quantified: compactness and

major axis length of signal. The compactness represents the mean squared distance of the object's pixels from the centroid divided by the area. The major axis length represents the pixels' length of the major axis of the ellipse that has the same normalised second central moments as the region. A more tightly packed and organized epithelial cell layer will have a more continuous pattern of tight junctions leading to objects with a long length axis and a high compactness value.

4.8. Adenoviral Preparation

For the generation of shRNA-carrying adenoviruses (AdV), pIPspAdapt-based constructs were transiently transfected with AdV5.Fib50 helper DNA into PER.C6/E2A producer cells as previously described [64,65]. The produced AdV were propagated by infecting PER.C6/E2A cells again. Throughout procedures, PER.C6/E2A cells were cultured in DMEM supplemented with 10% FBS (Gibco, Waltham, MA, USA) and 10 mM MgCl₂. Finally, titers of the crude lysates were determined as described [66].

For transduction efficiency determination, a knock-in AdV for ZsGreen was used; The ZsGreen reporter-gene construct was adapted from the pZsGreen-C1 vector (Clontech, Kusatsu, Japan. A 3x NLS sequence was cloned directly downstream from the ZsGreen open reading frame for nuclear expression. The ZsGreen-3xNLS sequence was cloned into an AdV adapter plasmid containing a CMV promoter by standard restriction enzyme digestion and ligation.

Viruses were selected based on their ability to reduce CCL20 production by Caco-2 cells (see Appendix B).

4.9. Adenoviral Transduction

One day after seeding, Caco-2 cells were exposed apically to different shRNA-carrying recombinant AdV for 6 h (MOI of 5 IU/cell) in absence of penicillin/streptomycin on an interval rocker switching between a +7° and -7° inclination every 8 min (37 °C, 5% CO₂). After transduction, medium was replaced with 50 µL of Caco-2 medium in medium inlets and outlets and plates were put back on the interval rocker (37 °C, 5% CO₂) for the rest of the experiment.

4.10. Transduction Efficiency

Caco-2 cells treated with a ZsGreen-expressing virus were imaged 72 h after transduction to determine transduction efficiency. Cells were stained for 30 min at 37 °C with NucBlue™ Live ReadyProbes™ Reagent (Thermo Fisher, Waltham, MA, USA) following the manufacturer's instructions and were then imaged on the InCell 6000 (GE Healthcare Life Sciences, Marlborough, MA). The transduction efficiency was calculated with an in-house algorithm quantifying the number of ZsGreen-positive cells relative to the number of total nuclei.

4.11. Quantitative PCR

Total RNA was isolated from Caco-2 tubules using a RNeasy Mini Kit (QIAGEN, Hilden, Germany) and converted to cDNA using TaqMan™ Reverse Transcription Reagents (Applied Biosystems, Waltham, MA, USA) according to the manufacturer's instructions. Real-time quantitative amplification (qPCR) was then performed using TaqMan® Fast Advanced MasterMix (Applied Biosystems, Foster City, CA, USA) on a LightCycler® 480 instrument. Probes for MYD88 (Life Technologies, Hs01573837_g1; Carlsbad, CA, USA), RELA (Life Technologies, Hs00153294_m1) and GAPDH (Life Technologies, Hs02758991_g1; Carlsbad, CA, USA) were used.

4.12. Compound Exposure

Four days after seeding, Caco-2 cells were pre-treated apically and basally with TPCA-1 (Sigma-Aldrich, St. Louis, MI, USA) compound in a concentration range from 0.005 to 20 µM in a final DMSO concentration of 0.22%. After a pre-exposure of 2 h, basal medium was removed

and replaced with cytokine-triggering medium (IL-1 β , IFN- γ and TNF- α at 2, 100 and 100 ng/mL, respectively) in presence of the compound for another 72 h.

4.13. Viability Assay

AlamarBlue Cell Viability Reagent (Thermo Fisher, Waltham, MA, USA) was pre-mixed in Caco-2 medium in a 1:10 ratio and 50 μ L was added to medium inlets and outlets. Plates were incubated at 37 $^{\circ}$ C for 4 h and fluorescence signals were measured (Excitation: 530–560 nm, Emission: 590 nm) on a multi-well plate fluorimeter (Fluoroskan Ascent FL, Thermo Fisher, Waltham, MA, USA).

4.14. Statistics and Data Analysis

Data was analyzed using GraphPad Prism software version 6 (GraphPad Software, La Jolla, CA, USA). Unless stated otherwise, values are expressed as mean \pm standard error of the mean (SEM). When two groups of data were analyzed, a two-tailed, unpaired Student's *t*-test was used to determine the statistical significance. When three or more groups were analyzed, parametrical or robust ANOVA were used to determine the statistical significance, depending on the presence of outliers. Differences with $p \leq 0.05$ were considered significant (*ns* $p > 0.05$, * $p \leq 0.05$, ** $p \leq 0.01$, *** $p \leq 0.001$, **** $p \leq 0.0001$). All graphs shown contain results from one representative experiment containing at least three technical replicates. The exact number of replicates in each condition is presented in the legend of each figure.

Author Contributions: C.B. and E.N. designed and performed experimental work and redacted the manuscript. Y.X.C. and G.v.M. helped with experimental work. E.D.E. designed algorithms and performed image analysis. H.W. helped with statistical analysis. A.N. and S.J.T. assisted with TEER measurements. J.S., H.L.L., D.K., K.S.E., J.J., P.V. and R.A.J.J. overviewed the research and contributed to writing the manuscript.

Funding: This work was supported by the European Union's Horizon 2020 research and innovation programme under the Marie Skłodowska-Curie [grant agreements #674983 (ITN-MIMIC) and #641639 (ITN-BIOPOL)].

Acknowledgments: Authors would like to thank Andre van Marle for assistance with adenoviral knowledge as well as Thomas van Es, Ayleen Kartono and Anaïs Legent for execution of early experimental work.

Conflicts of Interest: E.N., A.N., D.K., H.L.L., S.J.T., R.A.J.J. and P.V. are employees of Mimetas BV, which is marketing the OrganoPlate and the OrganoTEER. P.V., S.J.T. and J.J. are shareholders of that same company. OrganoPlate is a registered trademark of Mimetas BV. The authors have no additional financial interests.

Abbreviations

AdV	Adenovirus
AJ	Adherens junction
CD	Crohn's disease
DC	Dendritic cell
ECM	Extracellular matrix
IBD	Inflammatory bowel disease
IEC	Intestinal epithelial cells
iPSC	Induced pluripotent stem cell
NEAA	Non-essential amino acids
PBMC	Peripheral blood mononuclear cells
RQ	Relative quantification
TEER	Trans epithelial electrical resistance
TJ	Tight junction
UC	Ulcerative colitis

Appendix A Supplementary Methods

Appendix A.1 Cells

Peripheral blood mononuclear cells (PBMCs) were isolated from buffy coats (Sanquin, Amsterdam, The Netherlands) by standard Ficoll-PaqueTM density centrifugation and CD14⁺ cells were then positively-isolated using LS Columns from MACS Cell Separation system (Miltenyi, Bergisch Gladbach, Germany). Isolated CD14⁺

cells were cultured in RPMI supplemented with 10% heat-inactivated-FBS (Gibco, Waltham, MA, USA), 1% Penicillin/Streptomycin (Gibco, Waltham, MA, USA), [60 ng/mL] of GM-CSF (ImmunoTools, Friesoythe, Germany) and [40 ng/mL] of IL-4 (ImmunoTools, Friesoythe, Germany) for 7 days to differentiate towards dendritic cells (DCs).

Appendix A.2 Optimization of the Immune-Relevant Trigger

An immune-relevant trigger was first set-up in the Transwell system (Corning, Figures A1 and A2). 42,900 Caco-2 cells were seeded on top of a 96-well plate Transwell insert and were triggered at Day 16 with human recombinant cytokines IL-1 β , IFN- γ and TNF- α (ImmunoTools, Friesoythe, Germany). Basal supernatants were harvested at Day 19 and cytokine secretion was assessed by Luminex. The trigger leading to the highest secretion of cytokines by Caco-2 cells (IL-1 β , IFN- γ and TNF- α at 1, 50 and 50 ng/mL respectively) was then compared to the effect of UV-irradiated *E. coli*-activated DCs. To do so, 42,900 Caco-2 cells were seeded on top of a 96-well plate Transwell insert and DCs were added to the basal compartment in amounts ranging from 20,000 to 125,000 at Day 9. DCs were triggered with UV-irradiated *E. coli* (ATCC, #25922; Manassas, VA, USA) until Day 19 where apical and supernatants were harvested and cytokine secretion was assessed by Luminex.

Appendix A.3 Selection of Viruses

Several putative positive- and negative-control AdV were screened for their ability to reduce CCL-20 secretion by Caco-2 cells seeded on top of a Transwell insert and triggered at Day 9 with a cytokine cocktail (IL-1 β , IFN- γ and TNF- α at 1, 50 and 50 ng/mL respectively, Figure A4). Putative positive-control viruses needed to reduce CCL-20 secretion by at least 40% compared to non transduced conditions whereas CCL-20 expression of Caco-2 cells transduced with putative negative-control viruses could not differ from non-transduced conditions by more than 25%. Based on those criteria, luc_a and mmNr1h3_a were chosen as negative control AdV and MYD88_d and RELA_a as positive control AdV.

Table A1. Putative negative-control shRNA viruses tested.

Insert Name	Target Sequence
aveGFP_a	GCCACAACGTCTATATCAT
ffluc_a	GCAGAAGCTATGAAACGAT
ffluc_b	GCATGCCAGAGATCCTATT
luc_a *	GGTTACCTAAGGGTGTGGC
mmNr1h3_a *	CACACATATGTGGAGGCC

* Virus selected for this study.

Table A2. Putative positive-control shRNA viruses tested.

Insert Name	Target Sequence
MYD88_a	GGAACAGACAAACTATCGA
MYD88_b	GGTTGTCTCTGATGATTAC
MYD88_c	GACTTCCAGACCAAATTTG
MYD88_d *	GGTTCATCACTGTCTGCGA
MYD88_e	CTGCTCTCAACATGCGAGT
RELA_a *	GATTGAGGAGAAACGTAAA
RELA_b	GTACCCTGAGGCTATAACT

* Virus selected for this study.

Appendix B Supplementary Data

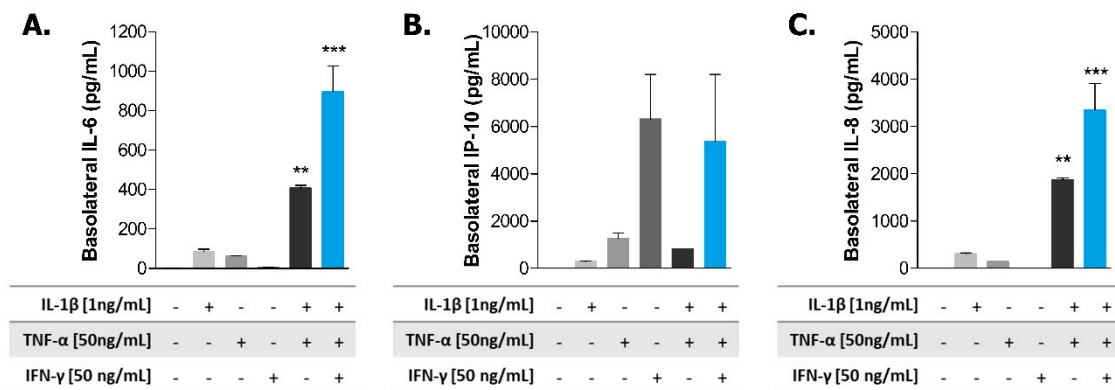


Figure A1. Optimization of the cytokine trigger composition in the Transwell system. Basal secretion of IL-6 (A), IP-10 (B) and IL-8 (C) by Caco-2 cells at Day 19 after a 72 h trigger with the indicated cytokines. Data is represented as mean ± SEM. * $p < 0.05$; ** $p < 0.01$; *** $p < 0.001$ by one-way ANOVA with Dunnett’s post-hoc test compared to non-triggered condition ($n = 2$).

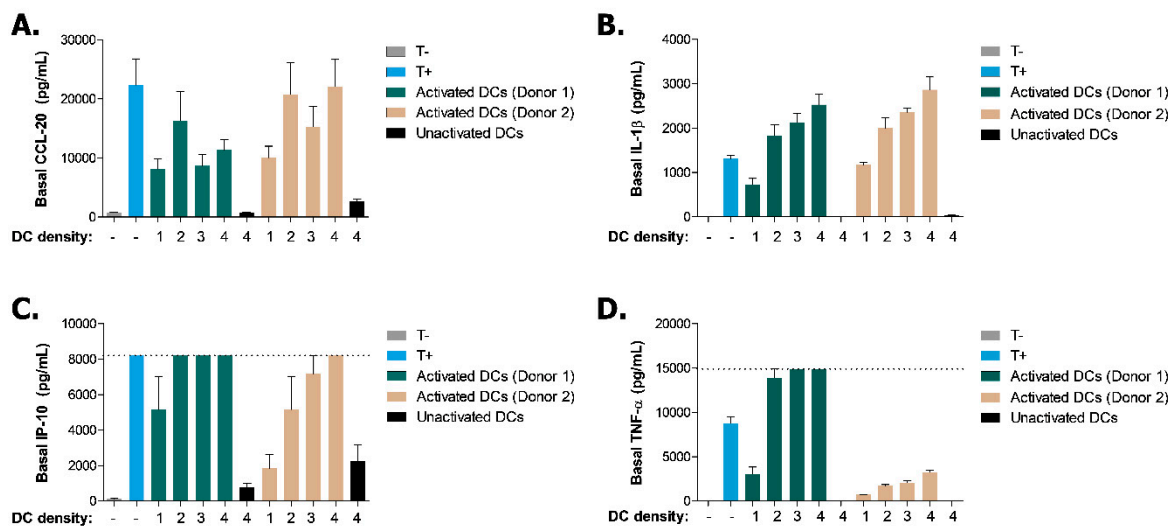


Figure A2. Effect of a cytokine trigger and the presence of activated-dendritic cells on the cytokine release of Caco-2 cells. Basal production of CCL-20 (A), IL-1β (B), IP-10 (C) and TNF-α (D) assessed by Luminex at Day 19. Caco-2 cells were either left non-triggered (T-) or triggered (T+) with cytokines IL-1β, TNF-α and IFN-γ (1, 50, 50 ng/mL respectively) or co-cultured with *E. coli*-activated DCs from two donors (DC density; 1 = 20,000, 2 = 55,000, 3 = 90,000, 4 = 125,000) or non-activated DCs for 72 h. Data is represented as mean ± SEM. Dotted line depicts the maximum detection range of the assay ($n = 2-4$).

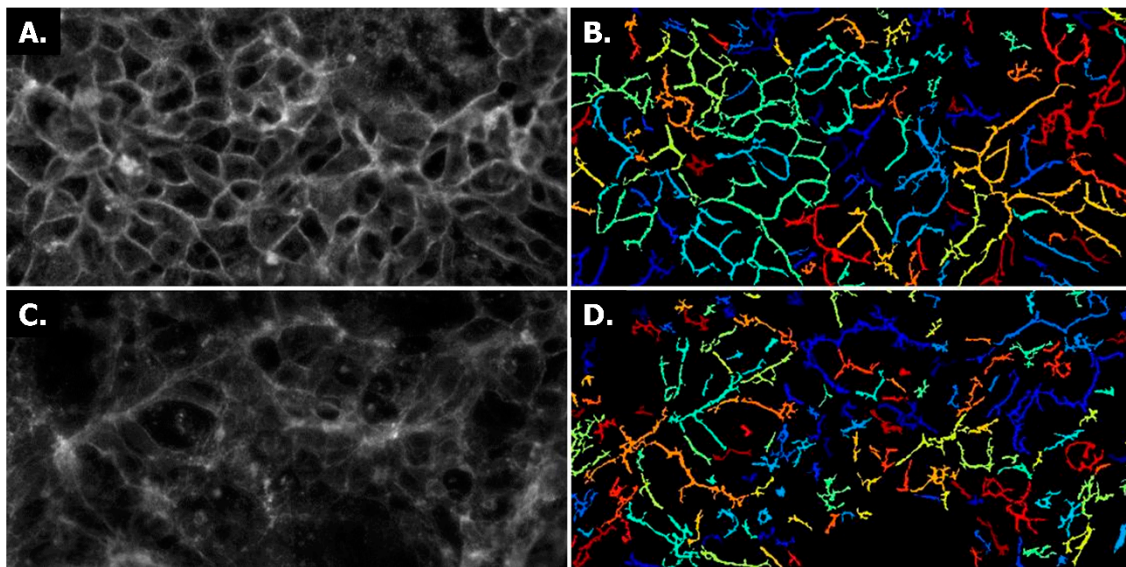


Figure A3. E-CADHERIN immunocytochemistry signal segmentation of triggered and non-triggered Caco-2 tubules using Cell Profiler. Raw input images of non-triggered (A) and triggered (C) Caco-2 tubules at Day 11 with their respective segmented masks (B and D) from the Cell Profiler analysis.

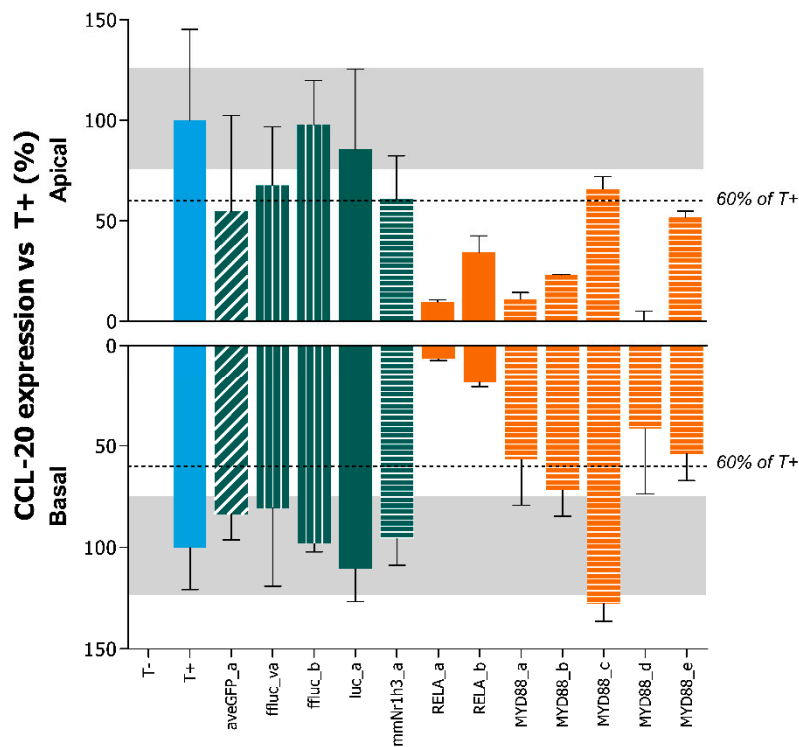


Figure A4. Selection of positive- and negative-control viruses based on CCL-20 production. Apical and basal production of CCL-20 by transduced Caco-2 cells (MOI 8–65) assessed by Luminex at Day 12 after a 72 h trigger with cytokines IL-1 β , TNF- α and IFN- γ (1, 50, 50 ng/mL respectively). Grey areas depict a 25% range from T+ and dotted lines depict a 40% reduction from T+. Data is represented as mean \pm range of data ($n = 2-4$). Conditions with non-transduced cells are shown in blue, putative negative control viruses in green and putative positive control viruses in orange.

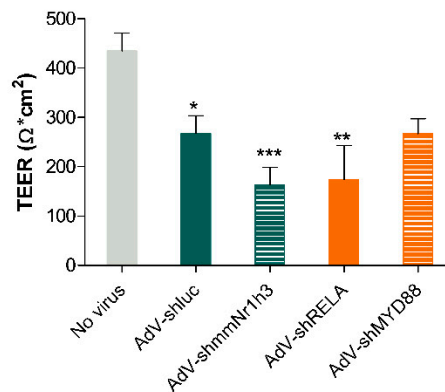


Figure A5. Adenoviral transduction of Caco-2 tubules cause a reduction of TEER values. TEER values of transduced Caco-2 tubules at Day 4. Data is presented as mean \pm SEM. * $p \leq 0.05$; ** $p \leq 0.01$; *** $p \leq 0.001$; **** $p \leq 0.0001$ by one-way ANOVA with Bonferroni post-hoc test compared to No virus condition ($n = 5-12$).

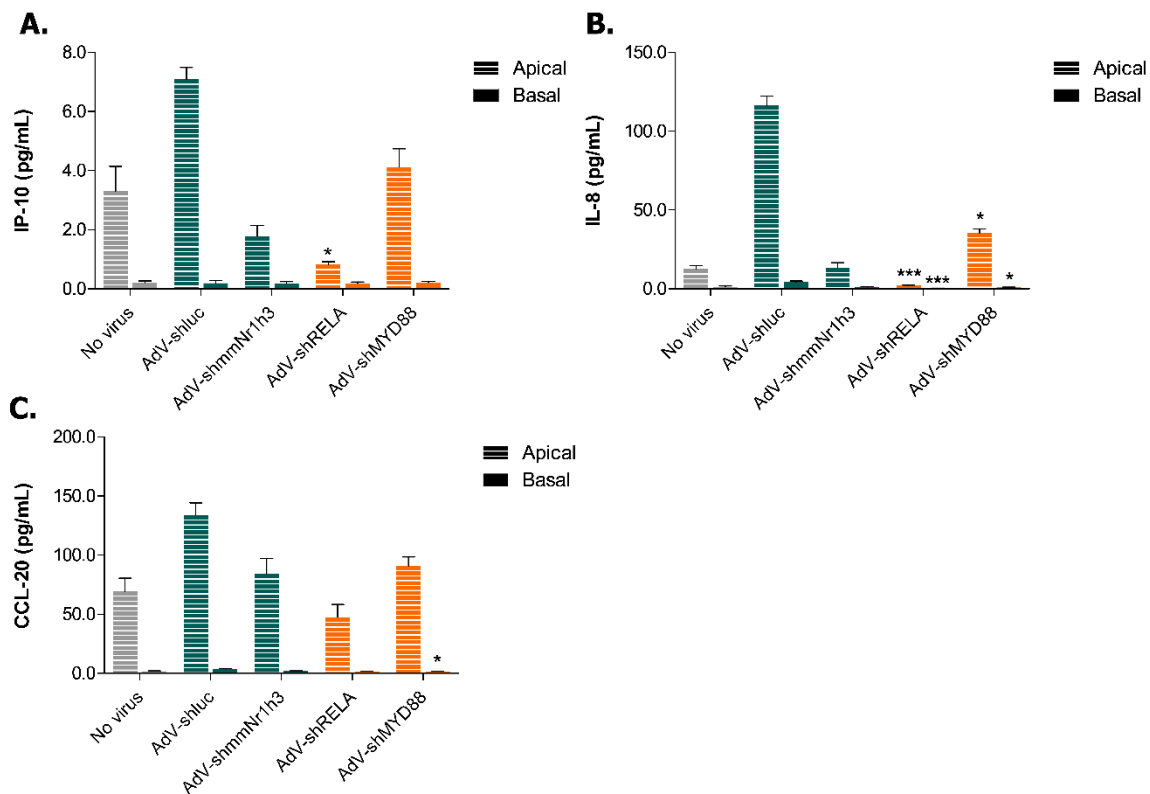


Figure A6. Knockdown of inflammatory effectors decreases basal cytokine secretion in non-triggered Caco-2 tubules. Secretion of IP-10 (A), IL-8 (B) and CCL-20 (C) cytokines in apical and basal compartments of non-triggered Caco-2 tubules at Day 7. Data is represented as mean \pm SEM. *, $p < 0.05$; **, $p < 0.01$; ***, $p < 0.001$ by two-way ANOVA with ArcSinh transformation and Holm corrected post-hoc test compared to AdV-shluc ($n = 3-5$). Non-transduced condition is shown in grey, negative control viruses in green and viruses carrying shRNA for inflammatory effectors in orange.

References

- De Souza, H.S.P.; Fiocchi, C.; Iliopoulos, D. The IBD interactome: An integrated view of aetiology, pathogenesis and therapy. *Nat. Rev. Gastroenterol. Hepatol.* **2017**, *14*, 739–749. [[CrossRef](#)] [[PubMed](#)]
- Kaplan, G.G. The global burden of IBD: From 2015 to 2025. *Nat. Rev. Gastroenterol. Hepatol.* **2015**, *12*, 720–727. [[CrossRef](#)] [[PubMed](#)]

3. Burisch, J.; Jess, T.; Martinato, M.; Lakatos, P.L. The burden of inflammatory bowel disease in Europe. *J. Crohn's Colitis* **2013**, *7*, 322–337. [[CrossRef](#)] [[PubMed](#)]
4. De Souza, H.S.P.; Fiocchi, C. Immunopathogenesis of IBD: Current state of the art. *Nat. Rev. Gastroenterol. Hepatol.* **2016**, *13*, 13–27. [[CrossRef](#)] [[PubMed](#)]
5. Matsuoka, K.; Kanai, T. The gut microbiota and inflammatory bowel disease. *Semin. Immunopathol.* **2015**, *37*, 47–55. [[CrossRef](#)] [[PubMed](#)]
6. Pedersen, J.; Coskun, M.; Soendergaard, C.; Salem, M.; Nielsen, O.H. Inflammatory pathways of importance for management of inflammatory bowel disease. *World J. Gastroenterol.* **2014**, *20*, 64–77. [[CrossRef](#)] [[PubMed](#)]
7. Atreya, R.; Neurath, M.F. IBD pathogenesis in 2014: Molecular pathways controlling barrier function in IBD. *Nat. Rev. Gastroenterol. Hepatol.* **2015**, *12*, 37–38. [[CrossRef](#)] [[PubMed](#)]
8. Carter, M.J.; Lobo, A.J.; Travis, S.P.L.; IBD Section, British Society of Gastroenterology. Guidelines for the management of inflammatory bowel disease in adults. *Gut* **2004**, *53* (Suppl. 5), V1–V16. [[CrossRef](#)] [[PubMed](#)]
9. Mizoguchi, A. Animal Models of Inflammatory Bowel Disease. *Prog. Mol. Biol. Transl. Sci.* **2012**, *105*, 263–320. [[PubMed](#)]
10. Tsilingiri, K.; Barbosa, T.; Penna, G.; Caprioli, F.; Sonzogni, A.; Viale, G.; Rescigno, M. Probiotic and postbiotic activity in health and disease: Comparison on a novel polarised ex-vivo organ culture model. *Gut* **2012**, *61*, 1007–1015. [[CrossRef](#)] [[PubMed](#)]
11. Mokry, M.; Middendorp, S.; Wiegerinck, C.L.; Witte, M.; Teunissen, H.; Meddens, C.A.; Cuppen, E.; Clevers, H.; Nieuwenhuis, E.E.S. Many Inflammatory Bowel Disease Risk Loci Include Regions That Regulate Gene Expression in Immune Cells and the Intestinal Epithelium. *Gastroenterology* **2014**, *146*, 1040–1047. [[CrossRef](#)] [[PubMed](#)]
12. McKay, D.M.; Philpott, D.J.; Perdue, M.H. Review article: In vitro models in inflammatory bowel disease research—A critical review. *Aliment. Pharmacol. Ther.* **1997**, *11* (Suppl. 3), 70–80. [[CrossRef](#)] [[PubMed](#)]
13. Eri, R.; McGuckin, M.A.; Wadley, R. T cell transfer model of colitis: A great tool to assess the contribution of T cells in chronic intestinal inflammation. *Methods Mol. Biol.* **2012**, *844*, 261–275. [[PubMed](#)]
14. Roy, U.; Galvez, E.J.C.; Iljazovic, A.; Lesker, T.R.; Blazejewski, A.J.; Pils, M.C.; Heise, U.; Huber, S.; Flavell, R.A.; Strowig, T. Distinct Microbial Communities Trigger Colitis Development upon Intestinal Barrier Damage via Innate or Adaptive Immune Cells. *Cell Rep.* **2017**, *21*, 994–1008. [[CrossRef](#)] [[PubMed](#)]
15. Prinz, F.; Schlange, T.; Asadullah, K. Believe it or not: How much can we rely on published data on potential drug targets? *Nat. Rev. Drug Discov.* **2011**, *10*, 712. [[CrossRef](#)] [[PubMed](#)]
16. Fritschfredin, M.; Vidal, A.; Utkovic, H.; Gotlind, Y.; Willen, R.; Jansson, L.; Hultgrenhornquist, E.; Melgar, S. The application and relevance of ex vivo culture systems for assessment of IBD treatment in murine models of colitis. *Pharmacol. Res.* **2008**, *58*, 222–231. [[CrossRef](#)] [[PubMed](#)]
17. Vadstrup, K.; Galsgaard, E.D.; Gerwien, J.; Vester-Andersen, M.K.; Pedersen, J.S.; Rasmussen, J.; Neermark, S.; Kiszka-Kanowitz, M.; Jensen, T.; Bendtsen, F. Validation and Optimization of an Ex Vivo Assay of Intestinal Mucosal Biopsies in Crohn's Disease: Reflects Inflammation and Drug Effects. *PLoS ONE* **2016**, *11*, e0155335. [[CrossRef](#)] [[PubMed](#)]
18. Hilgers, A.R.; Conradi, R.A.; Burton, P.S. Caco-2 Cell Monolayers as a Model for Drug Transport Across the Intestinal Mucosa. *Pharm. Res.* **1990**, *7*, 902–910. [[CrossRef](#)] [[PubMed](#)]
19. Edmondson, R.; Broglie, J.J.; Adcock, A.F.; Yang, L. Three-dimensional cell culture systems and their applications in drug discovery and cell-based biosensors. *Assay Drug Dev. Technol.* **2014**, *12*, 207–218. [[CrossRef](#)] [[PubMed](#)]
20. Kim, H.J.; Li, H.; Collins, J.J.; Ingber, D.E. Contributions of microbiome and mechanical deformation to intestinal bacterial overgrowth and inflammation in a human gut-on-a-chip. *Proc. Natl. Acad. Sci. USA* **2016**, *113*, E7–E15. [[CrossRef](#)] [[PubMed](#)]
21. Kim, H.J.; Huh, D.; Hamilton, G.; Ingber, D.E. Human gut-on-a-chip inhabited by microbial flora that experiences intestinal peristalsis-like motions and flow. *Lab Chip* **2012**, *12*, 2165–2174. [[CrossRef](#)] [[PubMed](#)]
22. Kasendra, M.; Tovaglieri, A.; Sontheimer-Phelps, A.; Jalili-Firoozinezhad, S.; Bein, A.; Chalkiadaki, A.; Scholl, W.; Zhang, C.; Rickner, H.; Richmond, C.A.; et al. Development of a primary human Small Intestine-on-a-Chip using biopsy-derived organoids. *Sci. Rep.* **2018**, *8*, 2871. [[CrossRef](#)] [[PubMed](#)]
23. Lee, J.; Choi, J.-H.; Kim, H.J. Human gut-on-a-chip technology: Will this revolutionize our understanding of IBD and future treatments? *Expert Rev. Gastroenterol. Hepatol.* **2016**, *10*, 883–885. [[CrossRef](#)] [[PubMed](#)]

24. Toepke, M.W.; Beebe, D.J. PDMS absorption of small molecules and consequences in microfluidic applications. *Lab Chip* **2006**, *6*, 1484. [[CrossRef](#)] [[PubMed](#)]
25. Halldorsson, S.; Lucumi, E.; Gómez-Sjöberg, R.; Fleming, R.M.T. Advantages and challenges of microfluidic cell culture in polydimethylsiloxane devices. *Biosens. Bioelectron.* **2015**, *63*, 218–231. [[CrossRef](#)] [[PubMed](#)]
26. Trietsch, S.J.; Naumovska, E.; Kurek, D.; Setyawati, M.C.; Vormann, M.K.; Wilschut, K.J.; Lanz, H.L.; Nicolas, A.; Ng, C.P.; Joore, J.; et al. Membrane-free culture and real-time barrier integrity assessment of perfused intestinal epithelium tubes. *Nat. Commun.* **2017**, *8*, 262. [[CrossRef](#)] [[PubMed](#)]
27. Coler, R.N.; Bertholet, S.; Moutaftsi, M.; Guderian, J.A.; Windish, H.P.; Baldwin, S.L.; Laughlin, E.M.; Duthie, M.S.; Fox, C.B.; Carter, D.; et al. Development and characterization of synthetic glucopyranosyl lipid adjuvant system as a vaccine adjuvant. *PLoS ONE* **2011**, *6*, e16333. [[CrossRef](#)] [[PubMed](#)]
28. De Castro, C.P.; Jones, S.A.; Ni Cheallaigh, C.; Hearnden, C.A.; Williams, L.; Winter, J.; Lavelle, E.C.; Mills, K.H.G.; Harris, J. Autophagy regulates IL-23 secretion and innate T cell responses through effects on IL-1 secretion. *J. Immunol.* **2012**, *189*, 4144–4153. [[CrossRef](#)] [[PubMed](#)]
29. Gad, M.; Ravn, P.; Soborg, D.A.; Lund-Jensen, K.; Ouwehand, A.C.; Jensen, S.S. Regulation of the IL-10/IL-12 axis in human dendritic cells with probiotic bacteria. *FEMS Immunol. Med. Microbiol.* **2011**, *63*, 93–107. [[CrossRef](#)] [[PubMed](#)]
30. Podolin, P.L.; Callahan, J.F.; Bolognese, B.J.; Li, Y.H.; Carlson, K.; Davis, T.G.; Mellor, G.W.; Evans, C.; Roshak, A.K. Attenuation of murine collagen-induced arthritis by a novel, potent, selective small molecule inhibitor of I κ B Kinase 2, TPCA-1 (2-[(aminocarbonyl)amino]-5-(4-fluorophenyl)-3-thiophenecarboxamide), occurs via reduction of proinflammatory cytokines and. *J. Pharmacol. Exp. Ther.* **2005**, *312*, 373–381. [[CrossRef](#)] [[PubMed](#)]
31. Ivanenkov, Y.A.; Balakin, K.V.; Lavrovsky, Y. Small molecule inhibitors of NF- κ B and JAK/STAT signal transduction pathways as promising anti-inflammatory therapeutics. *Mini Rev. Med. Chem.* **2011**, *11*, 55–78. [[CrossRef](#)] [[PubMed](#)]
32. Vulto, P.; Podszun, S.; Meyer, P.; Hermann, C.; Manz, A.; Urban, G.A. Phaseguides: A paradigm shift in microfluidic priming and emptying. *Lab Chip* **2011**, *11*, 1596. [[CrossRef](#)] [[PubMed](#)]
33. Srinivasan, B.; Kolli, A.R.; Esch, M.B.; Abaci, H.E.; Shuler, M.L.; Hickman, J.J. TEER measurement techniques for in vitro barrier model systems. *J. Lab. Autom.* **2015**, *20*, 107–126. [[CrossRef](#)] [[PubMed](#)]
34. Van De Walle, J.; Hendrickx, A.; Romier, B.; Larondelle, Y.; Schneider, Y.-J. Inflammatory parameters in Caco-2 cells: Effect of stimuli nature, concentration, combination and cell differentiation. *Toxicol. In Vitro* **2010**, *24*, 1441–1449. [[CrossRef](#)] [[PubMed](#)]
35. Coskun, M. Intestinal epithelium in inflammatory bowel disease. *Front. Med.* **2014**, *1*, 24. [[CrossRef](#)] [[PubMed](#)]
36. Karayiannakis, A.J.; Syrigos, K.N.; Efstathiou, J.; Valizadeh, A.; Noda, M.; Playford, R.J.; Kmiot, W.; Pignatelli, M. Expression of catenins and E-cadherin during epithelial restitution in inflammatory bowel disease. *J. Pathol.* **1998**, *185*, 413–418. [[CrossRef](#)]
37. Zbar, A.P.; Simopoulos, C.; Karayiannakis, A.J. Cadherins: An integral role in inflammatory bowel disease and mucosal restitution. *J. Gastroenterol.* **2004**, *39*, 413–421. [[CrossRef](#)] [[PubMed](#)]
38. Hanby, A.M.; Chinery, R.; Poulosom, R.; Playford, R.J.; Pignatelli, M. Downregulation of E-cadherin in the reparative epithelium of the human gastrointestinal tract. *Am. J. Pathol.* **1996**, *148*, 723–729. [[PubMed](#)]
39. Lawrence, T. The Nuclear Factor NF- κ B Pathway in Inflammation. *Cold Spring Harb. Perspect. Biol.* **2009**. [[CrossRef](#)] [[PubMed](#)]
40. Tran, R.; Myers, D.R.; Denning, G.; Shields, J.E.; Lytle, A.M.; Alrowais, H.; Qiu, Y.; Sakurai, Y.; Li, W.C.; Brand, O.; et al. Microfluidic Transduction Harnesses Mass Transport Principles to Enhance Gene Transfer Efficiency. *Mol. Ther.* **2017**, *25*, 2372–2382. [[CrossRef](#)] [[PubMed](#)]
41. Zou, J.; Shankar, N. Roles of TLR/MyD88/MAPK/NF- κ B Signaling Pathways in the Regulation of Phagocytosis and Proinflammatory Cytokine Expression in Response to *E. faecalis* Infection. *PLoS ONE* **2015**, *10*, e0136947. [[CrossRef](#)] [[PubMed](#)]
42. DiMasi, J.A.; Grabowski, H.G.; Hansen, R.W. Innovation in the pharmaceutical industry: New estimates of R&D costs. *J. Health Econ.* **2016**, *47*, 20–33. [[PubMed](#)]
43. Adams, C.P.; Brantner, V.V. Spending on new drug development. *Health Econ.* **2010**, *19*, 130–141. [[CrossRef](#)] [[PubMed](#)]

44. Franzen, N.; van Harten, W.H.; Retèl, V.P.; Loskill, P.; van den Eijnden-van Raaij, J.; IJzerman, M. Impact of organ-on-a-chip technology on pharmaceutical R&D costs. *Drug Discov. Today* **2019**, *24*, 1720–1724. [[PubMed](#)]
45. Maznah, I. The use of Caco-2 cells as an in vitro method to study bioavailability of iron. *Malays. J. Nutr.* **1999**, *5*, 31–45. [[PubMed](#)]
46. Hellinger, É.; Veszelka, S.; Tóth, A.E.; Walter, F.; Kittel, Á.; Bakk, M.L.; Tihanyi, K.; Háda, V.; Nakagawa, S.; Duy, T.D.H.; et al. Comparison of brain capillary endothelial cell-based and epithelial (MDCK-MDR1, Caco-2, and VB-Caco-2) cell-based surrogate blood–brain barrier penetration models. *Eur. J. Pharm. Biopharm.* **2012**, *82*, 340–351. [[CrossRef](#)] [[PubMed](#)]
47. Odijk, M.; Van Der Meer, A.D.; Levner, D.; Kim, H.J.; Van Der Helm, M.W.; Segerink, L.I.; Frimat, J.P.; Hamilton, G.A.; Ingber, D.E.; Van Den Berg, A. Measuring direct current trans-epithelial electrical resistance in organ-on-a-chip microsystems. *Lab Chip* **2015**, *15*, 745–752. [[CrossRef](#)] [[PubMed](#)]
48. Ligumsky, M.; Simon, P.L.; Karmeli, F.; Rachmilewitz, D. Role of interleukin 1 in inflammatory bowel disease–enhanced production during active disease. *Gut* **1990**, *31*, 686–689. [[CrossRef](#)] [[PubMed](#)]
49. Ghosh, S.; Chaudhary, R.; Carpani, M.; Playford, R. Interfering with interferons in inflammatory bowel disease. *Gut* **2005**, *55*, 1071–1073. [[CrossRef](#)] [[PubMed](#)]
50. Dionne, S.; Hiscott, J.; D’Agata, I.; Duhaime, A.; Seidman, E.G. Quantitative PCR Analysis of TNF- α and IL-1 β mRNA Levels in Pediatric IBD Mucosal Biopsies. *Dig. Dis. Sci.* **1997**, *42*, 1557–1566. [[CrossRef](#)] [[PubMed](#)]
51. Matsuda, R.; Koide, T.; Tokoro, C.; Yamamoto, T.; Godai, T.; Morohashi, T.; Fujita, Y.; Takahashi, D.; Kawana, I.; Suzuki, S.; et al. Quantitative Cytokine mRNA Expression Profiles in the Colonic Mucosa of Patients with Steroid Naïve Ulcerative Colitis During Active and Quiescent Disease. *Inflamm. Bowel Dis.* **2009**, *15*, 328–334. [[CrossRef](#)] [[PubMed](#)]
52. Neurath, M.F. Cytokines in inflammatory bowel disease. *Nat. Rev. Immunol.* **2014**, *14*, 329–342. [[CrossRef](#)] [[PubMed](#)]
53. Onyiah, J.C.; Colgan, S.P. Cytokine responses and epithelial function in the intestinal mucosa. *Cell. Mol. Life Sci.* **2016**, *73*, 4203–4212. [[CrossRef](#)] [[PubMed](#)]
54. Panja, A.; Goldberg, S.; Eckmann, L.; Krishen, P.; Mayer, L. The regulation and functional consequence of proinflammatory cytokine binding on human intestinal epithelial cells. *J. Immunol.* **1998**, *161*, 3675–3684. [[PubMed](#)]
55. Muise, A.M.; Walters, T.D.; Glowacka, W.K.; Griffiths, A.M.; Ngan, B.-Y.; Lan, H.; Xu, W.; Silverberg, M.S.; Rotin, D. Polymorphisms in E-cadherin (CDH1) result in a mis-localised cytoplasmic protein that is associated with Crohn’s disease. *Gut* **2009**, *58*, 1121–1127. [[CrossRef](#)] [[PubMed](#)]
56. Heller, F.; Florian, P.; Bojarski, C.; Richter, J.; Christ, M.; Hillenbrand, B.; Mankertz, J.; Gitter, A.H.; Bürgel, N.; Fromm, M.; et al. Interleukin-13 is the key effector Th2 cytokine in ulcerative colitis that affects epithelial tight junctions, apoptosis, and cell restitution. *Gastroenterology* **2005**, *129*, 550–564. [[CrossRef](#)] [[PubMed](#)]
57. Andrews, C.; McLean, M.H.; Durum, S.K. Cytokine Tuning of Intestinal Epithelial Function. *Front. Immunol.* **2018**, *9*, 1270. [[CrossRef](#)] [[PubMed](#)]
58. Eckmann, L.; Jung, H.C.; Schurer-Maly, C.; Panja, A.; Morzycka-Wroblewska, E.; Kagnoff, M.F. Differential cytokine expression by human intestinal epithelial cell lines: Regulated expression of interleukin 8. *Gastroenterology* **1993**, *105*, 1689–1697. [[CrossRef](#)]
59. Workman, M.J.; Gleeson, J.P.; Troisi, E.J.; Estrada, H.Q.; Kerns, S.J.; Hinojosa, C.D.; Hamilton, G.A.; Targan, S.R.; Svendsen, C.N.; Barrett, R.J. Enhanced Utilization of Induced Pluripotent Stem Cell–Derived Human Intestinal Organoids Using Microengineered Chips. *Cell. Mol. Gastroenterol. Hepatol.* **2018**, *5*, 669–677.e2. [[CrossRef](#)] [[PubMed](#)]
60. Zuo, T.; Ng, S.C. The Gut Microbiota in the Pathogenesis and Therapeutics of Inflammatory bowel disease. *Front. Microbiol.* **2018**, *9*, 2247. [[CrossRef](#)] [[PubMed](#)]
61. Manichanh, C.; Borruel, N.; Casellas, F.; Guarner, F. The gut microbiota in IBD. *Nat. Rev. Gastroenterol. Hepatol.* **2012**, *9*, 599–608. [[CrossRef](#)] [[PubMed](#)]
62. Ni, J.; Wu, G.D.; Albenberg, L.; Tomov, V.T. Gut microbiota and IBD: Causation or correlation? *Nat. Rev. Gastroenterol. Hepatol.* **2017**, *14*, 573–584. [[CrossRef](#)] [[PubMed](#)]
63. Carpenter, A.E.; Jones, T.R.; Lamprecht, M.R.; Clarke, C.; Kang, I.H.; Friman, O.; Guertin, D.A.; Chang, J.H.; Lindquist, R.A.; Moffat, J.; et al. CellProfiler: Image analysis software for identifying and quantifying cell phenotypes. *Genome Biol.* **2006**, *7*, R100. [[CrossRef](#)] [[PubMed](#)]

64. Arts, G.-J.; Langemeijer, E.; Tissingh, R.; Ma, L.; Pavliska, H.; Dokic, K.; Dooijes, R.; Mesic, E.; Clasen, R.; Michiels, F.; et al. Adenoviral vectors expressing siRNAs for discovery and validation of gene function. *Genome Res.* **2003**, *13*, 2325–2332. [[CrossRef](#)] [[PubMed](#)]
65. Michiels, F.; van Es, H.; van Rompaey, L.; Merchiers, P.; Francken, B.; Pittois, K.; van der Schueren, J.; Brys, R.; Vandersmissen, J.; Beirinckx, F.; et al. Arrayed adenoviral expression libraries for functional screening. *Nat. Biotechnol.* **2002**, *20*, 1154–1157. [[CrossRef](#)] [[PubMed](#)]
66. Rippmann, J.F.; Schoelch, C.; Nolte, T.; Pavliska, H.; van Marle, A.; van Es, H.; Prestle, J. Improved lipid profile through liver-specific knockdown of liver X receptor alpha in KKAY diabetic mice. *J. Lipid Res.* **2009**, *50*, 22–31. [[CrossRef](#)] [[PubMed](#)]



© 2019 by the authors. Licensee MDPI, Basel, Switzerland. This article is an open access article distributed under the terms and conditions of the Creative Commons Attribution (CC BY) license (<http://creativecommons.org/licenses/by/4.0/>).

Chapter 6

Developing a complex tetra co-culture model suitable for modelling the inflamed intestinal mucosa in a 3D microfluidic platform - a plug and play approach

The main goal of this chapter was to establish a plug and play tetra-coculture model that comprise of several interacting cell types typical for the human gut.

Author contributions

I developed the concept of a tetra co-culture and optimized the parameters. Performed the experiments and developed assays needed for the characterization of the mucus layer and the viability of the culture. Data in figure 6-6 A:C was performed by my intern GV.Moolenbroek.

Introduction

One of the major functions of the human intestine is to provide a protective epithelial barrier between the body and the digestive environment. Additionally, the interplay of commensal microbes of the gut microbiome with the gut tissue and the host immune system significantly contributes to intestinal homeostasis (Round and Mazmanian 2009; Garrett, Gordon, and Glimcher 2010). Crohn's disease (CD) and ulcerative colitis (UC), collectively referred to as inflammatory bowel diseases (IBD), are both associated with an increased permeability of the epithelial barrier and a dysregulated immune response. Although, the aetiology of these chronic inflammatory and relapsing diseases remains an enigma, it is known that environmental, genetic, immunological and microbial factors play a role (Orholm et al. 1991; Liu et al. 2015; Ananthakrishnan 2015; Frank et al. 2007). An increasing amount of evidence suggests that the onset and development of IBD is caused by an excessive immune response to the gut commensal microbiome in the intestinal mucosa in genetically predisposed individuals, accelerated by environmental influences (Abraham and Cho 2009; De Souza and Fiocchi 2016).

In the previous chapters I showed a simple gut-on-a-chip model that was based on Caco-2 that not only can be used as a healthy models for toxicological screenings but also to mimic characteristics of inflammatory bowel disease when specific molecular cues are applied (Beaurivage et al. 2019; Trietsch et al. 2017a). However, inflammatory processes in the gut are multifactorial and in their development not only factors but also several types of cells are involved, therefore depending of the therapeutic approach require altered complexity. In this chapter I wanted to account for the mucus producing epithelium and immune cells interactions in modelling various elements of gut physiology and inflammation. The simple Caco-2 model was further expanded to account for the mucus producing epithelium and immune cells interactions. This new

model therefore comprises of a tubular co-culture of enterocyte like Caco-2 and HT29-MTX-E12 cells, which are terminally differentiated HT29 clone into mucus secreting goblet like cells. A mixture of both in physiologically relevant ratios are seeded in the top compartment of the chip and a co-culture of immune competent cells THP-1 and MUTZ-3 seeded in the bottom compartment, with a collagen I extracellular matrix (ECM) lining the middle channel. To mimic intestinal inflammation, the model was exposed to various cytokines, whose effect was assessed by measuring the transepithelial electrical resistance (TEER) and the secretion of pro-inflammatory cytokines in both the apical and the basal compartments. Finally, I was involved in the assessment the applicability of the model in screening anti-inflammatory compounds Overall, this 3D multicellular perfused intestine-on-a-chip model provides the versatile modularity of mimicking key features of intestinal inflammation and can, therefore, further support drug screening efforts and provide a platform for personalized medicine.

Materials and methods

Cell culture

The human colon adenocarcinoma cell line Caco-2 (86010202, Sigma) is cultured in T75 flasks in Eagle's minimum essential medium (EMEM; 30-2003, ATCC) supplemented with 10% fetal bovine serum (FBS; 16140-071, Gibco), 1% non-essential amino acids (NEAA; 11140-050, Life Tech) and 1% penicillin-streptomycin (P4333, Sigma). The human colon cell line HT29-MTX-E16 (86010202, Sigma) is cultured in T75 flasks in Dulbecco's modified Eagle medium (DMEM; D6546, Sigma) supplemented with 10% FBS (16140-071, Gibco), 1% NEAA (11140-050, Life Tech), 1% Glutamax (35050-061, Gibco) and 1% penicillin-streptomycin (P4333, Sigma-). The human acute monocytic leukemia cell line THP-1 (Tib-202, ATCC) is cultured in T25 in Roswell Park Memorial Institute 1640 medium (RPMI; R0883, Sigma) supplemented with 10% FBS

(16140-071, Gibco), 1% Glutamax (35050-061, Gibco) and 1% penicillin-streptomycin (P4333, Sigma). THP-1 cells are differentiated towards macrophages in 6-well plates by exposure to 5 ng/ml PMA (phorbol 12-myristate 13-acetate) in the medium. After 72h, the medium is replaced with standard culture medium for 24h, after which the cell culture is trypsinized with TrypLE™ Express (12604-013, Life Tech) for seeding in the OrganoPlate®. The human acute myelomonocytic leukemia cell line MUTZ-3 (ACC 295, DSMZ) is cultured in T25 flasks in alpha-minimum essential medium (M4526, Sigma) supplemented with 20% FBS (16140-071, Gibco), 1% Glutamax (35050-061, Gibco), 1% penicillin-streptomycin (P4333, Sigma) and a 10% conditioned medium of confluent layers of 5637 cells (HTB-9, ATCC). The cells are cultured in a humidified incubator (37°C, 5% CO₂) and maintained by adding fresh medium every 2-3 days. All experiments are performed on Caco-2, HT29-MTX E12, THP-1 and MUTZ-3 cells between passage 53 and 60, 53 and 58, 6 and 14 or 6 and 9, respectively. The cells are routinely tested for mycoplasma contamination and found negative.

OrganoPlate® culture

This study employed OrganoPlate® three-lanes (Mimetas BV, the Netherlands) with 400 µm x 220 µm (w x h) channels. The PhaseGuides™ had dimensions of 100 µm x 55 µm (w x h). Before ECM loading, each observation window is filled with 50 µl HBSS to prevent dehydration and to provide optical clarity. Next, 2 µl of ECM composed of 4 mg/ml collagen-I (Cultrex 3D collagen-I Rat Tail, 5 mg/ml, 3447-020-01, AMSbio), 100 mM HEPES (15630-122, Thermo Fisher, Waltham, MA, USA) and 3.7 mg/ml NaHCO₃ (S5761, Sigma) is dispensed in the gel inlet. After incubation for 15 min at 37°C, 20 µl HBSS is added on top of the gel inlet, and the plate is incubated overnight in a humidified incubator at 37°C. Caco-2 and HT29-MTX-E12 cells are trypsinized with 0.25% Trypsin (15290-046, Gibco) and 0.53 mM EDTA (AM9260G, Ambion),

aliquoted, and pelleted (200 x g, 5 min). A suspension of Caco-2 and HT29 cells (concentration of 1×10^7 cells/ml) is prepared in a ratio of 6:1 in EMEM supplemented Caco-2 medium. Subsequently, a 2- μ l cell suspension is injected into the inlet of the top medium channel, after which 50 μ l of medium is added to the same well. The OrganoPlate[®] is placed on the side for 3.5 hours at 37°C to allow the cells to sediment and attach to the ECM. Next, an additional 50 μ l of culture medium is added to each of the remaining inlets and outlets of the top and bottom medium channels. Subsequently, the OrganoPlate[®] is placed horizontally in a humidified incubator (37°C, 5% CO₂) on an interval rocker switching between a +7° and -7° inclination every 8 min (Mimetas Rocker Mini, Mimetas BV), allowing bi-directional flow. The medium is refreshed every 2-3 days. At day 4 of culture, differentiated THP-1 and MUTZ-3 are collected, aliquoted and pelleted (300 x g, 5 min). A cell suspension of THP-1 and MUTZ-3 cells (concentration 3×10^6 cells/ml) is prepared in a ratio of 1:1 in EMEM supplemented Caco-2 medium. The medium in the bottom perfusion channel of each chip is aspirated, and 2 μ l of cell suspension is injected into the inlet of the bottom medium channel. Because the channels are wet, and the capillary force is lost, the cells are forced through the channel by pipetting 0.5 μ l cell suspension from the outlet into the inlet. This process is repeated 3 times, after which the OrganoPlate[®] is placed on the side for 30 min at 37°C to allow the immune cells to attach to the ECM. Subsequently, the medium present in the top medium channel is aspirated, and 50 μ l of fresh EMEM supplemented Caco-2 medium is added to all inlets and outlets of the top and bottom medium channels. The plate is again placed horizontally on the interval rocker. Experiments involving compound exposure for inducing or preventing inflammation are all performed at day 4 or 5 of culture.

Immunohistochemistry

Cultures in the OrganoPlate® are fixed with 3.7% formaldehyde (252549, Sigma) in phosphate-buffered saline (PBS; 20012068, Life Tech) for 10 min, then washed twice for 5 min with PBS, and permeabilized with 0.3% Triton X-100 (T8787, Sigma) in PBS for 10 min. Next, the cultures are washed with 4% FCS (16140-071, Gibco) in PBS and incubated with blocking solution (2% FCS, 2% bovine serum albumin (BSA) [A2153, Sigma]; and 0.1% Tween20 [P9416, Sigma] in PBS) for 40 min. The cells are then incubated with primary antibodies for 60 min at room temperature (RT), washed twice, incubated with secondary antibodies for 30 min at RT, and washed twice with 4% FCS in PBS. The following antibodies are used for immunohistochemical analysis: mouse anti-acetylated tubulin (1:2000, T6793, Sigma); rabbit anti-occludin (1:100, 71-1500, Thermo Fisher); mouse anti-ezrin (1:50, 610602, BD Transduction); rabbit anti-ZO-1 (1:125, 617300, Invitrogen); rabbit isotype (86199, Life Tech); mouse isotype (86599, Life Tech); goat anti-rabbit AlexaFluor 488 (1:250, A11008, Thermo Fisher); and goat anti-mouse AlexaFluor 555 (1:250, A21422, Life Tech). Finally, the nuclei are stained with Hoechst 33342 (H3570, Thermo Fisher), and the cells are stored in PBS. The cultures are imaged with ImageXpress Micro XLS- High Content Imaging Systems (Molecular Devices, US).

TEER measurements

The transepithelial electrical resistance (TEER) in the cultures in the OrganoPlate® is measured by using an automated multichannel impedance spectrometer (OrganoTEER, Mimetas BV). An electrode board containing gold electrodes that matched the OrganoPlate® three-lane layout was cleaned with 70% ethanol an hour before measurement. Prior to measurement, 50 µl of Caco-2 culture medium was added to all inlets and outlets, and the OrganoPlate® was placed on a rocker platform (7°, 8min) for 30 min in a humidified incubator (37°C, 5% CO₂) for equilibration. Subsequently, the OrganoPlate® was placed in the OrganoTEER device and point-impedance

measurements are performed with a frequency range of 10 Hz to 1 MHz (41 points; precision, 0.2) at RT. The corresponding software automatically generated TEER values per chip in Ohm (Ω). These values are normalized to Ohm.cm² by multiplication with the surface area of the tubule-ECM interface (0.0057 cm²).

Gene expression analysis

Epithelial tubes composed of Caco-2 and HT29-MTX-E12 cells are harvested from the top medium channel of the OrganoPlate[®] by using RLT lysis buffer (79216, Qiagen). RNA was extracted by using the RNeasy Micro kit (74004, Qiagen) and purified in accordance with the manufacturer's protocol. M-MLV reverse transcriptase (28025013, Thermo Fisher) was used to synthesize complementary DNA by following the manufacturer's protocol. The following probes are used in this study: MUC2 (forward: 5'-ACTGCGAGCAGTGTGTCTGT-3', reverse: 5'-AGGTGTACGTCTTCCCATCG-3'); MUC5AC (forward: 5'-AGGCCTGTGTCTGCACCTAC-3', reverse: 5'-CAGGGGTAGACCCTCCTCTC-3'); MUC12 (forward: 5'-CCTGGAAACCTTAGCACCAG-3', reverse: 5'-GACAGACGCATTGTTTTCCAT-3'); MUC13 (forward: 5'-TCCTCCTCAGATTACCAAGCA-3', reverse: 5'-GTTTAGGGTGCTGGTCTCCA-3'); MUC16 (forward: 5'-GGTGGACATCCATGTGACAG-3', reverse: 5'-TCCTAGGTTGGTGATGGTGA-3'); MUC20 (forward: 5'-TCCCTCCGACTACAACCAAC-3', reverse: 5'-ACCTCCATTTTCACCTGCAC-3'); and ACTB (forward: 5'-CTCTTCCAGCCTTCCTTCCT-3', reverse: 5'-AGCACTGTGTTGGCGTACAG-3') are used. Quantitative PCR was performed by using FastStart Essential DNA Green Master (06402712001, Roche) on the LightCycler[®] 96 system (Roche Molecular Systems Inc., Switzerland). Data are analyzed with the corresponding software, and expression levels of β -actin are used as the reference for normalization.

Alcian blue staining

Cultures in the OrganoPlate[®] are fixed with 0.1% glutaraldehyde (G5882, Sigma) in Hank's Balanced Salt solution (HBSS; H6648, Sigma) for 20 min at RT and then washed three times with HBSS. Next, the cultures are exposed to 1% Alcian blue (B8438, Sigma) prepared in 3% acetic acid (A6238, Sigma; pH 2.5) and incubated for 2 h by placing the OrganoPlate[®] on a rocker platform (8 min, 7°). Alcian blue was used to detect acidic mucous substances in the tubular structures. Subsequently, the cells are washed once with 3% acetic acid and two times with HBSS and then stored in HBSS. Image acquisition was performed by using the EVOS[™] FL Auto 2 Imaging System (Thermo Fisher, USA).

Cytokine kinetics in the OrganoPlate[®]

To determine the diffusion of potentially inflammatory cytokines either released by the immune cells or added to the system, the kinetics of several cytokines in the OrganoPlate[®] was assessed. A total of 2 μ l of ECM composed of 4 mg/ml collagen-I, 100 mM HEPES, and 3.7 mg/ml NaHCO₃ was dispensed into the gel inlet. After incubation for 15 min at 37°C, 20 μ l HBSS was added on top of the gel inlet, and the plate is incubated in a humidified incubator at 37°C overnight. Next, 50 μ l of a cytokine mixture composed of 0.5 mg/ml fluorescein isothiocyanate (FITC)-dextran (150 kDa; 46946, Sigma), 100 ng/ml TNF α (210-TA-020, R&D systems), 100 ng/ml interleukin (IL)-1 β (11340015, Immunotools), in Caco-2 complete medium was added to the inlet and outlet of each top medium channel in a OrganoPlate[®] three-lane. In the bottom medium channel, 50 μ l of Caco-2 complete medium was added to the inlet and outlet. The OrganoPlate[®] was then placed on a rocker platform (8 min, 7°), and medium was collected from the apical (top) and basolateral (bottom) compartments after 0.5, 1, 2, 6, 24, and 72 h for quantification of IL-8, TNF α and IL-1 β using human IL-1 beta/IL-1F2 DuoSet ELISA (DY201-05, R&D systems) and human TNF-alpha

DuoSet ELISA (DY210-05, R&D systems), respectively, in accordance with the manufacturer's protocol. Additionally, the diffusion of FITC–dextran was assessed by fluorescent imaging with ImageXpress XLS Micro (Molecular Devices, USA).

Immune cell functionality in the OrganoPlate®

To determine the functionality of the immune cells in the OrganoPlate®, 6000 differentiated THP-1 and/or MUTZ-3 cells are seeded in the top compartment of a three-lane chip in mono- or coculture against a collagen-I ECM. The cells are exposed to 0, 1, 10, and 100 ng/ml lipopolysaccharide (LPS; L2630, Sigma) in the apical (top) compartment. Medium was collected from the apical and basolateral compartments at 24, 48, and 72 h after exposure, and the concentration of IL-8 (CXCL8) was quantified by using the human IL-8/CXCL8 DuoSet ELISA kit (DY208, R&D systems) in accordance with the manufacturer's protocol. The absorbance of the samples at 450 nm was measured by using the Multiskan™ FC Microplate Photometer (Thermo Fisher).

Induction of inflammation

The tetra-culture model in the OrganoPlate® was exposed to 200 ng/ml TNF α and IL-1 β (11340015, Immunotools) on the apical and basolateral sides (top and bottom medium channels) on day 4 of culture. This was done by replacing the cell-culture medium in the inlets and outlets of the bottom and/or top medium channels with 50 μ l of medium containing the inflammatory trigger(s). TNF α and IL-1 β are dissolved in sterile PBS and sterile Milli-Q water, respectively. The cultures are exposed to the cytokines for 72 h on a rocker platform for interval measurements of phase-contrast imaging, barrier integrity (fluorescent probe assay and TEER measurements), and cytokine secretion. Finally, the cultures in the OrganoPlate® are fixed with 3.7% formaldehyde and stored in PBS at +4°C.

Cytokine secretion analysis

Media in the top and bottom medium channels are collected, and samples from the inlets and outlets are pooled. The concentration of IL-8 (CXCL8) was quantified by using the human IL-8/CXCL8 DuoSet ELISA kit (DY208, R&D systems) in accordance with the manufacturer's protocol. The absorbance of the samples at 450 nm was measured by using the Multiskan™ FC Microplate Photometer (Thermo Fisher).

Barrier integrity assay in the OrganoPlate®

All medium was aspirated from the chips, and 20 µl of medium without a fluorescent compound is added to the basal side of the chips (inlets and outlets of the gel channel and the bottom medium channel). Medium containing 0.5 mg/ml tetramethylrhodamine isothiocyanate (TRITC)–dextran (4.4 kDa; T1037, Sigma) was added to the top medium channel, which contained the epithelial vessel of Caco-2 and HT29-MTX-E12 cells. Subsequently, leakage of the fluorescent dye from the lumen of the tube into the ECM compartment was imaged over time with ImageXpress XLS Micro (Molecular Devices, USA). The ratio between the fluorescent signals in the basal and apical compartments of the tube was analysed by using FiJi (Schindelin et al., 2012).

Compound exposure to prevent inflammation

To determine the protective effect of anti-inflammatory compounds on the inflamed tetra-culture, cells in the OrganoPlate® were pre-treated with 1 µM TPCA-1 (2559, Tocris) on both the apical and basolateral sides or only on the basolateral side for 6 h, respectively. Subsequently, the medium was replaced with medium containing the cytokine trigger (200 ng/ml TNF- α and IL-1 β on both sides) and anti-inflammatory compound. The cultures are placed on the rocker platform and exposed to the cytokines and anti-inflammatory compound for interval measurements at 24, 48

and 72 h of phase-contrast imaging, barrier integrity (fluorescent probe assay and TEER measurements), and cytokine secretion. Finally, the cultures in the OrganoPlate[®] are fixed with 3.7% formaldehyde.

Statistics and data analysis

Image analysis was performed by using FiJi. Data analysis was performed by using Excel (Microsoft office 2016) and GraphPad Prism 6 (GraphPad Software Inc., USA). All data are expressed as mean \pm standard deviation (SD) of at least three individual chips ($n = 3$). Statistical analysis was performed by two-way analysis of variance with Tukey's multiple comparisons test, unless stated otherwise. Statistical significance was considered at $p < 0.05$.

Results

Schematic overview of the co-cultures -on-a-chip

To establish a 3D in vitro multicellular microfluidic intestinal model, we adapted and improved a previously published intestine-on-a-chip model, in which used polarized, leak-tight Caco-2 tubules (Trietsch et al., 2017). To better recapitulate the intestinal physiology and increase the model complexity and cell-to-cell interaction, additional cell types are added to the system. The microfluidic device used in this study, the OrganoPlate[®] three-lane, contains 40 microfluidic chips embedded in a standard 384-well microtiter plate format (**Fig. 6-1A**). Each chip comprises three adjacent culture channels that are linked to 9 wells of the microtiter plate, which serve as channel inlets and outlets. The channels join in the centre of the chip, where they are separated by two capillary pressure barriers called PhaseGuides[™]. The center well also serves as an observation window for monitoring the culture and for readout purposes.

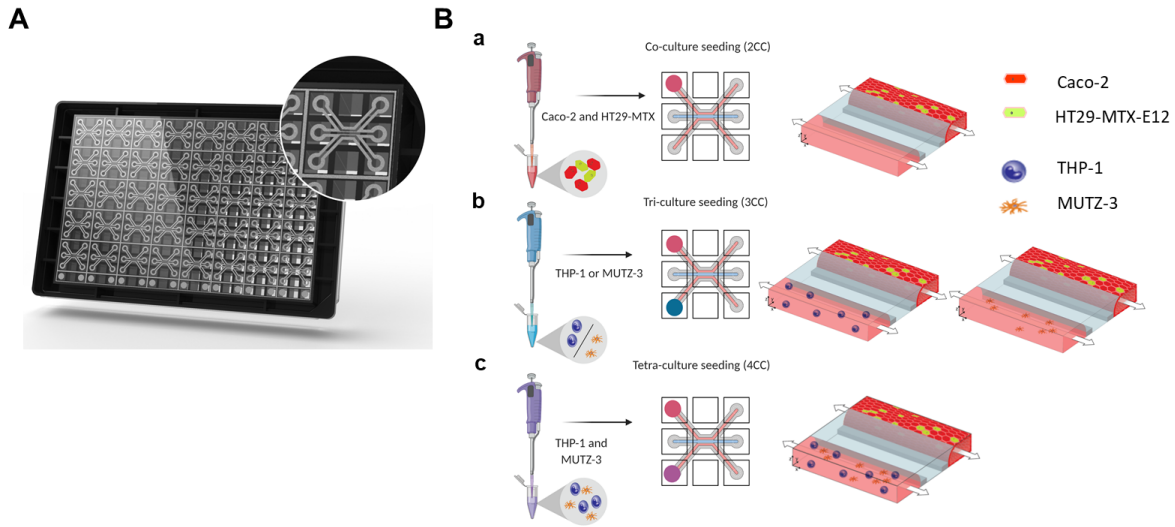


Figure 6.1 Development of a complex tetra co-culture intestinal model

A. Bottom view of the 3-lane OrganoPlate platform with 40 microfluidic cell culture chips embedded in a standard 384-well microtiter plate. Zoom-in image showing one microfluidic chip consisting of three channels: two medium perfusion channels and a gel channel in the middle. B. Schematic representation of the seeding strategy for establishing a plug and play model either co-culture, tri-culture and tetra-culture intestine on-a-chip. After patterning a collagen I ECM (*light blue*) into the middle channel of the chip between two phaseguides, a mixture of Caco-2 and HT29-MTX cells is seeded in the top channel (a). By placing the plate on its side, cells are allowed to settle against the ECM and upon starting medium perfusion flow, cells start to grow into a tubular structure covering the channel and the ECM surface. Once a confluent tubular structure has been obtained, usually at day 4 of culture, differentiated THP-1 and/or MUTZ-3 are added to the bottom perfusion channel (b,c). After an attachment period against the ECM, medium perfusion flow is restarted.

The methodology for establishing a membrane-free multicellular intestine-on-a-chip model is schematically illustrated in (**Fig. 6-1B**). The ECM loading for all of the complex co-cultures was the same and described more in details by (Trietsch et al. 2017a; Beurivage et al. 2019) however in short, an ECM gel composed of collagens added to the middle channel of each chip. The liquefied ECM enters the channels by capillary action, and, owing to the meniscus-pinning effect of the PhaseGuides™, doesn't overflow into the adjacent channels. After ECM gelation, a single-cell mixture of Caco-2 and HT29-MTX-E12 cells in medium (6:1 ratio) was loaded into the top

medium channel, and the cells are allowed to attach to the ECM by placing the plate on its side in vertical position. This step was the same for the co-culture (2CC), tri-culture (3CC) and the tetra-culture (4CC) (**Fig. 6-1B-a-c**). Subsequently, the plate was placed horizontally on an interval rocker platform to induce perfusion flow through gravity-driven liquid levelling between the reservoirs. Upon perfusion flow, the cells start to proliferate and line all surfaces of the medium channel. After an establishment of a confluent tubular structure, either a single cell suspension of differentiated THP-1 and of MUTZ-3 cells in medium (**Fig. 6-1B-b**) or a mixture of both in 1:1 ratio was loaded into the bottom medium channel(**Fig. 6-1B-c**), and the cells are allowed to attach to the ECM. Because these cells are grown in suspension they will not form a tubular structure against the ECM. Both the apical (lumen of the tube) and basolateral (accessible from the bottom medium channel) sides can be perfused with medium, exposed to compounds, and assessed for cytokine release. The optimization and the development of the culture was done in two phases due to the need for adding of up to 4 different cell types in one microfluidic chip, all of which have their specific cell culturing setup. In phase I the epithelial layer of Caco-2 /HT29-MTX co-culture was optimized and characterized and in phase II the optimized epithelial layer was tested with the immune cells separately and combined to deliver a high throughput and stable over time co-culture that can be used for phenotypic study.

Optimization of the Caco-2 /HT29-MTX intestinal model (2CC)

To increase the complexity and translatability, the Caco-2 model previously published was modified to also contain mucus-producing HT29-MTX-E12 cells. The seeding and culture conditions for the intestinal co-culture model (Caco-2/HT-29-MTX) were optimized first by testing the media in which the cells can be cultured **Fig. 2A**. The optimal media for culturing the co-culture was determined to be Caco-2 (EMEM) media. Tubules cultured in EMEM media didn't

invade the ECM and stayed stable for 11-15 days (data not shown). Furthermore, the ECM supporting the epithelial layer was tested and for the tubule formation a Collagen I was most successful in maintaining leak tight barrier **Fig. 2B**. shows the barrier integrity assay assessed by using a fluorescent probe (the 4.4-kDa TRITC–dextran probe), which was

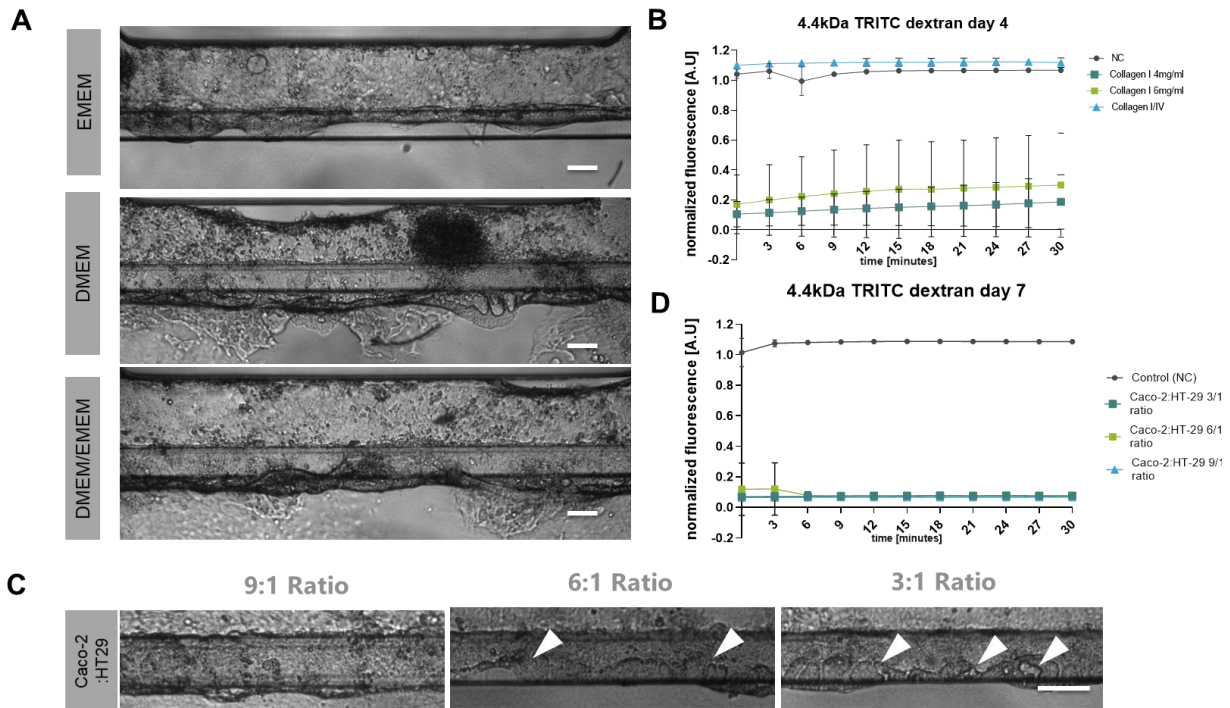


Figure 6.2 Optimization of mucus producing tubules

A Phase-contrast images of Caco-2 and HT29-MTX-E12 tubules at day 11 cultured in different medias, EMEM, DMEM and a 1:1 mixture of DMEM and EMEM. B. Barrier integrity assessment of the epithelial tube in the tetra-culture model after 6 days of culture under perfusion. A fluorescent probe (the 4.4-kDa TRITC1–dextran probe) was added to the lumen of the tube and assessed for leakage into the adjacent ECM channel. The ratio is determined and where the cells form a leak tight barrier exp. Collagen I 4mg/mL ratio is lower, whereas the no-cells control or the there is the ECM with collagen I/IV mixtures there is a higher and close to 1 ratio showing clear leakage of the dye into the ECM compartment. C. Phase-contrast images of Caco-2 and HT29-MTX-E12 tubules at day 11 seeded in 9:1, 6:1 and 3:1 ratio. Arrows pointing at the goblet cells location and the morphological differences between seeding ratios. Scale bar 100um.

perfused in the lumen of the gut tubule. The leakage of the fluorescent probe into the ECM compartment was determined and normalized to the fluorescence in the lumen of the tube. The BI assay was also performed to the leak tightness of the ratios between Caco2 and HT-29 MTX cells at day 7 **Fig. 2D**. All the physiologically relevant ratios were found to form a leak tight barrier between day 4-6 (data not shown) but a fully established by BI assay at day 7 **Fig. 2C** shows a phase-contrast image of a three-lane chip in an OrganoPlate[®] with the different seeding ratios of Caco-2 and HT-29MTX cells on day 4 of culture (2CC) of a single chip.

Characterization of the Caco-2 /HT29-MTX intestinal model (2CC)

The expression of key markers in the co-culture model in the OrganoPlate[®] was assessed by using an immunofluorescence-based approach in combination with high-content microscopy. A 3D reconstruction of a gut tubule consisting of Caco-2 and HT29-MTX-E12 cells was shown in **Figure 6-3A**. It demonstrates a tubular structure that has formed with cells lining the ECM and walls of the medium channel, which indicates the presence of a clear lumen with accessibility to both apical and basolateral sides. Furthermore, the coculture of Caco-2 and HT29-MTX-E12 cells displays brush-border formation and tight junctions, as shown by the expression of ezrin and ZO-1, respectively (**Fig. 6-3B**). Finally, the mucus production of the co-culture was assessed as tubular structures composed of only Caco-2 or HT29-MTX-E12 and a coculture of both cells in the OrganoPlate[®] are stained with Alcian blue on day 4 of culture. As shown in **Fig. 6-3C**, the monoculture of HT29-MTX-E12 showed the highest level of staining. Interestingly, the Caco-2 monoculture also displayed staining of mucins, but to a lower extent than the HT29-MTX-12 tubules. The coculture of Caco-2 and HT29-MTX-E12 showed an intermediate level of staining. **Fig.6-3D** shows a merge of phase contrast image and staining for MUC2 (red) and MUC5AC (yellow) expressed by the 6:1 ratio co-culture of Caco-2 and HT-29-MTX. The optimal ratio for

mucus production and barrier integrity was determined to be 6:1 Caco-2/HT-29MTX and this was used for the complex co-cultures.

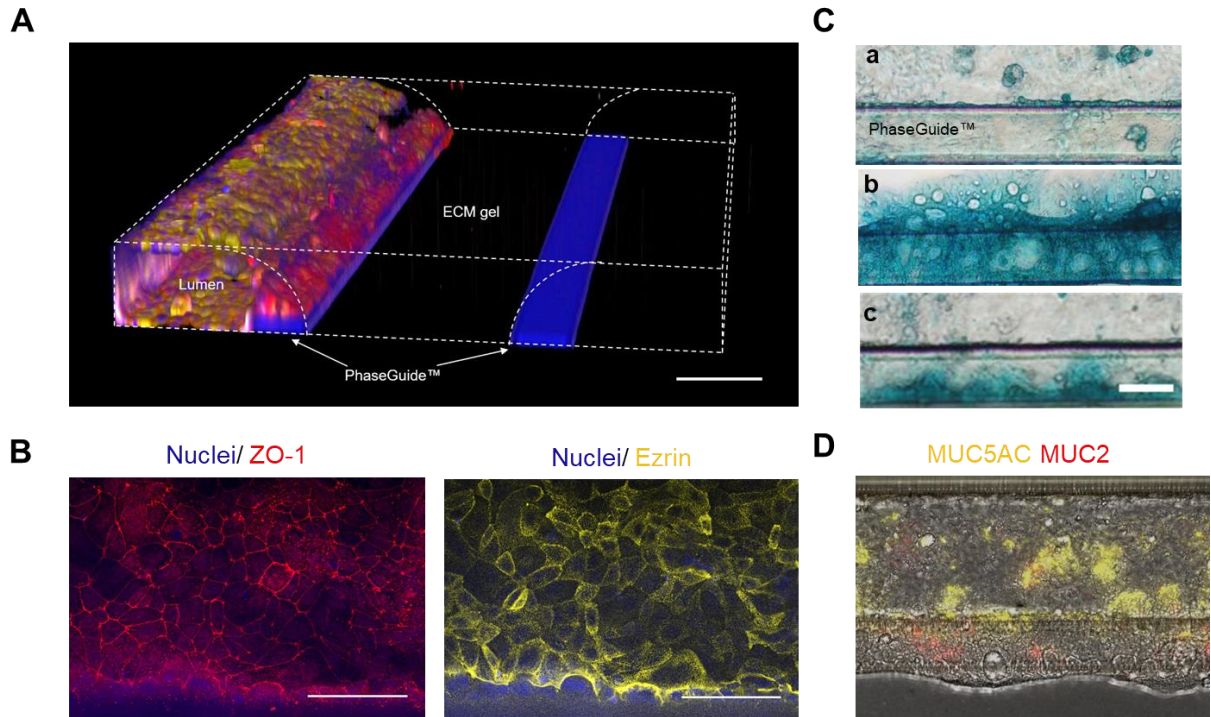


Figure 6.3 Characterization of mucus producing 2CC

A. 3D reconstruction of a confocal z-stack at 10x magnification, showing a tubular epithelial structure of Caco-2 and HT29-MTX cells against a collagen-I ECM patterned in the middle compartment. The tube was stained for acetylated tubulin (red), occludin (yellow), and DNA (blue). B. Representative immunofluorescent max projections of the epithelial tube in the 2CC set up at 20x magnification stained for Ezrin (yellow), ZO-1 (red) and DNA (blue). C. Alcian blue staining in a monoculture of Caco-2 or HT29-MTX cells or a coculture of Caco-2 and HT29-MTX cells in a three-lane OrganoPlate[®] on day 4. Acidic glycosaminoglycans produced and secreted by the cells into the lumen of the tube are visualized in blue. All cultures were fixed on day 4 of culture. D. Immunofluorescent image merged with a PhC image of the cells at day 7. The cells are stained for MUC5AC (yellow) and MUC2 (red). Scale bars in white are 100 μm (A), 50 μm (B)

Optimization of the tetra co-culture intestinal model (4CC)

In order to obtain a model that more closely reflects the physiological cellular composition of the intestine, immune cells were added to the OrganoPlate®. The seeding and culture conditions for the intestinal tetra-culture model were optimized by testing different parameters such configuration of cells relative to the epithelial layer (**Fig. 6-4 A**) in this experiment cells were seeded either embedded in the ECM or added to the bottom perfusion channel. **Fig. 6-4 B** shows that when cells are added in the bottom channel the barrier is maintained and tubules are more leak-tight as the fluorescent probe is retained in the lumen of the tubule at day 7. Moreover **Fig. 6-4 C** shows the percentages of leak-tight versus leaky tubules in both seeding methods at day 7. The viability of the culture was also assessed and even though there were no significant differences, the seeding in the bottom channel had produced more viable cells **Fig. 6-4 C,D**. To show the functionality of both THP-1 and MUTZ-3 cells, mono- and co-cultures of the immune cells (6000 cells per chip) were seeded in the top compartment and exposed to different concentrations of LPS **Fig. 6-4F**. IL-8 secretion was assessed which shows the individual and combined contributions of the different cell types of its release after 24, 48, and 72 h of trigger exposure. Combining THP-1 and MUTZ-3 cells results in a synergistic release of IL-8 into the medium in the apical compartment.

After the optimization steps the complex tetra co-culture was assessed for expression of relevant markers involved in the barrier integrity and polarization and the mucus production and by immunofluorescence. The coculture of Caco-2 and HT29-MTX-E12 cells displays brush-border formation and tight junctions, as shown by the expression of ezrin and ZO-1, respectively (**Fig. 6-5A**). Moreover, the genes MUC5AC, MUC12, MUC13, MUC16, and MUC20 all showed a fold-change increase in expression levels after 48 h (day 5) and 72 h (day 6) of culture relative to the

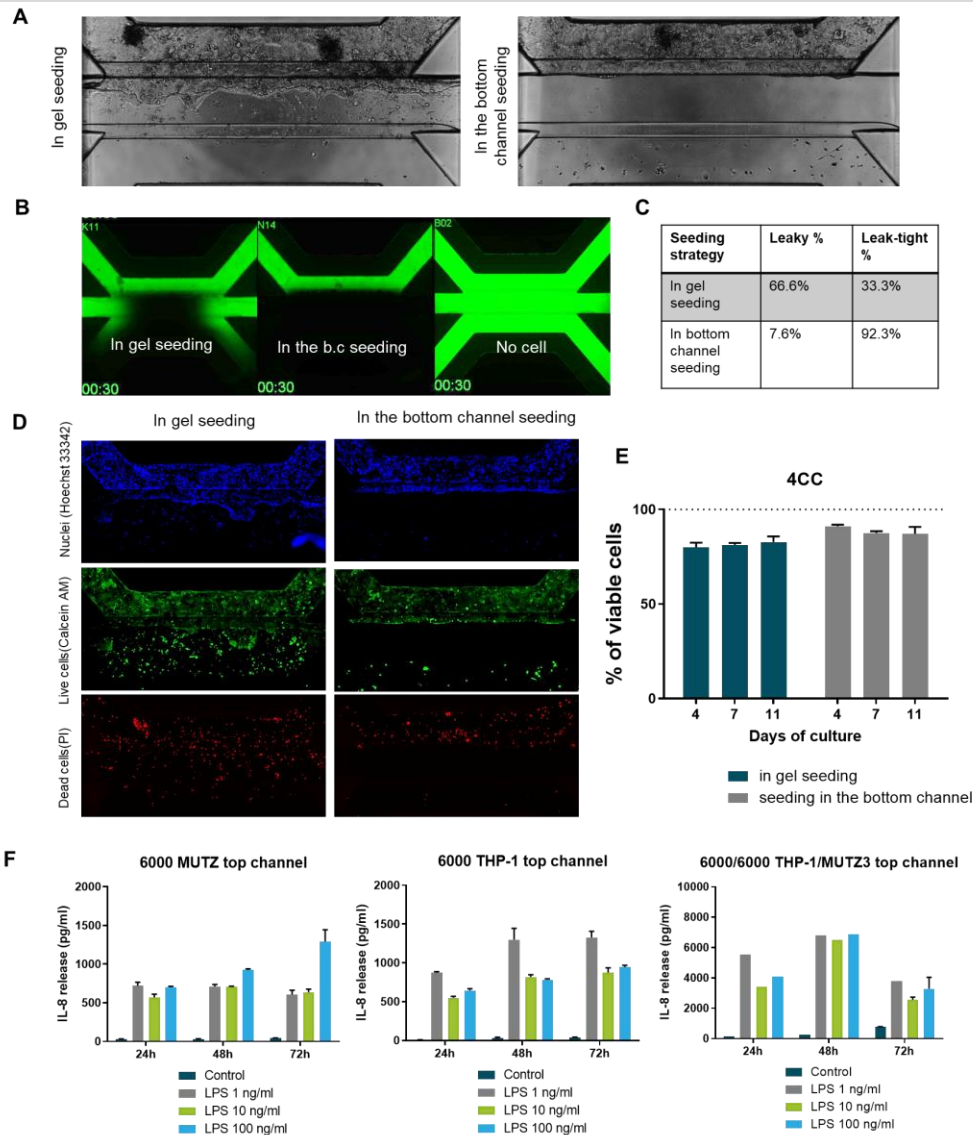


Figure 6.4 Optimization of the tetra co-culture model

A. Phase-contrast images of seeding of seeding strategy of immune cells THP-1 and MUTZ-3 were added either embedded in the ECM matrix (in gel seeding) or added to the bottom medium compartment (in bottom channel seeding) B. Barrier integrity assay performed in 4CC, immune cells are seeded in the gel or in the bottom channel. Images taken at 30 min also showing the No cell control C table showing the percentage of leaky and leaktight tubules on day 7 D. Live dead staining of both seeding strategy of immune cells. Tetra-culture was stained at day 7. Nuclei were stained with Hoechst 33324 (blue) live cells were stained with Calcein AM (green) and dead cells are stained with Propidium Iodine (PI) (red). E Quantification of Live dead assay at day 4, day 7 and day 11 for the 4CC model and both seeding strategies. Data is represented in percentages of dead cells over total cells (n=3 chips). F Eliza performed for secreted IL-8 after stimulation of mono and co-cultures of THP-1 and MUTZ-3 (n=3-5 chips).

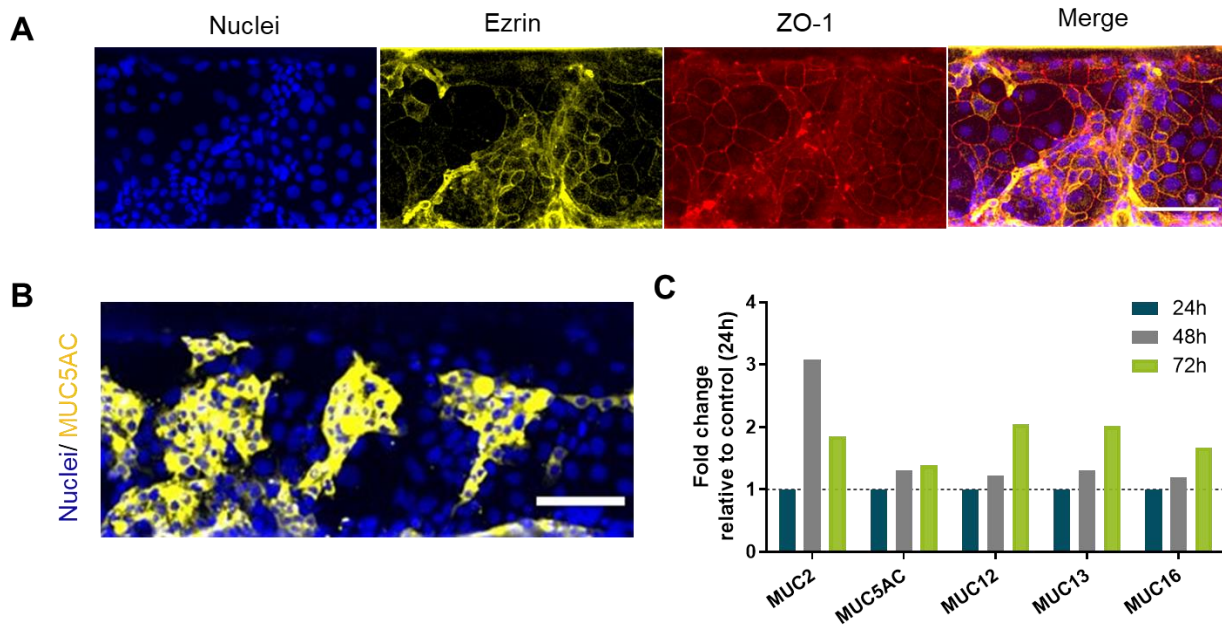


Figure 6.5 Characterization of the tetra co-culture (4CC)

A. Representative immunofluorescent max projections of the epithelial tube in the tetra-culture at day 4 set up at 20x magnification stained for Ezrin (yellow), ZO-1 (red) and DNA (blue). B. Max projection of an stained tubular structure of Caco-2 and HT29-MTX cells in the top compartment of a 3-lane OrganoPlate at day 4 of culture. Cells are stained for MUC5AC (yellow) and DNA (blue). Scale bar in white is 50 μm . C. Expression of genes involved in the production of mucus by the co-culture of Caco-2 and HT29-MTX cultured in the 3-lane OrganoPlate at day 4 (24h), 5 (48h) and 6 (72h). Data is represented as fold change and normalized to 24h datapoints

expression levels at 24 h (day 4) (**Fig. 6-5C**). The results of immunofluorescent staining of MUC5AC showed clear local expression of mucin in the co-culture tubule (**Fig. 6-5B**).

Mimicking intestinal inflammation

To mimic intestinal inflammation LPS was used, however, even though immune cells were responsive the epithelial cells didn't respond to the addition of LPS (data not shown) That is why the determination of the diffusion kinetics of product of immune activation was assessed $\text{TNF}\alpha$, and $\text{IL-1}\beta$ were added—together with the 150-kDa FITC-dextran—to the top (apical) medium compartment of a chip containing only ECM in the middle compartment (**Fig. 6-6A**).

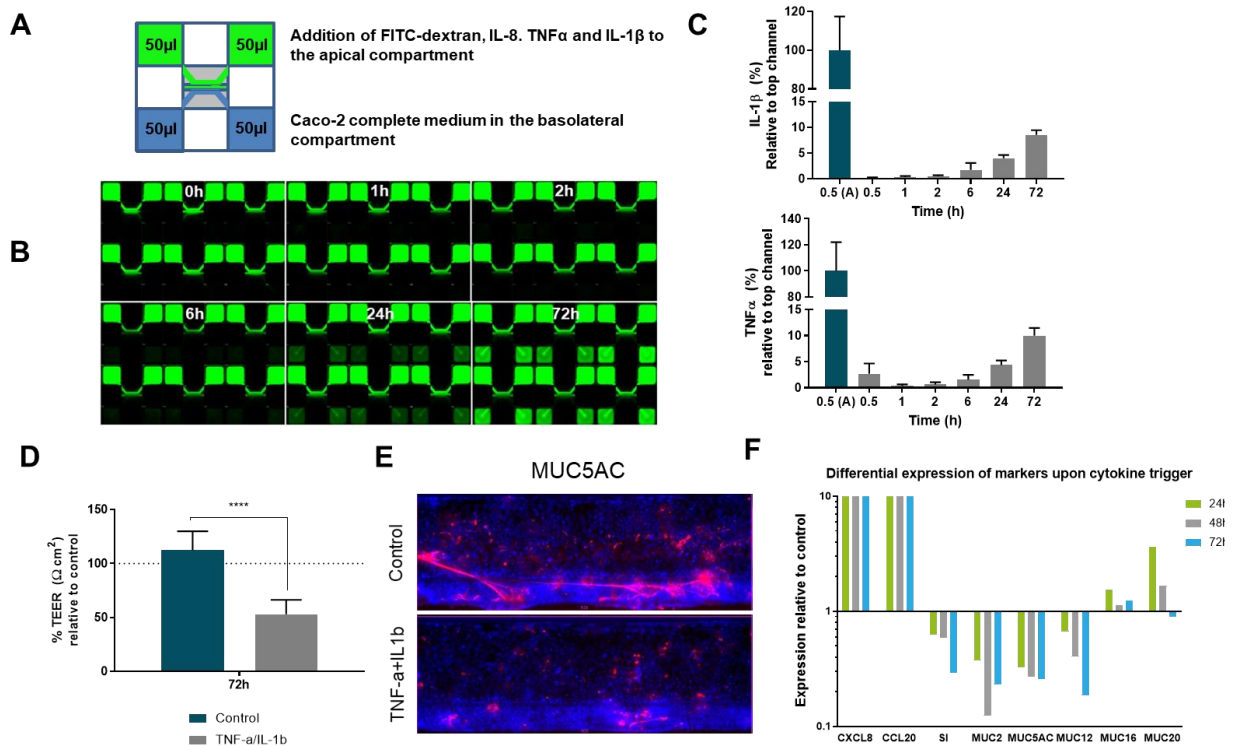


Figure 6.6 Trigger dynamics and inducing inflammation in the 4CC

A TNF α and IL1 β were added to the top medium compartment together with 150 kDa FITC-dextran (50 μ l to in- and outlet) of chips containing only a collagen-I ECM in the middle compartment. Standard Caco-2 complete medium was added to bottom compartment (50 μ l to in- and outlet). The plate was placed on the rocker platform to induce perfusion through the channels. B Real-time imaging of interval measurements at 0, 1, 2, 6, 24 and 72 hours showed the diffusion of the fluorescent FITC-dextran dye over time in the chip. C Cytokine analysis on medium samples from the bottom medium compartment showed the detectability of TNF- α and IL1 β over time. D the effect of the cytokines, on transepithelial electrical resistance (TEER) at 72 hours after exposure. Data is represented in percentages and normalized to the 2h non-exposed condition (n=4). E. fluorescent images of tubules stained for MUC5AC (red) after 72h triggered with the cytokine cocktail. F. Expression of genes involved in inflammation differentiation and the production of mucus by the co-culture of Caco-2 and HT29-MTX cultured in the 3-lane OrganoPlate at day 4 (24h), 5 (48h) and 6 (72h). Data is represented as fold change and normalized to 24h datapoints

Real-time imaging for interval measurement showed diffusion of the dye over time in the chip (**Fig. 6-6B**). Cytokine analysis of medium samples containing TNF α , and IL-1 β revealed that, 10.1%, and 8.5% of these cytokines reached the bottom medium channel after 72 h, respectively

(Fig. 6-6C). Overall, these results indicate that the cytokines can cross the collagen-I ECM by passive diffusion and reach the other compartment, however at very low rate .

Knowing this the mimicking of intestinal inflammation in the tetra-culture model was done by exposing the 4CC model TNF α and IL-1 β on both apical and basolateral sides on day 4-5 of culture for 24h, 48h and 72 h (Fig. 6-6 D,E,F). This inflammation cocktail and exposure strategy was found to be the most effective in inducing a drop in barrier integrity (Fig.6-6D) and increasing the expression of marker of inflammation like IL-8, CCL20 decreasing mucus production and markers of differentiation like Sucrase-Isomaltose detected by RT-qPCR (Fig.6-6F) Decrease in the expression of MUC5AC after cytokine trigger was also detected by immunofluorescence (Fig.6-6E).

Preventing intestinal inflammation

Finally we assess the applicability of the tetra-culture model for screening anti-inflammatory compounds, the tetra-culture (4CC) was pre-treated with 1 μ M TPCA-1 for 6 h prior the addition of the inflammatory cocktail (TNF α and IL-1 β) in the extended presence of the compound (Fig. 6-7A). TEER measurements revealed a significant difference in TEER between the treated and non-treated chips in the presence of TNF α and IL-1 β after 72 h of exposure. TPCA-1-treated cultures triggered with TNF α and IL-1 β retained TEER values similar to those of the vehicle control (Fig. 6-7B). Furthermore, IL-8 levels in medium samples from the apical and basolateral sides are assessed after 24, 48, and 72 h. The results showed increased IL-8 secretion in cultures exposed to TNF α and IL-1 β (both apical and basolateral sides) than in non-treated cultures (Fig. 6-7C). Of note, TPCA-1 pre-treatment significantly hampered IL-8 release, as evident upon comparing TPCA-1-treated cells with -treated cells. This effect of TPCA-1 in decreasing IL-8 secretion is observed in both apical and basolateral samples when the cultures are exposed to both

TNF α and IL-1 β . In summary, these results showed that treatment of cultures with the anti-inflammatory compound TPCA-1 could prevent inflammatory status in the cells.

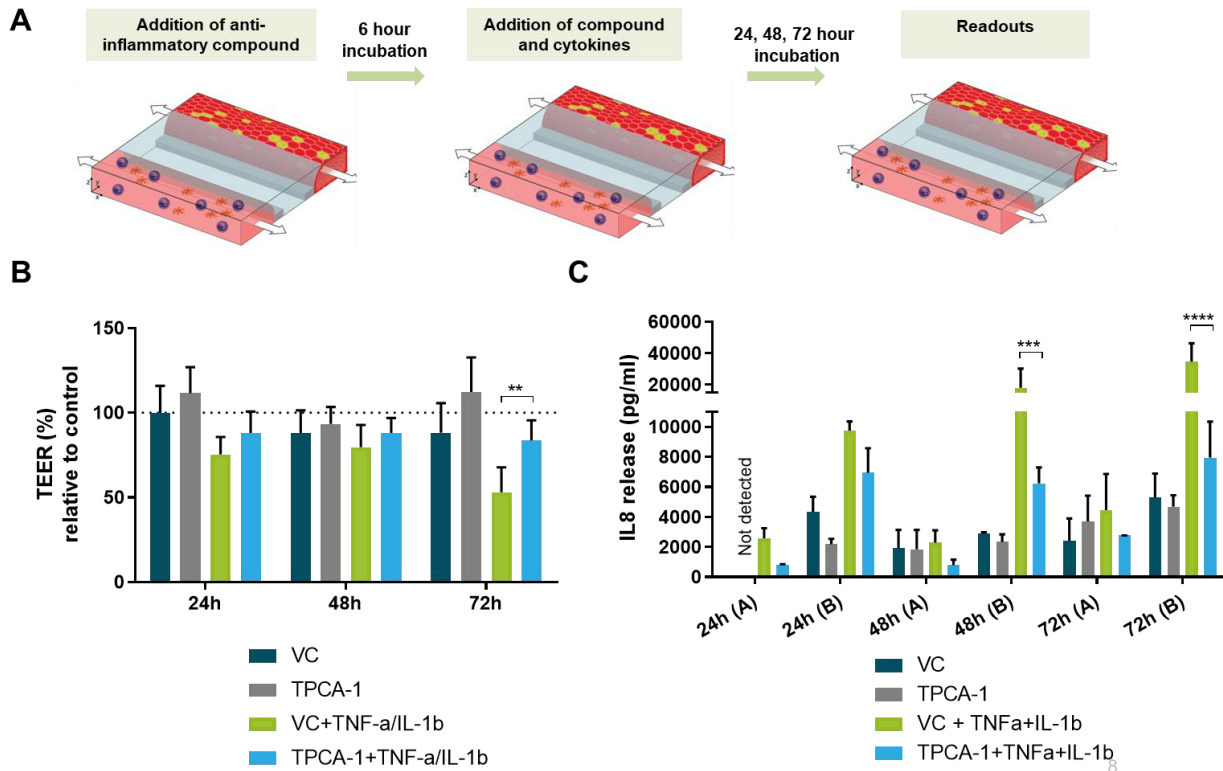


Figure 6.7 Prevention of the intestinal inflammatory-like phenotype induced by cytokines in the intestine on-a-chip model by addition of the anti-inflammatory compound TPCA-1

A Schematic overview of the exposure strategy in the tetra-culture intestine-on-a-chip model. Cultures were pre-treated with 1 μ M TPCA-1 and incubated for 6 hours under perfusion. Next, the cultures were exposed to TPCA-1 and cytokines (TNF α and/or IL1 β) followed by incubation for 24, 48 or 72 hours on the rocker platform. Finally, the morphology, barrier integrity and release of cytokines were assessed in the cultures. B To determine the cytokine effect and the anti-inflammatory action of the TPCA-1 on the culture, transepithelial electrical resistance (TEER) of the epithelial barriers was assessed at 24, 48 and 72 hours after exposure to the cytokines. Data is represented in percentages and normalized to the 24h non exposed condition (VC) (n=4-9 chips). C The secretion of the pro-inflammatory cytokine IL-8 was assessed in the apical (A) (Caco-2/HT29-MTX) and basolateral (B) (THP-1 and MUTZ-3) in the triggered and non-triggered conditions at 24, 48 and 72h after exposure to the cytokines. ***, p<0.001; ****, p<0.0001. (n \geq 3 chips).

Discussion

In this study, a complex 3D multicellular Plug and play intestine-on-a-chip model was developed in which it is possible to mimic intestinal inflammation, as demonstrated by the loss of barrier function and production of cytokines. Moreover, this simple and reproducible tool kit can be used in its highest complexity 4CC or lowest 2CC depending on the research question posed.

The complexity of the model is achieved by creating a tubular structure comprising a co-culture of Caco-2 cells and the mucus-producing HT29-MTX-E12 cells against a collagen-I ECM. Additionally, a coculture of immune-competent cells THP-1 and MUTZ-3 is established by adding the cells to the basal medium compartment. Moreover, Caco-2 and HT29-MTX-E12 coculture (2CC) formed confluent and polarized tubular structures against the collagen-I ECM in the OrganoPlate[®], with a stable barrier function over time. The model was capable of mucus secretion, as evident from the staining and gene expression results. This is extremely important if microbiota is also included at some point in the culture because it is known that the presence of a mucus layer is important in *in-vitro* modelling because more often pathogens cause different pathology compared to no mucus containing models (Navabi, McGuckin, and Lindén 2013a).

Furthermore, by exposing the cultures to TNF α and/or IL-1 β , an inflammatory state was induced, characterized by cytokine release (IL-8) and a decrease in TEER values and decrease secretion of mucus components like MUC12 and MUC16, characteristic for UC patients (Yamamoto-Furusho et al. 2015). These cytokines proved to be more effective than LPS in activating the epithelium. The immune-cell functionality of the model was determined by exposing monocultures or cocultures of differentiated THP-1 and MUTZ-3 cells to various concentrations of LPS. We showed a concentration- and cell-number-dependent increase in IL-8 release by both cells and observed a synergetic effect in the cocultures. The induced inflammatory state of the cultures in the tetra-culture model could be prevented by treatment with the anti-inflammatory

compound TPCA-1; this result is evident from the decreased secretion of IL-8 and retention of barrier function in treated cultures at levels similar to those observed in untreated cultures.

Compared to Transwell cultures, other intestine-on-a-chip systems, and animal models, this platform has considerable throughput capacity because of its ability to accommodate 40 independent intestinal cultures in parallel (Trietsch et al. 2017a; Beurivage et al. 2019). Finally, this type of organ-on-a-chip systems provide versatile modularity for studying the individual contribution of each factor, thus paving the way towards unravelling the underlying pathophysiology of intestinal inflammation, which is not possible in any animal model.

In summary, in this chapter I showed the development and characterization of a robust, high-throughput, 3D multicellular perfused intestine-on-a-chip model in which could be used to mimic mucosal inflammation, as demonstrated by the loss of barrier function and production of cytokines. Additionally, this model can be applied for screening anti-inflammatory compounds. Overall, this model allows the versatile modularity of mimicking key features of intestinal inflammation, which positions it at the forefront of high-throughput screening efforts for supporting drug discovery and providing a platform for personalized medicine. This extremely important for the pharmaceutical industry knowing that when organs on a chip are implemented in a standard drug development process one estimate shows an overall reduction of 10–26% in total costs, calculated savings per new drug reaching the market of up to 631 million euros (DiMasi, Grabowski, and Hansen 2016; Adams and Brantner 2010).

Chapter 7

Directed differentiation of induced pluripotent stem cells towards gut-on-a-chip in a 3D microfluidic platform

The main goal of this study was to develop and optimize a method for the generation of intestinal tubules from iPSC. Moreover to characterize the gut-on-a-chip model and show applicability for IBD modelling.

Authors contributions

I developed the concept of directed on plate differentiation, wrote the project plan, designed and performed the optimization experiments (figure 2, figure A1 (A,B) and figure A2) at Sheffield University, I was involved in planning and analysis of data for all of the figures and wrote the manuscript with the comments of the authors.

DIRECTED ON PLATE DIFFERENTIATION OF INDUCED PLURIPOTENT STEM CELLS TOWARDS GUT-ON-A-CHIP MODEL IN A HIGH-THROUGHPUT PLATFORM

Elena Naumovska ^{1,3,†}, Germaine Aalderink ^{1†}, Christian Vong Valencia ², Kinga Kosim ^{1,2}, Stephen Brown ², Kai S. Erdmann ² and Dorota Kurek ^{1,*}

¹ Mimetas BV, J.H. Oortweg 16, 2333 CH Leiden, The Netherlands; e.naumovska@mimetas.com (E.N.); k.kosim@mimetas.com (K.K), aalderink.germaine@gmail.com (G.A)

² Department of Biomedical Sciences, University of Sheffield, Western Bank, S10 2TN Sheffield, United Kingdom; k.erdmann@sheffield.ac.uk (K.E), s.brown@sheffield.ac.uk (S.B), cwongvalencia1@sheffield.ac.uk (C.V)

* Correspondence: d.kurek@mimetas.com (D.K.); +31-8588-83161 (DK),

† These authors contributed equally to this work.

Abstract: The absence of patient specific intestinal in-vitro models impairs drug discovery and development processes. Current static models lack the cellular complexity and genetic variability found in patient-derived samples. Organoids represent a possible solution to this problem as they allow to produce all cell types inhabiting the intestine from induced pluripotent stem cells (iPSC) within a three-dimensional structure. Unfortunately, organoids have enclosed lumens and are usually embedded in Matrigel dome making them difficult and labor-intensive tools for high throughput studies. In this study, we directly differentiated induced pluripotent stem cells towards intestinal-like phenotype within a microfluidic device to produce tubules with an accessible lumen and a basolateral side. Within 14 days differentiation in OrganoPlates, the iPSC lose their stem cell markers and acquire mature intestinal marker expression, while maintaining a leak-tight barrier. These iPSCs derived gut tubules show physiologically relevant Transepithelial electrical resistance (TEER), as well as a powerful response to pro-inflammatory trigger. Therefore, iPSC-derived intestinal-like tubules directly differentiated in microfluidic devices hold the potential as an efficiently produced, patient specific, high-throughput model that can be further optimized for disease modelling and drug candidate screening.

Keywords: iPSC; directed differentiation; gut-on-a-chip; Organ-on-a-Chip; microfluidic, 3D, high-throughput; disease modeling

1. Introduction

In-vitro models that closely mimic the human intestinal epithelium and its physiology are important tools for drug development processes as oral drug delivery is the preferred route of administration [1]. These models have enormous potential to improve and speed up studies of absorption, drug metabolism and interactions as well as associated toxicology. Therefore, patient specific absorption models that take the gut complexity, passive transport, active transport and patient variability into consideration could be highly valuable in the evaluation of candidate drugs [2].

One potential cell source for building such models are intestinal organoids derived from induced pluripotent stem cells (iPSC) [3]. As opposed to human embryonic and adult stem cells, there are no ethical concerns in using iPSC cells in research and the material is patient specific and easy to acquire. Moreover, their ability to differentiate into the major cell types of the intestinal epithelium makes them a useful tool to investigate the intestinal epithelium's role in health and disease in vitro. Nevertheless, a major limitation of organoid culture is the overall closed

conformation, which makes the apical-luminal surface of the epithelium inaccessible [4]. Embedding 3D organoids into a gel matrix restricts the accessibility to compounds for transport studies and limits the ability of real-time imaging. Additionally, organoids are usually difficult and costly to produce [5,6].

In our study we focused on overcoming some of the hurdles in intestinal in-vitro modelling for high-throughput drug discovery. These include robustness, reproducibility, cost-effectiveness and patient specificity. In a proof of principle study, by using induced pluripotent stem cells we developed a protocol for directed differentiation of iPSC into 3D gut-like tubules in microfluidic cell culture devices without the need for an intermediary organoid step. This directed differentiation of iPSC in the microfluidic system could combine quick establishment of the model with patient-specific cells thus decreasing costs and increasing physiological relevance. These gut tubules are accessible from both apical and basal side which allows for the assessment of barrier function, transport activity, real-time drug absorption and quantification of cytokines production.

2. Results

2.1. Directed on Organoplate differentiation of iPSC towards gut-on-a-chip

In this study, iPSC derived intestinal tubules were differentiated in the 3-lane OrganoPlate platform which contains 40 independent microfluidic chips (**Fig. 1A**) that have 3 microfluidic channels with dedicated inlets and outlets. The 3D culture can be monitored in real-time through an observation window (**Fig. 1B**). Extracellular matrix (ECM) is introduced into the middle channel where it creates a meniscus after which iPSC are seeded against the ECM gel in the top channel (**Fig. 1C**). The experimental scheme is shown in (**Fig. 1D**). iPSC were seeded directly in OrganoPlate and after 2 days differentiation was started for 2 days in Definitive endoderm (DE) media, 3 days of Hindgut (HG) media and 7 to 24 days in the Mature Intestine (MI) media.

To optimize the attachment of iPSC in the OrganoPlate several conditions were tested including ECM composition (collagen 4mg/ml and Matrigel) and coating strategies with recombinant human Vitronectin (rhVTN), Laminin and no coating (**Fig.A1**). The stem cells attached to all coatings but detached from Laminin on day 4 and did not attach properly in the chips without coating. Moreover, conditions containing Matrigel as ECM and coated with Laminin or VTN were more likely to remodel the ECM, whereas chips having Collagen and rhVTN as coating remained more stable (**Fig.A1.B**). Once we established and optimized the seeding strategy, we applied a 3-step directed differentiation protocol adapted for differentiation in microfluidic devices (**Fig 1D**). In the first step, the definitive endoderm (DE) differentiation is achieved by treating the iPSC for 24h with Wnt-agonist CHIR99021, followed by a medium only treatment. Moreover, to assess the differentiation potential of iPSC towards DE we performed a small endodermal screen as described by Siler et al. (**Fig. SA2.A**). iPSC were treated with either 3 or 4 μ M CHIR99021 in RPMI/B27 +/- insulin in RPMI-1640 Medium on day 2 and RPMI/B27 +/- insulin in RPMI-1640 on day 3. We did not observe any morphological differences between the conditions and all of the treated cells were able to form tubules (**Fig. 2A**). There were no significant changes in the DE and HG marker expression as tested by RT-qPCR. However, when we tested the development of barrier integrity by TEER measurements we saw a small but not significant improvement of barrier integrity in the 3 μ M CHIR99021 in RPMI/B27 + insulin in RPMI-1640 medium condition. Uniform expression of FOXA2 and SOX17 endodermal markers on day 4 confirms successful differentiation towards definitive endoderm (**Fig. 2B**).

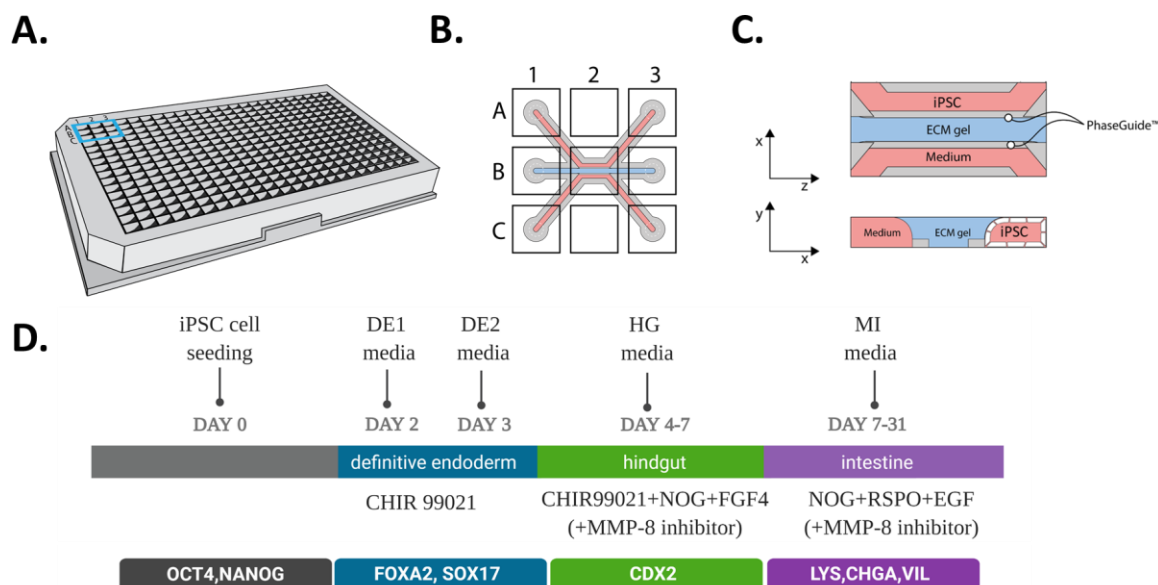


Figure 1. Seeding and differentiation of hiPSC in the 3-lane OrganoPlate. A. Schematic representation of the 3-lane OrganoPlate. Each individual chip is spanning nine connecting wells (blue) B. One chip contains three microfluidic channels all having top, middle and bottom inlets (A1, B1 and C1) and outlets (A3, B3 and C3) and an observation window (B2) for real-time assays. C. hiPSC cell seeding in a microfluidic chip on a parallel and transversal view; single iPSC are seeded in the top channel and are left to adhere flat for up to 24h after which media is added and perfusion started, cells start to form tubules growing against the ECM gel (blue). D. Schematic of workflow for directed on plate differentiation of iPSC into gut tubules.

2.2.

Activation and inhibition of several signaling pathways like Notch, Wnt, phosphoinositide-3-kinase and BMP are important for the intestinal differentiation [7]. Therefore, in the second step we examined whether DE cells can be differentiated further towards hindgut (HG), cells were treated additionally with CHIR 99020, BMP-antagonist Noggin (NOG) and Fibroblast growth factor 4 (FGF4) for 3 additional days. On day 7 post-seeding, cells started expressing intestinal progenitor cell marker caudal type homeobox 2 (CDX2, transcription factor important for intestinal development (Fig.2D). Moreover, cells downregulated the expression of pancreatic progenitor cell marker pancreatic and duodenal homeobox 1 (PDX1) (Fig.A2.B), confirming that the cells were of a posterior nature. Furthermore, the iPSC-derived gut-like cells showed homogeneous staining for CDX2 (Fig.2C). This result suggests that most of the undifferentiated human iPS cells were successfully differentiated towards intestinal lineage.

In the last step of the differentiation a mature intestinal media (MI) was added to direct the CDX2+ cells towards mature intestinal cells. The medium was enriched with epidermal growth factor (EGF), Wnt agonist R-spondin1 (Rspo1) and Noggin (NOG) emanating the signalling molecules from supporting mesenchyme for stem cell homeostasis [8]. On day 14 (a week after starting with MI media), expression of mature intestinal markers was detected by qPCR and the expression was pronounced at 28. Stem cell marker Leucine-rich repeat-containing G-protein coupled receptor 5 (LGR5), goblet cell marker Mucin-2 (MUC2) and brush border sucrase-isomaltase (SI) were both readily detected and on levels similar to human colon organoids and Caco-2 (Fig.2E). Additionally, we detected expression of Paneth cell marker Lysozyme (LYZ), enterocyte cell marker Villin-1 (VIL1) and neuroendocrine cell marker Chromogranin A (CHGA) which were distributed throughout the tubule (Fig.2F).

Next, we tested the applicability of our model for drug studies. Therefore, we first examined the gene expression levels of the drug metabolizing enzymes cytochrome P450 3A4 (CYP3A4) and multidrug resistance protein 1 (MDR1) and by real-time RT-PCR analysis. The gene expression

levels of both CYP3A4 and MDR1 in the hiPSC derived tubules were lower than those in the human colon organoids however when compared to Caco-2 cells the hiPSC derived tubules had 4 times higher expression level of CYP3A4. (Fig 2G)

One of the major obstacles during the development of this model was the invasion of cells into the Collagen I ECM which usually happened at the second step or the HG stage, approximately 9 days of iPSC post-seeding. While invasion and remodelling of the ECM are normal processes in the epithelium of the gut, in our case it often affected barrier integrity and thus TEER measurements. Initially, we attempted to apply cost-effective solutions where we increased concentration of ECM in order to strengthen the gel and reduce the movement of the gel, however with limited success. Therefore, we looked into preventing ECM breakdown by inhibition of matrix metalloproteinases (MMPs). We tested both a MMP-8 specific inhibitor (CAS 236403-25-1) and a broad spectrum MMP-inhibitor Marimastat (CAS 154039-60-8) at 10 μ M concentration [9] added from day 4 onwards. The addition of MMP-8 inhibitor prevented the invasion of cells into the ECM, helped in maintaining tubule stability (Fig.A3A) and did not affect the expression of mature intestinal markers (Fig.A3B). Broad spectrum MMP-inhibitor (Marimastad), even though completely stopped invasion, affected also cell morphology (Fig.S3A).

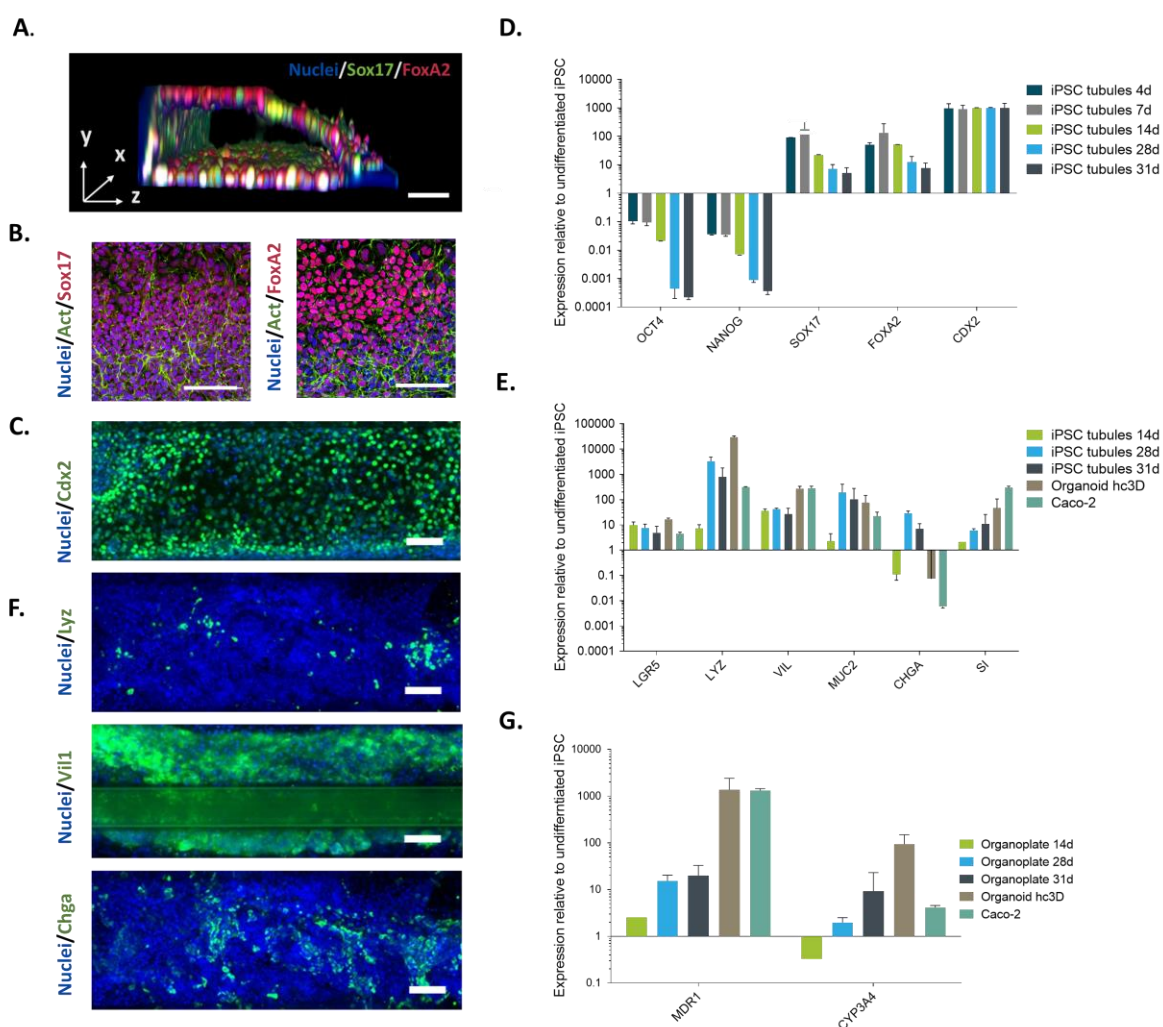


Figure 2. Differentiation and characterization of hiPSC into human intestinal-like tubules. A. 3D reconstruction image of an iPSC derived tubule at Day 4 stained using antibodies for SOX17 (green), FOXA2 (red) or DAPI for DNA (blue). Representative 10X images of iPSC tubules stained for Definitive endoderm markers B. SOX17 and C. FOXA2 at day 4 D. Hindgut marker CDX2 at day 7 and E. intestinal markers Lysozyme (LYZ), Villin (VIL) and Chromogranin A (CHGA) at day 14

(green). Nuclei were stained with DAPI (blue) to visualize the overall morphology. Scale bars=100 μ m. Gene expression was measured using TaqMan qRT-PCR from hiPSC tubules at different differentiation stages (HG) for the 3 μ M CHIR99021 in RPMI supplemented with either B27 +/- insulin. The following genes were analysed: F. Pluripotency: POU class 5 homeobox 1 (POU5F1); Nanog homeobox (NANOG) Primitive Streak; forkhead box a2 (FOXA2) and Definitive Endoderm: FOXA2, SRY (sex determining region Y)-box 17 (SOX17), markers for Posterior Gut Homeobox protein CDX-2. G. Intestinal markers: Leucine-rich repeat-containing G-protein coupled receptor 5 (LGR5) ,Mucin-2 (MUC2) , Lysozyme (LYZ), Villin-1 (VIL1) Chromagranin A (CHGA) and sucrase-isomaltase (SI) (G.) Relative mRNA expression of MDR1 (P-gp) and CYP3A4 in iPSC-derived intestine-like tubules on day 14, day 28 and day 31, human adult colon organoids and Caco-2 cells. Expression levels were normalized to ACTIN, data represented as mean \pm SD relative to the expression in undifferentiated miFF1 hiPSC (N=2, n \geq 2-3) The Y-axis represents the LOG10 relative quantification (RQ). All samples were normalized to beta-actin (ACTB) and depicted as relative to undifferentiated hiPSC. Caco-2 cells and primary colon organoid were also included to compare the gene expression and to follow the differentiation of our model during the different stages. Data is presented as the average of two independent experiments +/- SD (n=3).

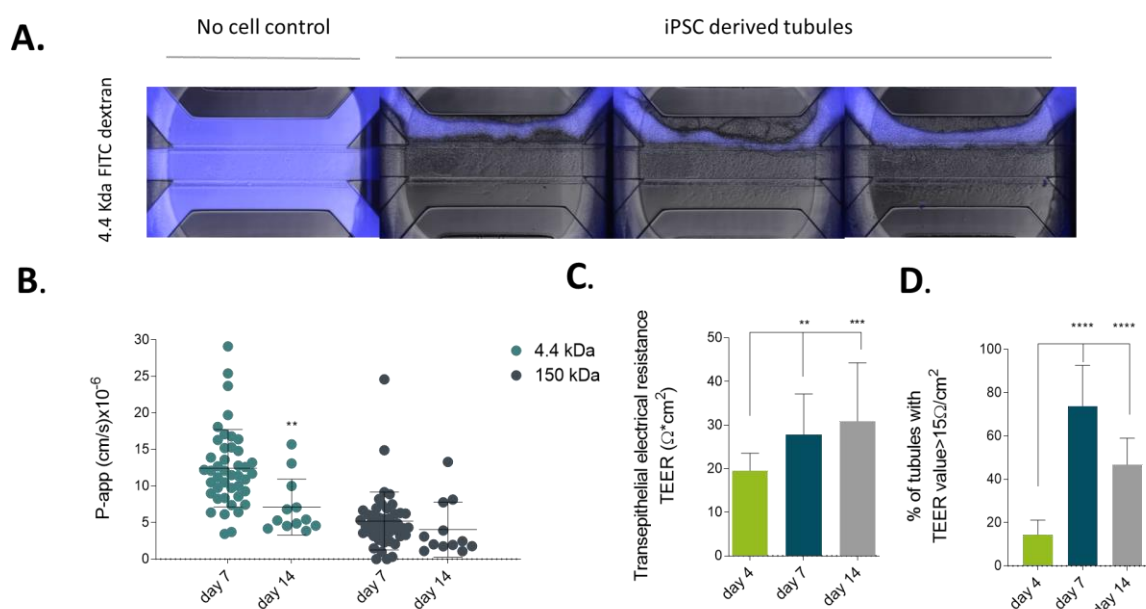


Figure 3. Barrier integrity in miFF1-derived intestinal-like tubules. A. Fluorescent and phase contrast images of microfluidic chips perfused with fluorescent molecules using 4.4 kDa TRITC-Dextran for 15 min on day 25 of culture B. P-app value calculated with the Barrier Integrity assay using both 4.4 kDa TRITC-dextran and 150 kDa FITC-dextran at day 7 and day 14. Data is represented as mean \pm SD Significance was detected by two-way Anova, $n \geq 12$. C. Transepithelial electrical resistance (TEER) measurements of iPSC derived intestine-like tubules between day 4 and day 14 of culture (N=3, $n \geq 110$). (C.) Percentage of iPSC derived intestine-like tubules between day 4 and day 14 of culture having TEER values above 15 $\Omega \cdot \text{cm}^2$. Significance was detected by ordinary one-way Anova with Dunnett's multiple comparison test. Data is represented as mean \pm SD. (N=3, $n \geq 110$), ns $p > 0.05$, * $p \leq 0.05$, ** $p \leq 0.01$, *** $p \leq 0.001$, **** $p \leq 0.0001$.

2.3. iPSC derived gut-like tubules develop a physiologically relevant barrier

To determine whether the hiPS derived tubules could be applicable to drug permeability studies, we evaluated barrier function of the tubules by performing a real-time barrier integrity assay (BI assay) previously described by Trietisch et al. and Beurivage et. al [10,11] and

transepithelial electrical resistance (TEER) measurements. For the BI assay high molecular weight probes (150 kDa FITC-dextran) and low molecular weight probes (4.4 kDa TRITC-dextran) were added to the medium that was subsequently perfused through the lumen of the tubule. The permeability of the fluorescent particles was quantified by determining the fluorescence levels in the basal gel region and normalizing it to the fluorescence in the lumen of the tubule to compensate for bleaching effects. This data was then used to calculate the apparent permeability value or P-app. Tubules became more leak-tight over time and appeared to be most leak-tight on day 14, with a P-app score of 4.03×10^{-6} cm/s for 150 kDa Dextran and 7.12×10^{-6} cm/s for 4.4 kDa. The TEER measures the integrity of tight junction dynamics in cell culture models of endothelial and epithelial monolayers. Tubules were subjected to TEER measurement after confluency was reached on day 4 until day 14 (Fig.3C). TEER values reached a plateau of $30.91 \pm 13.37 \Omega$ cm on day 14 and maintained this plateau at least until day 21 (data not shown). Interestingly, approximately 90% of tubules developed a barrier starting from day 7 (Fig.3D) These iPSC derived gut-like tubules exhibited TEER values similar to intestinal tissue within 2 weeks of differentiation [12].

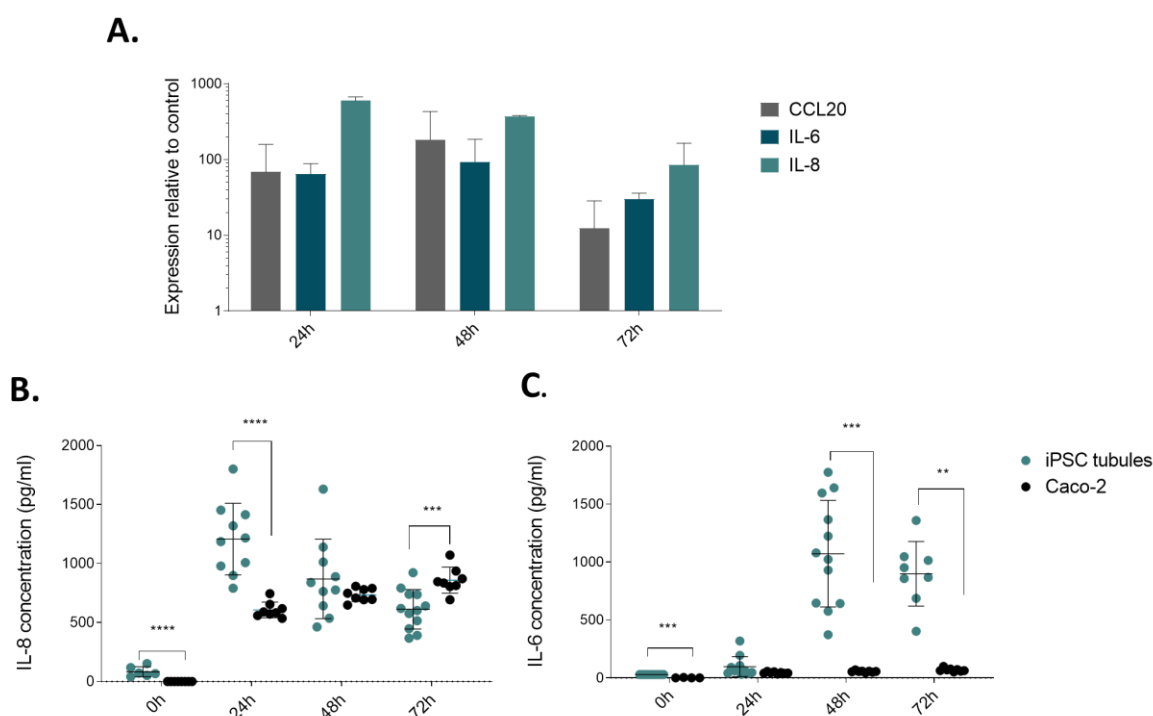


Figure 4. hiPSC derived gut tubules are suitable for modeling inflammatory conditions. Gene expression analysis of hiPSC derived gut tubules for CCL20 A., IL-8 B., and IL-6 C. after cytokine trigger at 24h, 48h and 72h. Data is represented as mean \pm SD normalized to ACTIN expression ($n=2-3$). Secretion of IL-8 B. and IL-6 C. in apical and basal compartments of triggered hiPSC derived gut tubules (blue) and Caco-2 tubules (gray) Significance was determined with Multiple t-tests (one per row) and discovery determined using Two-stage linear step-up procedure of Benjamini, Krieger and Yekutieli, with $Q = 1\%$. Each row was analyzed individually, without assuming a consistent SD. Data is represented as mean \pm SD. ($n \geq 5$) ns $p > 0.05$, * $p \leq 0.05$, ** $p \leq 0.01$, *** $p \leq 0.001$, **** $p \leq 0.0001$.

2.4. iPSC derived tubules are suitable for IBD modeling

We further tested our model applicability for disease modeling of inflammatory bowel disease. We applied inflammatory trigger composed of TNF- α IL-1B IFN- γ [11,13] in combination known to be upregulated in several inflammatory conditions. We focused on specific aspects of intestinal inflammation like expression and secretion of pro-inflammatory cytokines by activated epithelial cells. CCL20 is a chemo attractant to recruit circulating Th17 cells to sites of inflammation, IL-6 is a cytokine which main function is the regulation of T cell balance and IL-8 is a powerful neutrophil

chemoattractant found in inflamed mucosa. Once added to the tubules, the cytokine cocktail upregulated mRNA expression and maximal expression was observed after 48h for CCL20 and IL6 and highest expression levels for CXCL8 are at 24h (Fig 4A).

We next investigated the release of IL-6 and IL-8 by iPSC gut tubules compared to Caco-2 tubules, in response to cytokine cocktail exposure, using enzyme-linked immunosorbent assay (ELISA). IL-8 production after addition of the inflammatory trigger in the iPSC tubules was significantly increased after the first 24 hours and then decreased significantly for each of the following 24 hours, decreasing from a mean of 1206 ± 303 pg/mL to 869 ± 336 pg/mL at 48 hours and 613 ± 167 pg/mL at 72 hours. The IL-8 secretion of Caco-2 tubules showed a reversed tendency increasing from 607 ± 66 pg/mL at 24h, 734 ± 55 pg/mL at 48 and 859 ± 109 pg/mL at 72h (Fig 4B).

After cytokine stimulation the IL-6 production was high for the iPSC derived tubules 97.40 ± 86.5 pg/mL, 1072 ± 460 pg/mL and 898 ± 278 pg/mL at 24h, 48h and 72h respectively. Caco-2 tubules had low IL-6 production at all of the time points (Fig 4C).

3. Discussion

In summary, we developed a modified organoid differentiation protocol [3,14] that can be used effectively to directly differentiate iPSC in a microfluidic platform (OrganoPlates), towards gut like tubules showing relevant intestinal marker expression. We also demonstrate that these tubules can be used for disease modeling and the recapitulation of key aspects of IBD pathogenesis in a high throughput manner. This work provides a foundation for upcoming large-scale 3D microfluidic modeling of IBD and screening of relevant therapeutic targets, allowing us to further study and understand gut inflammation. The main purpose of this study was to develop a method to generate iPSC derive gut-like tubules directly on a high throughput platform the OrganoPlate without the long and labor-intensive organoid generation step. We also show applicability of our model for barrier integrity studies by performing a large scale TEER measurement (N=110) over 14 days of culture in the microfluidic device. Thus, showing that our model is capable of developing a barrier integrity starting from day 4 and reaching levels similar to in-vivo situation in 14 days [12] with the addition of MMP-8 inhibitor. In contrast, average TEER values for Caco-2 cultures ranges between $500\text{--}1500 \Omega\text{cm}^2$ [15,16]. For the applicability of the model in drug discovery studies, it should be noted that the P-gp (MDR1) expression is lower than the human colon Organoids and Caco-2 tubules. P-gp expression has been previously described in stem cell differentiated gut-like tissue [17] and these results suggest that our hiPSC derived gut-like tubules resemble more the fetal tissue rather than the adult one. Fortunately, the expression of both P-gp and CYP3A4 hold induction potential with the addition of different molecules [18–20].

Lastly, we were able to validate the applicability of our system for modeling an inflammatory condition in the gut, like inflammatory bowel disease. By applying a cytokine trigger optimized previously for mimicking IBD-like symptoms in epithelial cells we were able to observe a response similar to in-vivo situation in the iPSC-derived intestinal-like tubules [11,23]. The iPSC-derived intestinal-like tubules showed a significant increase in IL-6 and IL-8 release after 48 and 24 hours respectively. While Caco-2 cells are capable of producing IL-8 after several days of culture [24] in the literature there is conflicting evidence regarding IL-6 secretion by Caco-2 and in our experiments we were not able to detect it [25,26]. It is understandable, knowing that the effect of Interleukin-6 in the intestinal epithelium is to increase proliferation and survival by an autocrine signaling mechanism [27]. Moreover, the only cells that express IL-6 receptors are crypt Paneth cells [13,28]. Caco-2 cells, when differentiated resemble enterocytes of the small intestine therefore they are unable to produce IL-6 in large quantities [29] and in our previous experiments we were unsuccessful in measuring the IL-6 production of Caco-2. This difference makes our model more physiologically relevant in disease modeling than with using secondary cell lines which are considered currently as the “golden standard” model.

In conclusion, in this proof-of-principle study we demonstrated that iPSC can be successfully directed towards 3D gut-like phenotype in a robust, reproducible and cost-effective manner, all in a

high-throughput microfluidic device and within 14 days post seeding. Moreover, the iPSC develops into physiologically relevant leak-tight tubules with the expression of intestinal markers similar to existing models and with significant response to inflammatory triggers. This will allow to efficiently establish patient specific in vitro models for drug discovery and for studying inflammatory processes in the intestine.

4. Materials and Methods

4.1. Ethics Statement

The research described here has been performed according to applicable Dutch and UK national ethics regulations and was conducted within MIMETAS BV (Leiden, The Netherlands) and the University of Sheffield (Sheffield, United Kingdom).

4.2. Cells

Human induced pluripotent stem cells (hiPSC; miFF1 UOSi001-A) were obtained from the University of Sheffield (Sheffield, United Kingdom) were cultured standard gas atmosphere with 95% humidity and 5% CO₂ at 37°C in feeder-free conditions using 0.5 mg/mL Vitronectin Recombinant Human Protein (Thermo Fisher Scientific No. A14700) coated 6 well plates. Routine passaging of cells was performed with 0.5 mM EDTA (Thermo Fisher Scientific, 15-575-020). Essential 8 medium (Thermo Fisher Scientific No. A1517001) supplemented with 10 µM Y-27623 ROCK inhibitor (Merck No. 688000-1MG) was used in the first 24h post passaging.

Human colon adenocarcinoma cell line Caco-2 (ECACC 86010202) was cultured as described earlier [10,11].

Human Colon Organoids were obtained from the Hubrecht institute (Utrecht, Netherlands) and cultured as described previously [30].

Cell were routinely tested against mycoplasma contamination and were found negative.

4.3. OrganoPlate Seeding and Tubule Formation

ECM loading was prepared as described previously in a 3-lane 400 µm Organoplate (Mimetas No. 4003-400-B). In short 1.5-2 µL of 6.64 mg/mL collagen-I (Corning,354249) were dispensed into the middle inlet. The Organoplate were placed in the incubator for 15 min to allow the polymerization of the collagen-I gel. After solidification of the gel, 30 µL HBSS was placed in the middle inlet to prevent the gel from drying out and the plate was placed back into the incubator until use. Then the Organoplate were coated with 0.5 mg/mL Vitronectin Recombinant Human Protein (Thermo Fisher Scientific, A14700) diluted in ice cold PBS added in the top medium inlet for 60 min at room temperature (RT) before seeding. Cells were dissociated to a single cell suspension and the concentration was adjusted to 5,000 cells/µL in mTeSR medium supplemented with 10 µM Y-27623 ROCK inhibitor. HBSS was removed from gel inlets and 2 µL cell suspension was inserted in the top medium outlet. 1 µL of liquid was removed from the top medium inlet to assist the seeding of cells in a coated channel. After which 50 µL of mTeSR medium (STEMCELL Technologies,85850) supplemented with 10 µM Y-27623 ROCK inhibitor was added to the top medium inlet to prevent evaporation. The Organoplate was placed flat and static in a humidified chamber to allow the cells attachment for 6 hours. Subsequently 50 µL of mTeSR medium was added to the top medium inlet, bottom medium inlet and outlet as well. Cells were then incubated in a humidified chamber on a Rocker with 7 °/8 angle/inclination overnight to induce a bi-directional flow.

4.4. Directed on plate differentiation of iPSC

After the initial 48 hours of mTeSR medium in the Organoplate, cells were given definitive endoderm differentiation medium Table A1. After x days the differentiation on the definitive

endoderm was completed, the cultures were started on Hindgut differentiation medium Table A1. These conditions were maintained for 72 hours. Cells were further directed towards mature intestine with mature intestine medium table A1 for an additional two to three weeks, with medium changes every 3 to 4 days (**Table A1**). 10 μ M MMP-8 inhibitor (Fischer Scientific No. 44-423-7) or 10 μ M Marimastat (MERCK, M2699) were added to cultures to reduce invasion of cells into the ECM.

4.5. Barrier integrity assay (BI assay)

Barrier integrity assay was performed as described earlier. using 0.5 mg/ml FITC-dextran (150kDa, Sigma No. 46946) and TRITC-dextran (4.4 kDa, Sigma No. T1037) and imaged using an ImageXpress XLS Micro HCI system for 15 min, with an interval of 3 min. The ratio between the fluorescent signal in the basal and apical region of the tube was analyzed using Fiji and Papp value was calculated as. Cell-free chips were taken as negative controls.

4.6. TEER Measurements

Transepithelial electrical resistance (TEER) was measured at different time points using an automated multichannel impedance spectrometer designed for use with the OrganoPlate (OrganoTEER, Mimetas). Before measurement, medium was added in the middle inlets and outlets and the OrganoPlate was returned in the incubator (37°C, 5% CO₂) to equilibrate for an hour. The electrodeboard of the OrganoTEER is matched to the OrganoPlate such that when an OrganoPlate is placed in the OrganoTEER, electrode pairs are dipped in the medium in all inlet and outlet wells connecting to the basal and apical side of all tubes. Point impedance measurements were performed by frequency sweep from 5Hz to 1MHz (75 points at precision 0) with TEER values going up to 1000 Ω ·cm². Data was analyzed using the OrganoTEER software, which automatically extracts the TEER contribution (in Ohm) from the measured spectra and normalizes it to Ohm·cm² by multiplying by the tubule-ECM interface (estimated at 0.0056 cm²).

4.7. Cytokine trigger and ELISA for activation molecules

iPSC and Caco-2 tubules treated with cytokine-triggering medium comprised from IL-1 β , IFN- γ and TNF- α at 50, 50 and 50 ng/mL respectively (Immunotools) for 24,48 and 72h. Medium was collected from the Top and Bottom inlets and outlets, pooled and stored at -80°C until analysis. CXCL6 and CXCL8 secretion were quantified using the Human IL-6 DuoSet ELISA (RD systems No. DY206) and Human IL-8/CXCL8 DuoSet ELISA (RD systems No. DY208), respectively, according to the manufacturer's instructions.

4.8. Immunocytochemistry (ICC)

Cells were fixated with 3.7% formaldehyde in HBSS at RT for 15 min. Cells were washed twice with PBS for 5min and subsequently washed once with 4% Fetal bovine serum (FCS) in PBS for 5 min. Following a permeabilized with 0.3% Triton X-100 in PBS for 10 min. After which cells were washed with 4% Fetal bovine serum (FCS) in PBS for 5 min and blocked with 2 % FCS, 2% Bovine serum albumin (BSA), 0.1% Tween20 in PBS for 30 min. Blocking solution was removed and primary antibodies in blocking solution were incubated overnight. Cells were washed with 4%Fetal bovine serum (FCS) in PBS twice for 3 min subsequently incubated with secondary antibodies for 30 min followed by washing step and nuclei staining with Hoechst 33342. Antibodies used Primary: SOX17 (R&D Systems, MAB19241 1/100), FOXA2 (R&D Systems AF2400. 1/100) CDX2 (R&D Systems, AF3665, 1/100), Villin (Santa cruz, 58897, 1/200), Chromagranin A (Rabbit Santa, cruz13090, 1/200), Muc-2(Thermo Fischer,MA5-12178, 1/100), Lysozyme (Thermo Fischer, MA1-82873,1/200) LGR5 (Sanbio, TA503316 1/100), Isotype Rabbit (Life Technologies, 86199, 1/250) Isotype Goat (Life Technologies, 026202, 1/250), Isotype Mouse (Invitrogen, 08-6599 1/250),

Secondary: Goat Alexa Fluor 488 (Invitrogen, A11055 1/250) Mouse Alexa Fluor 555(Life Technologies,1736967, 1/250), Rabbit Alexa Fluor 647 (MERCK, SAB460177 1/250) and cell stains

Actin Green(LifeTechnologies,R37110),ActinRed(LifeTechnologies,R37112), Hoechst 33342 (Thermo Fischer,H3570, 1/1000).

4.9. Quantitative Real-Time Polymerase Chain Reaction-SYBRGREEN

Total RNA was isolated using RNeasy Micro kit (Qiagen No. 74004) according to manufacturer instructions, two to three chips were pooled into one sample. We first determined the RNA concentration with NanoDrop OneC Microvolume UV-Vis Spectrophotometer (Thermo Fischer) and adjusted to a min concentration of 30 ng/ μ L in DEPC-treated milliQ water. Then we proceeded with adding the isolated RNA and a MasterMix to Applied Biosystems™ MicroAmp™ Optical 8-Tube Strip with Attached Optical Caps, 0.2 mL (Thermo Fisher, 15527575) to convert RNA to cDNA. Finally, qPCR was performed by using FastStart Essential DNA Green Master (Roche, 06402712001) for SYBR Green I-based real-time PCR and FastStart Essential DNA Probe Master (Roche, 06402682001) for TaqMan based real-time PCR.

SYBR Green primers used during experiments. GeneID, NCBI number, Primer sequence 5' - 3':

ACTB NM_001101.3

F: CTCTCCAGCCTTCCTCCT R: AGCACTGTGTTGGCGTACAG,

SI NM_001041.3

F: GTAAGGAGAAACCGGGAAGC R: TGTCCATGGTCATGCAAATC,

CYP3A4NM_001202855.3

F: TTTACCCAATAAGGCACCACC R: TTGCAGACCCTCTCAAGTC

CXCL6 NM_002993.4

F: TGTTTACGCGTTACGCTGAG R: AACTTGCTTCCCGTTCTTCA

CXCL8 NM_000584.4

F: CAAGAGCCAGGAAGAAACCA R: ACTCCTTGGCAAAACTGCAC

CCL20 NM_004591.3

F: GCAAGCAACTTTGACTGCTG R: GATGTCACAGCCTTCATTGG

TaqMan probes for:

OCT4 Hs04260367_gH FAM 77 NANOG Hs04260366_g1 FAM 99 SOX17 Hs00751752_s1 FAM 149 FOXA2 Hs05036278_s1 FAM 144 CDX2 Hs01078080_m1 FAM 81 PDX1 Hs00236830_m1 FAM 73 LGR5 Hs00969422_m1 FAM 61 LYZ Hs00426232_m1 FAM 67 VIL1 Hs01031722_g1 FAM 72 MUC2 Hs00159374_m1 FAM 81 CHGA Hs00900375_m1 FAM 88 ABCB1 Hs00184491_m1 FAM 110 ACTB Hs01060665_g1 VIC 63 06402712001)

Results were normalized relative to ACTIN expression for both Taqman and SybrGreen experiments.

4.10. Statistics and Data Analysis

Data was analyzed using GraphPad Prism software version 7 (GraphPad Software, La Jolla, CA, USA). Unless stated otherwise, values are expressed as mean \pm Standard Deviation (SD). ANOVA and student t-test were used to determine the statistical significance. Differences with $p < 0.05$ were considered significant (ns $p > 0.05$, * $p < 0.05$, ** $p < 0.01$, *** $p < 0.001$, **** $p < 0.0001$). All graphs shown contain results from one or two representative experiments containing at least three technical replicates (chips). Number of chips used are described in the figure legends.

4.11. Graphics

Graphics in figure 1D are made with BioRender.com

Author Contributions: EN developed the concept of directed differentiation in OrganoPlate®. EN, GA, DK designed the study. EN, GA, KK and CVV performed experiments and data analysis. SB and CVV optimized the differentiation cocktail with small adjustments from EN and GA. EN and GA wrote the manuscript with comments from the authors D.K., K.E. DK, KE and SB oversaw the research.

Funding: This work was supported by the European Union's Horizon 2020 research and innovation programme under the Marie Skłodowska-Curie grant agreement #674983 (ITN-MIMIC).

Conflicts of Interest: E.N.,KK, D.K., are employees of Mimetas BV, which is marketing the OrganoPlate and the OrganoTEER. OrganoPlate is a registered trademark of Mimetas BV. The authors have no additional financial interests.

Abbreviations

CD Crohn's disease

CYP Cytochrome P450

EGF Epidermal growth factor

ESCs Embryonic stem cells

FGF4 Fibroblast growth factor 4

IBD Inflammatory bowel disease

iPSC induced pluripotent stem cells

LGR5 Leucine-rich-repeat-containing G-protein-coupled receptor 5

MMP Matrix metalloproteinase

P-gp P-glycoprotein

RNase Ribonuclease

ROCK Rho-associated protein kinase

TEER Trans epithelial electrical resistance

UC Ulcerative colitis

Appendix A – Supplementary data

Table A1. Components of directed differentiation media

Stage of differentiation	Abbreviation	Component	Final concentration	Supplier	Cat.No
Definitive endoderm	DE1	RPMI-1640 Medium	/	Sigma-Aldrich	R0883
		Penicillin-Streptomycin	1x	Sigma-Aldrich	P4333
		Non-essential amino acids	1x	Gibco	11140035
		B27 with insulin	1x	Gibco	17504-044
		CHIR99021	3 uM	Bio-Techne	4423
	DE2	RPMI-1640 Medium	/	Sigma-Aldrich	R0883
		Penicillin-Streptomycin	1x	Sigma-Aldrich	P4333
		Non-essential amino acids	1x	Gibco	11140035
		B27 with insulin	1x	Gibco	17504-044
	Hindgut	HG	RPMI-1640 Medium	/	Sigma-Aldrich
Penicillin-Streptomycin			1x	Sigma-Aldrich	P4333
Non-essential amino acids			1x	Gibco	11140035
FBS			2%	ATCC	30-2020
CHIR99021			2 uM	Bio-Techne	4423
FGF 4			500ng/mL	Peprtech	100-31
Noggin			100ng/mL	Peprtech	120-10C
Mature intestine	MI	DMEM/F12 Medium	/	Gibco	31331-028
		HEPES	15mM	Gibco	15630-056
		Penicillin-Streptomycin	1x	Sigma-Aldrich	P4333
		Non-essential amino acids	1x	Gibco	11140035
		B27 with insulin	1x	Gibco	17504-044
		Noggin	100 ng/mL	Peprtech	120-10C
		R-spondin	500 ng/mL	Peprtech	120-38
		EGF	100 ng/mL	Sigma-Aldrich	E9644-.2MG
		MMP-8	10 uM	Fisher Scientific	4442371MG

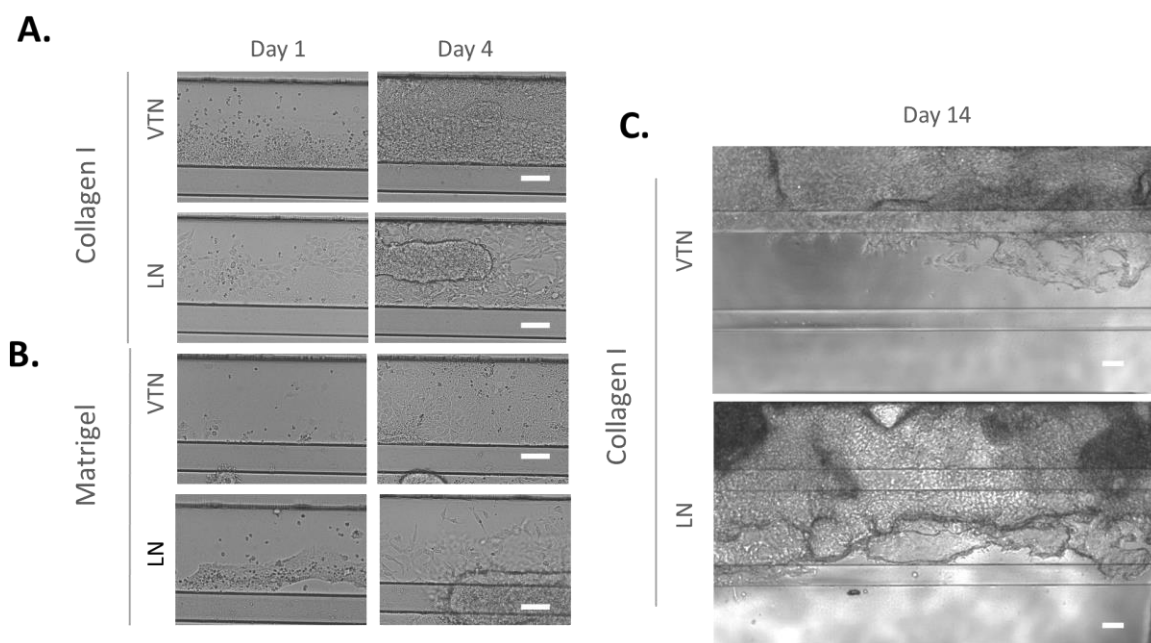


Figure A1. Optimization of ECM and coating strategy for better attachment and tubule maintenance of iPSC. Representative 10X phase contrast images of iPSC derived tubules at Day 1 and 4 cultured on either Collagen I (A) and either human recombinant vitronectin (VTN) or laminin (LN) as coating strategy or Matrigel as ECM (B) and either human recombinant vitronectin (VTN) or laminin (LN) as coating strategy (C). Representative 10X phase contrast images of iPSC derived tubules at Day 14 with Collagen I as ECM and either VTN or LN as a coating strategy. Scale bars=100μm

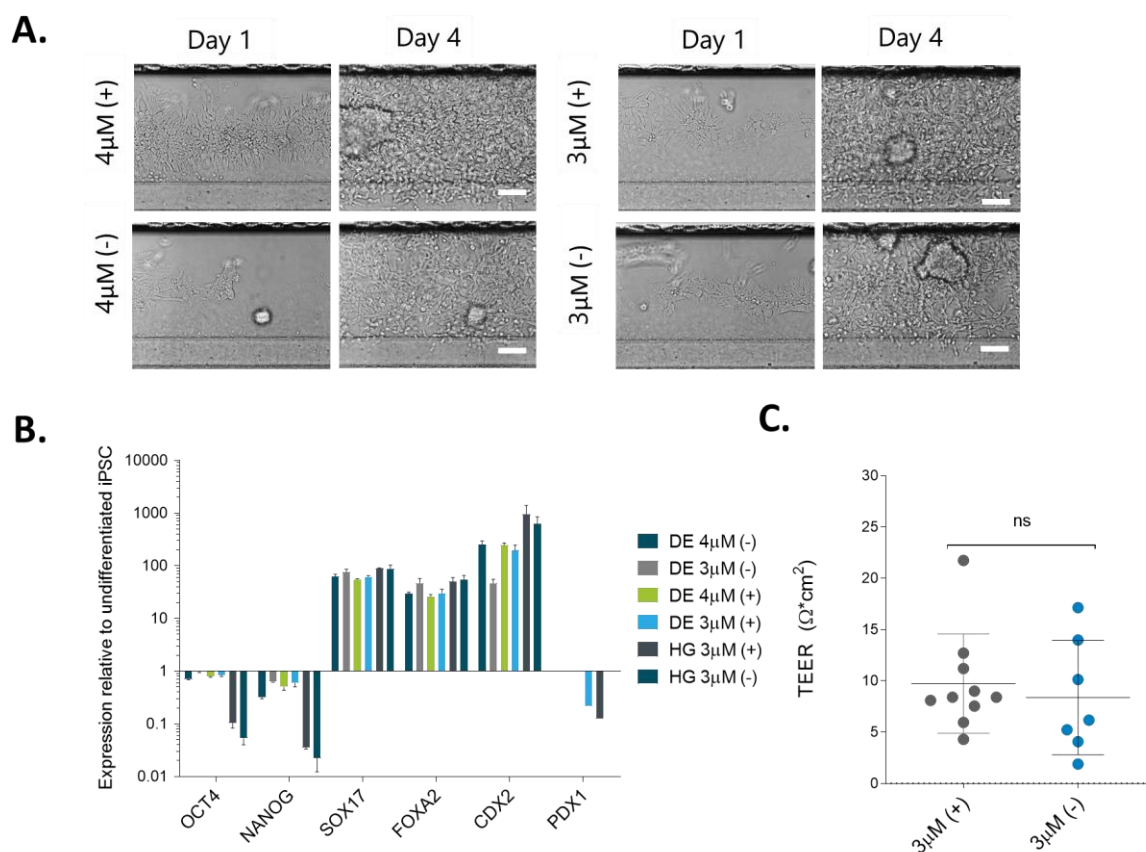


Figure A2 Endodermal potential screen and barrier integrity of iPSC. A. Representative 10X phase contrast images of iPSC derived tubules at Day 1 and 4 cultured under four different conditions 3 or 4 μ M CHIR99021 in RPMI supplemented with either B27 +/- insulin. Scale bars=100 μ m B. Gene expression were measured using TaqMan pRT-PCR at Day 4 (DE) for all four conditions and Day 7 (HG) for the 3 μ M CHIR99021 in RPMI supplemented with either B27 +/- insulin. The following genes were analysed: Pluripotency: POU class 5 homeobox 1 (POU5F1); Nanog homeobox (NANOG) Primitive Streak; forkhead box a2 (FOXA2) and Definitive Endoderm:FOXA2, SRY (sex determining region Y)-box 17 (SOX17) and markers for Anterior Gut: pancreatic and duodenal homeobox 1 (PDX1) and Posterior Gut Homeobox protein CDX-2. The Y-axis represents the LOG10 relative quantification (RQ). All samples were normalized to beta-actin (ACTB), and to undifferentiated hiPSC. Data is presented as the average of two independent experiments +/- SD (N=2, n \ge 3). C. TEER measurements of Day 4 hiPSC derived tubules at DE stage Significance was detected by ordinary one-way Anova. Data is represented as mean \pm SD. (N=1, n \ge 6), ns p > 0.05, * p \le 0.05, ** p \le 0.01, *** p \le 0.001, **** p \le 0.0001.

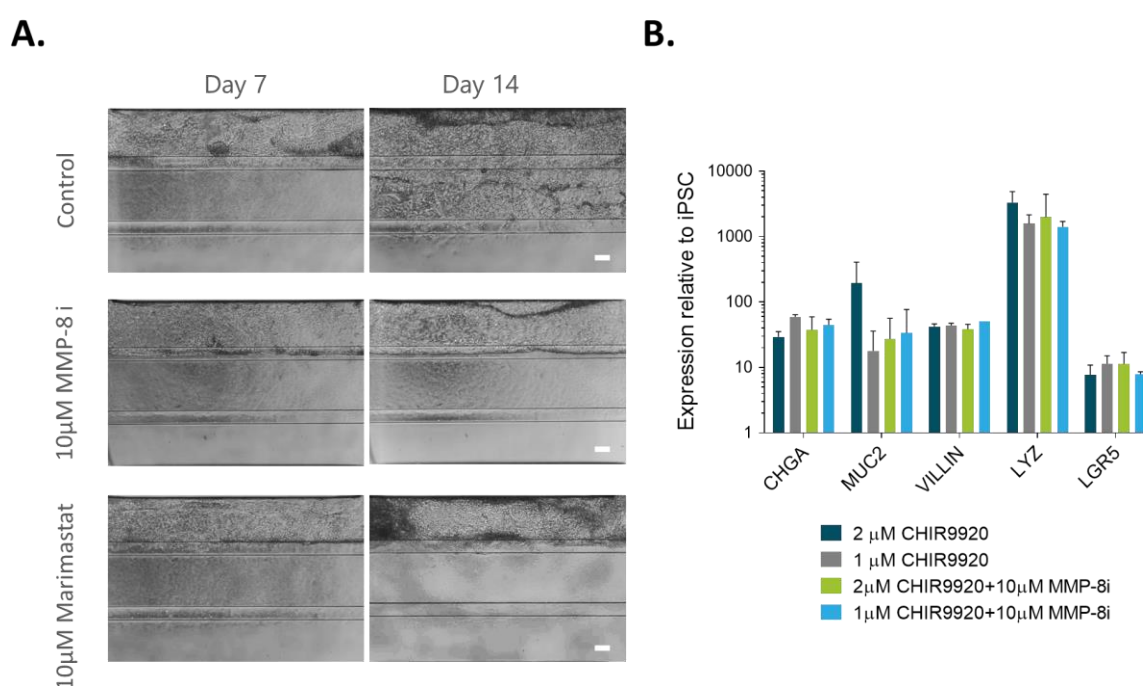


Figure A3. Maintenance of tubular shape of differentiated iPSC derived gut-like tubules within a microfluidic device with matrix metalloproteinases inhibitors. A. Representative 10x phase contrast images on day 7 and day 14 per condition. Scale bars=100 μ m B. Gene expression measured using TaqMan qRT-PCR at day 28 from hiPSC derived gut-like tubules. The following genes were analyzed Leucine-rich repeat-containing G-protein coupled receptor 5 (LGR5), Mucin-2 (MUC2), Lysozyme (LYZ), Villin-1 (VIL1) and Chromogranin A (CHGA) The Y-axis represents the LOG10 relative quantification (RQ). All samples were normalized to beta-actin (ACTB) and expressed as relative to undifferentiated hiPSC. Data is presented as the average of two independent experiments +/- SD (n \ge 3).

References

1. Jain, K.K. Drug Delivery Systems - An Overview. In: 2008; pp. 1–50.
2. Elliott, N.T.; Yuan, F. A Review of Three-Dimensional In Vitro Tissue Models for Drug Discovery and Transport Studies. *J. Pharm. Sci.* **2011**, *100*, 59–74.
3. Kraiczy, J.; Zilbauer, M. Intestinal Epithelial Organoids as Tools to Study Epigenetics in Gut Health and Disease. *Stem Cells Int.* **2019**, *2019*, 7242415.
4. Sato, T.; Vries, R.G.; Snippert, H.J.; van de Wetering, M.; Barker, N.; Stange, D.E.; van Es, J.H.; Abo, A.; Kujala, P.; Peters, P.J.; et al. Single Lgr5 stem cells build crypt-villus structures in vitro without a mesenchymal niche. *Nature* **2009**, *459*, 262–5.
5. Lukovac, S.; Roeselers, G. *Intestinal Crypt Organoids as Experimental Models*; Springer, 2015; ISBN 9783319157917.
6. Wallach, T.E.; Bayrer, J.R. Intestinal Organoids: New Frontiers in the Study of Intestinal Disease and Physiology. *J. Pediatr. Gastroenterol. Nutr.* **2017**, *64*, 180–185.
7. Sato, T.; Vries, R.G.; Snippert, H.J.; van de Wetering, M.; Barker, N.; Stange, D.E.; van Es, J.H.; Abo, A.; Kujala, P.; Peters, P.J.; et al. Single Lgr5 stem cells build crypt-villus structures in vitro without a mesenchymal niche. *Nature* **2009**, *459*, 262–265.
8. Smith, N.R.; Davies, P.S.; Silk, A.D.; and M. H. Wong Epithelial and mesenchymal contribution to the niche: a safeguard for intestinal stem cell homeostasis. *Gastroenterology* **2012**, *143*, 1426–1430.
9. Tonn, J.C.; Kerkeay, S.; Hanke, A.; Bouterfa, H.; Mueller, J.G.; Wagner, S.; Hamilton, G.; Roosen, K. Effect of synthetic matrix-metalloproteinase inhibitors on invasive capacity and proliferation of human malignant gliomas in vitro. *Int. J. Cancer* **1999**, *80*, 764–772.
10. Trietsch, S.J.; Naumovska, E.; Kurek, D.; Setyawati, M.C.; Vormann, M.K.; Wilschut, K.J.; Lanz, H.L.; Nicolas, A.; Ng, C.P.; Joore, J.; et al. Membrane-free culture and real-time barrier integrity assessment of perfused intestinal epithelium tubes. *Nat. Commun.* **2017**, *8*, 262.
11. Beurivage, C.; Naumovska, E.; Chang, Y.X.; Elstak, E.D.; Nicolas, A.; Wouters, H.; van Moolenbroek, G.; Lanz, H.L.; Trietsch, S.J.; Joore, J.; et al. Development of a Gut-On-A-Chip Model for High Throughput Disease Modeling and Drug Discovery. *Int. J. Mol. Sci.* **2019**, *20*, 5661.
12. Sjöberg, Å.; Lutz, M.; Tannergren, C.; Wingolf, C.; Borde, A.; Ungell, A.-L. Comprehensive study on regional human intestinal permeability and prediction of fraction absorbed of drugs using the Ussing chamber technique. *Eur. J. Pharm. Sci.* **2013**, *48*, 166–180.
13. Andrews, C.; McLean, M.H.; Durum, S.K. Cytokine Tuning of Intestinal Epithelial Function. *Front. Immunol.* **2018**, *9*, 1270.
14. Kasendra, M.; Tovaglieri, A.; Sontheimer-Phelps, A.; Jalili-Firoozinezhad, S.; Bein, A.; Chalkiadaki, A.; Scholl, W.; Zhang, C.; Rickner, H.; Richmond, C.A.; et al. Development of a primary human Small Intestine-on-a-Chip using biopsy-derived organoids. *Sci. Rep.* **2018**, *8*.
15. Srinivasan, B.; Kolli, A.R.; Esch, M.B.; Abaci, H.E.; Shuler, M.L.; Hickman, J.J. TEER Measurement Techniques for In Vitro Barrier Model Systems. *J. Lab. Autom.* **2015**, *20*, 107–126.
16. Takenaka, T.; Harada, N.; Kuze, J.; Chiba, M.; Iwao, T.; Matsunaga, T. Human small intestinal epithelial cells differentiated from adult intestinal stem cells as a novel system for predicting oral drug absorption in humans. *Drug Metab. Dispos.* **2014**, *42*, 1947–1954.
17. Ozawa, T.; Takayama, K.; Okamoto, R.; Negoro, R.; Sakurai, F.; Tachibana, M.; Kawabata, K.; Mizuguchi, H.; Frank, R.; Hargreaves, R.; et al. Generation of enterocyte-like cells from human induced pluripotent stem cells for drug absorption and metabolism studies in human small intestine. *Sci. Rep.*

- 2015, 5, 16479.
18. Onozato, D.; Yamashita, M.; Nakanishi, A.; Akagawa, T.; Kida, Y.; Ogawa, I.; Hashita, T.; Iwao, T.; Matsunaga, T. Generation of Intestinal Organoids Suitable for Pharmacokinetic Studies from Human Induced Pluripotent Stem Cells. *Drug Metab. Dispos.* **2018**, *46*, 1572–1580.
 19. Westphal, K.; Weinbrenner, A.; Zschiesche, M.; Franke, G.; Knoke, M.; Oertel, R.; Fritz, P.; von Richter, O.; Warzok, R.; and T. Hachenberg; et al. Induction of P-glycoprotein by rifampin increases intestinal secretion of talinolol in human beings: a new type of drug/drug interaction. *Clin. Pharmacol. Ther.* **2000**, *68*, 345–355.
 20. Negoro, R.; Takayama, K.; Nagamoto, Y.; Sakurai, F.; Tachibana, M.; Mizuguchi, H. Modeling of drug-mediated CYP3A4 induction by using human iPS cell-derived enterocyte-like cells. *Biochem. Biophys. Res. Commun.* **2016**, *472*, 631–636.
 21. Reitman, M.L.; Chu, X.; Yabut, J.; Venkatasubramanian, R.; Zajic, S.; Stone, J.A.; Ding, Y.; Witter, R.; Gibson, C.; Roupe, K.; et al. Rifampin's acute inhibitory and chronic inductive drug interactions: experimental and model-based approaches to drug–drug interaction trial design. *Clin. Pharmacol. Ther.* **2010**, *89*, 234–242.
 22. Niemi, M.; Backman, J.T.; Fromm, M.F.; Neuvonen, P.J.; Kivivstö, K.T. Pharmacokinetic interactions with rifampicin : clinical relevance. *Clin. Pharmacokinet.* **2003**, *42*, 819–850.
 23. Andrews, C.; McLean, M.H.; Durum, S.K. Cytokine Tuning of Intestinal Epithelial Function. *Front. Immunol.* **2018**, *9*, 1270.
 24. Van De Walle, J.; Hendrickx, A.; Romier, B.; Larondelle, Y.; Schneider, Y.-J. Inflammatory parameters in Caco-2 cells: Effect of stimuli nature, concentration, combination and cell differentiation. *Toxicol. Vitro.* **2010**, *24*, 1441–1449.
 25. Vitkus, S.J.D.; Hanifin, S.A.; McCee, D.W. Factors affecting Caco-2 intestinal epithelial cell interleukin-6 secretion. *Vitro. Cell. Dev. Biol. - Anim.* **1998**, *34*, 660–664.
 26. Workman, M.J.; Gleeson, J.P.; Troisi, E.J.; Estrada, H.Q.; Kerns, S.J.; Hinojosa, C.D.; Hamilton, G.A.; Targan, S.R.; Svendsen, C.N.; Barrett, R.J. Enhanced Utilization of Induced Pluripotent Stem Cell-Derived Human Intestinal Organoids Using Microengineered Chips. *Cell. Mol. Gastroenterol. Hepatol.* **2018**, *5*, 669-677.e2.
 27. Jeffery, V.; Goldson, A.J.; Dainty, J.R.; Chieppa, M.; Sobolewski, A. IL-6 Signaling Regulates Small Intestinal Crypt Homeostasis. *J. Immunol.* **2017**, *199*, 304–311.
 28. Kuhn, K.A.; Manieri, N.A.; Liu, T.C.; Stappenbeck, T.S. IL-6 stimulates intestinal epithelial proliferation and repair after injury. *PLoS One* **2014**, *9*.
 29. Galvez-Llompарт, M.; Del Carmen Recio Iglesias, M.; Gálvez, J.; García-Domenech, R. Novel potential agents for ulcerative colitis by molecular topology: Suppression of IL-6 production in Caco-2 and RAW 264.7 cell lines. *Mol. Divers.* **2013**, *17*, 573–593.
 30. Sato, T.; Vries, R.G.; Snippert, H.J.; Van De Wetering, M.; Barker, N.; Stange, D.E.; Van Es, J.H.; Abo, A.; Kujala, P.; Peters, P.J.; et al. Single Lgr5 stem cells build crypt-villus structures in vitro without a mesenchymal niche. *Nature* **2009**, *459*, 262–265.

Chapter 8 Discussion

Benefit of Organs on a chip (OOC)

Efficiency in pharmaceutical research can be greatly increased by mainly improving the ratio between the investment (input) and the go-to market of new drugs (output). It is known that main drivers of costs are the direct costs per project and the cycle time which is the success rates of drugs versus the development time. Cost of different R&D phases differs significantly and failure clinical phases are considered as a major driver of R&D costs, thus, better models in the preclinical phases are needed (Franzen et al. 2019).

Organs-on-chips are micro engineered biomimetic systems that show wide range of applications as they represent key functional units of living human organs. The advantage over existing models comes from three main aspects that can be implemented in these platforms: 3D microenvironment interactions, cell–cell interfaces and complex organ-specific mechanical and biochemical microenvironments. These miniaturized tissues and organs on a chip can considerably change the existing R&D framework (Esch, Bahinski, and Huh 2015). If organs on a chip are implemented in standard drug development process, one estimate shows an overall reduction of 10–26% of total costs. These are calculated savings per new drug reaching the market of up to 631 million euros (DiMasi, Grabowski, and Hansen 2016).

No single model can rule them all

In this thesis, I focused in building models that fit a specific research question. This is true especially for developing high throughput models for drug development and I believe that the research question defines the choice of the cellular model. This means that when modelling a complex idiopathic disease, depending on the research question, the model can be simple or more

complex. Therefore, I worked on developing different health and diseased models of the intestine which can be applied at different stages in the drug development pipeline. For example, simple Caco-2 tubules can be a very useful tool for the early phases in the drug development process such as target selection process due to the ease of use and the cost effectiveness.

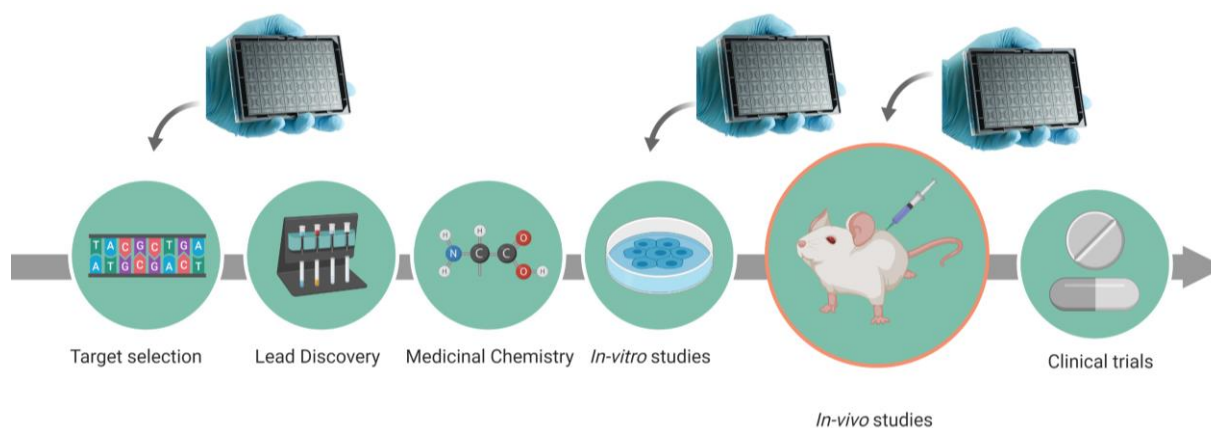


Figure 8.1 Applicability of Organs-on-a-chip in the drug development pipeline

These “simple” models are very valuable instruments for addressing specific known mechanism of action of a certain disease. Complex co-cultures or iPSC derived patient specific tubules that bring higher complexity, genetic variability and functionality, can be used later on in this process. For example, assessment of the long-term effect of medicines and for improving vastly current *in vitro* studies. Likewise, more complex models containing several different tissues/organs interconnected on chip can be used for further optimizing drug candidate selection process. This in turn will drastically decrease the number of animal models used for testing or maybe in the future even completely substitute the *in vivo* pre-clinical stage. Therefore, I expect that in the future there will be a modular approach in drug discovery process, where different organs-on-a-chip covering all levels and types of organs can be easily combined as prebuilt modules and applied for a specific application and thus speeding up the process and reducing costs drastically.

Modelling IBD with organs-on-a-chip

Due to the multifactorial nature of IBD, it is difficult to pinpoint and understand the underlying mechanisms for the development of the disease. Yet, it is more challenging to model complex disease in one single chip of a microfluidics platform. Nevertheless, OOC platforms gives us the possibility to make these high throughput models as simple as possible, but not “simpler”. Furthermore, we are able to incorporate different components involved in the development of the disease and dissect their individual contribution in the disease development and progression. OOC platforms can be used for modelling both healthy and diseased models of the intestine and study interactions between drugs, cells, signalling molecules and immune system as separate events and thus apply more simplistic approach. Therefore, assessing the possibility of medicines to repair the barrier integrity after integrity loss, there is no need for complex model. In this case a simple Caco-2 model will be enough to fast test large library of compounds that can be useful for repairing the barrier integrity. Barrier integrity reparation, is a promising step in the treatment of IBD, but not the complication that needs to be solved. For this reason, in this thesis instead of developing only one, the work describes development and characterization of four different models with increasing level of complexity. The models described in the thesis can be used for observing different characteristics of inflammatory bowel disease.

Chapter 4 describes the building and characterizing a healthy intestinal model on the OrganoPlate by using Caco-2 cells. It mainly focusses on important factors to consider when developing 3D high-throughput models for drug discovery. These are have highly robust and reliable system, preferably accessible from apical and basal side. Using ‘reverse engineering’, I was involved in development of a system that is suitable for high-throughput studies which include toxicity screening, real-time imaging of transport and barrier integrity. The aim was modelling the intestine

as close as possible, by having the correct cell type, ECM component and microenvironment without compromising of throughput. Even though, cancer cells were used, Caco-2 cells, they are known to differentiate into enterocyte like cells once confluent. Moreover, Caco-2 cells are known as the “golden standard” in drug discovery research since the 50’s, as they have good correlation to human jejunum and differentiated Caco-2 are used in drug absorption studies, especially for passively absorbed drugs (Sun et al. 2008). For the extracellular matrix, Collagen I was used which is one of the major collagen types of the intestine, representing approximately 68%, followed by Collagen III and collagen V with 20% and 12%, respectively (Graham et al. 1988). In our system, the cells were also exposed to fluid shear stress by applying a bidirectional and pulsatile flow with mean flow rate of 2.02 $\mu\text{L}/\text{min}$ and mean shear stress of 0.13 dyne/cm^2 . This is as similar as possible to physiological values, knowing that depending on digesta properties the intestinal fluid flow varies between 0.002 and 0.08 dyne/cm^2 (Lentle and Janssen 2008). After applying these physiological stimuli the model showed major improvement over standard 2D culture models (Ghaffarian and Muro 2013). One of these improvements was the accelerated maturation and polarization of the Caco-2 tubules as they did differentiate in 4 days compared to the 21 days needed for 2D cultures (Hilgers, Conradi, and Burton 1990; Trietsch et al. 2017a). This in turn significantly reduces time and costs associated with standard 2D cultures. More importantly, our approach increases the physiological relevance of the system and allowed more sensitive, real-time interrogation of compound effects on barrier integrity. The 3D model has closer physiologically relevant response in the case of Aspirin, but not quite the same due to the simplistic nature of the system (use of only of enterocytes like cells). Caco-2 cells are used extensively in Organs-on-chip platforms which report superior characteristics to our model like villi structures and different cell types (H. J. Kim et al. 2012a, 2016). However, the goal of the thesis wasn’t direct

competition with other gut-on-a-chip platforms, rather development of high throughput system suitable for drug discovery purposes, which most of the platforms that I will discuss are lacking. To my knowledge the OrganoPlate is the only microfluidics system compatible with all standard laboratory equipment and suitable for this purpose.

In my hands, I couldn't see formation of villi or crypt structures, which may be due to the lack of cyclic stretching. However, this villi formation still needs to be confirmed whether is due to the side effect of the stretching of the membrane or simply several layers of cells on top of each other. Additionally, the literature consensus is that Caco-2 cells only develop in enterocyte like cells of the small intestine (Lea 2015), therefore I doubt that they can differentiate into Paneth or Goblet cells, without the application of differentiation stimuli like in the case of differentiating them in M-cell like phenotype when RajiB lymphoma cells are present (Simon-Assmann et al. 2007). Nevertheless, at the same time I do acknowledge that Caco-2 are heterogenous population with lab to lab variations which can be constantly seen in reported TEER values (Srinivasan et al. 2015a). That is why the tubules were constantly assessed by immunofluorescence for intestinal markers specific for other cell types in the intestinal epithelium like Paneth and goblet cells and were found negative.

In Chapter 5 the "simple" Caco-2 model was further developed by applying specific downstream cues of immune activation to recapitulate aspects of the inflammatory bowel disease like barrier disruption and cell activation (McCole 2014). The choice of using cytokine induced IBD modelling was mainly because of the idiopathic nature of IBD where there is an unchecked and excessive immune response towards common microflora. The optimized cytokine cocktail was comprised by several pro-inflammatory cytokines like IL-1 β , INF-gamma and TNF- α fairly known from literature to be the main culprits for severity of IBD in both UC and CD patients

(Strober and Fuss 2011). This cocktail is mainly chosen to affect the intestinal epithelium, since in this setup only the epithelial compartment was present. The cytokine concentrations used were higher than reported in literature (Singh et al. 2016; Ogawa et al. 2012), however reported values are from systemic measurements from blood samples, whereas the localized levels are presumed to be in much higher quantities. The model showed suitability for target discovery and validation as AdV transduction performed directly on plate. The selected recombinant adenoviruses were expressing effective shRNAs, to two well-characterized inflammatory molecules, MYD88 and RELA. The importance of MyD88 come from the possibility of Toll like receptor adaptor protein to activate series of signalling modules and ultimately leading to the downstream activation of several transcription factors like NF- κ B, AP-1, STATs, Elk-1, IRF or CREB (Cario 2010). Moreover, the model was used for testing novel IBD therapeutics like 2-[(aminocarbonyl)amino]-5-(4-fluorophenyl)-3-thiophen carboxamide (TPCA-1), which is a direct dual inhibitor of STAT3 and NF- κ B (Nan et al. 2014). When added, TPCA-1 was effective suppressor of cell activation and restoring the barrier integrity after cytokine trigger, making the IBD model suitable for phenotypic studies and investigation of drugs that have the potential of preventing barrier integrity loss.

There are also other methods to model IBD and that is to harness the potential of Crispr-Cas9 which in my opinion is a powerful tool to make a precision genetic modification in cells (Morgens et al. 2017) . Applying this tool, however is quite impractical, primarily because Caco-2 are near tetraploid cells (Bezrookove et al. 2003). In addition to this, as mentioned in the introduction, no single gene is responsible in the development of IBD. Except for few very early onset cases of IBD (Moran et al. 2013; Kotlarz et al. 2012), considered to be monogenic forms, IBD is a multigenetic, multifactorial and multi cellular disease (Loddo and Romano 2015) .

In chapter 6, I focused on increasing the complexity of the model and investigating the effect of added immune cells and thereby examining the crosstalk between epithelium and the immune system. Both intestinal epithelium and immune system modulate the immune response and intestinal barrier function through either secreting cytokines and chemokines or through direct cell-cell interaction (Shan et al. 2013; Liang et al. 2006). I worked in the developing and characterization a tetra co-culture model consisting of enterocyte like Caco-2, the mucus producing HT29-MTX-E12 (Navabi, McGuckin, and Lindén 2013b), immune competent cells monocyte/macrophages THP-1 (Genin et al. 2015) and dendritic MUTZ-3 cells (Masterson, Sombroek, De Gruijl, et al. 2002). The ratio of seeding of the human intestinal cell lines Caco-2 and HT29-MTX-E12 were kept in physiological relevant ratios knowing that the absorptive to mucus producing cells may vary from 9:1 to 3:1 ratio or 5%-16% of goblet cell in the intestinal epithelium (Y. S. Kim and Ho 2010), depending on which part of the intestine is modelled (Kleiveland and Kleiveland 2015). As immune component immortalized monocyte-like cell line THP-1 and CD34⁺ dendritic cell precursor cell line MUTZ-3 are both widely used to study immune responses *in vitro* (Daigneault et al. 2010; Schwende et al. 1996; Masterson, Sombroek, de Gruijl, et al. 2002). In addition to showing the mucus production by the intestinal epithelial compartment, in this model the immune cell functionality was showed by exposing either monocultures or co-cultures of differentiated THP-1 and MUTZ-3 to various concentrations of LPS. Here, a concentration and cell number dependent increased release of IL-8 by both cells and found a synergetic effect in the co-culture settings. These results confirm the functionality of the cells in the OrganoPlate and are in line with previous *in vitro* model findings where the inflamed intestinal mucosa is an adequate tool for the screening of novel IBD drugs and formulations that would influence both the intestinal epithelial cells and infiltrating innate immune cells. This in turn

combines the convenience of *in vitro* studies with the complexity of pathophysiological changes of inflamed mucosal tissue.

The tetra-culture intestinal inflammation model could further be improved to more representative and robust inflammatory bowel disease model. The complexity could be enhanced by addition of intestinal microbiota to the lumen of the epithelial tubule as it has shown to have an important role in maintaining homeostasis in the gut (Pearce, Coia, et al. 2018; J. Lee, Choi, and Kim 2016). Even though the use of these cell lines allows controlled and reproducible data, they often fail to completely recapitulate the *in vivo* intestinal phenotypes. Alternatively, the addition of primary intestinal cells like iPSC-derived cells (Workman et al. 2018) or intestinal organoids (Kasendra et al. 2018b) could serve as valuable sources to increase the physiological relevance of the model.

In line with this, I focused in mimicking a more physiologically relevant gut-on-a-chip in chapter 7 that can at the same time be more sustainable sources of human cells, especially disease-specific cells. From iPSC and Organoids, I believe that the LGR5⁺ Organoids derived gut-on-a-chip models are better models because they are derived from adult stem cells, express all markers and are previously shown that can be used for different applications mentioned in this thesis (Kasendra et al. 2018b, 2020). However one drawback of the LGR5⁺ is that the organoids derived from adult stem cells generate only the epithelial layer which leads to the stem cell niche to not be supported once the differentiation is started. Thus, the viability of the differentiated cells will be 5-6 days, which is their intrinsic programmed lifespan (Park et al. 2016). That is why I decided to use iPSC cells. Organoids derived from iPSC (Forbester et al. 2015; Hannan et al. 2013; Forbester et al. 2019) do not only differentiate into the epithelial layer, but also to the stromal layer. Therefore the stem cell niche is supported by factors secreted by the stromal cells like Wnt and R-spondin3 (Aoki et al. 2016; Kabiri et al. 2014). In this chapter, I showed that iPSC can be successfully directed

towards intestinal epithelium, directly on the plate in a robust way and without the need of long and labour-intensive organoid steps and thereby shortening the time and reagents required for the derivation of iPSC differentiated gut tubules, from 2 months to 14-21 days. The accelerated culture developed barrier integrity starting from day 4, but reached small intestinal TEER values at day 14 (Sjöberg et al. 2013). In contrast to Caco-2 whose average TEER is 10 to 30 times higher than the physiologically relevant values (Srinivasan et al. 2015b; Takenaka et al. 2014), The tubules expressed relevant markers, but under expressed drug relevant transporters like P-gp (MDR1) which was actually in line with previous findings in stem cell differentiated gut-like tissue (Ozawa et al. 2015). This is due mainly of their foetal-like phenotype (Spinelli, Guillot, and De Coppi 2013).

The system applicability for modelling an inflammatory condition in the gut like inflammatory bowel disease was validated. Application of the previously optimized cytokine cocktail for mimicking IBD-like symptoms in epithelial cells, a response similar to *in vivo* situation was observed (Andrews, McLean, and Durum 2018). The iPSC-derived intestinal-like tubules had an immediate response and significant increase of IL-6 and IL-8 after 48 and 24 hours respectively. Especially interesting was the detection of IL-6, a cytokine produced by and affecting crypt Paneth cells, which is responsible for the increase of proliferation and survival of the intestinal epithelium by an autocrine signalling mechanism, but overall not produced by Caco-2 cells (Andrews, McLean, and Durum 2018; Jeffery et al. 2017).

In conclusion, the model described in chapter 7, is more physiologically relevant than the ones described in the previous chapters making this patient-specific model valuable tool for drug discovery studies especially the ones involving rare diseases. However, it is a proof of principle and the model needs to be further validated.

Taken together, in this thesis I was involved in the development of four different models that can be applied in the drug development process, from target validation to personalized medicine. Once implemented in standard procedures, the models should significantly decrease the costs of these processes bringing the necessary drugs to the patient. It is worth to mention that the research on organs-on-a-chip is evolving constantly and with the recent improvements in the field, there is still a lot of work until these systems become the new golden standard in drug development studies. Thus far the most important thing to confirm is whether this improved physiological relevance in these systems closely corresponds to better drug predictivity.

Outlook

High-throughput organ on chip platforms have the potential to play transformative role across the drug discovery and development field. This is not only because they can decrease the time needed for approval of medicines, but also decrease the cost associated to this process, by increasing the pre-clinical relevance. I believe that extensive and rigorous validation needs to be performed in these platforms to closely compare the data acquired, both from the animal studies, but most importantly to compare them to the clinical trials data. This will truly show the potential for OOC to transform the pharma industry. Moreover, I do believe that with the future advances of stem cells technology, both iPSC and organoid, these platforms can be used as personalized models for developing medicines specific for the given individual and also for the development of medicines for rare diseases based on patient specific biomarkers.

References

- Abraham, Clara, and Judy H Cho. 2009. "Inflammatory Bowel Disease." *Bmj*, 2066–78. <https://doi.org/10.1056/NEJMra0804647>.
- Abreu, Maria T. 2010. "Toll-like Receptor Signalling in the Intestinal Epithelium: How Bacterial Recognition Shapes Intestinal Function." *Nature Reviews Immunology*. <https://doi.org/10.1038/nri2707>.
- Abusleme, L., and N. M. Moutsopoulos. 2017. "IL-17: Overview and Role in Oral Immunity and Microbiome." *Oral Diseases*. Blackwell Publishing Ltd. <https://doi.org/10.1111/odi.12598>.
- Acuner Ozbabacan, Saliha Ece, Attila Gursay, Ruth Nussinov, and Ozlem Keskin. 2014. "The Structural Pathway of Interleukin 1 (IL-1) Initiated Signaling Reveals Mechanisms of Oncogenic Mutations and SNPs in Inflammation and Cancer." Edited by Yu Xia. *PLoS Computational Biology* 10 (2): e1003470. <https://doi.org/10.1371/journal.pcbi.1003470>.
- Adams, Christopher Paul, and Van Vu Brantner. 2010. "Spending on New Drug Development." *Health Economics* 19 (2): 130–41. <https://doi.org/10.1002/hec.1454>.
- Ahluwalia, Bani, Maria K. Magnusson, and Lena Öhman. 2017. "Mucosal Immune System of the Gastrointestinal Tract: Maintaining Balance between the Good and the Bad." *Scandinavian Journal of Gastroenterology* 52 (11): 1185–93. <https://doi.org/10.1080/00365521.2017.1349173>.
- Ahluwalia, Bani, Luiza Moraes, Maria K. Magnusson, and Lena Öhman. 2018a. "Immunopathogenesis of Inflammatory Bowel Disease and Mechanisms of Biological Therapies." *Scandinavian Journal of Gastroenterology*. Taylor and Francis Ltd. <https://doi.org/10.1080/00365521.2018.1447597>.
- . 2018b. "Immunopathogenesis of Inflammatory Bowel Disease and Mechanisms of Biological Therapies." *Scandinavian Journal of Gastroenterology* 53 (4): 379–89. <https://doi.org/10.1080/00365521.2018.1447597>.
- Al-Sadi, Rana M, and Thomas Y Ma. 2007. "IL-1beta Causes an Increase in Intestinal Epithelial Tight Junction Permeability." *Journal of Immunology (Baltimore, Md. : 1950)* 178 (7): 4641–49. <https://doi.org/10.4049/jimmunol.178.7.4641>.
- Alberts, Bruce, Alexander Johnson, Julian Lewis, Martin Raff, Keith Roberts, and Peter Walter. 2002. "Cell Junctions."
- Ananthakrishnan, Ashwin N. 2015. "Epidemiology and Risk Factors for IBD." *Nature Reviews Gastroenterology and Hepatology* 12 (4): 205–17. <https://doi.org/10.1038/nrgastro.2015.34>.
- Andrews, Caroline, Mairi H. McLean, and Scott K. Durum. 2018. "Cytokine Tuning of Intestinal Epithelial Function." *Frontiers in Immunology* 9 (June): 1270. <https://doi.org/10.3389/fimmu.2018.01270>.

- Aoki, Reina, Michal Shoshkes-Carmel, Nan Gao, Soona Shin, Catherine L. May, Maria L. Golson, Adam M. Zahm, et al. 2016. "Foxl1-Expressing Mesenchymal Cells Constitute the Intestinal Stem Cell Niche." *CMGH* 2 (2): 175–88. <https://doi.org/10.1016/j.jcmgh.2015.12.004>.
- Araújo, Francisca, Carla Pereira, Joana Costa, Cristina Barrias, Pedro L. Granja, and Bruno Sarmento. 2016. "In Vitro M-like Cells Genesis through a Tissue-Engineered Triple-Culture Intestinal Model." *Journal of Biomedical Materials Research Part B: Applied Biomaterials* 104 (4): 782–88. <https://doi.org/10.1002/jbm.b.33508>.
- Arebi, Naila, Ravi Misra, Omar Faiz, Pia Munkholm, and Johan Burisch. 2018. "Epidemiology of Inflammatory Bowel Disease in Racial and Ethnic Migrant Groups." *World Journal of Gastroenterology*. Baishideng Publishing Group Co., Limited. <https://doi.org/10.3748/wjg.v24.i3.424>.
- Assche, Gert v., Severine Vermeire, and Paul Rutgeerts. n.d. "Mucosal Healing and Anti TNFs in IBD."
- Atreya, Raja, Michael Zimmer, Brigitte Bartsch, Maximilian J Waldner, Imke Atreya, Helmut Neumann, Kai Hildner, et al. 2011. "Antibodies against Tumor Necrosis Factor (TNF) Induce T-Cell Apoptosis in Patients with Inflammatory Bowel Diseases via TNF Receptor 2 and Intestinal CD14⁺ Macrophages." *Gastroenterology* 141 (6): 2026–38. <https://doi.org/10.1053/j.gastro.2011.08.032>.
- Barker, Nick, Johan H. van Es, Jeroen Kuipers, Pekka Kujala, Maaïke van den Born, Miranda Cozijnsen, Andrea Haegebarth, et al. 2007. "Identification of Stem Cells in Small Intestine and Colon by Marker Gene Lgr5." *Nature* 449 (7165): 1003–7. <https://doi.org/10.1038/nature06196>.
- Beaurivage, Claudia, Elena Naumovska, Yee Xiang Chang, Edo D. Elstak, Arnaud Nicolas, Heidi Wouters, Guido van Moolenbroek, et al. 2019. "Development of a Gut-On-A-Chip Model for High Throughput Disease Modeling and Drug Discovery." *International Journal of Molecular Sciences* 20 (22): 5661. <https://doi.org/10.3390/ijms20225661>.
- Béduneau, Arnaud, Camille Tempesta, Stéphane Fimbel, Yann Pellequer, Vincent Jannin, Frédéric Demarne, and Alf Lamprecht. 2014. "A Tunable Caco-2/HT29-MTX Co-Culture Model Mimicking Variable Permeabilities of the Human Intestine Obtained by an Original Seeding Procedure." *European Journal of Pharmaceutics and Biopharmaceutics* 87 (2): 290–98. <https://doi.org/10.1016/j.ejpb.2014.03.017>.
- Bein, Amir, Woojung Shin, Sasan Jalili-Firoozinezhad, Min Hee Park, Alexandra Sontheimer-Phelps, Alessio Tovaglieri, Angeliki Chalkiadaki, Hyun Jung Kim, and Donald E. Ingber. 2018. "Microfluidic Organ-on-a-Chip Models of Human Intestine." *CMGH*. Elsevier Inc. <https://doi.org/10.1016/j.jcmgh.2017.12.010>.
- Berger, A. 2000. "Science Commentary: Th1 and Th2 Responses: What Are They?" *British Medical Journal*. BMJ Publishing

- Group. <https://doi.org/10.1136/bmj.321.7258.424>.
- Bezrookove, Vladimir, Ron Smits, Gabriela Moeslein, Riccardo Fodde, Hans Johannes Tanke, Anton Klaas Raap, and Firouz Darroudi. 2003. "Premature Chromosome Condensation Revisited: A Novel Chemical Approach Permits Efficient Cytogenetic Analysis of Cancers." *Genes, Chromosomes and Cancer* 38 (2): 177–86. <https://doi.org/doi:10.1002/gcc.10268>.
- Bjarnason, I, C O'Morain, A J Levi, and T J Peters. 1983. "Absorption of 51chromium-Labeled Ethylenediaminetetraacetate in Inflammatory Bowel Disease." *Gastroenterology* 85 (2): 318–22. <http://www.ncbi.nlm.nih.gov/pubmed/6407889>.
- Bonnans, Caroline, Jonathan Chou, and Zena Werb. 2014. "Remodelling the Extracellular Matrix in Development and Disease." *Nature Reviews Molecular Cell Biology*. Nature Publishing Group. <https://doi.org/10.1038/nrm3904>.
- Brewer, Matthias, Markus Utech, Andrei I. Ivanov, Ann M. Hopkins, Charles A. Parkos, and Asma Nusrat. 2005. "Interferon- γ Induces Internalization of Epithelial Tight Junction Proteins via a Macropinocytosis-like Process." *The FASEB Journal* 19 (8): 923–33. <https://doi.org/10.1096/fj.04-3260com>.
- Burisch, Johan, Tine Jess, Matteo Martinato, and Peter L. Lakatos. 2013. "The Burden of Inflammatory Bowel Disease in Europe." *Journal of Crohn's and Colitis* 7 (4): 322–37. <https://doi.org/10.1016/j.crohns.2013.01.010>.
- Cadwell, Ken. 2010. "Crohn's Disease Susceptibility Gene Interactions, a NOD to the Newcomer ATG16L1." *Gastroenterology* 139 (5): 1448–50. <https://doi.org/10.1053/j.gastro.2010.09.023>.
- Capaldo, Christopher T., and Asma Nusrat. 2009. "Cytokine Regulation of Tight Junctions." *Biochimica et Biophysica Acta - Biomembranes*. <https://doi.org/10.1016/j.bbamem.2008.08.027>.
- Cario, Elke. 2010. "Toll-like Receptors in Inflammatory Bowel Diseases: A Decade Later." *Inflammatory Bowel Diseases*. <https://doi.org/10.1002/ibd.21282>.
- Chen, Shuai, Ralf Einspanier, and Jennifer Schoen. 2015. "Transepithelial Electrical Resistance (TEER): A Functional Parameter to Monitor the Quality of Oviduct Epithelial Cells Cultured on Filter Supports." *Histochemistry and Cell Biology* 144 (5): 509–15. <https://doi.org/10.1007/s00418-015-1351-1>.
- Cho, Judy H., and Steven R. Brant. 2011. "Recent Insights into the Genetics of Inflammatory Bowel Disease." *Gastroenterology* 140 (6): 1704-1712.e2. <https://doi.org/10.1053/j.gastro.2011.02.046>.
- Chudy-Onwugaje, Kenechukwu O, Kaci E Christian, Francis A Farraye, and Raymond K Cross. 2019. "A State-of-the-Art Review of New and Emerging Therapies for the Treatment of IBD." *Inflammatory Bowel Diseases* 25 (5): 820–30. <https://doi.org/10.1093/ibd/izy327>.

- Cintolo, Marcello. 2016. "Mucosal Healing in Inflammatory Bowel Disease: Maintain or de-Escalate Therapy." *World Journal of Gastrointestinal Pathophysiology* 7 (1): 1. <https://doi.org/10.4291/wjgp.v7.i1.1>.
- Clark, Allison, and N ria Mach. 2016. "Role of Vitamin D in the Hygiene Hypothesis: The Interplay between Vitamin D, Vitamin D Receptors, Gut Microbiota, and Immune Response." *Frontiers in Immunology* 7: 627. <https://doi.org/10.3389/fimmu.2016.00627>.
- Cohen, B. L., H. Zo ga, S. A. Shah, N. Leleiko, S. Lidofsky, R. Bright, N. Flowers, et al. 2014. "Fatigue Is Highly Associated with Poor Health-Related Quality of Life, Disability and Depression in Newly-Diagnosed Patients with Inflammatory Bowel Disease, Independent of Disease Activity." *Alimentary Pharmacology and Therapeutics* 39 (8): 811–22. <https://doi.org/10.1111/apt.12659>.
- Coskun, Mehmet. 2014. "Intestinal Epithelium in Inflammatory Bowel Disease." *Frontiers in Medicine* 1: 24. <https://doi.org/10.3389/fmed.2014.00024>.
- Costa, Joana, and Arti Ahluwalia. 2019. "Advances and Current Challenges in Intestinal in Vitro Model Engineering: A Digest." *Frontiers in Bioengineering and Biotechnology*. Frontiers Media S.A. <https://doi.org/10.3389/fbioe.2019.00144>.
- Daigneault, Marc, Julie A. Preston, Helen M. Marriott, Moira K B Whyte, and David H. Dockrell. 2010. "The Identification of Markers of Macrophage Differentiation in PMA-Stimulated THP-1 Cells and Monocyte-Derived Macrophages." *PLoS ONE* 5 (1). <https://doi.org/10.1371/journal.pone.0008668>.
- Dawson, A., C. Dyer, J. Macfie, J. Davies, L. Karsai, J. Greenman, and M. Jacobsen. 2016. "A Microfluidic Chip Based Model for the Study of Full Thickness Human Intestinal Tissue Using Dual Flow." *Biomicrofluidics* 10 (6): 064101. <https://doi.org/10.1063/1.4964813>.
- DiMasi, Joseph A., Henry G. Grabowski, and Ronald W. Hansen. 2016. "Innovation in the Pharmaceutical Industry: New Estimates of R&D Costs." *Journal of Health Economics* 47 (May): 20–33. <https://doi.org/10.1016/j.jhealeco.2016.01.012>.
- Eckmann, Lars, and Michael Karin. 2005. "NOD2 and Crohn's Disease: Loss or Gain of Function?" *Immunity*. Cell Press. <https://doi.org/10.1016/j.immuni.2005.06.004>.
- Ek, Weronica E., Mauro D'Amato, and Jonas Halfvarson. 2014. "The History of Genetics in Inflammatory Bowel Disease." *Annals of Gastroenterology* 27 (4): 294–303.
- Elia, Paula Peruzzi, Yolanda Faia M. Tolentino, Claudio Bernardazzi, and Heitor Siffert Pereira de Souza. 2015. "The Role of Innate Immunity Receptors in the Pathogenesis of Inflammatory Bowel Disease." *Mediators of Inflammation* 2015: 1–10. <https://doi.org/10.1155/2015/936193>.

- Esch, Eric W., Anthony Bahinski, and Dongeun Huh. 2015. "Organs-on-Chips at the Frontiers of Drug Discovery." *Nature Reviews Drug Discovery*. Nature Publishing Group. <https://doi.org/10.1038/nrd4539>.
- Forbester, Jessica L., David Goulding, Ludovic Vallier, Nicholas Hannan, Christine Hale, Derek Pickard, Subhankar Mukhopadhyay, and Gordon Dougan. 2015. "Interaction of Salmonella Enterica Serovar Typhimurium with Intestinal Organoids Derived from Human Induced Pluripotent Stem Cells." *Infection and Immunity* 83 (7): 2926–34. <https://doi.org/10.1128/IAI.00161-15>.
- Forbester, Jessica L., Nicholas Hannan, Ludovic Vallier, and Gordon Dougan. 2019. "Derivation of Intestinal Organoids from Human Induced Pluripotent Stem Cells for Use as an Infection System." In *Methods in Molecular Biology*, 1576:157–69. Humana Press Inc. https://doi.org/10.1007/7651_2016_7.
- Frank, Daniel N, Allison L St Amand, Robert A Feldman, Edgar C Boedeker, Noam Harpaz, and Norman R Pace. 2007. "Molecular-Phylogenetic Characterization of Microbial Community Imbalances in Human Inflammatory Bowel Diseases." *Proceedings of the National Academy of Sciences* 104(34): 13780–85. <https://doi.org/10.1073/pnas.07066625104>.
- Franzen, Nora, W. H. van Harten, Valesca P. Retèl, P. Loskill, J. van den Eijnden-van Raaij, and Maarten IJzerman. 2019. "Impact of Organ-on-a-Chip Technology on Pharmaceutical R&D Costs." *Drug Discovery Today*. Elsevier Ltd. <https://doi.org/10.1016/j.drudis.2019.06.003>.
- Gao, Dan, Hongxia Liu, Jin Ming Lin, Yini Wang, and Yuyang Jiang. 2013. "Characterization of Drug Permeability in Caco-2 Monolayers by Mass Spectrometry on a Membrane-Based Microfluidic Device." *Lab on a Chip* 13 (5): 978–85. <https://doi.org/10.1039/c2lc41215b>.
- Garrett, WS, JI Gordon, and LH Glimcher. 2010. "Homeostasis and Inflammation in the Intestine." *Cell* 140 (6): 859–70. <https://doi.org/10.1016/j.cell.2010.01.023>.
- Gassler, Nikolaus. 2017. "Paneth Cells in Intestinal Physiology and Pathophysiology." *World Journal of Gastrointestinal Pathophysiology* 8 (4): 150–60. <https://doi.org/10.4291/wjgp.v8.i4.150>.
- Gaudino, Stephen J., and Pawan Kumar. 2019. "Cross-Talk between Antigen Presenting Cells and T Cells Impacts Intestinal Homeostasis, Bacterial Infections, and Tumorigenesis." *Frontiers in Immunology*. Frontiers Media S.A. <https://doi.org/10.3389/fimmu.2019.00360>.
- Genin, Marie, Francois Clement, Antoine Fattaccioli, Martine Raes, and Carine Michiels. 2015. "M1 and M2 Macrophages Derived from THP-1 Cells Differentially Modulate the Response of Cancer Cells to Etoposide." *BMC Cancer* 15 (1).

<https://doi.org/10.1186/s12885-015-1546-9>.

- Gent, A E, M D Hellier, R H Grace, E T Swarbrick, and D Coggon. 1994. "Inflammatory Bowel Disease and Domestic Hygiene in Infancy." *Lancet (London, England)* 343 (8900): 766–67. <http://www.ncbi.nlm.nih.gov/pubmed/7907734>.
- Geremia, Alessandra, Paolo Biancheri, Philip Allan, Gino R. Corazza, and Antonio Di Sabatino. 2014a. "Innate and Adaptive Immunity in Inflammatory Bowel Disease." *Autoimmunity Reviews* 13 (1): 3–10. <https://doi.org/10.1016/J.AUTREV.2013.06.004>.
- . 2014b. "Innate and Adaptive Immunity in Inflammatory Bowel Disease." *Autoimmunity Reviews* 13 (1): 3–10. <https://doi.org/10.1016/J.AUTREV.2013.06.004>.
- Ghaffarian, Rasa, and Silvia Muro. 2013. "Models and Methods to Evaluate Transport of Drug Delivery Systems across Cellular Barriers." *Journal of Visualized Experiments : JoVE*, no. 80. <https://doi.org/10.3791/50638>.
- Graham, Martin F., Robert F. Diegelmann, Charles O. Elson, William J. Lindblad, Nancy Gotschalk, Steffen Gay, and Renate Gay. 1988. "Collagen Content and Types in the Intestinal Strictures of Crohn's Disease." *Gastroenterology* 94 (2): 257–65. [https://doi.org/10.1016/0016-5085\(88\)90411-8](https://doi.org/10.1016/0016-5085(88)90411-8).
- Groschwitz, Katherine R., and Simon P. Hogan. 2009. "Intestinal Barrier Function: Molecular Regulation and Disease Pathogenesis." *Journal of Allergy and Clinical Immunology* 124 (1): 3–20. <https://doi.org/10.1016/j.jaci.2009.05.038>.
- Halldorsson, Skarphedinn, Edinson Lucumi, Rafael Gómez-Sjöberg, and Ronan M.T. Fleming. 2015. "Advantages and Challenges of Microfluidic Cell Culture in Polydimethylsiloxane Devices." *Biosensors and Bioelectronics* 63 (January): 218–31. <https://doi.org/10.1016/J.BIOS.2014.07.029>.
- Hamman, J H, P H Demana, and E I Olivier. 2007. "Targeting Receptors, Transporters and Site of Absorption to Improve Oral Drug Delivery." *Drug Target Insights* 2: 71–81. <http://www.ncbi.nlm.nih.gov/pubmed/21901064>.
- Hampton, Tracy. 2017. "Organoids Reveal Clues to Gut-Brain Communication." *JAMA* 318 (9): 787. <https://doi.org/10.1001/jama.2017.11545>.
- Hannan, Nicholas R.F., Robert P. Fordham, Yasir A. Syed, Victoria Moignard, Andrew Berry, Ruben Bautista, Neil A. Hanley, Kim B. Jensen, and Ludovic Vallier. 2013. "Generation of Multipotent Foregut Stem Cells from Human Pluripotent Stem Cells." *Stem Cell Reports* 1 (4): 293–306. <https://doi.org/10.1016/j.stemcr.2013.09.003>.
- Henry, T. Lynch, E. Brand Randall, and Y. Locker Gershon. 2004. "Inflammatory Bowel Disease in Ashkenazi Jews: Implications for Familial Colorectal Cancer." *Familial Cancer* 3 (3–4): 229–32. <https://doi.org/10.1007/s10689-004-9548-9>.

- Hidalgo, I J, T J Raub, and R T Borchardt. 1989. "Characterization of the Human Colon Carcinoma Cell Line (Caco-2) as a Model System for Intestinal Epithelial Permeability." *Gastroenterology* 96 (3): 736–49. <http://www.ncbi.nlm.nih.gov/pubmed/2914637>.
- Hilgers, Allen R., Robert A. Conradi, and Philip S. Burton. 1990. "Caco-2 Cell Monolayers as a Model for Drug Transport Across the Intestinal Mucosa." *Pharmaceutical Research: An Official Journal of the American Association of Pharmaceutical Scientists* 7 (9): 902–10. <https://doi.org/10.1023/A:1015937605100>.
- Hillman, Ethan T., Hang Lu, Tianming Yao, and Cindy H. Nakatsu. 2017. "Microbial Ecology along the Gastrointestinal Tract." *Microbes and Environments*. Japanese Society of Microbial Ecology. <https://doi.org/10.1264/jsme2.ME17017>.
- Hoefkens, Eveline, Kris Nys, Jestinah M John, Kristel Van Steen, Ingrid Arijs, Jan Van der Goten, Gert Van Assche, et al. 2013. "Genetic Association and Functional Role of Crohn Disease Risk Alleles Involved in Microbial Sensing, Autophagy, and Endoplasmic Reticulum (ER) Stress." *Autophagy* 9 (12): 2046–55. <https://doi.org/10.4161/autophagy.26337>.
- Hold, Georgina L, Megan Smith, Charlie Grange, Euan Robert Watt, Emad M El-Omar, and Indrani Mukhopadhyay. 2014. "Role of the Gut Microbiota in Inflammatory Bowel Disease Pathogenesis: What Have We Learnt in the Past 10 Years?" *World Journal of Gastroenterology* 20 (5): 1192–1210. <https://doi.org/10.3748/wjg.v20.i5.1192>.
- Homer, Craig R., Amy L. Richmond, Nancy A. Rebert, Jean-Paul Achkar, and Christine McDonald. 2010. "ATG16L1 and NOD2 Interact in an Autophagy-Dependent Antibacterial Pathway Implicated in Crohn's Disease Pathogenesis." *Gastroenterology* 139 (5): 1630-1641.e2. <https://doi.org/10.1053/j.gastro.2010.07.006>.
- Hu, Zhang Zhi, Hongzhan Huang, Cathy H. Wu, Mira Jung, Anatoly Dritschilo, Anna T. Riegel, and Anton Wellstein. 2011. "Omics-Based Molecular Target and Biomarker Identification." *Methods in Molecular Biology (Clifton, N.J.)* 719: 547–71. https://doi.org/10.1007/978-1-61779-027-0_26.
- Huet, G, I Kim, C de Bolos, J M Lo-Guidice, O Moreau, B Hemon, C Richet, P Delannoy, F X Real, and P Degand. 1995. "Characterization of Mucins and Proteoglycans Synthesized by a Mucin-Secreting HT-29 Cell Subpopulation." *Journal of Cell Science* 108 (Pt 3 (March): 1275–85. <http://www.ncbi.nlm.nih.gov/pubmed/7622610>.
- Idriss, Haitham T., and James H. Naismith. 2000. "TNF α and the TNF Receptor Superfamily: Structure-function Relationship(S)." *Microscopy Research and Technique* 50 (3): 184–95. [https://doi.org/10.1002/1097-0029\(20000801\)50:3<184::AID-JEMT2>3.0.CO;2-H](https://doi.org/10.1002/1097-0029(20000801)50:3<184::AID-JEMT2>3.0.CO;2-H).
- Jeffery, Victoria, Andrew J. Goldson, Jack R. Dainty, Marcello Chieppa, and Anastasia Sobolewski. 2017. "IL-6 Signaling Regulates Small Intestinal Crypt Homeostasis." *The Journal of Immunology* 199 (1): 304–11.

<https://doi.org/10.4049/jimmunol.1600960>.

- Joossens, Marie, Geert Huys, Margo Cnockaert, Vicky De Preter, Kristin Verbeke, Paul Rutgeerts, Peter Vandamme, and Severine Vermeire. 2011. "Dysbiosis of the Faecal Microbiota in Patients with Crohn's Disease and Their Unaffected Relatives." *Gut* 60 (5): 631–37. <https://doi.org/10.1136/gut.2010.223263>.
- Junaid, Abidemi, Alireza Mashaghi, Thomas Hankemeier, and Paul Vulto. 2017. "An End-User Perspective on Organ-on-a-Chip: Assays and Usability Aspects." *Current Opinion in Biomedical Engineering* 1 (March): 15–22. <https://doi.org/10.1016/J.COBME.2017.02.002>.
- Kabiri, Zahra, Gediminas Greicius, Babita Madan, Steffen Biechele, Zhendong Zhong, Hamed Zaribafzadeh, Edison, et al. 2014. "Stroma Provides an Intestinal Stem Cell Niche in the Absence of Epithelial Wnts." *Development (Cambridge)* 141 (11): 2206–15. <https://doi.org/10.1242/dev.104976>.
- Kaplan, Gilaad G. 2015a. "The Global Burden of IBD: From 2015 to 2025." *Nature Reviews Gastroenterology & Hepatology* 12 (12): 720–27. <https://doi.org/10.1038/nrgastro.2015.150>.
- . 2015b. "The Global Burden of IBD: From 2015 to 2025." *Nature Reviews Gastroenterology and Hepatology*. Nature Research. <https://doi.org/10.1038/nrgastro.2015.150>.
- Kasendra, Magdalena, Raymond Luc, Jianyi Yin, Dimitris V. Manatakis, Gauri Kulkarni, Carolina Lucchesi, Josiah Sliz, et al. 2020. "Duodenum Intestine-Chip for Preclinical Drug Assessment in a Human Relevant Model." *ELife* 9 (January). <https://doi.org/10.7554/eLife.50135>.
- Kasendra, Magdalena, Alessio Tovaglieri, Alexandra Sontheimer-Phelps, Sasan Jalili-Firoozinezhad, Amir Bein, Angeliki Chalkiadaki, William Scholl, et al. 2018a. "Development of a Primary Human Small Intestine-on-a-Chip Using Biopsy-Derived Organoids." *Scientific Reports* 8 (1): 2871. <https://doi.org/10.1038/s41598-018-21201-7>.
- . 2018b. "Development of a Primary Human Small Intestine-on-a-Chip Using Biopsy-Derived Organoids." *Scientific Reports* 8 (1). <https://doi.org/10.1038/s41598-018-21201-7>.
- . 2018c. "Development of a Primary Human Small Intestine-on-a-Chip Using Biopsy-Derived Organoids." *Scientific Reports* 8 (1): 2871. <https://doi.org/10.1038/s41598-018-21201-7>.
- Kenny, Eimear E, Itsik Pe'er, Amir Karban, Laurie Ozelius, Adele A Mitchell, Sok Meng Ng, Monica Erazo, et al. 2012. "A Genome-Wide Scan of Ashkenazi Jewish Crohn's Disease Suggests Novel Susceptibility Loci." *PLoS Genetics* 8 (3): e1002559. <https://doi.org/10.1371/journal.pgen.1002559>.
- Kikut, Justyna, Nina Konecka, Maciej Ziętek, and Małgorzata Szczuko. 2018. "Inflammatory Bowel Disease Etiology: Current

-
- Knowledge.” *Pteridines* 29 (1): 206–14. <https://doi.org/10.1515/pteridines-2018-0020>.
- Kim, Duk Hwan, and Jae Hee Cheon. 2017. “Pathogenesis of Inflammatory Bowel Disease and Recent Advances in Biologic Therapies.” *Immune Network*. Korean Association of Immunologists. <https://doi.org/10.4110/in.2017.17.1.25>.
- Kim, Hyun Jung, Dongeun Huh, Geraldine Hamilton, and Donald E. Ingber. 2012a. “Lab on a Chip Human Gut-on-a-Chip Inhabited by Microbial Flora That Experiences Intestinal.” *Lab on a Chip* 12: 2165–74. <https://doi.org/10.1039/c2lc40074j>.
- . 2012b. “Human Gut-on-a-Chip Inhabited by Microbial Flora That Experiences Intestinal Peristalsis-like Motions and Flow.” *Lab on a Chip* 12 (12): 2165. <https://doi.org/10.1039/c2lc40074j>.
- Kim, Hyun Jung, Hu Li, James J. Collins, and Donald E. Ingber. 2016. “Contributions of Microbiome and Mechanical Deformation to Intestinal Bacterial Overgrowth and Inflammation in a Human Gut-on-a-Chip.” *Proceedings of the National Academy of Sciences of the United States of America* 113 (1): E7–15. <https://doi.org/10.1073/pnas.1522193112>.
- Kim, Young S., and Samuel B. Ho. 2010. “Intestinal Goblet Cells and Mucins in Health and Disease: Recent Insights and Progress.” *Current Gastroenterology Reports*. Springer. <https://doi.org/10.1007/s11894-010-0131-2>.
- Kleiveland, Charlotte R., and Charlotte R. Kleiveland. 2015. “Co-Cultivation of Caco-2 and HT-29MTX.” In *The Impact of Food Bioactives on Health: In Vitro and Ex Vivo Models*, 135–40. Springer International Publishing. https://doi.org/10.1007/978-3-319-16104-4_13.
- Kotlarz, Daniel, Rita Beier, Dhaarini Murugan, Jana Diestelhorst, Ole Jensen, Kaan Boztug, Dietmar Pfeifer, et al. 2012. “Loss of Interleukin-10 Signaling and Infantile Inflammatory Bowel Disease: Implications for Diagnosis and Therapy.” *Gastroenterology* 143 (2): 347–55. <https://doi.org/10.1053/j.gastro.2012.04.045>.
- Lamb, Christopher Andrew, Nicholas A. Kennedy, Tim Raine, Philip Anthony Hendy, Philip J. Smith, Jimmy K. Limdi, Bu’Hussain Hayee, et al. 2019. “British Society of Gastroenterology Consensus Guidelines on the Management of Inflammatory Bowel Disease in Adults.” *Gut*. NLM (Medline). <https://doi.org/10.1136/gutjnl-2019-318484>.
- Laukoetter, Mike G, Porfirio Nava, and Asma Nusrat. 2008. “Role of the Intestinal Barrier in Inflammatory Bowel Disease.” *World Journal of Gastroenterology* 14 (3): 401. <https://doi.org/10.3748/wjg.14.401>.
- Lea, Tor. 2015. “Caco-2 Cell Line.” In *The Impact of Food Bioactives on Health: In Vitro and Ex Vivo Models*, 103–11. Springer International Publishing. https://doi.org/10.1007/978-3-319-16104-4_10.
- Lee, Jaewon, Jin-Ha Choi, and Hyun Jung Kim. 2016. “Human Gut-on-a-Chip Technology: Will This Revolutionize Our Understanding of IBD and Future Treatments?” [Http://Dx.Doi.Org/10.1080/17474124.2016.1200466](http://Dx.Doi.Org/10.1080/17474124.2016.1200466).
- Lee, Sung Hee. 2015. “Intestinal Permeability Regulation by Tight Junction: Implication on Inflammatory Bowel Diseases.”

-
- Intestinal Research* 13 (1): 11–18. <https://doi.org/10.5217/ir.2015.13.1.11>.
- Lentle, R. G., and P. W. M. Janssen. 2008. “Physical Characteristics of Digesta and Their Influence on Flow and Mixing in the Mammalian Intestine: A Review.” *Journal of Comparative Physiology B* 178 (6): 673–90. <https://doi.org/10.1007/s00360-008-0264-x>.
- Liang, Spencer C., Xiang-Yang Tan, Deborah P. Luxenberg, Rieyz Karim, Kyriaki Dunussi-Joannopoulos, Mary Collins, and Lynette A. Fouser. 2006. “Interleukin (IL)-22 and IL-17 Are Coexpressed by Th17 Cells and Cooperatively Enhance Expression of Antimicrobial Peptides.” *The Journal of Experimental Medicine* 203 (10): 2271–79. <https://doi.org/10.1084/jem.20061308>.
- Liu, Jimmy Z., Suzanne Van Sommeren, Hailiang Huang, Siew C. Ng, Rudi Alberts, Atsushi Takahashi, Stephan Ripke, et al. 2015. “Association Analyses Identify 38 Susceptibility Loci for Inflammatory Bowel Disease and Highlight Shared Genetic Risk across Populations.” *Nature Genetics* 47 (9): 979–86. <https://doi.org/10.1038/ng.3359>.
- Loddo, Italia, and Claudio Romano. 2015. “Inflammatory Bowel Disease: Genetics, Epigenetics, and Pathogenesis.” *Frontiers in Immunology* 6: 551. <https://doi.org/10.3389/fimmu.2015.00551>.
- Marks, D J B, and A W Segal. 2008. “Innate Immunity in Inflammatory Bowel Disease: A Disease Hypothesis.” *The Journal of Pathology* 214 (2): 260–66. <https://doi.org/10.1002/path.2291>.
- Martels, Julius Z.H. von, Mehdi Sadaghian Sadabad, Arno R. Bourgonje, Tjasso Blokzijl, Gerard Dijkstra, Klaas Nico Faber, and Hermie J.M. Harmsen. 2017. “The Role of Gut Microbiota in Health and Disease: In Vitro Modeling of Host-Microbe Interactions at the Aerobe-Anaerobe Interphase of the Human Gut.” *Anaerobe*. Academic Press. <https://doi.org/10.1016/j.anaerobe.2017.01.001>.
- Masterson, Allan J., Claudia C. Sombroek, Tanja D. de Gruijl, Yvo M. F. Graus, Hans J. J. van der Vliet, Sinéad M. Loughheed, Alfons J. M. van den Eertwegh, Herbert M. Pinedo, and Rik J. Scheper. 2002. “MUTZ-3, a Human Cell Line Model for the Cytokine-Induced Differentiation of Dendritic Cells from CD34+precursors.” *Blood* 100 (2). <http://www.bloodjournal.org/content/100/2/701.long?sso-checked=true>.
- Masterson, Allan J., Claudia C. Sombroek, Tanja D. De Gruijl, Yvo M.F. Graus, Hans J.J. Van Der Vliet, Sinéad M. Loughheed, Alfons J.M. Van Den Eertwegh, Herbert M. Pinedo, and Rik J. Scheper. 2002. “MUTZ-3, a Human Cell Line Model for the Cytokine-Induced Differentiation of Dendritic Cells from CD34+ Precursors.” *Blood* 100 (2): 701–3. <https://doi.org/10.1182/blood.V100.2.701>.
- Matricon, Julien, Nicolas Barnich, and Denis Ardid. 2010. “Immunopathogenesis of Inflammatory Bowel Disease.” *Self/Nonself*

-
- 1 (4): 299–309. <https://doi.org/10.4161/self.1.4.13560>.
- McCole, Declan F. 2014. “IBD Candidate Genes and Intestinal Barrier Regulation.” *Inflammatory Bowel Diseases*. Lippincott Williams and Wilkins. <https://doi.org/10.1097/MIB.0000000000000090>.
- McKay, D. M., D. J. Philpott, and M. H. Perdue. 1997. “Review Article: In Vitro Models in Inflammatory Bowel Disease Research - A Critical Review.” *Alimentary Pharmacology and Therapeutics, Supplement*. <https://doi.org/10.1111/j.1365-2036.1997.tb00811.x>.
- Mogensen, Trine H. 2009. “Pathogen Recognition and Inflammatory Signaling in Innate Immune Defenses.” *Clinical Microbiology Reviews*. American Society for Microbiology (ASM). <https://doi.org/10.1128/CMR.00046-08>.
- Molodecky, Natalie A., and Gilaad G. Kaplan. 2010a. “Environmental Risk Factors for Inflammatory Bowel Disease.” *Gastroenterology and Hepatology*. Millenium Medical Publishing. <https://doi.org/10.1111/jgh.2010.25.issue-2>.
- . 2010b. “Environmental Risk Factors for Inflammatory Bowel Disease.” *Gastroenterology and Hepatology*. <https://doi.org/10.1111/jgh.2010.25.issue-2>.
- Moran, Christopher J, Thomas D Walters, Cong-Hui Guo, Subra Kugathasan, Christoph Klein, Dan Turner, Victorien M Wolters, et al. 2013. “IL-10R Polymorphisms Are Associated with Very-Early-Onset Ulcerative Colitis.” *Inflammatory Bowel Diseases* 19 (1): 115–23. <https://doi.org/10.1002/ibd.22974>.
- Morgens, David W, Michael Wainberg, Evan A Boyle, Oana Ursu, Carlos L Araya, C Kimberly Tsui, Michael S Haney, et al. 2017. “Genome-Scale Measurement of off-Target Activity Using Cas9 Toxicity in High-Throughput Screens.” *Nature Communications* 8 (May): 15178. <https://doi.org/10.1038/ncomms15178>.
- Mow, William S., Eric A. Vasiliauskas, Ying-Chao Lin, Phillip R. Fleshner, Konstantinos A. Papadakis, Kent D. Taylor, Carol J. Landers, et al. 2004. “Association of Antibody Responses to Microbial Antigens and Complications of Small Bowel Crohn’s Disease.” *Gastroenterology* 126 (2): 414–24. <https://doi.org/10.1053/j.gastro.2003.11.015>.
- Mulder, Daniel J., Angela J. Noble, Christopher J. Justinich, and Jacalyn M. Duffin. 2014. “A Tale of Two Diseases: The History of Inflammatory Bowel Disease.” *Journal of Crohn’s and Colitis* 8 (5).
- Muzes, Györgyi, Béla Molnár, Zsolt Tulassay, and Ferenc Sipos. 2012. “Changes of the Cytokine Profile in Inflammatory Bowel Diseases.” *World Journal of Gastroenterology* 18 (41): 5848–61. <https://doi.org/10.3748/wjg.v18.i41.5848>.
- Nan, Jing, Yuping Du, Xing Chen, Qifeng Bai, Yuxin Wang, Xinxin Zhang, Ning Zhu, et al. 2014. “TPCA-1 Is a Direct Dual Inhibitor of STAT3 and NF-KB and Regresses Mutant EGFR-Associated Human Non-Small Cell Lung Cancers.” *Molecular Cancer Therapeutics* 13 (3): 617–29. <https://doi.org/10.1158/1535-7163.MCT-13-0464>.

- Nasseri-Moghaddam, Siavosh. 2012. "Inflammatory Bowel Disease." *Middle East Journal of Digestive Diseases* 4 (2): 77–89.
<http://www.ncbi.nlm.nih.gov/pubmed/24829639>.
- Navabi, Nazanin, Michael A. McGuckin, and Sara K. Lindén. 2013a. "Gastrointestinal Cell Lines Form Polarized Epithelia with an Adherent Mucus Layer When Cultured in Semi-Wet Interfaces with Mechanical Stimulation." *PLoS ONE* 8 (7).
<https://doi.org/10.1371/journal.pone.0068761>.
- . 2013b. "Gastrointestinal Cell Lines Form Polarized Epithelia with an Adherent Mucus Layer When Cultured in Semi-Wet Interfaces with Mechanical Stimulation." Edited by Benoit Foligne. *PLoS ONE* 8 (7): e68761.
<https://doi.org/10.1371/journal.pone.0068761>.
- Negróni, Anna, Maria Pierdomenico, Salvatore Cucchiara, and Laura Stronati. 2018a. "NOD2 and Inflammation: Current Insights." *Journal of Inflammation Research* 11: 49–60. <https://doi.org/10.2147/JIR.S137606>.
- . 2018b. "NOD2 and Inflammation: Current Insights." *Journal of Inflammation Research* Volume 11 (February): 49–60.
<https://doi.org/10.2147/JIR.S137606>.
- Nemeth, Zoltan H, Dorian A Bogdanovski, Patricia Barratt-Stopper, Samantha R Paglinco, Luca Antonioli, and Rolando H Rolandelli. 2017. "Crohn's Disease and Ulcerative Colitis Show Unique Cytokine Profiles." *Cureus*, April.
<https://doi.org/10.7759/cureus.1177>.
- Neurath, Markus F. 2014. "Cytokines in Inflammatory Bowel Disease." *Nature Reviews Immunology* 14 (5): 329–42.
<https://doi.org/10.1038/nri3661>.
- Ng, Siew C, Charles N Bernstein, Morten H Vatn, Peter Laszlo Lakatos, Edward V Loftus, Curt Tysk, Colm O'Morain, Bjorn Moum, Jean-Frédéric Colombel, and Epidemiology and Natural History Task Force of the International Organization of Inflammatory Bowel Disease (IOIBD). 2013. "Geographical Variability and Environmental Risk Factors in Inflammatory Bowel Disease." *Gut* 62 (4): 630–49. <https://doi.org/10.1136/gutjnl-2012-303661>.
- Noble, Colin, Elaine Nimmo, Daniel Gaya, Richard K Russell, and Jack Satsangi. 2006. "Novel Susceptibility Genes in Inflammatory Bowel Disease." *World Journal of Gastroenterology* 12 (13): 1991–99.
<https://doi.org/10.3748/wjg.v12.i13.1991>.
- Noguchi, Eiichiro, Yoichiro Homma, Xiaoyan Kang, Mihai G Netea, and Xiaojing Ma. 2009. "A Crohn's Disease–Associated NOD2 Mutation Suppresses Transcription of Human IL10 by Inhibiting Activity of the Nuclear Ribonucleoprotein HnRNP-A1." *Nature Immunology* 10 (5): 471–79. <https://doi.org/10.1038/ni.1722>.
- Ogawa, Kotaro, Takayuki Matsumoto, Motohiro Esaki, Takehiro Torisu, and Mitsuo Iida. 2012. "Profiles of Circulating

- Cytokines in Patients with Crohn's Disease under Maintenance Therapy with Infliximab." *Journal of Crohn's and Colitis* 6 (5): 529–35. <https://doi.org/10.1016/j.crohns.2011.10.010>.
- Orholm, Marianne, Pia Munkholm, Ebbe Langholz, Ole Haagen Nielsen, Thorkild I. A. Sørensen, and Vibeke Binder. 1991. "Familiar Occurance of Inflammatory Bowel Disease." *N Engl J Med* 324 (2): 84–88. <https://doi.org/10.1056/NEJM199101103240203>.
- Ozawa, Tatsuya, Kazuo Takayama, Ryota Okamoto, Ryosuke Negoro, Fuminori Sakurai, Masashi Tachibana, Kenji Kawabata, et al. 2015. "Generation of Enterocyte-like Cells from Human Induced Pluripotent Stem Cells for Drug Absorption and Metabolism Studies in Human Small Intestine." *Scientific Reports* 5 (November): 16479. <https://doi.org/10.1038/srep16479>.
- Park, Jung Ha, Takenori Kotani, Tasuku Konno, Jajar Setiawan, Yasuaki Kitamura, Shinya Imada, Yutaro Usui, et al. 2016. "Promotion of Intestinal Epithelial Cell Turnover by Commensal Bacteria: Role of Short-Chain Fatty Acids." *PLoS ONE* 11 (5). <https://doi.org/10.1371/journal.pone.0156334>.
- Parlato, Marianna, Garabet Yeretssian, Marianna Parlato, and Garabet Yeretssian. 2014. "NOD-Like Receptors in Intestinal Homeostasis and Epithelial Tissue Repair." *International Journal of Molecular Sciences* 15 (6): 9594–9627. <https://doi.org/10.3390/ijms15069594>.
- Pearce, Sarah C., Arwa Al-Jawadi, Kunihiro Kishida, Shiyan Yu, Madeleine Hu, Luke F. Fritzkly, Karen L. Edelblum, Nan Gao, and Ronaldo P. Ferraris. 2018. "Marked Differences in Tight Junction Composition and Macromolecular Permeability among Different Intestinal Cell Types." *BMC Biology* 16 (1): 19. <https://doi.org/10.1186/s12915-018-0481-z>.
- Pearce, Sarah C., Heidi G. Coia, J. P. Karl, Ida G. Pantoja-Feliciano, Nicholas C. Zachos, and Kenneth Racicot. 2018. "Intestinal in Vitro and Ex Vivo Models to Study Host-Microbiome Interactions and Acute Stressors." *Frontiers in Physiology*. Frontiers Media S.A. <https://doi.org/10.3389/fphys.2018.01584>.
- Peterson, Lance W., and David Artis. 2014a. "Intestinal Epithelial Cells: Regulators of Barrier Function and Immune Homeostasis." *Nature Reviews Immunology* 14 (3): 141–53. <https://doi.org/10.1038/nri3608>.
- . 2014b. "Intestinal Epithelial Cells: Regulators of Barrier Function and Immune Homeostasis." *Nature Reviews Immunology*. Nature Publishing Group. <https://doi.org/10.1038/nri3608>.
- Pott, Johanna, and Mathias Hornef. 2012. "Innate Immune Signalling at the Intestinal Epithelium in Homeostasis and Disease." *EMBO Reports* 13 (8): 684. <https://doi.org/10.1038/EMBOR.2012.96>.
- Roda, Giulia, Alessandro Sartini, Elisabetta Zambon, Andrea Calafiore, Margherita Marocchi, Alessandra Caponi, Andrea

-
- Belluzzi, and Enrico Roda. 2010. "Intestinal Epithelial Cells in Inflammatory Bowel Diseases." *World Journal of Gastroenterology* 16 (34): 4264–71. <https://doi.org/10.3748/wjg.v16.i34.4264>.
- Round, June L., and Sarkis K. Mazmanian. 2009. "The Gut Microbiota Shapes Intestinal Immune Responses during Health and Disease." *Nature Reviews Immunology* 9 (5): 313–23. <https://doi.org/10.1038/nri2515>.
- Russel, M G, F H Nieman, J M Bergers, and R W Stockbrügger. 1996. "Cigarette Smoking and Quality of Life in Patients with Inflammatory Bowel Disease. South Limburg IBD Study Group." *European Journal of Gastroenterology & Hepatology* 8 (11): 1075–81. <http://www.ncbi.nlm.nih.gov/pubmed/8944369>.
- Sato, Toshiro, Robert G. Vries, Hugo J. Snippert, Marc van de Wetering, Nick Barker, Daniel E. Stange, Johan H. van Es, et al. 2009. "Single Lgr5 Stem Cells Build Crypt-Villus Structures in Vitro without a Mesenchymal Niche." *Nature* 459 (7244): 262–65. <https://doi.org/10.1038/nature07935>.
- Sato, Toshiro, Robert G. Vries, Hugo J. Snippert, Marc Van De Wetering, Nick Barker, Daniel E. Stange, Johan H. Van Es, et al. 2009. "Single Lgr5 Stem Cells Build Crypt-Villus Structures in Vitro without a Mesenchymal Niche." *Nature* 459 (7244): 262–65. <https://doi.org/10.1038/nature07935>.
- Schokker, Dirkjan, Gosse Veninga, Stephanie A. Vastenhouw, Alex Bossers, Freddy M. de Bree, Lucia M.T.E. Kaal-Lansbergen, Johanna M.J. Rebel, and Mari A. Smits. 2015. "Early Life Microbial Colonization of the Gut and Intestinal Development Differ between Genetically Divergent Broiler Lines." *BMC Genomics* 16 (1). <https://doi.org/10.1186/s12864-015-1646-6>.
- Schreiber, Stefan, Philip Rosenstiel, Mario Albrecht, Jochen Hampe, and Michael Krawczak. 2005. "Genetics of Crohn Disease, an Archetypal Inflammatory Barrier Disease." *Nature Reviews Genetics* 6 (5): 376–88. <https://doi.org/10.1038/nrg1607>.
- Schroder, Kate, Paul J. Hertzog, Timothy Ravasi, and David A. Hume. 2004. "Interferon- γ : An Overview of Signals, Mechanisms and Functions." *Journal of Leukocyte Biology* 75 (2): 163–89. <https://doi.org/10.1189/jlb.0603252>.
- Schwende, Heike, Edith Fitzke, Petra Ambs, and Peter Dieter. 1996. "Differences in the State of Differentiation of THP-1 Cells Induced by Phorbol Ester and 1,25-Dihydroxyvitamin D3." *Journal of Leukocyte Biology* 59 (4): 555–61. <https://doi.org/10.1002/jlb.59.4.555>.
- Shah, Pranjul, Joëlle V. Fritz, Enrico Glaab, Mahesh S. Desai, Kacy Greenhalgh, Audrey Frachet, Magdalena Niegowska, et al. 2016a. "A Microfluidics-Based in Vitro Model of the Gastrointestinal Human-Microbe Interface." *Nature Communications* 7 (1): 1–15. <https://doi.org/10.1038/ncomms11535>.
- . 2016b. "A Microfluidics-Based in Vitro Model of the Gastrointestinal Human-Microbe Interface." *Nature Communications* 7 (1): 11535. <https://doi.org/10.1038/ncomms11535>.

-
- Shan, Meimei, Maurizio Gentile, John R Yeiser, A Cooper Walland, Victor U Bornstein, Kang Chen, Bing He, et al. 2013. "Mucus Enhances Gut Homeostasis and Immunoregulatory Signals." *Science (New York, N.Y.)* 342 (447): 447–53. <https://doi.org/10.1126/science.1237910>.
- Shaw, Michael H., Nobuhiko Kamada, Neil Warner, Yun-Gi Kim, and Gabriel Nuñez. 2011. "The Ever-Expanding Function of NOD2: Autophagy, Viral Recognition, and T Cell Activation." *Trends in Immunology* 32 (2): 73–79. <https://doi.org/10.1016/j.it.2010.12.007>.
- Shen, Le, Eric D Black, Edwina D Witkowski, Wayne I Lencer, Vince Guerriero, Eveline E Schneeberger, and Jerrold R Turner. 2006. "Myosin Light Chain Phosphorylation Regulates Barrier Function by Remodeling Tight Junction Structure." *Journal of Cell Science* 119 (Pt 10): 2095–2106. <https://doi.org/10.1242/jcs.02915>.
- Shi, Yan-Hong, Jin-Jing Xiao, Rong-Peng Feng, Yu-Ying Liu, Min Liao, Xiang-Wei Wu, Ri-Mao Hua, and Hai-Qun Cao. 2017. "Factors Affecting the Bioaccessibility and Intestinal Transport of Difenoconazole, Hexaconazole, and Spirodiclofen in Human Caco-2 Cells Following *in Vitro* Digestion." *Journal of Agricultural and Food Chemistry* 65 (41): 9139–46. <https://doi.org/10.1021/acs.jafc.7b02781>.
- Shim, Kyu Young, Dongwook Lee, Jeonghun Han, Nam Trung Nguyen, Sungsu Park, and Jong Hwan Sung. 2017a. "Microfluidic Gut-on-a-Chip with Three-Dimensional Villi Structure." *Biomedical Microdevices* 19 (2). <https://doi.org/10.1007/s10544-017-0179-y>.
- . 2017b. "Microfluidic Gut-on-a-Chip with Three-Dimensional Villi Structure." *Biomedical Microdevices* 19 (2): 37. <https://doi.org/10.1007/s10544-017-0179-y>.
- Sidiq, Tabasum, Sayuri Yoshihama, Isaac Downs, and Koichi S. Kobayashi. 2016. "Nod2: A Critical Regulator of Ileal Microbiota and Crohn's Disease." *Frontiers in Immunology*. Frontiers Media S.A. <https://doi.org/10.3389/fimmu.2016.00367>.
- Siegmund, Britta, and Martin Zeitz. 2011. "Innate and Adaptive Immunity in Inflammatory Bowel Disease." *World Journal of Gastroenterology* 17 (27): 3178–83. <https://doi.org/10.3748/wjg.v17.i27.3178>.
- Simon-Assmann, P., N. Turck, M. Sidhoum-Jenny, G. Gradwohl, and M. Kedinger. 2007. "In Vitro Models of Intestinal Epithelial Cell Differentiation." In *Cell Biology and Toxicology*, 23:241–56. <https://doi.org/10.1007/s10565-006-0175-0>.
- Sinagoga, Katie L, and James M Wells. 2015. "Generating Human Intestinal Tissues from Pluripotent Stem Cells to Study Development and Disease." *The EMBO Journal* 34 (9): 1149–63. <https://doi.org/10.15252/embj.201490686>.
- Singh, Udai P., Narendra P. Singh, E. Angela Murphy, Robert L. Price, Raja Fayad, Mitzi Nagarkatti, and Prakash S. Nagarkatti.

-
2016. "Chemokine and Cytokine Levels in Inflammatory Bowel Disease Patients." *Cytokine* 77 (January): 44–49.
<https://doi.org/10.1016/j.cyto.2015.10.008>.
- Sjöberg, Åsa, Mareike Lutz, Christer Tannergren, Caroline Wingolf, Anders Borde, and Anna-Lena Ungell. 2013.
"Comprehensive Study on Regional Human Intestinal Permeability and Prediction of Fraction Absorbed of Drugs Using
the Ussing Chamber Technique." *European Journal of Pharmaceutical Sciences* 48 (1–2): 166–80.
<https://doi.org/10.1016/j.ejps.2012.10.007>.
- Sosa-Hernández, Juan Eduardo, Angel M. Villalba-Rodríguez, Kenya D. Romero-Castillo, Mauricio A. Aguilar-Aguila-Isaías,
Isaac E. García-Reyes, Arturo Hernández-Antonio, Ishtiaq Ahmed, Ashutosh Sharma, Roberto Parra-Saldívar, and Hafiz
M.N. Iqbal. 2018. "Organs-on-a-Chip Module: A Review from the Development and Applications Perspective."
Micromachines. MDPI AG. <https://doi.org/10.3390/mi9100536>.
- Souza, Heitor S. P. de, Claudio Fiocchi, and Dimitrios Iliopoulos. 2017. "The IBD Interactome: An Integrated View of
Aetiology, Pathogenesis and Therapy." *Nature Reviews Gastroenterology & Hepatology* 14 (12): 739–49.
<https://doi.org/10.1038/nrgastro.2017.110>.
- Souza, Heitor S.P. De, and Claudio Fiocchi. 2016. "Immunopathogenesis of IBD: Current State of the Art." *Nature Reviews
Gastroenterology and Hepatology* 13 (1): 13–27. <https://doi.org/10.1038/nrgastro.2015.186>.
- Souza, Heitor S P de, and Claudio Fiocchi. 2016. "Immunopathogenesis of IBD: Current State of the Art." *Nat Rev Gastroenterol
Hepatol* 13 (1): 13–27. <http://dx.doi.org/10.1038/nrgastro.2015.186>.
- Spinelli, Valentina, Pascale V. Guillot, and Paolo De Coppi. 2013. "Induced Pluripotent Stem (IPS) Cells from Human Fetal
Stem Cells (HFSCs)." *Organogenesis*. Taylor & Francis. <https://doi.org/10.4161/org.25197>.
- Srinivasan, Balaji, Aditya Reddy Kolli, Mandy Brigitte Esch, Hasan Erbil Abaci, Michael L. Shuler, and James J. Hickman.
2015a. "TEER Measurement Techniques for In Vitro Barrier Model Systems." *Journal of Laboratory Automation*. SAGE
Publications Inc. <https://doi.org/10.1177/2211068214561025>.
- . 2015b. "TEER Measurement Techniques for In Vitro Barrier Model Systems." *Journal of Laboratory Automation* 20
(2): 107–26. <https://doi.org/10.1177/2211068214561025>.
- Strober, Warren, and Ivan J. Fuss. 2011. "Proinflammatory Cytokines in the Pathogenesis of Inflammatory Bowel Diseases."
Gastroenterology 140 (6): 1756–1767.e1. <https://doi.org/10.1053/j.gastro.2011.02.016>.
- Sun, Huadong, Edwin Cy Chow, Shanjun Liu, Yimin Du, and K Sandy Pang. 2008. "The Caco-2 Cell Monolayer: Usefulness
and Limitations." *Expert Opinion on Drug Metabolism & Toxicology* 4 (4): 395–411.

<https://doi.org/10.1517/17425255.4.4.395>.

- Takenaka, T, N Harada, J Kuze, M Chiba, T Iwao, and T Matsunaga. 2014. "Human Small Intestinal Epithelial Cells Differentiated from Adult Intestinal Stem Cells as a Novel System for Predicting Oral Drug Absorption in Humans." *Drug Metabolism and Disposition* 42: 1947–54. <https://doi.org/10.1124/dmd.114.059493>.
- Tau, G., and P. Rothman. 1999. "Biologic Functions of the IFN- γ Receptors." *Allergy: European Journal of Allergy and Clinical Immunology*. NIH Public Access. <https://doi.org/10.1034/j.1398-9995.1999.00099.x>.
- Tontini, Gian Eugenio, Maurizio Vecchi, Luca Pastorelli, Markus F. Neurath, and Helmut Neumann. 2015. "Differential Diagnosis in Inflammatory Bowel Disease Colitis: State of the Art and Future Perspectives." *World Journal of Gastroenterology* 21 (1): 21–46. <https://doi.org/10.3748/wjg.v21.i1.21>.
- Travassos, Leonardo H, Leticia A M Carneiro, Mahendrasingh Ramjeet, Seamus Hussey, Yun-Gi Kim, João G Magalhães, Linda Yuan, et al. 2010. "Nod1 and Nod2 Direct Autophagy by Recruiting ATG16L1 to the Plasma Membrane at the Site of Bacterial Entry." *Nature Immunology* 11 (1): 55–62. <https://doi.org/10.1038/ni.1823>.
- Trietsch, Sebastiaan J., Guido D. Israëls, Jos Joore, Thomas Hankemeier, Paul Vulto, A. Abbott, V. M. Weaver, et al. 2013. "Microfluidic Titer Plate for Stratified 3D Cell Culture." *Lab on a Chip* 13 (18): 3548. <https://doi.org/10.1039/c3lc50210d>.
- Trietsch, Sebastiaan J., Elena Naumovska, Dorota Kurek, Meily C. Setyawati, Marianne K. Vormann, Karlijn J. Wilschut, Henriëtte L. Lanz, et al. 2017a. "Membrane-Free Culture and Real-Time Barrier Integrity Assessment of Perfused Intestinal Epithelium Tubes." *Nature Communications*. <https://doi.org/10.1038/s41467-017-00259-3>.
- . 2017b. "Membrane-Free Culture and Real-Time Barrier Integrity Assessment of Perfused Intestinal Epithelium Tubes." *Nature Communications* 8 (1): 262. <https://doi.org/10.1038/s41467-017-00259-3>.
- Utech, Markus, Andrei I. Ivanov, Stanislav N. Samarin, Matthias Bruewer, Jerrold R. Turner, Randall J. Mrsny, Charles A. Parkos, and Asma Nusrat. 2005. "Mechanism of IFN- γ -Induced Endocytosis of Tight Junction Proteins: Myosin II-Dependent Vacuolarization of the Apical Plasma Membrane." *Molecular Biology of the Cell* 16 (10): 5040–52. <https://doi.org/10.1091/mbc.e05-03-0193>.
- Valatas, Vassilis, Eirini Filidou, Ioannis Drygiannakis, and George Kolios. 2017. "Stromal and Immune Cells in Gut Fibrosis: The Myofibroblast and the Scarface." *Annals of Gastroenterology* 30 (4): 393–404. <https://doi.org/10.20524/aog.2017.0146>.
- Vancamelbeke, Maaïke, and Séverine Vermeire. 2017. "The Intestinal Barrier: A Fundamental Role in Health and Disease." *Expert Review of Gastroenterology and Hepatology*. Taylor and Francis Ltd.

<https://doi.org/10.1080/17474124.2017.1343143>.

- Viswanathan, Pragasam, Yuvashree Muralidaran, and Gokulakannan Ragavan. 2017. "Challenges in Oral Drug Delivery: A Nano-Based Strategy to Overcome." *Nanostructures for Oral Medicine*, January, 173–201. <https://doi.org/10.1016/B978-0-323-47720-8.00008-0>.
- Wang, Pingzhang, Wenling Han, and Dalong Ma. 2016. "Electronic Sorting of Immune Cell Subpopulations Based on Highly Plastic Genes." *The Journal of Immunology* 197 (2): 665–73. <https://doi.org/10.4049/jimmunol.1502552>.
- Williams, C.F., G.E. Walton, L. Jiang, S. Plummer, I. Garaiova, and G.R. Gibson. 2015. "Comparative Analysis of Intestinal Tract Models." *Annual Review of Food Science and Technology* 6 (1): 329–50. <https://doi.org/10.1146/annurev-food-022814-015429>.
- Workman, Michael J, John P Gleeson, Elissa J Troisi, Hannah Q Estrada, S Jordan Kerns, Christopher D Hinojosa, Geraldine A Hamilton, Stephan R Targan, Clive N Svendsen, and Robert J Barrett. 2018. "Enhanced Utilization of Induced Pluripotent Stem Cell-Derived Human Intestinal Organoids Using Microengineered Chips." *Cellular and Molecular Gastroenterology and Hepatology* 5 (4): 669-677.e2. <https://doi.org/10.1016/j.jcmgh.2017.12.008>.
- Yamamoto-Furusho, Jesús K, Ilse Ascaño-Gutiérrez, Janette Furuzawa-Carballeda, and Gabriela Fonseca-Camarillo. 2015. "Differential Expression of MUC12, MUC16, and MUC20 in Patients with Active and Remission Ulcerative Colitis." *Mediators of Inflammation* 2015: 659018. <https://doi.org/10.1155/2015/659018>.
- Yamamoto, Soichiro, and Xiaojing Ma. 2009. "Role of Nod2 in the Development of Crohn's Disease." *Microbes and Infection* 11 (12): 912–18. <https://doi.org/10.1016/j.micinf.2009.06.005>.
- Zaidi, M. Raza, and Glenn Merlino. 2011. "The Two Faces of Interferon- γ in Cancer." *Clinical Cancer Research*. NIH Public Access. <https://doi.org/10.1158/1078-0432.CCR-11-0482>.
- Zuo, Tao, and Siew C. Ng. 2018. "The Gut Microbiota in the Pathogenesis and Therapeutics of Inflammatory Bowel Disease." *Frontiers in Microbiology* 9 (September): 2247. <https://doi.org/10.3389/fmicb.2018.02247>.